





# **WATER BALANCE MODELING WITH EXPLICIT ICE-FLOW DYNAMICS**

Von der Fakultät für Bauingenieurwesen und Geodäsie  
der Gottfried Wilhelm Leibniz Universität Hannover

zur Erlangung des akademischen Grades  
Doktor-Ingenieurin  
- Dr.-Ing. -

genehmigte Dissertation

von

María Herminia Pesci, M.Sc.  
geboren am 13. Juli 1988 in Totoras (Argentinien)

2024

Referent: Prof. Dr.-Ing. Kristian Förster  
Korreferent: Prof. Dr.-Ing. Markus Disse

Tag der Promotion: 02.02.2024

# Acknowledgments

First and foremost I would like to give my greatest thank to my doctoral thesis supervisor and mentor, Kristian Förster. His guidance, support, experience and patience were invaluable to me during this journey. Even before, while working as a student assistant and helping with teaching, I have been able to form myself in the field of hydrology, confirming my desire of becoming a professional in the topic.

I would also like to thank Prof. Disse, for agreeing to be co-examiner for this thesis, and Prof. Achmus for being part of the committee. A big thanks goes to PD Jörg Dietrich, also for his willingness to be part of the committee but specially for the shared moments and given confidence during teaching.

I am very grateful to Prof. Haberlandt, for grating me the opportunity to be part of the Institute over the past four years, which would not have been so incredible if it were not for my colleagues. I am deeply grateful to Luisa, for her time in helping me improve this manuscript, for her advice, her patience and her boundless willingness to support me in teaching. I am also very thankful to Golbarg and Ross, with whom I also have spent most of my time at the Institute and who have always gave me the right perspective. In addition, a warm thanks to Ronja, Adina and Zoë, even though our paths crossed for a shorter time, you made my journey very enjoyable. I would also like to extend my thanks to Larissa, for being part of our small working group and always giving me useful advice regarding glaciers. Lastly, I am very grateful to my former colleagues with whom I shared at least some time at the Institute.

I would like to express my gratitude towards my DIRT-X project colleagues for the collaborative discussions, conferences, manuscripts and meetings that we participated in together. I really enjoyed working with experts from all over Europe. A warm thanks also for Philipp Schulte Overberg, who worked as a student assistant and prepared the past climate data for my simulations. Moreover, thanks to Dr. Thomas Bosshard, colleague at SMHI, who provided me with the future climate datasets. I would also like to thank Dr. Jörg Schulla (developer of WaSiM) and the OGGM community, for providing help whenever I required it.

Finally, thank you to my friends in Hannover, my WATENV classmates, especially my *latinos* friends. Thank you to my partner Gunnar, for being a great support. And the greatest thanks goes to Spain and Argentina, to my family and friends, who are always with me no matter the distance.

# Declaration

I, María Herminia Pesci, hereby declare that:

1. I know the regulations for the doctoral candidates at Leibniz University of Hannover and I have met all the requirements. I agree with an examination under the provisions of the doctoral regulations.
2. I have completed the thesis independently, and where I have consulted other works, to the best of my knowledge, this is always clearly attributed.
3. I have not paid any third party to contribute to the content of my dissertation. The scientific work has not been acquired or conveyed, either in part or in full, by a third party for payment or any other consideration.
4. This work contains no material which has been accepted for the award of any other degree or diploma at any other university or tertiary institution.
5. The same or partly similar work has not been submitted at any other university or academic institution.
6. I agree that my thesis can be used for verifying the compliance with scientific standards in particular using electronic data processing programs.

Hamburg, 19.02.2024

---

Place and Date



---

María Herminia Pesci, M.Sc.

# Abstract

Mountains, the *water towers* of the world, are capable of storing water and releasing it to lower elevations, hence ensuring water supply to the lowlands. In mountainous regions, higher precipitation amounts and low temperatures favor the presence of glaciers, which act as vast reservoirs of fresh water being stored in the form of snow, firn and ice. Glaciers primarily release water due to melt, resulting in a decrease in their volume and area. In the matter of changing climate, anthropogenic causes lead to rising temperatures, which are projected to continuously do so until the end of the century. This inevitable results in glacier volume loss and increased glacier runoff, which at some point will reach a maximum (*peak water*). Beyond this point, glacier volume continues to decrease and the water balance surplus cannot be sustained due to the lack of glacier runoff. This matter contributes to sea-level rise on a global scale, while changes in the runoff regime and water shortage can be awaited at the local and regional levels.

Accurate prediction of glacier evolution and runoff becomes crucial for the assessment of changes in catchment hydrology. In this sense, glacio-hydrological models are extremely valuable as they can predict both glacier and hydrological processes. Yet, the limited available glacier measurements (e.g. long-term mass balances) poses a challenge to model glacier evolution. To address this issue, simplified and empirical methods, such as the Volume-Area (VA) scaling approach, are commonly utilized. Even though good estimates can be expected for hundreds of glaciers, its application at the catchment scale is somewhat controversial due to the difficulty in selecting representative scaling parameters (e.g. representative thickness) for a single glacier. On the other hand, the emergence of global glacier datasets enhances the development of (global) glacier models that implement more complex approaches to account for glacier evolution. Essentially, the flux of ice along the glacier's flowline is contemplated, thus relying on the actual physical forces that underlie the processes. Despite efforts to couple standalone glacier models to hydrological models, major limitations still persist: Either a single variable is transferred between models (e.g. glacier area), or inconsistencies in the driven climate dataset can be recognized.

For these reasons, the aim of this study is to go beyond existing *offline* coupled glacio-hydrological models (*offline* means that the models run separately but variables are transferred between them) by ensuring a consistent exchange of state variables between two independent models. More precisely, and being both models driven by the same climate dataset, glacier states (i.e. areas, ice thickness distribution, volumes and mass balances) are produced annually with the help of the Open Global Glacier Model (OGGM), based on explicit ice-flow dynamics, and later integrated into the fully-distributed and physically-based Water Flow and Balance Simulation Model (WaSiM). The developed WaSiM-OGGM coupling scheme, applied to the Gepatschalm catchment (Austria), demonstrates greater reliability in predicting glacier evolution and runoff when compared to the original WaSiM model with integrated VA scaling. Despite rather pessimistic results (with nearly 19% more glacier area loss by the end of the century under severe warming conditions), they share more affinity with other studies carried out in the European Alps. Furthermore, the pro-

posed coupling scheme could be implemented in catchments lacking glacier observations while providing a physically-based and fully-distributed representation of hydrological processes, including glacier evolution from any year in the past. Finally, the WaSiM-OGGM coupling scheme might serve as a powerful tool for the effective water resources management in vulnerable regions, especially in face of a changing climate.

**Keywords:** glacio-hydrological models, VA scaling, ice-flow dynamics, catchment runoff, offline coupling scheme

# Kurzfassung

Berge, die *Wassertürme* der Welt, können Wasser speichern und an die flacheren Regionen abgeben und so die Wasserversorgung des angrenzenden Flachlandes sicherstellen. In Gebirgsregionen ermöglichen höhere Niederschlagsmengen und niedrige Temperaturen das Vorkommen von Gletschern, die als riesige Frischwasserspeicher in Form von Schnee, Firn und Eis wirken. Gletscher geben vor allem durch Schmelzen Wasser ab, was zu einer Verringerung ihres Volumens und ihrer Oberfläche führt. Im Zusammenhang mit der Klimaänderung führen anthropogene Ursachen zu einem Anstieg der Temperaturen, der bis zum Ende des Jahrhunderts anhalten wird. Dies führt unvermeidlich zu einem Gletscherschwund und einer Zunahme des Gletscherabflusses, der irgendwann ein Maximum (*peak water*) erreichen wird. Nach Erreichen des Maximums, nimmt das Gletschervolumen weiter ab und der Wasserbilanzüberschuss kann aufgrund des fehlenden Gletscherabflusses nicht aufrechterhalten werden. Dieser Umstand trägt auf globaler Ebene zum Anstieg des Meeresspiegels bei, während auf lokaler und regionaler Ebene Veränderungen im Abflussregime und Wassermangel zu erwarten sein können.

Eine genaue Vorhersage der Gletscherentwicklung und des Abflusses ist für die Bewertung von Veränderungen in der Hydrologie von Einzugsgebieten wichtig. In diesem Sinne sind glazio-hydrologische Modelle äußerst wertvoll, da sie sowohl Gletscher als auch hydrologische Prozesse vorhersagen können. Die begrenzte Verfügbarkeit von Gletschermessungen (z.B. langfristige Massenbilanzen) stellt jedoch eine Herausforderung für die Modellierung der Gletscherentwicklung dar. Um dieses Problem zu überwinden, werden oft vereinfachte und empirische Methoden wie der Volumen-Fläche (Volume-Area, VA) Skalierungsansatz verwendet. Auch wenn gute Schätzungen für Hunderte von Gletschern zu erwarten sind, ist die Anwendung auf der Einzugsgebietebene umstritten, da es schwierig ist, repräsentative Skalierungsparameter (z.B. eine repräsentative Eisdicke) für einen einzelnen Gletscher auszuwählen. Die jüngsten Erhebungen globaler Gletscherdatensätze hingegen fördern die Entwicklung von (globalen) Gletschermodellen, die auf komplexeren Ansätzen beruhen, um die Gletscherentwicklung zu berücksichtigen. Im Wesentlichen wird der Eisfluss entlang der Fließlinie des Gletschers betrachtet, wobei man sich auf die tatsächlichen physikalischen Kräfte stützt, die hinter den Prozessen stehen. Trotz der Versuche, eigenständige Gletschermodelle mit hydrologischen Modellen zu koppeln, gibt es nach wie vor große Einschränkungen: Entweder wird nur eine einzige Variable zwischen den Modellen übertragen (z.B. die Gletscheroberfläche), oder es sind Inkonsistenzen in den zugrunde liegenden Klimadatensätzen erkennbar.

Aus diesen Gründen besteht das Ziel dieser Arbeit darin, über die bestehenden *offline* gekoppelten glazio-hydrologischen Modelle (*offline* heißt die Modelle laufen unabhängig voneinander, aber die Variablen werden zwischen ihnen übertragen) hinauszugehen und einen konsistenten Austausch von Zustandsvariablen zwischen zwei unabhängigen Modellen zu ermöglichen. Da beide Modelle mit demselben Klimadatensatz betrieben werden, werden die Gletscherzustände (d.h. Oberflächen, Eisdickenverteilung, Volumen und Massenbilanzen) mit Hilfe des Open Global Glacier Model (OGGM), das auf expliziter Eis-



flussdynamik basiert, jährlich erstellt und später in das flächendifferenzierte und physikalisch basierte Water Flow and Balance Simulation Model (WaSiM) integriert. Das entwickelte WaSiM-OGGM-Kopplungsschema, das auf das Einzugsgebiet der Gepatschalm (Österreich) angewandt wird, zeigt eine größere Zuverlässigkeit bei der Vorhersage der Gletscherentwicklung und des Abflusses im Vergleich zum ursprünglichen WaSiM-Modell mit integrierter VA-Skalierung. Trotz der eher pessimistischen Ergebnisse (mit fast 19% mehr Gletscheroberflächenverlust bis zum Ende des Jahrhunderts unter starken Erwärmungsbedingungen), stimmen sie besser mit anderen Studien überein, die in den europäischen Alpen durchgeführt wurden. Darüber hinaus kann das vorgeschlagene Kopplungsschema in Einzugsgebieten ohne Gletscherbeobachtungen implementiert werden, was eine physikalisch basierte und flächendifferenzierte Darstellung der hydrologischen Prozesse ermöglicht, einschließlich der Gletscherentwicklung von einem beliebigen Jahr in der Vergangenheit. Das WaSiM-OGGM-Kopplungsschema könnte ein leistungsfähiges Instrument für die effektive Bewirtschaftung von Wasserressourcen in gefährdeten Regionen sein, insbesondere angesichts des sich ändernden Klimas.

**Schlagwörter:** Glazio-hydrologische Modelle, VA-Skalierung, Eisflussdynamik, Einzugsgebietsabfluss, Offline-Kopplungsschema

# Contents

<b>1</b>	<b>Introduction</b>	<b>1</b>
1.1	Background and motivation . . . . .	1
1.2	Objectives . . . . .	4
1.3	Research questions . . . . .	4
1.4	Structure of the thesis . . . . .	5
<b>2</b>	<b>State of the art</b>	<b>7</b>
2.1	Water balance in mountainous regions . . . . .	7
2.2	Glaciers . . . . .	9
2.2.1	Introduction to glaciers . . . . .	9
2.2.2	Glacier mass balance . . . . .	11
2.2.3	Glacier measurements . . . . .	12
2.3	Modeling . . . . .	14
2.3.1	Water balance modeling . . . . .	14
2.3.2	Glacier modeling . . . . .	16
2.3.3	Glacio-hydrological modeling . . . . .	20
2.3.4	Optimization and uncertainties in modeling . . . . .	23
<b>3</b>	<b>Study area and data</b>	<b>27</b>
3.1	Study area . . . . .	27
3.2	Data . . . . .	28
3.2.1	Land cover and soil classification . . . . .	28
3.2.2	Glaciers . . . . .	29
3.2.3	Snow . . . . .	31
3.2.4	Climate . . . . .	32
3.2.5	Runoff . . . . .	34
<b>4</b>	<b>Water balance modeling</b>	<b>35</b>
4.1	Model resolution and simulation period . . . . .	36
4.2	Precipitation correction . . . . .	37
4.3	Interpolation of meteorological data . . . . .	38
4.4	Radiation correction . . . . .	39
4.5	Evapotranspiration . . . . .	40
4.6	Interception . . . . .	40
4.7	Snow accumulation and melt . . . . .	41
4.7.1	Snow accumulation . . . . .	41
4.7.2	Snow melt . . . . .	42
4.8	Soil model . . . . .	43
4.8.1	Unsaturated zone model . . . . .	43
4.8.2	Groundwater model . . . . .	44

4.9	Discharge routing . . . . .	44
<b>5</b>	<b>Glacier modeling</b>	<b>45</b>
5.1	WaSiM VA scaling glacier model . . . . .	45
5.1.1	Glacier mass balance . . . . .	46
5.1.2	Glacier retreat and advance . . . . .	47
5.1.3	Routing of melt components to the catchment outlet . . . . .	48
5.2	The Open Global Glacier Model . . . . .	48
5.2.1	General workflow . . . . .	48
5.2.2	Glacier flowlines . . . . .	50
5.2.3	Glacier mass balance . . . . .	51
5.2.4	Glacier ice thickness inversion . . . . .	51
<b>6</b>	<b>WaSiM-OGGM coupling scheme</b>	<b>53</b>
6.1	Main capabilities of the models . . . . .	53
6.2	Assumptions . . . . .	55
6.3	First WaSiM run with resampling of climate data . . . . .	56
6.3.1	Sensitivity analysis . . . . .	57
6.3.2	Calibration and validation of the model . . . . .	58
6.3.3	Generation of monthly climate grids . . . . .	59
6.4	OGGM run and processing of glacier outputs . . . . .	60
6.4.1	Calibration of the mass balance model . . . . .	60
6.4.2	Sensitivity analysis of the mass balance model parameters . . . . .	62
6.4.3	Dynamic runs . . . . .	63
6.4.4	From "1.5D" to 2D geometries . . . . .	65
6.4.5	Distributed ice thickness . . . . .	68
6.4.6	Glacier volumes . . . . .	69
6.5	Coupling the models: final WaSiM run with optimization . . . . .	70
6.5.1	Multi-data optimization . . . . .	72
6.5.2	Uncertainties . . . . .	76
6.5.3	Future projections . . . . .	78
<b>7</b>	<b>Results and discussion</b>	<b>79</b>
7.1	First WaSiM run with resampling of climate data . . . . .	79
7.1.1	Sensitivity analysis . . . . .	79
7.1.2	Calibration and validation of the model . . . . .	80
7.1.3	Generation of monthly climate grids . . . . .	84
7.1.4	WaSiM VA scaling glacier model . . . . .	85
7.2	OGGM run and processing of glacier outputs . . . . .	85
7.2.1	Sensitivity analysis of the mass balance model parameters . . . . .	86
7.2.2	Calibration of the mass balance model . . . . .	90
7.2.3	Dynamic runs . . . . .	90
7.2.4	From "1.5D" to 2D geometries . . . . .	92
7.2.5	Distributed ice thickness . . . . .	93
7.2.6	Glacier volumes . . . . .	95
7.3	Coupling the models: final WaSiM run with optimization . . . . .	95
7.3.1	Multi-data optimization . . . . .	95
7.3.2	Uncertainties . . . . .	98
7.4	Comparison: WaSiM VA scaling vs. WaSiM-OGGM coupling scheme . . . . .	101

7.4.1	Historical period . . . . .	101
7.4.2	Future projections . . . . .	103
7.5	Application of the coupling scheme in another catchment . . . . .	111
7.5.1	First WaSiM run with resampling of climate data . . . . .	111
7.5.2	OGGM run and processing of glacier outputs . . . . .	112
7.5.3	Coupling the models: final WaSiM run with optimization . . . . .	112
7.5.4	Results of the coupling scheme in Rofenache . . . . .	113
<b>8</b>	<b>Conclusions and outlook</b>	<b>117</b>
8.1	Conclusions . . . . .	117
8.2	Limitations and Outlook . . . . .	120
	<b>GitHub Repository and code availability</b>	<b>125</b>
	<b>Bibliography</b>	<b>127</b>
	<b>Appendix</b>	<b>145</b>
<b>A</b>	<b>Observed data</b>	<b>145</b>
A.1	Glaciers . . . . .	145
A.2	Climate . . . . .	146
<b>B</b>	<b>Performance measures</b>	<b>148</b>
<b>C</b>	<b>Model runs</b>	<b>151</b>
C.1	Additional results: first WaSiM run with resampling of climate data . . . . .	151
C.2	Additional results: OGGM run and processing of glacier outputs . . . . .	154
C.3	Additional results: coupling scheme . . . . .	157
C.4	Additional results: comparison WaSiM VA scaling vs. WaSiM-OGGM coupling scheme . . . . .	158
C.5	Additional results: application of the coupling scheme in another catchment	161
<b>D</b>	<b>GitHub repository</b>	<b>163</b>

# List of Figures

1.1	Example of runoff evolution and peak water . . . . .	2
1.2	Research questions . . . . .	5
2.1	Hydrological cycle . . . . .	7
2.2	Snow metamorphosis . . . . .	10
2.3	Glacier as a system . . . . .	10
2.4	Glacier mass balance and evolution models . . . . .	17
2.5	Stresses acting on a glacier . . . . .	19
2.6	Online and offline coupled models . . . . .	22
2.7	Examples of uncertainty sources . . . . .	26
3.1	Study area . . . . .	27
3.2	Land cover and soil classification . . . . .	29
3.3	Glacier outlines . . . . .	30
3.4	Elevation dependency of meteorological variables . . . . .	32
4.1	WaSiM model structure . . . . .	36
4.2	WaSiM simulation period . . . . .	37
4.3	Bilinear interpolation of meteorological variables . . . . .	39
5.1	Input grids for VA scaling glacier approach in WaSiM . . . . .	45
5.2	OGGM workflow . . . . .	49
5.3	Main flowline along one glacier . . . . .	50
5.4	Flowlines along Gepatschferner . . . . .	51
5.5	Discrete volume of ice along a flowline . . . . .	52
6.1	General workflow of the coupling scheme . . . . .	54
6.2	Coupling scheme: first step . . . . .	56
6.3	Coupling scheme: second step . . . . .	60
6.4	Initialization methods in OGGM . . . . .	64
6.5	From "1.5D" to 2D geometries . . . . .	66
6.6	Distributed ice thickness . . . . .	69
6.7	Interpolation of ice thickness from flowlines . . . . .	69
6.8	Glacier volumes . . . . .	70
6.9	Coupling scheme: third step . . . . .	71
6.10	WaSiM-OGGM coupling scheme simulation period . . . . .	72
6.11	Detailed workflow of the coupling scheme with multi-data optimization. . . . .	74
6.12	Example of the SCE-UA method . . . . .	77
7.1	Sensitivity analysis results from WaSiM . . . . .	80
7.2	Observed and simulated runoff during the calibration period - WaSiM . . . . .	81
7.3	Observed and simulated glacier areas - WaSiM . . . . .	82

7.4	Observed and simulated SWE - WaSiM . . . . .	83
7.5	Monthly temperature and precipitation grids from WaSiM . . . . .	84
7.6	Mass balance from the VA scaling approach in WaSiM . . . . .	86
7.7	OGGM sensitivity analysis - Test A . . . . .	87
7.8	OGGM sensitivity analysis - Test B . . . . .	87
7.9	OGGM sensitivity analysis - Test C . . . . .	88
7.10	OGGM sensitivity analysis - Test E . . . . .	88
7.11	OGGM sensitivity analysis - Test F . . . . .	89
7.12	OGGM sensitivity analysis - errors . . . . .	89
7.13	Observed and simulated mass balance at the tongue of Gepatschferner . .	91
7.14	Simulation results from OGGM's dynamic run . . . . .	91
7.15	Observed and simulated 2D glacier areas from OGGM . . . . .	93
7.16	Distributed ice thickness from OGGM . . . . .	94
7.17	Simulated (and observed) mean ice thickness for three glaciers . . . . .	94
7.18	Convergence of the multi-objective function during optimization . . . . .	96
7.19	Observed and simulated runoff - optimized coupling scheme . . . . .	98
7.20	Uncertainties in model initialization . . . . .	99
7.21	Uncertainties in model parameters . . . . .	100
7.22	Comparison of simulated runoff for the historical period . . . . .	102
7.23	Comparison of simulated runoff for the future period . . . . .	104
7.24	Historical and future glacier evolution . . . . .	106
7.25	Influence of "b" parameter in simulation results . . . . .	108
7.26	Future evolution of climate variables and annual runoff . . . . .	110
7.27	Study area: Rofenache catchment . . . . .	112
7.28	Observed and simulated runoff - coupling scheme (Rofenache) . . . . .	113
7.29	Observed and simulated 2D glacier areas - coupling scheme (Rofenache) .	114
7.30	Flowlines of Vernagtferner . . . . .	114
7.31	Glacier mass balances of three reference glaciers (Rofenache) . . . . .	116
8.1	GitHub repository . . . . .	125
A.1	Mass balance measurements at the tongue of Gepatschferner . . . . .	145
A.2	GPR locations for ice thickness measurements . . . . .	146
A.3	Example of the kNN method . . . . .	146
A.4	Mean daily values of meteorological variables . . . . .	147
B.1	Example of POD and FAR determination . . . . .	149
C.1	Observed and simulated runoff at Gepatschalm - WaSiM . . . . .	153
C.2	Observed and simulated runoff during the validation periods - WaSiM . . .	153
C.3	Observed and simulated snow coverage (28.12.2016) . . . . .	154
C.4	Observed and simulated snow coverage (19.04.2018) . . . . .	154
C.5	Sensitivity analysis results for other glaciers - OGGM . . . . .	155
C.6	Calibrated values precipitation factor - OGGM . . . . .	156
C.7	Observed and simulated runoff at Gepatschalm - coupling scheme . . . . .	157
C.8	Observed and simulated runoff for other model configurations - coupling scheme . . . . .	157
C.9	Observed and simulated 2D glacier areas for other model configurations - coupling scheme . . . . .	158

C.10	Cumulative mass balance for other model configurations - coupling scheme	158
C.11	Observed and simulated mass balance at the tongue of Gepatschferner - comparison . . . . .	159
C.12	Errors - mass balance at the tongue of Gepatschferner . . . . .	159
C.13	Projected glacier coverage: VA scaling vs. Coupling scheme . . . . .	160
C.14	Future evolution of annual runoff under different climate models - OGGM .	161
C.15	Simulation results from OGGM's dynamic run (Rofenache) . . . . .	161
C.16	Calibrated values precipitation factor - OGGM (Rofenache) . . . . .	162
C.17	Simulated (and observed) mean ice thickness for three glaciers (Rofenache)	162
D.1	Example of flow of files and scripts - GitHub repository . . . . .	166



## List of Tables

3.1	GCMs and RCMs considered for the prediction of the catchment's response in the future. . . . .	34
4.1	Summary of the main processes included in WaSiM. . . . .	35
6.1	Criteria for evaluating the calibration performance . . . . .	59
6.2	Glacier parameters involved in the mass balance model . . . . .	61
6.3	Sensitivity test runs in OGGM . . . . .	63
7.1	Parameters adjusted during optimization of the coupling scheme . . . . .	96
7.2	Performance measures of the coupling scheme . . . . .	97
7.3	Water balance in the historical period . . . . .	103
B.1	Criteria for evaluating model performance during calibration and validation of the models . . . . .	150
C.1	Selected parameters for the sensitivity test - WaSiM . . . . .	152
C.2	Parameters adjusted during calibration of the model - WaSiM . . . . .	153
C.3	Simulated ice thickness values - OGGM . . . . .	156
C.4	Parameters adjusted during optimization - coupling scheme (Rofenache) . . . . .	162

# Abbreviations

- AGI** Austrian Glacier Inventory
- ASCII** American Standard Code for Information Interchange
- AWS** Automatic weather station
- BE** Benchmark efficiency
- CRS** Coordinate reference system
- DEM** Digital Elevation Model
- ELA** Equilibrium line altitude
- EPSG** European Petroleum Survey Group Geodesy
- FAR** False alarm rate
- FAST** Fourier amplitude sensitivity test
- GCM** Global climate model
- GPR** Ground-penetrating radar
- IDW** Inverse distance weight
- INCA** Integrated Newcasting Analysis Data
- KGE** Kling-Gupta efficiency
- kNN** k-Nearest Neighbor
- LAI** Leaf area index
- LIA** Little Ice Age
- m a.s.l.** meters above sea level
- MB** Mass balance
- MBE** Mean bias error
- NSE** Nash-Sutcliffe efficiency
- OGGM** Open Global Glacier Model
- PBIAS** Percentage bias

**POD** Probability of detection

**RCM** Regional climate model

**RCP** Representative concentration pathway

**RGI** Randolph Glacier Inventory

**RMSE** Root mean square error

**RSR** Root mean square error standard deviation ratio

**SCE-UA** Shuffled Complex Evolution Algorithm (University of Arizona)

**SIA** Shallow ice approximation

**SMB** Specific mass balance

**SPOTPY** Statistical Parameter Optimization Tool for Python

**SWE** Snow water equivalent

**UPH** Unsolved problems in hydrology

**VA** Volume-Area

**WaSiM** Water flow and balance simulation model

**WGS** World Geodetic System

**WGMS** World Glacier Monitory Service



# Chapter 1

## Introduction

### 1.1 Background and motivation

Water resources are of vital importance to ensure that basic human needs are fulfilled. Domestic and industrial use, hydropower generation and irrigation are typical examples of activities that rely on water, including as well the sustainability of ecosystems. In this context, mountainous regions play a fundamental role. They are not only responsible for ensuring water availability in high altitudes, but also in the contiguous lowlands, which represent almost 39% of the global land mass (Viviroli et al., 2020). Mountains have been considered to be the *water towers* of the world, since they are able to store water and redistribute it in terms of runoff to the lowlands (Viviroli et al., 2007). Moreover, mountainous areas are characterized by high precipitation amounts and low temperature values. In most cases, these conditions favor the presence of glaciers, which are huge reservoirs of fresh water being stored in form of snow, firn and ice. Even though the changes in glacier volumes might only be visible after years or centuries (*long-term storage*), the seasonal changes in their storage (water stored in winter due to precipitation and released in summer by melting) have major implications for the hydrology at a shorter time scale (*intermediate-term storage*) (Jansson et al., 2003).

Among other meteorological variables, temperature and precipitation are the main atmospheric drivers of changes in high mountainous regions, primarily affecting the cryosphere components (like snow and glaciers, Pepin et al., 2022). Temperature increases detected during the last decades can be predominantly attributed to anthropogenic factors, being greenhouse gas emissions the major cause (e.g. Bonfils et al., 2008). In addition, future projections based on General Circulation Models (GCMs) and Regional Climate Models (RCMs) reveal that temperature will continue to increase, which might also lead to the decrease on solid precipitation in mountainous regions (Hock et al., 2019). The projected climatic and socio-economic changes (e.g. increasing temperatures, growth in population) are expected to have a profound impact on the *water towers* of the world, making them in some regions extremely vulnerable (Immerzeel et al., 2020). This issue could be greatly intensified by the accelerating glacier mass loss, which is even expected to lead to completely ice-free areas by the end of the century in some parts of the world (e.g. in Europe, Zekollari et al., 2019). Yet, this matter is not surprising. In particular in Europe, it began to be on the spotlight mostly after the heatwave of 2003, which was considered to be a year with extreme negative glacier mass balance for the European Alps. Unfortunately, that year was not unique (e.g. other extremes were observed during the years 2018 and 2022) and the prognoses for the future are not encouraging either (Voordendag, 19.9.2023). In other

regions, like the Himalaya–Hindu Kush region in Asia (that is home to approx. 50% of the world's population), glacier runoff practically ensures a dry-season water supply (Barnett et al., 2005). Thus, accelerating glacier mass loss and its potential water shortage may lead to serious consequences for the residents of this region. In addition, the steep slopes in mountainous areas, in combination with high runoff values, can favor erosion processes and the consequent transport of soil sediments (Schmidt et al., 2022). If reservoirs are located downstream, expected sedimentation loads might have a negative impact on their operation, such as on hydropower generation.

In order to assess the long-term water availability in glacierized regions, it is essential to understand the role of glacier melt in runoff generation (Clason et al., 2022). The retreat of glaciers results in an increased glacier runoff, which at some point will reach a maximum, known as *peak water* (Figure 1.1, Huss and Hock, 2018). After this point is met, glacier runoff will ultimately decrease due to the reduction on the glacier volume and water shortage can be awaited.

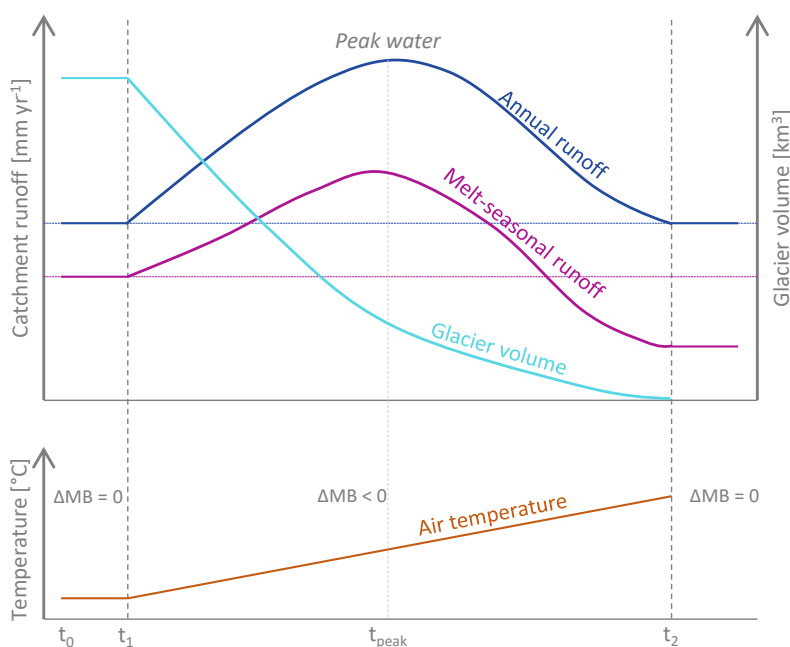


Figure 1.1: Example of annual and melt-season runoff evolution in glacierized catchments, in response to increasing temperatures. The peak water refers to the maximum glacier runoff. At the beginning ( $t_0$ ), the glacier is in equilibrium and therefore no runoff associated to glacier volume reduction is generated. Once the temperature begins to increase ( $t_1$ ), the glacier retreats while runoff reaches its maximum and then starts to decrease again. At the end ( $t_2$ ), when the glacier is again in equilibrium or completely melted, the annual runoff equals the value at the beginning, since other water balance components (e.g. rainfall) compensate the lack of glacier melt in the runoff generation (adapted from Huss and Hock, 2018).

For a correct and sustainable management of the water resources, the prediction of glacier evolution and the impact on runoff becomes indispensable (Bolch et al., 2022). Glacio-hydrological models are valuable tools, since they can combine the modeling of both, catchment hydrology and glaciers, thus providing a more detailed representation of all involved processes (van Tiel et al., 2020). However, the inclusion of glacier evolution is still a challenging issue. First, the limited available measurements (i.e. long-term glacier mass balance, Naz et al., 2014) together with unknown initial conditions of glaciers (e.g. areas and volumes), yield to higher uncertainties that could be translated into misinterpretations of water availability. Second, due to the complexity of the involved processes, many models

still rely on empirical and simplified approaches to determine glacier evolution. One widely used example is the Volume-Area (VA) scaling approach (e.g. Bahr et al., 1997). The method allows to determine glacier volume by simply scaling the observed area. Yet, the main drawback of the method is the applicability in local and regional studies, since a representative mean ice thickness (*scaling parameter*) is usually chosen for all considered glaciers, which may not accurately reflect the true thickness distribution or variability within the study area. More recently, the Randolph Glacier Inventory (RGI Consortium, 2017) together with glacier mass change observations (Hugonnet et al., 2021; Zemp et al., 2019) around the globe, have been proving to be a valuable resource for moving a step forward in (global) glacier modeling. The finer level of detail provided by such datasets facilitates the integration of more complex approaches when predicting the evolution of glaciers, hence allowing more reliable estimates of water availability. By using these approaches and under some assumptions, the modeling of glacier evolution acquires a more physically-based representation, since the determination of the glacier volume is based on the actual flux of ice along a flowline (ice-flow dynamics), and not only, for example, on an empirical relation (Zekollari et al., 2022).

Consequently, the integration of ice-flow dynamics into hydrological models might help to improve the prediction of runoff in glacierized catchments, in view to the more accurate representation of glacier processes. On the one hand, the description of glacier processes adopts an individual perspective, as the flux of ice along the flowlines is unique to each glacier. In this way, model parameters can be adjusted at a glacier basis, hence the rough approximation of representative (*global*) parameters for all glaciers (e.g. the *scaling parameter* involved in the empirical VA scaling approach) might be handled. On the other hand, the actual physical drivers of glacier processes are contemplated, which include internal deformation of ice and basal sliding (e.g. Cuffey and Paterson, 2010). So far, different attempts have been made to couple standalone glacier models to hydrological models, but a few limitations can be recognized. First, a distinction between *online* (also known as *fully coupling*) and *offline* coupling must be drawn. While an *online* coupling ensures that the feedback between the two independent models is given at every time step, an *offline* coupling can be just considered as the transfer of data from one model to the other. Examples of *online* coupled models are very narrow and can only be applicable if both models share the same input data and spatio-temporal resolution (e.g. Naz et al., 2014). On the contrary, examples of *offline* coupled models are more common. In these cases, the problematic of working with completely different spatio-temporal scales may be tackled, since the continuous feedback between models is not further required. Typically, glacier areas are obtained from the glacier model and then used as input data for running the following hydrological model (e.g. Stoll et al., 2020). Likewise, in other cases, glacier runoff is the selected variable to be transferred between models (e.g. Wiersma et al., 2022). Nevertheless, other essential attributes are often omitted, like glacier volume or mass balance, which might help to constrain model uncertainties (for instance, by the reduction of model parameters that need to be calibrated). Besides, in various (*offline*) cases, the individual models do not share the same driven climate dataset, which may result on a coupled approach subjected to inconsistencies (e.g. Khadka et al., 2020).

In light of the possible concerns that runoff from glacierized catchments may imply to future water availability, the DIRT-X Project (<https://dirtx-reservoirs4future.eu/>) aimed to predict the hydro- and morphological response of distinct catchments. With focus on the glacio-hydrological processes in two European catchments (Gepatsch reservoir in Austria



and Banja reservoir in Albania, the latter without glaciers), this thesis was developed at the Leibniz Universität Hannover, as part of the Project. More specifically, an *offline* coupling scheme is developed, in which glacier evolution (studied at a glacier basis following the actual flow of ice) is integrated into a hydrological model. This coupling scheme aims to go beyond existing *offline* approaches, due to a consistent exchange of state variables and fluxes between both models. To achieve this, annual estimates of glacier areas, thickness distributions, volumes and mass balances are produced by the **Open Global Glacier Model (OGGM)**, Maussion et al., 2019) and integrated into the **Water Flow and Balance Simulation Model (WaSiM)**, Schulla, 1997), being both models driven by the same input climate dataset. The main objectives of this thesis are therefore enumerated in the next section.

## 1.2 Objectives

While keeping the primary focus on the prediction of runoff in glacierized catchments, the main objectives of this thesis are:

1. To benefit from a freely available, fully-distributed, physically-based water balance model with an integrated VA scaling approach to account for glacier evolution.
2. To benefit from an open-source, state-of-the-art, global glacier modeling framework, capable to simulate ice-flow dynamics for (almost) every glacier in the world.
3. To profit from the publicly available emerging global datasets that are used in the glacier model, thus reducing the manual adjustment of the model's configuration and leave model parameters with their default values whenever possible.
4. To integrate the main capabilities of each individual model into a consistent coupling scheme, in which also their strengths are complemented.
5. To supplant the rather simple, empirical VA scaling approach by a process-based, more sophisticated flowline model to study glacier evolution.
6. To bridge the gap between global glacier modeling (including global available datasets) and catchment hydrology.
7. To support hydrological modeling with more detailed glacier representations, yet without increasing the required expertise on glacier modeling.
8. To develop a modeling tool that may facilitate the task of predicting runoff in glacierized catchments, whilst ensuring sufficient reliability and robustness of the model.

## 1.3 Research questions

It is well known among the hydrological sciences that, although many advances have been made in recent times to overcome the problems related to water availability, there are still issues that require further research. Within the framework of the **23 unsolved problems**

in hydrology (UPH, Blöschl et al., 2019), one of them addresses the effects of changing climate on the response of glacierized catchments. More specifically, problem number 2 points out: "How will cold region runoff and groundwater change in a warmer climate (e.g. with glacier melt and permafrost thaw)?" Additionally, with interest in modeling methods, problem number 19 reveals: "How can hydrological models be adapted to be able to extrapolate to changing conditions, including changing vegetation dynamics?". While bearing in mind these two unsolved problems in hydrology and the above-mentioned objectives, this thesis aims to partially but consistently contribute to the solution of the problems. Therefore, the key research questions that are being addressed in this thesis are:

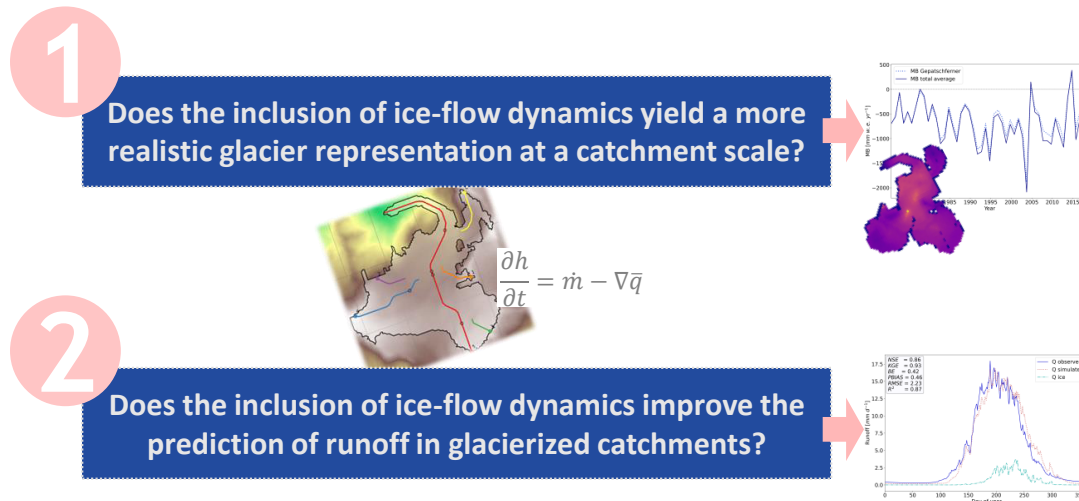


Figure 1.2: Key research questions that are being addressed in this thesis.

While the first question focuses primarily on the accurate representation of glacier processes, the second one comprises the complete hydrological response of the catchment, under given climatic conditions. To address the first question, model results in terms of glacier areas, ice thickness distributions, volumes and mass balances are evaluated, whereas total runoff and the contribution from glacier melt is assessed when dealing with the second question. Furthermore, the evaluation is not just limited to historical simulations, but also predictions under different climatic conditions in the future are contemplated. This enables to gain deeper insight on the changing conditions of glacierized catchments and also assist in the feasible solutions for two of the 23 unsolved problems in hydrology.

## 1.4 Structure of the thesis

The thesis is structured in eight chapters:

**Chapter 1: Introduction** describes the background and motivation of this thesis. Moreover, the main objectives and key research questions are presented.

**Chapter 2: State of the art** gives an insight into the water balance in mountainous regions, focusing mainly on glacier processes (including different measurements). Moreover, it provides an overview of the theoretical background and current developments on water balance and glacier modeling, as well as on coupled glacio-hydrological

models. In addition, insights into optimization strategies and uncertainty sources are also presented.

**Chapter 3: Study area and data** describes the study area in which the thesis is focused, together with a description of all the input data used in the study.

**Chapter 4: Water balance modeling** provides a detailed description of the water balance model WaSiM used for the simulations, with all the corresponding processes involved.

**Chapter 5: Glacier modeling** presents the glacier model integrated in the water balance model (VA scaling) and the separate and independent global glacier model OGGM.

**Chapter 6: WaSiM-OGGM coupling scheme** explains all the steps required to develop the coupling scheme, in which the glacier evolution determined with the ice-flow dynamics (OGGM) is integrated into the hydrological simulations (WaSiM), highlighting the novelty of introducing a glacier-based representation of ice thickness distribution. This chapter includes a detailed description of the processing of inputs and outputs, the optimization of the models and the analysis of possible uncertainties.

**Chapter 7: Results and discussion** depicts all the intermediate results from the separate runs with WaSiM and OGGM and the final results obtained from the coupling scheme, including the evaluation of different sources of uncertainties. Moreover, a comparison between the results from the WaSiM run with integrated VA scaling glacier approach and the coupling scheme itself is performed. Part of these results can be found in *Pesci, M.H., Schulte Overberg, P., Bosshard, T. and Förster, K. (2023): "From global glacier modeling to catchment hydrology: bridging the gap with the WaSiM-OGGM coupling scheme", *Frontiers in Water* 5, Article 1296344, [doi.org/10.3389/frwa.2023.1296344](https://doi.org/10.3389/frwa.2023.1296344). (This article is part of the special topic "Water and Hazards in Mountainous Regions in a Changing Climate")*. Finally, the applicability of the developed coupling scheme in another catchment is also presented.

**Chapter 8: Conclusions and outlook** summarizes the main findings of the thesis, focusing specially on the key research questions. Besides, an outlook for further research is given.

# Chapter 2

## State of the art

### 2.1 Water balance in mountainous regions

The hydrological cycle and its components are depicted in Figure 2.1. The first driver of the cycle is the evapotranspiration of water from the oceans and land, which is lifted to the atmosphere in form of vapor and finally turned into precipitation. Then, precipitation can fall as rain or snow, the latest contributing to the increase of snow and ice areas. Precipitation can either (i) be intercepted by vegetation, (ii) infiltrate into the soil or (iii) flow over the land surface (Maidment, 1993; Mohajerani et al., 2021):

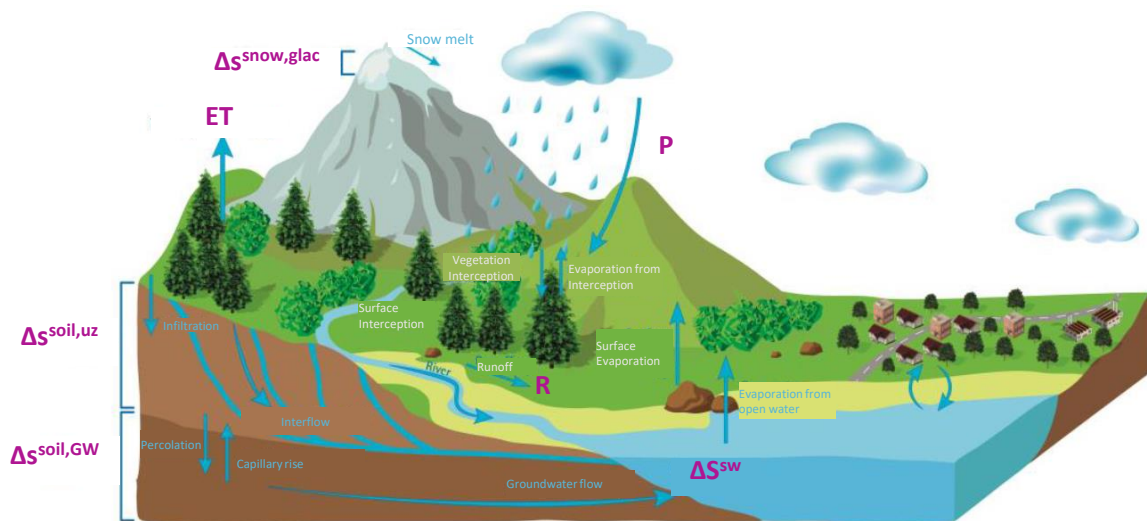


Figure 2.1: Hydrological cycle in a mountainous region (adapted from European Commission, 2015).

- (i) **Interception:** Precipitation that is intercepted by vegetation can then return to the atmosphere as evaporation.
- (ii) **Infiltration:** While part of the precipitation only reaches the upper layer of the soil and evaporates from its surface or transpires through vegetation, the rest can move into deeper layers of soil, reaching finally the groundwater storage.
- (iii) **Runoff:** The remaining part of the precipitation becomes surface runoff, which travels over the land surface reaching at the end the water bodies, including the oceans, where the hydrological cycle starts again.

All these hydrological processes lead to water flows, which enter (inflows) and leave (outflows) the catchment (control volume). The difference between inflows and outflows is described by the water balance, which is based on the conservation of mass. The water balance of a catchment can be expressed by terms of Equation 2.1 (e.g. Weingartner et al., 2007):

$$P = ET + R + \Delta S \quad (2.1)$$

The first term of the water balance equation refers to the precipitation ( $P$ ), which represents the amount of water that enters the catchment. Usually, this term can be directly determined by measurements, thanks to meteorological stations located within or around the catchment. However, in high mountainous regions, the network of meteorological stations decrease with altitude, which makes the computation of  $P$  less accurate. In addition, solid precipitation is affected by errors due to wetting and evaporation losses and wind-induced undercatch, hence a correction of its measured value is required in such regions (Goodison et al., 1998; Hanzer et al., 2016; Weingartner et al., 2007).

The second water balance component is the evapotranspiration ( $ET$ ), which represents the amount of water that goes back to the atmosphere in form of water vapor (either by evaporation or transpiration). In glacierized catchments, located in mountainous regions, this component is typically very small (e.g. Kormann et al., 2016) and although it can be measured, it is commonly assumed constant. The values depend on the type of surface, since vegetated areas are more prone to increase  $ET$ , compared to, for example, glacierized surfaces (Psenner, 2007; Hanzer et al., 2016). However, snow sublimation could significantly influence the water balance in alpine regions, especially where wind reaches higher velocities (like in mountain ridges, Strasser et al., 2008). Since this process affects the storage of snow in a glacier, it can be considered in the  $\Delta S^{Snow,Glaciers}$  component of the water balance, as shown afterward in this Section.

Following up, runoff ( $R$ ) is the next water balance component, which encompasses the remaining amount of water that exits the catchment. If gauging stations are available, then this component can be directly measured at the outlet of the catchment. However, in some cases, measurements are not at hand and methods for predicting runoff are employed. For example, by using neighboring gauges or statistical methods, both requiring runoff information on neighboring catchments (Savenije et al., 2013).

The remainder of the water balance equation represents the changes in water storage ( $\Delta S$ ), which can be written as (Equation 2.2, Healy and Scanlon, 2018):

$$\Delta S = \Delta S^{Soil} + \Delta S^{SW} + \Delta S^{Snow,Glaciers} \quad (2.2)$$

The soil storage,  $\Delta S^{Soil}$ , can be divided into two parts, depending on the depth of the soil layer: (a) unsaturated zone, for the shallow parts of the soil and (b) groundwater zone (or saturated zone), for the deeper layers of the soil. In mountainous catchments, where the predominant hydrogeology type is non-aquiferous rocks with low permeability, the main contributor comes from the unsaturated zone. However, there are some exceptions. First of all, there has been remarkable advances towards a better understanding of groundwater processes in such regions, thus more measurements and modeling have been carried out related to the groundwater processes. Second, there are cases in which the underlying rock presents some fractures or formations (e.g. evaporitic layers, which are rocks that resulted from evaporation of water, Encyclopedia Britannica, 20/10/2023) that show an increased permeability, hence allowing the groundwater flow. Moreover, if a karst aquifer is present in

the area, water is able to flow through the tunnels that were created through the limestone dissolution (Cochand et al., 2019; Somers and McKenzie, 2020). As an example, Cochand et al., 2019 and Perico et al., 2022 showed that the groundwater storage can reach values up to 38% and 15% of the total precipitation during a snowmelt period, in alpine catchments in Switzerland and Italy, respectively. In addition, higher storage values can be observed for an Himalayan catchment (66%), where a fractured aquifer lies below the area (Andermann et al., 2012). Consequently, the groundwater storage in mountainous catchments is quite diverse and depends mainly on the hydrogeology of the region.

When looking at the change in storage of surface water bodies,  $\Delta S^{SW}$ , this could be significant, for example, if a lake (i.e. reservoir) is located in the catchment. Here,  $ET$  can reach higher values and more interactions between the water body and the soil layers can be expected. The inclusion of these two types of storage (soil and water bodies) in the water balance of a catchment, depend on several aspects, being even feasible to neglect those terms if the conditions are met.

Finally, solid precipitation can also be stored as snow and ice during cold periods and released during warm months, thus the change in water storage of snow and glaciers,  $\Delta S^{Snow,Glaciers}$ , becomes a fundamental component, especially when looking at long-term water balances. As an example, Killingtveit et al., 2003 found that for a catchment in Svalbard (Arctic Ocean, Norway), the average annual  $\Delta S$  of glaciers and snow was almost 40% of the mean precipitation for the period 1990-2001. Similarly, Singh and Jain, 2002 determined that this storage component represented almost 88% of the total average  $P$  of a catchment in the Tibetan Plateau, during a period of ten years. When looking at the Vernagt catchment in the European Alps (Austria), values close to 20% of the total precipitation were estimated for the period 1974-2005 (Psenner, 2007).

Since the focus of this thesis is given to the changes in glacierized areas and their influence on the water balance of a catchment, a detailed description of glacier processes is given in the following sections. First, an introduction of the glaciers as a system is provided in Section 2.2. The mass balance is introduced in Section 2.2.2 and a revision of the current measurement techniques is presented in Section 2.2.3.

## 2.2 Glaciers

### 2.2.1 Introduction to glaciers

Glaciers, huge reservoirs of fresh water that are part of the cryosphere, are in constant exchange of mass and energy with other components of the earth system, like the atmosphere or the hydrosphere. Glaciers are formed due to precipitation that falls as snow in high altitudes and which accumulates through long periods of time. Moreover, snow can also accumulate due to avalanches or being blown by wind. The snow that does not melt after one season, becomes firn. After some years, the deeper older layers of snow are transformed into ice, due to the reduction of the air-filled pores and the increase in density, result of the compaction generated by the fresher layers of snow (Benn and Evans, 2010). More specifically, the transformation of snow crystals into ice occurs due to the pressure, regelation (i.e. ice melting under pressure and refreezing when the pressure is reduced), molecular diffusion and convection in the pore space within the snowpack, usually known as *metamorphosis*

(Baumgartner and Liebscher, 1996). Figure 2.2 depicts the evolution (in days after snowfall) of the snow crystals until they become ice, due to isothermal metamorphosis. This process takes place due to a formation of a vapor pressure gradient between the higher vapor pressure over convex structures and the lower over concave surfaces (Baumgartner and Liebscher, 1996; Förster, 2013). All in all, this part of the glacier, in which it usually gains mass, is called the *accumulation area*.

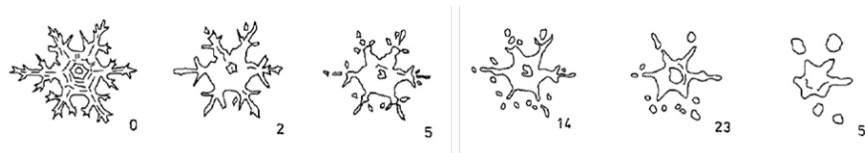


Figure 2.2: Evolution of snow crystals until they become ice, through (degradative) isothermal metamorphosis. The numbers indicate the age of snow (in days) after snowfall (Baumgartner and Liebscher, 1996)

On the contrary, other processes driven by gravitational forces and solar radiation contribute to the loss of glacier mass. Examples of these processes are evaporation, sublimation, avalanching, calving and melting, being the latter the principal contributor. These take place mainly in the lower altitudes and in the so-called *ablation area* (Benn and Evans, 2010; Hooke, 2020). Figure 2.3 schematizes the glacier as a system, with the main inputs that contribute to the formation of the accumulation area and the main outputs that intervene in the ablation area (calving only takes place in water-terminating glaciers). Furthermore, the equilibrium line altitude (ELA), which divides the accumulation from the ablation areas, is also indicated in the figure. Along the ELA, the mass balance (MB) of the glacier is zero, meaning that accumulation is equal to ablation (Section 2.2.2).

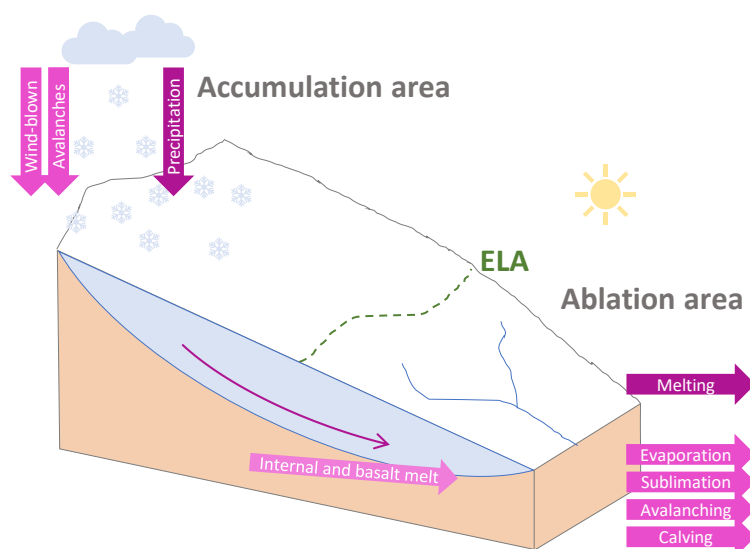


Figure 2.3: Glacier as a system: accumulation and ablation areas, inputs, outputs and equilibrium line altitude (ELA) (adapted from Hooke, 2020).

In the matter of changing climatic conditions, where temperatures have been already facing increments and are projected to sequentially rise in the future, mountain glaciers are experiencing a reduction of their size due to elevated melting rates. Apart from natural variability, anthropogenic causes also affect the glacier response, being the latter one more tangible since the 1990s (Intergovernmental Panel on Climate Change, 2023; Marzeion et al., 2014). Among the anthropogenic causes, greenhouse emissions are the principal contributors (Lee et al., 2023). Regardless the cause, two immediate consequences arise



from glacier shrinkage, depending on the considered scale: (i) global sea-level rise and (ii) changes in regional and local hydrology (e.g. Radić and Hock, 2014; Fischer et al., 2015a):

- (i) **Glaciers and global sea-level rise:** Many studies have been carried out focusing on the global scale of glaciers and their role in sea-level rise. Despite the small influence of mountain glaciers and ice caps in the Earth's ice volume (0.43 m of sea level equivalent, Huss and Farinotti, 2012), they are key contributors to sea-level rise (Braithwaite and Raper, 2002; Gardner et al., 2013; Oerlemans et al., 2007; Marzeion et al., 2012; Radić and Hock, 2011; Radić and Hock, 2014; Zemp et al., 2019). For example, Zemp et al., 2019, estimated a global sea-level rise (from glaciers) of 27 mm during the period 1969-2016, whereas Kaser et al., 2006 calculated values of 11 and 27 mm for the periods 1961-1990 and 2001-2004, respectively. When looking at the future, projected values suggest a possible sea-level rise between 60 to 150 mm by the end of the century (e.g. Church et al., 2001).
- (ii) **Glaciers and changes in regional/local hydrology:** The retreat (i.e. melting) of glaciers heavily influences the runoff regime of the catchment, which is characterized by low-flows during winter and high-flows during summer. Water supply, hydropower generation and sustainability of aquatic ecosystems are strongly dependent on the water availability, thus on the accessible water volume of glaciers (Hanzer et al., 2018; Huss and Hock, 2018; Radić and Hock, 2011). Yet, the water availability is not the same everywhere and depends, for example, on the climate regime that governs the region (Kaser et al., 2010). Concerning future climate, several studies conclude that the warming conditions will continue to accelerate the volume loss of glaciers, thus strongly affecting water availability. Consequences for the European Alps could be severe, as more than 80% of the initial ice volume is expected to be melted (from the 2000s) under strong warming (e.g. Compagno et al., 2021; Zekollari et al., 2019).

## 2.2.2 Glacier mass balance

Glacier mass balance represents an immediate and unfiltered reaction to atmospheric conditions, making it one of the crucial variables necessary for monitoring the climate system (Zemp et al., 2009). The mass balance of a glacier refers to the rate of mass change over a defined period of time and is done between the accumulation and ablation areas, usually over one year (Figure 2.3). In general terms, it can be expressed by means of Equation 2.3 (e.g. Hooke, 2020), in which the dot indicates a mass change per time:

$$\dot{m} = \text{accumulation} + \text{ablation} \quad (2.3)$$

Where the ablation component is expressed as a negative number (Cogley et al., 2011). Commonly, the term specific mass balance (SMB) is used, referring to the change of mass per unit area. This term allows a fair comparison between glaciers of different sizes. The units of the specific mass balance are given in  $\text{kg m}^{-2}$  or millimeters of water equivalent (mm w.e.), being the latter possible because 1 kg of liquid water (with density of  $1000 \text{ kg m}^{-3}$ ) distributed over an area of  $1 \text{ m}^2$ , has a depth of 1 mm. The mass balance year is considered from the beginning of the accumulation season until the melting season, which for the Northern Hemisphere spans from 1<sup>st</sup> October to 30<sup>th</sup> September.

It is worth to highlight that although the mass balance of a glacier is a rate (change of mass per time), it is common in the glacier community to just refer to mass balance. For this reason, whenever the term *mass balance* is mentioned in the following parts of this thesis, it refers to the rate described by Equation 2.3, and to the specific mass balance (expressed in mm w.e. or m w.e.).

### 2.2.3 Glacier measurements

Even though glaciers have been a subject of study for many centuries, measurements on their state date from the 19<sup>th</sup> century. During the so called *Little Ice Age* (LIA), which extended between the early 14<sup>th</sup> and the mid-19<sup>th</sup> centuries, cold conditions favored the expansion of mountain glaciers in the northern hemisphere, including the European Alps (Stephen and Rafferty, 2023). After the cold peak was achieved around the year 1850, Alpine glaciers have been retreating considerably, which for the European Alps meant reaching a 50% area reduction over the past 150 years (Zemp et al., 2008). A clear outcome of glacier retreat can be attributed to visible moraines, which refer to a ridge or mound formed at the margin of the glacier and contain glacial till (deposited material), indicating that that part was formerly glacierized (AntarcticGlaciers.org, 22/06/2020). Since that cold peak in 1850, regular measurements on glacier extents and mass balance components simultaneously began to become relevant (Fischer et al., 2015a).

In terms of glacier mass balance, its components can be determined by three common methods: the glaciological method, the hydrological method and glacier mass changes based on measurements from space. These methods are summarized in Sections 2.2.3.1 to 2.2.3.3. In addition, changes in the glacier's geometry can be evaluated in terms of aerial photographs (introduced in Section 2.2.3.4) and ice thicknesses can be measured at certain points along the glaciers (Section 2.2.3.5).

#### 2.2.3.1 Glaciological method for mass balance measurements

This is one of the most frequently used methods and consists on the direct measurement of accumulation and ablation components, done by snow pits and ablation stakes (Benn and Evans, 2010; Fischer, 2010). The measurements are carried out at an annual scale, coincident with the end of the mass balance year. Since it only provides information of a glacier at certain points, an extrapolation to the entire glacier's area has to be done. This extrapolation requires assumptions about how the mass balance is distributed, being the main source of uncertainty of this method.

#### 2.2.3.2 Hydrological method for mass balance measurements

This method is based on the water balance of the catchment. By knowing the values of  $P$ ,  $ET$  and  $R$  (Equation 2.1), the change of storage in snow and glacier can be directly calculated. However, a few inaccuracies in the method are expected. First of all, the water balance components are not always effectively measured and their values need to be estimated. For example, the main challenge presented by  $P$  is the extrapolation of point measurements to the entire catchment, especially due to its high variability in mountainous regions (e.g. Hagg et al., 2004). Similarly, direct measurements of  $ET$  are not easily

available. Besides, if the other storage components (i.e. soil, water bodies, Equation 2.2) are significant, then an accurate estimation of their values must also be ensured, making the method even more arduous.

### 2.2.3.3 Glacier mass balance changes measured from space

With the recent developments on satellite data, measurements on glacier mass balance changes can be determined directly for the whole glacier based basically on three types of techniques:

- (i) **Geodetic method:** From two Digital Elevation Models (DEMs) at different years and the known glacier outlines, the difference in volume can be determined. Then, the change in volume ( $\Delta V$ ) is converted into a change of mass by considering the (mean) density of the glacier ( $\rho$ ) (Fischer, 2011):

$$MB_{geo} = \Delta V \times \rho \quad (2.4)$$

This, however, is one of the main sources of uncertainties of this method, since the ice density is not homogeneous throughout the glacier. Also, there might be some inaccuracies on the DEM, due to, for example, empty gaps. Hence, the geodetic method is usually employed over periods no longer than 10 years (Berthier et al., 2023). One of the most recent and well-used datasets in modeling is the global dataset provided by Hugonnet et al., 2021. It contains average geodetic mass balance measurements for all glaciers, based on surface elevation changes at high spatio-temporal resolution from untapped satellite images. During the analyzed period (2000-2020, split into two parts), an average mass balance change of -813 mm w.e. was determined for all the glaciers in the European Alps, for example.

- (ii) **Altimetry method:** Within this method, radars or sensors measure the elevation of the Earth's surface by emitting a pulse, which travels back to the device. Then, the recorded time and the velocity of the traveling pulse are used to determine the distance, which at the ends leads to the topography of the glacier. Finally, the change in glacier thickness can be determined by two different altimetry measurements (Berthier et al., 2023).
- (iii) **Gravimetric method:** Employed by the Gravity Recovery and Climate Experiment (GRACE), this method provides direct measurements of glacier mass changes on a global scale. Compared to the other methods, no assumptions on ice density are needed, hence less uncertainties can be expected. The basic principle of the method consists on detecting changes in the Earth's gravitational field, by two satellites separated by a certain distance but in the same orbit (Benn and Evans, 2010; Berthier et al., 2023).

While the glaciological and hydrological methods are employed at a glacier (or catchment) basis, the remaining methods cover a global scale. In this sense, the World Glacier Monitoring Service (WGMS) offers a compilation on glaciological measurements from reference glaciers for long periods of time. Moreover, many recent datasets have been collecting information on mass balance changes all over the world, like the dataset provided by Hugonnet et al., 2021. These datasets are an essential aid when modeling, since they allow to calibrate and validate the models for performing simulations.

#### 2.2.3.4 Glacier extent

Another proper way of measuring the glacier's response to different climate conditions and its evolution throughout the years is analyzing the change in its extent (i.e. glacier area). After the end of the LIA, when glacier measurements began to become more regular, a set of aerial photographs has been compiled to build glacier inventories. Within these inventories, which can contain either global or regional information, the outlines of the glaciers can be delineated. At a global scale, the Randolph Glacier Inventory (RGI, Pfeffer et al., 2014), provides an up-to-date collection of glacier outlines for several regions all over the world. As an example of the regional scale, the Austrian Glacier Inventory (AGI, e.g. Lambrecht and Kuhn, 2007; Fischer et al., 2015a) offers a high-resolution inventory for all the glaciers in Austria. The earliest inventory created for the LIA (1850) and the changes compared to the year 1920, were estimated through moraines and terrestrial photogrammetry (e.g. Haggreén et al., 2007). The derivation of the latest inventories (e.g. year 2015) is based on lidar data and orthophotos, thus lower uncertainties are estimated in comparison to the earliest datasets.

#### 2.2.3.5 Glacier thickness

Apart from the changes in mass balance and glacier extent, estimations on glacier volumes are essential to assess the amount of water that is stored within the glacier (Farinotti et al., 2009). By knowing the glacier extent, the volume can be estimated from ice thickness measurements carried out by means of a Ground-penetrating Radar (GPR). Basically, the point thickness can be determined empirically by measuring the travel time of the signal, for a known signal velocity (Fischer and Kuhn, 2013).

The combination of all available measurements (i.e. mass balances, glacier extents, ice thickness) is a powerful tool not only for understanding the glaciers' behavior in the past, but also for making predictions in the future, with the use of computer models.

## 2.3 Modeling

Models are simplifications of the real world. Generally speaking, they combine observations (i.e. measurements) with methods that describe the processes that regulate the behavior of a system (Abdollahi et al., 2019). Depending on the target variable that is aimed to be modeled, they can be distributed into several groups. Section 2.3.1 describes the theory behind water balance models and their classification. Section 2.3.2 gives an overview of the modeling approaches for representing glacier evolution and Section 2.3.3 describes the water balance models with focus on glacier processes and the most recent advances in coupled glacio-hydrological models.

### 2.3.1 Water balance modeling

If the primary aim of the water balance model is to predict the water flows in a catchment, they are usually called *hydrological models*. Although the first steps in modeling date from the 1850s (e.g. Mulvaney, 1851), it was after 1960s when big progress was made

due to the advances in computations (Singh, 2018). Water balance models simulate all the components involved in Equation 2.1, with different level of detail, depending on the nature of the processes. Moreover, they can be grouped in point, regional or catchment-scale models and global models, being the latter able to model the components of the global water cycle. Although some argue that classifications of hydrological models are rather unnecessary (i.e. some terms are broadly used, hence the classification becomes pointless (Seibert and Bergström, 2022)), they can be allocated into distinct categories, depending on their structure, spatial discretization and stochasticity:

- (i) **Model structure:** When the underlying hydrological processes are not described, the model is known as a *black box*. An example are regression models. If, however, the processes are described through a set of mathematical equations where the modeler has a better understanding of what is happening behind these equations, then the model is considered *conceptual* (Beven, 2012). An example of a very popular and widely used conceptual (bucket-type) model is the HBV model (Bergström and Forsman, 1973). Finally, *physically-based* models rely on a detailed description of the processes, for example, by applying conservation of mass or energy. An example of a physically-based model is the WaSiM-ETH (Schulla, 1997), further used in this thesis.
- (ii) **Spatial discretization:** If the modeled catchment is treated as a single unit, then it is a *lumped* model. In this case, there is no spatial discretization of the catchment properties, being the parameters homogeneous and they usually rely on conceptual approaches (e.g. the GR4J model developed by Perrin et al., 2003). On the other hand, if the catchment is discretized in grid cells, where a detailed representation of parameters is given to each of those cells, then the model is *fully-distributed*. In this case, the heterogeneity of the catchment can be better related to the heterogeneity of the climate variables, like in WaSiM. There are also models that combine the characteristics of both, the *lumped* and *fully-distributed* models and result in a *semi-distributed* model. Within this kind of model, the catchment is divided into small subcatchments, each of them including Hydrological Response Units (HRUs) that summarize the main hydrological properties (such as soil types, Kalcic et al., 2015). An example of a semi-distributed model is the Soil and Water Assessment Tool (SWAT, Arnold et al., 1998).
- (iii) **Stochasticity:** Models can be either deterministic or stochastic. The latter is related to the randomness of the processes, which are described by probability distributions (Yevjevich, 1987). On the contrary, deterministic models are free of randomness and they always reproduce the same output, for the same input and parameters considered. Water balance models, like WaSiM, are assumed to be deterministic.

As introduced in Section 2.1, the water balance in mountainous regions is heavily influenced by the presence of glaciers. This inevitably leads to the need of incorporating glacier processes when performing model simulations at the catchment scale. Due to the complexity and spatial variability of such processes, the adoption of fully-distributed, physically-based and deterministic hydrological (or water balance) models seems crucial. Moreover, glacier processes necessitate adequate consideration (e.g. due to the detailed input data required). In terms of glacier modeling, many improvements have been achieved during the last years, especially due to the emergence of global datasets. For this reason, the following section

(2.3.2) first offers an overview on the development of glacier modeling and afterwards an introduction to glacio-hydrological models (i.e. hydrological models including glaciers) is done (Section 2.3.3).

## 2.3.2 Glacier modeling

Mass balance modeling is crucial when studying the evolution of glaciers. The gain and loss of mass of a glacier indicates how it behaves under the given climatic conditions or projected conditions in the future. Once the mass balance of the glacier is solved, the changes in glacier's geometry (area, thickness and volume) can be determined. To do so, different approaches can be used, ranging from empirical methods to ones that consider explicit ice-flow dynamics of the glacier. Figure 2.4 gives an overview of available models, ranging from low (left) to high (right) complexity. Examples of models with low complexity are those which rely on empirical methods, whereas ice-flow dynamic models (from 1- to 3 dimensions) are based on more complex approaches.

### 2.3.2.1 Glacier mass balance models

In essence, the purpose of a mass balance model is to estimate the change in mass of a glacier after a certain period of time (e.g. one year or one month). This is given by the accumulation (mass gain) and ablation (mass loss), as introduced in Section 2.2.2. Regardless what type of model is adopted, they all rely on climate variables as input data. Being precipitation and temperature the essential variables, the complexity of models can increase if other variables are considered (e.g. solar radiation). From empirical models based on linear or multiple regressions (e.g. Mutz and Aschauer, 2022) to those based on a temperature index (T-index) approach (e.g. Marzeion et al., 2012), it is feasible to estimate the mass balance at a glacier basis. The simplest formulation to calculate the melt rate (ablation) of the T-index method is represented by Equation 2.5 (Hock, 1999):

$$M = \begin{cases} DDF_{ice/firn/snow} \times T & T > 0 \\ 0 & T \leq 0 \end{cases} \quad (2.5)$$

Where:  $DDF_{ice/firn/snow}$  refer to the degree-day factors [ $\text{mm d}^{-1} \text{ } ^\circ\text{C}^{-1}$ ] for ice, firn and snow, and  $T$  is the measured air temperature [ $^\circ\text{C}$ ]. In the example shown in Equation 2.5, melt can take place as long as temperature is higher than  $0^\circ\text{C}$ .

Examples of more sophisticated, physically-based models are those based on energy balances (e.g. Klok and Oerlemans, 2002; Krampe et al., 2022; Machguth et al., 2006). In these cases, the model also considers the heat transfer between the glacier and the atmosphere, thus more variables describing the glacier need to be known beforehand, like the albedo of ice. In this case, the surface energy balance can be described by Equation 2.6 (Ohmura, 2001):

$$R + H + L_v E + C + M = 0 \quad (2.6)$$

Where:  $R$  accounts for the net radiation,  $H$  is the sensible heat flux,  $L_v$  is the latent heat of vaporization,  $E$  is the evaporation rate,  $C$  is the conductive heat flow in the subsurface and  $M$  is the latent heat for melting [ $\text{W m}^{-2}$ ].

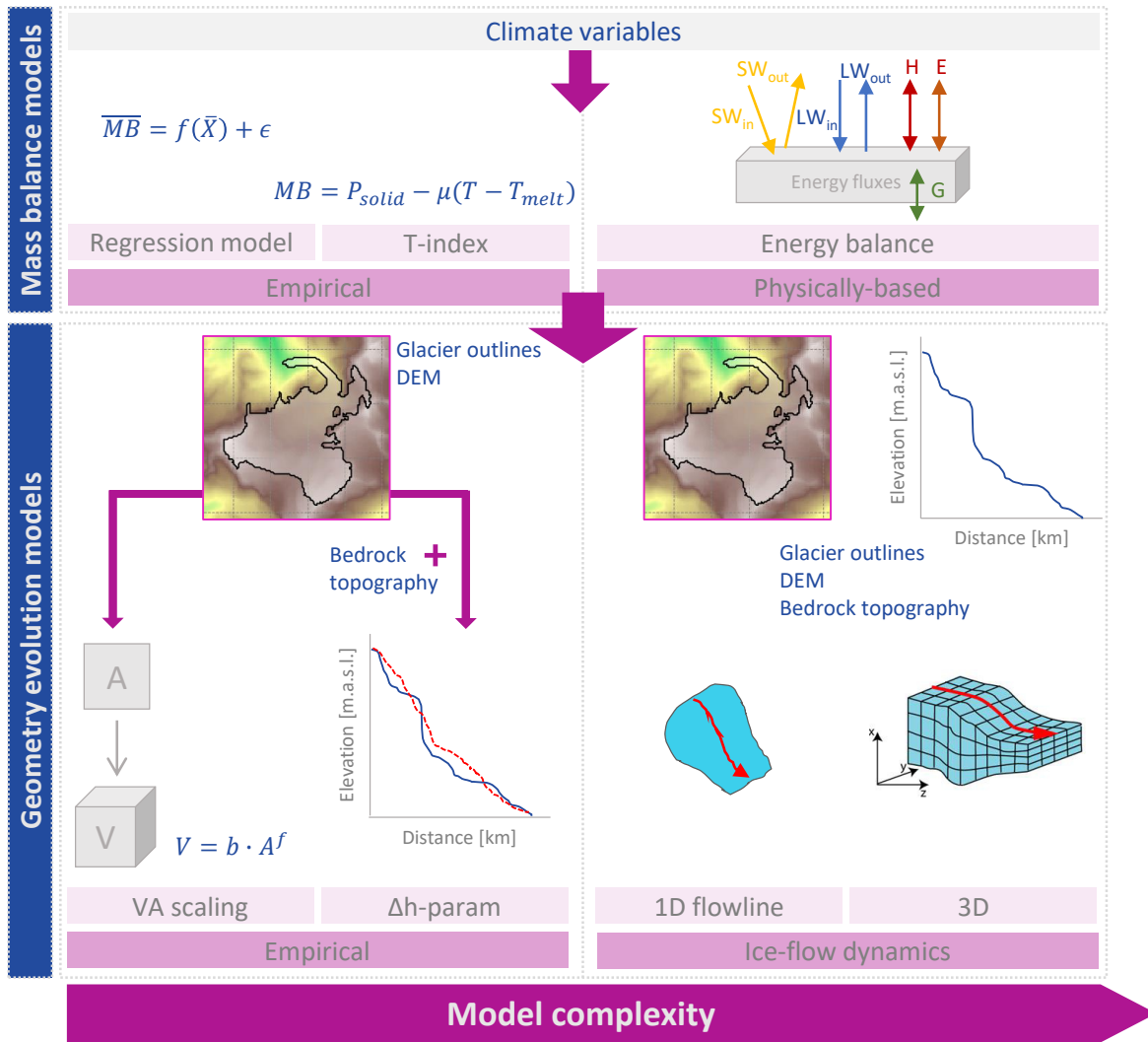


Figure 2.4: Examples of glacier mass balance models, from low (e.g. T-index) to high (e.g. energy balance) complexity and glacier evolution models, from low (e.g. the empirical VA scaling approach) to high (e.g. 3D ice-flow dynamics models) complexity (adapted from AntarcticGlaciers.org, 03/07/2023; Zekollari et al., 2022).

Even though the T-index is considered to be a rudimentary method because it only relies on temperature, its physical basis is attributed to the sensible heat (Ohmura, 2001). It is in fact a short form of the energy balance method, since temperature affects longwave atmospheric radiation and sensible heat flux (part of  $R$  and  $H$  in Equation 2.6, respectively).

The choice of the mass balance model depends on the available input data, measurements, modeled area and aim of the study, therefore models with higher complexity are not always the most suitable choice. Once the mass balance of the glacier is established, the evolution of its geometry can be analyzed by means of geometry evolution models. These are described in Sections 2.3.2.2 and 2.3.2.3.

### 2.3.2.2 Empirical methods for glacier evolution

Following the classification depicted in Figure 2.4, examples of geometry evolution models with lower complexity are those who rely on empirical relations. Within this group, the

Volume-Area (VA) scaling approach can be identified, which estimates the volume ( $V$ ) of a glacier based on its (observed) area ( $S$ ) by simply applying a scaling function, like the one described by Equation 2.7 (e.g. Chen and Ohmura, 1990a):

$$V \propto S^\gamma \quad (2.7)$$

This method was physically validated by Bahr et al., 1997 for a collection of glaciers and has been applied in numerous cases. In that study,  $\gamma$  was estimated to be 1.36. A distinct advantage of this method is that only the glacier's area is required and the scaling parameter could be fixed for the whole set of glaciers. However, it should be avoided when simulating single glaciers, since large errors can be achieved (for example, an error of 10% in the scaling parameter could lead to an error of 10% in the estimated volume, independently of the glacier's size) (Bahr et al., 2015). This finding was also justified by Farinotti and Huss, 2013, where more accurate volume results were obtained if applied to more than hundreds of glaciers and neglecting time-variation of the scaling parameters. Even though Radić et al., 2007 found that glaciers in non-steady state are described differently from those in steady state, they concluded that the VA scaling is accurate enough to predict volume changes in the future, being results close enough to those predicted by a flowline model.

By knowing the glacier bedrock topography, a spatial distribution of the glacier thickness change can be estimated by means of a  $\Delta h$ -parameterization (Equation 2.8), originally developed by Huss et al., 2010 for three distinct glacier size classes:

$$\Delta h = (h_\Gamma + a)^\gamma + b \times (h_\Gamma + a) + c \quad (2.8)$$

Where:  $h_\Gamma$  refers to the elevation range,  $\gamma$  prescribes the curvature of the function and  $a$ ,  $b$  and  $c$  are parameters that depend mainly on the glacier class. Then, by knowing the elevation  $h_0$  at time  $t_0$ , an estimation of the new glacier elevation  $h_1$  at time  $t_1$  can be achieved in terms of Equation 2.9 by applying an annual scaling factor  $f_s$ :

$$h_1 = h_0 + f_s \times \Delta h \quad (2.9)$$

This method, which is computationally cheaper compared to more complex ice-flow models, has been rapidly evolving and adapting to the need of modeling glaciers at a global scale. One of the first outcomes is the Global Glacier Evolution Model (GloGEM, Huss and Hock, 2015), initially created to predict global glacier change and sea-level rise driven by the ice melt from glaciers. More recently and focusing on a regional scale, a further development of the  $\Delta h$ -parameterization can be found in the open-source Python Glacier Evolution Model (PyGEM, Rounce et al., 2020a; Rounce et al., 2020b).

Due to the relatively simple application of the VA scaling and  $\Delta h$ -parameterization for estimating the evolution of glaciers, these two methods are widely utilized in combination with hydrological models for predicting runoff in glacierized catchments. These glacio-hydrological models are introduced in Section 2.3.3.

### 2.3.2.3 Ice-flow dynamics for glacier evolution

The next generation of models predicts glacier's evolution based on the transfer of mass through the glacier by gravity processes (driving forces). The high viscosity of ice and the very slow movement of the glacier allow to neglect inertial and acceleration forces, thus the



force balance is expressed by an equilibrium of stresses, like the example shown in Figure 2.5a (Cuffey and Paterson, 2010; Zekollari et al., 2022). In this figure, all involved stresses are included.

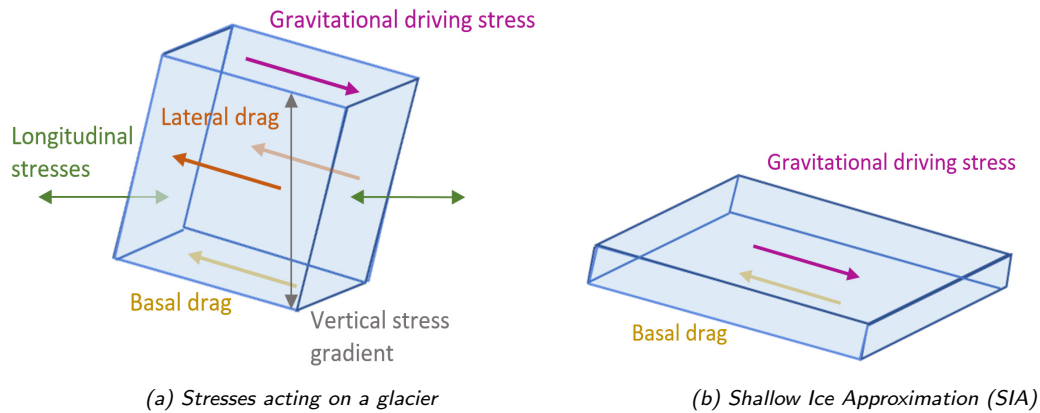


Figure 2.5: Driving and resisting stresses acting on a (block of) glacier: (a) considering all forces and (b) simplified model based on the Shallow Ice Approximation (SIA). Adapted from AntarcticGlaciers.org, 03/07/2023; Zekollari et al., 2022.

As the name depicts it, the main driver of the glacier's movement is the gravitational driving stress. As a reaction, the glacier resists with the basal drag. There are, however, other stresses that intervene and complement the resistance of the driving force, such as lateral drag, which originates from the contact between ice and the valley walls where the glacier lays (AntarcticGlaciers.org, 03/07/2023). Although such complete models consider all involved stresses, there are simplified approaches that help reducing computational times and are widely used, while still representing the phenomenon.

If the scales (stresses) in the longitudinal direction (glacier length and width) are much larger than those in the transversal direction (glacier thickness), the stresses can be reduced to the driving and basal drag (as shown in Figure 2.5b). This simplification, which is known as the Shallow Ice Approximation (SIA, Hutter, 1983), is adopted in many contemporary flowline models. Within these models, glacier evolution is estimated in terms of the ice thickness ( $h$ ) by the general Equation (2.10, e.g. Cuffey and Paterson, 2010; Farinotti et al., 2009):

$$\frac{\partial h}{\partial t} = \dot{m} - \nabla \cdot q \quad (2.10)$$

Where:  $\dot{m}$  is the mass balance [ $\text{m w.e. yr}^{-1}$ ] and  $\nabla \cdot q$  is the flux divergence [ $\text{m}^2 \text{ yr}^{-1}$ ], that depends on the basal drag (depicted in Figure 2.5b).

In order to solve Equation 2.10, many flowline models adopt an *explicit* numerical scheme, in which the state of a glacier at a later time step is determined analytically from a given time step (i.e. forward calculation). On the contrary, a few models rely on an *implicit* scheme, in which information on a future time step is used additionally. Since the latter is more complicated and computationally more expensive, the explicit scheme is mostly used by flowline models (Zekollari et al., 2022). Basically, the terms  $\dot{m}$  and  $\nabla \cdot q$  can be determined beforehand, so that Equation 2.10 allows the estimation of the change of ice thickness in time. Anyway, a more detailed explanation is given in Chapter 5.

Starting with the simplest approach in which ice is assumed to flow along a flowline, examples of models that rely on a 1D flowline representation are numerous. The first

attempts were already made around the year 1980, when, for example, Bindschadler et al., 1977 applied such method to describe the motion of a glacier in Alaska. Another example can be found in Kruss and Smith, 1982, where also a flowline model was used to represent the evolution of *Vernagtferner* in Austria. Later studies began to investigate the evolution of glaciers under climate warming, like Oerlemans et al., 1998, in which also Equation 2.10 was applied to twelve glaciers in different parts of the world.

More recently, Zekollari et al., 2019 benefit from GloGEM (Huss and Hock, 2015, introduced in Section 2.3.2.2) which is originally based on the  $\Delta h$ -parameterization method and extended it to include ice dynamics, following Equation 2.10. In their study, where GloGEMflow was applied to examine the future evolution of glaciers in the European Alps, they emphasized the importance of introducing ice dynamics. Moreover, with the emergence of global glacier datasets and the possibility to automatically solve Equation 2.10 for many glaciers simultaneously, the Open Global Glacier Model (OGGM, Maussion et al., 2019) is one of the newest models that explicitly account for glacier dynamics at a global scale. Because it is an open-source framework completely relying on publicly available data, it has been widely applied in several studies since its release. OGGM is used in this thesis for including explicit ice-flow dynamics into the water balance model and is introduced in detail in Chapter 5.

Finally, ice-flow dynamics can also be accounted for by 3D models. Although a higher level of detail of geometrical settings can be achieved by such models, the computational times are also considerably higher, compared to 1D flowline models. Some of these 3D models rely on the assumption of SIA, in which the continuity equation (Equation 2.10) is solved for every point on a 2D horizontal grid (e.g. Le Meur et al., 2007). There are, on the contrary, more sophisticated approaches that consider all terms involved in Figure 2.5a (e.g. Zekollari et al., 2014; van Tricht et al., 2023). In all cases, however, their applications are still limited to a single glacier or small group of glaciers, hence predictions at a regional and global scale are an ongoing challenge (Zekollari et al., 2022).

### 2.3.3 Glacio-hydrological modeling

The changes in glacier geometry strongly influences the hydrology at local and regional scales (Radić and Hock, 2014). There are, however, many other processes involved that affect the hydrological response of a catchment. Depending on the size of the catchment and the fraction of glacier coverage, glacier modeling plays a fundamental role, since an inaccurate representation of glacier retreat could lead to wrong runoff predictions at a decadal or multi-decadal scale (Stahl et al., 2008). Glacio-hydrological models are essentially catchment hydrological models that incorporate glacier processes to predict the response of highly-glaciated catchments (Stoll et al., 2020). From conceptual to fully-distributed and physically-based hydrological models, glacier processes are encompassed by several ways. Therefore, this section offers an overview of distinct glacio-hydrological models that are available and have been successfully applied in different catchments around the world, while giving insight about ongoing and future progress.

### 2.3.3.1 Glacio-hydrological models without considering glacier evolution

The ablation component of the glacier mass balance (i.e. melting of glaciers) directly affects the total runoff at the outlet of a catchment, being in some cases the major contributor in the generation of runoff, especially during summer. This suggests that, when pursuing runoff predictions, the sole inclusion of glacier mass balance into the hydrological model may be sufficient to account for glacier processes. Some studies do not account for changes in glacier geometry, since they only focus on specific events, or the simulation period is rather "short" (e.g. five to ten years) or because measurements show negligible changes between two certain years (Hanzer et al., 2016; Klok and Oerlemans, 2002; Schaepli et al., 2005; Tarasova et al., 2016). This assumption might hold true, because the movement of glaciers is rather slow (e.g. between 15 and 50 years per meter in mountain glaciers, Cuffey and Paterson, 2010) and a change in its geometry may only be visible after decades in some regions. Yet, the studies highlight the limitations on future projections, since the changes in glacier geometry will play a crucial role and cannot be neglected, especially under a warming climate.

### 2.3.3.2 Glacio-hydrological models including glacier evolution

When looking at multi-decadal scales, changes in glacier geometry must be considered (e.g. runoff projections under future climatic conditions). Hydrological models integrate glacier evolution by different ways. As depicted in Figure 2.4, glacier evolution models range from those based on empirical approaches (Section 2.3.2.2) to those relying on ice-flow dynamics (Section 2.3.2.3).

On the one hand, due to their lower required input data and computational times, the  $\Delta h$ -parameterization (Huss et al., 2010) has been successfully included in numerous hydrological models to account for glacier surface elevation changes (e.g. Duethmann et al., 2016; Hanzer et al., 2018; Li et al., 2015; Mackay et al., 2018; Seibert et al., 2018; Stoll et al., 2020). Similarly, the empirical VA scaling approach (Bahr et al., 1997) has been used to predict the evolution of glaciers based on observed areas (e.g. Kormann et al., 2016; Stahl et al., 2008; Verbunt et al., 2003; Zhang et al., 2012). The latter is the original glacier approach integrated in WaSiM, thus studied in more detailed in Chapter 5. On the other hand, more sophisticated ice-flow models have been also integrated into hydrological models to predict the response of glacierized catchments under changing climate, but to a lesser extent (e.g. Immerzeel et al., 2012; Wortmann et al., 2019).

### 2.3.3.3 Coupled glacio-hydrological models

So far, the term glacio-hydrological model referred to one single model, namely a hydrological model, that contains a sub-model for describing glacier processes. There are, however, other cases in which glacier processes are simulated separately by a stand-alone glacier model and the results are then coupled (i.e. integrated) to the hydrological model. These coupled models aim to exploit the capabilities of each independent model to provide a better representation of runoff in glacierized catchments.

In some cases, glacier evolution is based on empirical approaches, like the VA scaling approach (e.g. Stoll et al., 2020) or the  $\Delta h$ -parameterization, where even the latest gener-

ation of global glacier models are used (e.g. Wiersma et al., 2022). In other cases, on the contrary, glacier evolution models based on ice-flow dynamics are coupled to hydrological models (e.g. Naz et al., 2014). Additionally, the capabilities of global glacier models are also utilized (e.g. Khadka et al., 2020), gaining benefit not only of the available global datasets, but also of the possible application of such coupled models to predict runoff at a global scale.

Furthermore, the coupling between glacier and hydrological models can be classified into two groups, depending on how the inputs/outputs are transferred from one model to another (Figure 2.6). An *online* coupling aims to continuously integrate glacier processes (i.e. mass balance and/or glacier evolution) into the hydrological model, thus the feedback from one model to another is done at every time step. Moreover, both models are driven with the same climate input data. Oppositely, for an *offline* coupling, the continuous feedback between models is not required. In this case, the output produced by one model is used as input for the succeeding model. Still, a close similarity could be achieved to an online coupling if the same climate dataset is used in each separate model.

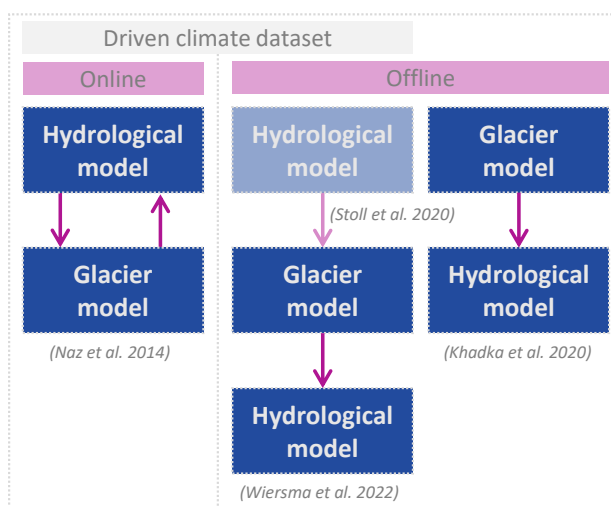


Figure 2.6: Examples of online and offline coupled glacio-hydrological models.

### 2.3.3.4 Snow modeling

With temperature as the main driver, the first step in the generation of glacier is the transformation from snow to ice (Cuffey and Paterson, 2010, Figure 2.3). After a few years, snow that was not subject to melt is converted into firn and then into ice, hence increasing the thickness and area of the glacier. Even though the focus was exclusively given to glacier modeling so far, it is also vital to understand how snow is represented in such glacio-hydrological models. Not only is snowmelt a major contributor to runoff generation in Alpine regions, but the spatial distribution of snow exerts a huge impact on glacier evolution (Schöber et al., 2010). In this context, significant progress has been made to more accurately represent snow accumulation in high-mountainous regions, accounting for the complexity of the terrain (i.e. steep slopes), wind (Warscher et al., 2013) and interception processes (Förster et al., 2018). Particularly in Alpine regions, the steep slopes, high wind velocities and scarce vegetated areas favor the transport and consequent deposition of snow in wind-sheltered areas. If these snow redistribution processes are not considered during

modeling, unrealistic "snow towers" can be formed at high elevations, hence underestimating the amount of water (snowmelt) that is then able to contribute to runoff generation (Freudiger et al., 2017). Various glacio-hydrological models based on physical processes, like WaSiM, enable the consideration of snow redistribution processes, which are therefore explained in detail in Chapter 4 (Section 4.7).

Similar to the case of glaciers, snowmelt can be represented by diverse methods, ranging from simple T-index approaches to more sophisticated energy balance models. Moreover, the inclusion of snow measurements during calibration and validation of the glacio-hydrological models helps to constrain the uncertainty of involved parameters, while obtaining reliable results of runoff predictions (e.g. Hofmeister et al., 2022; Schattan et al., 2020; Schöber et al., 2014; Thornton et al., 2021).

### 2.3.4 Optimization and uncertainties in modeling

Glacio-hydrological models aim to accurately represent hydrological processes in glacierized catchments, make predictions into the future and support decision-making in the field of water resources management (Chen et al., 2017b; van Tiel et al., 2020; Zhao et al., 2019). However, modeling the response of highly glacierized catchments faces some major challenges. First, the runoff dynamics is not the same for all parts within the catchment. While runoff in the non-glacierized parts respond mainly to precipitation, runoff in the glacierized parts of the catchment react mainly to temperature and radiation variations (van Tiel et al., 2020). Although a good model performance can be obtained in terms of total runoff, deficiencies in modeling one component might be compensated by the other (i.e. low ice melt might be compensated by high rainfall rates).

Second, the changes in glacier coverage directly alters the runoff in the glacierized parts of the catchment, hence a reliable estimation of glacier evolution should be ensured (Chen and Ohmura, 1990b). However, as already described in the previous sections, glacier processes are very complex. Accelerating glacier melt results in a reduction of the glacier volume and increased runoff (Hanzer et al., 2018; Koboltschnig and Schöner, 2011; Marzeion et al., 2012), whereas the contribution of the glacier melt to the runoff will ultimately decrease over a long period of time due to the reduction on the glacier volume (Chen et al., 2017b; Huss et al., 2008). As introduced in Figure 1.1, the time in which the glacier provides its maximum contribution to runoff is known as *peak water* (Huss and Hock, 2018). Besides, the spatial distribution of climate variables in such high-mountainous catchments show a clear dependence on elevation. Unfortunately, due to the complex terrain, high-resolution datasets are limited (e.g. difficulties to install measurement devices), hence increasing modeling complexity even more (Naz et al., 2014).

#### 2.3.4.1 Model optimization

Model parameterization can turn into an arduous task, not only due to scarce available datasets, but also because the number of parameters involved in all processes may be high. During model optimization (also referred to as calibration), different model parameter sets are used to describe the processes while evaluating the performance of the model. This evaluation can be done in terms of an objective function, in which simulated values are compared to observations. Then, the parameter set that yields the best model perfor-

mance (usually, this is equivalent to obtain the minimum objective function) is selected for further applications of the model. However, as the number of parameters increases, the optimization becomes problematic, since several parameter sets might equitably reproduce the observed behavior of the catchment (Liu et al., 2021). This concept, which is known as equifinality (Beven and Freer, 2001; Beven, 2006), cannot be avoided, but the integration of more observational datasets might help to constrain it (e.g. Chen et al., 2017a; Gupta et al., 1998). The uncertainties associated with model parameters could be important and should be assessed, together with other sources of uncertainty (Section 2.3.4.2).

Although runoff is the primary observed dataset used when optimizing a glacio-hydrological model (e.g. according to the reviews done by Chen et al., 2017b and van Tiel et al., 2020), several studies demonstrate that the inclusion of an additional dataset usually leads to more reliable results (*Multi-data optimization*, e.g. Muñoz et al., 2021). These dataset can include glacier mass balances (e.g. Duethmann et al., 2016; Hanzer et al., 2016; Konz and Seibert, 2010; Stahl et al., 2008; Schaefli et al., 2005; Tarasova et al., 2016), glacier outlines or areas (e.g. Kormann et al., 2016; Naz et al., 2014; Tarasova et al., 2016) and snow measurements (e.g. Chen et al., 2017a; Hanzer et al., 2016; Hofmeister et al., 2023; Naz et al., 2014; Parajka et al., 2007; Schöber et al., 2010; Thornton et al., 2021). Besides, several objective functions can be used when evaluating the performance of the model (*Multi-criteria optimization* e.g. Gupta et al., 1998; Parajka et al., 2007; Tarasova et al., 2016).

The optimization process can be done either manually or automatically. A manual optimization implies that the adjustment of model parameters is done by trial and error, so this process, together with the estimation of related uncertainties could be very arduous. On the contrary, an automatic optimization can be performed with the help of computer-based algorithms, thus reducing times and the amount of expertise needed. However, the judgment of the modeler should always accompany the evaluation of such automatic algorithms (Pechlivanidis et al., 2011). Finally, once the optimization procedure is complete and the "best" parameter set is obtained, a verification of the model should be carried out. This verification (validation) consists on evaluating the performance of the optimized model but with a different dataset (Klemeš, 1986). This can be done, for example, by running the model on a different time period (known as split sample test) or by applying the optimized model to another catchment.

### 2.3.4.2 Uncertainties in modeling

The main sources of uncertainty encompassed in glacio-hydrological modeling are mostly related to (Beven and Binley, 2014; Beven and Lamb, 2017; Liu and Gupta, 2007; Liu et al., 2021):

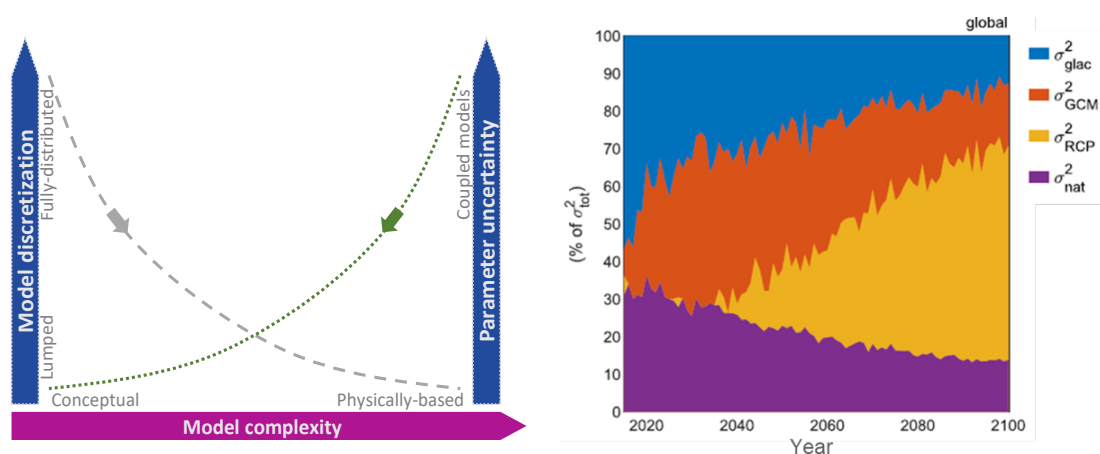
- (i) **Observed data:** Uncertainties in meteorological input data can be attributed, for example, to scarce observations (which is common in high-mountainous regions, Chen et al., 2017b), undercatch of precipitation due to wind processes (Freudiger et al., 2017) unknown spatial variation or inhomogeneities in the measurements, which can propagate to model results (Hofmeister et al., 2023). Besides, the datasets that are used as target variables during optimization of the model, entail other sources of uncertainty. These variables are, for instance, runoff, glacier observations (e.g. mass balance, areas) and snow measurements (e.g. depth and coverage). Uncertainties

can appear either due to human misinterpretation (e.g. reading errors) or because the variable is obtained through calculation from another measured data (e.g. snow water equivalent obtained from measured snow depth, Jonas et al., 2009).

- (ii) **Model parameters:** These uncertainties arise from the equifinality concept, when non-unique parameter sets yield equally good model performances during the optimization process (Gupta et al., 2005). Furthermore, errors in observational data (e.g. runoff) can also propagate and increase parameter uncertainty (McIntyre et al., 2002). Model parameter uncertainty can be evaluated in terms of stability (parameters are stable if similar values are obtained for different optimization periods) and identifiability (parameters are identifiable if different parameter sets lead to different model results, e.g. Gelleszun et al., 2017; Tarasova et al., 2016).
- (iii) **Model structure:** These uncertainties are related to the unknown nature of the processes and simplifications made to represent them within the model. The reduction in model assumptions by introducing for example more physically-based methods, might lead to a decrease on such uncertainties (Moges et al., 2021), at the expense of a more complex model. Similarly, the selection of a simple model with coarse model discretization (e.g. lumped model), might result in higher parameter uncertainty. The interaction between model structure and parameter uncertainty is depicted in Figure 2.7a. For a fully-distributed model, an increase in model complexity might reduce the uncertainties on model structure (gray dashed line), whereas a decrease in parameter uncertainty can be achieved by decreasing model complexity (green pointed line). The point at which both curves meet, can be considered as a desired compromise between model discretization, complexity and parameter uncertainty. This figure also suggests that more complex physically-based and coupled models, tend to have greater uncertainties as regards their parameters instead of model structure. For this reason, parameter uncertainty is studied later on this thesis.
- (iv) **Initial (boundary) conditions:** The initial conditions have a considerable influence on the hydrological response of the catchment. These can refer, for instance, to soil moisture (Yu et al., 2019) or initial ice thickness estimation (Naz et al., 2014). The model requires time until the (unknown) initial conditions reach an "optimal" state. This period, which can take from one to several years, is known as warm-up period (Kim et al., 2018). This type of uncertainty can be critical in glacier modeling, since the initial state of the glaciers could have a tremendous impact on the simulation results and is described in more detail in the following.

Particularly in glacier modeling, the uncertainties derived from unknown initial conditions play a fundamental role (Maussion et al., 2019). An inaccurate initialization of the glacier states might lead to huge errors in the prediction of runoff, since an under- or overestimation of the glacier geometry (i.e. areas and ice thickness) could lead to a misinterpretation of the water that might be available in the catchment.

When modeling glacier evolution in the past, sometimes an estimation of the initial conditions is required due to the lack of observed data. This can be achieved, for example, with the initialization method developed by Eis et al., 2019, in which current glacier states and past climatic conditions are used to initialize OGGM in the past. In this approach, a series of possible glacier states are studied and the "best" candidate is selected. However, uncertainty increases when going farther in the past and the non-unique solution of glacier



(a) Interaction between model structure and parameter uncertainty (b) Relative contribution of uncertainty sources to the total uncertainty of projected glacier mass change

Figure 2.7: (a) Interaction between model structure and model parameter uncertainty. Increase in model complexity, model discretization and parameter uncertainty. The gray dashed curve indicates the decrease in bias due to model discretization, whereas the green pointed curve indicates a decrease in parameter uncertainty due to a decrease in model complexity (adapted from Moges et al., 2021). (b) Relative contribution of different uncertainty sources ( $\sigma_{glac}^2$ : glacier model,  $\sigma_{GCM}^2$ : climate model,  $\sigma_{RCP}^2$ : emission scenario,  $\sigma_{nat}^2$ : internal climate variability or natural climate fluctuations) to the total uncertainty ( $\sigma_{tot}^2$ ) of projected glacier mass change accumulated since the year 2015 and for the global scale (Marzeion et al., 2020).

candidates cannot be avoided. Later on, Eis et al., 2021 introduced a validation of the method to real-world applications, in which a calibration step is performed a priori to reduce the mismatch between the results and current glacier geometry, thus restricting the uncertainty in model initialization. Another common way to initialize glacier models is to perform a spinup, in which the model runs until glaciers are in dynamical equilibrium (this is a necessary assumption for the ice thickness inversion applied in OGGM, for instance, OGGM, 2023).

Similarly, when the objective pursued by the models is to predict the evolution of glaciers and the hydrological response of the catchment in the future, uncertainties in climate change projections emerge. At a global scale, such uncertainties could be very important (Viviroli et al., 2011) and also at a regional scale are expected to be remarkably larger than uncertainties arising from model parameterization in hydrological models, for example (e.g. Kingston et al., 2011; Pesci et al., 2023a; Wagner et al., 2017). Likewise, for glacier projections, Marzeion et al., 2020 showed that the main source of uncertainty comes from the emission scenarios, being uncertainty of the glacier model itself much smaller (Figure 2.7b).



# Chapter 3

## Study area and data

This chapter describes the study area (Section 3.1) and the input data (Section 3.2) used in all the modeling steps considered within this thesis. Appendix A complements this section with additional information about observed datasets.

### 3.1 Study area

The study area is the *Gepatschalm* catchment, located in the Kaunertal region, in the Ötztal Alps (Austria). Figure 3.1 (a) shows the location of the study area within Austria, whereas (b) shows the catchment in detail.

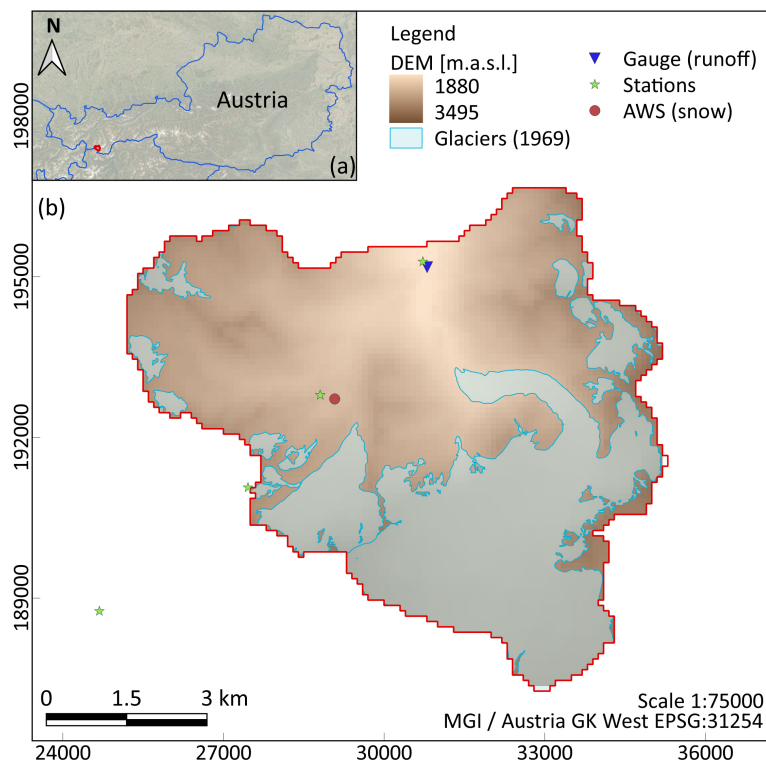


Figure 3.1: Study area: (a) location within Austria and (b) catchment with Digital Elevation Model (DEM), glacier coverage for the year 1969, available gauging station for runoff and Automatic Weather Station (AWS) for snow measurements.

Gepatschalm occupies a total surface of 57.5 km<sup>2</sup>, from which a significant part is

covered by glaciers (47% during the year 1969, according to the Austrian Glacier Inventory (AGI, Fischer et al., 2015c)). Furthermore, it presents a highly varying topography: values of around 1800 m a.s.l. can be reached at the outlet of the catchment, in the vicinities of the Gepatsch reservoir, whereas the highest altitudes can reach values of approximately 3500 m a.s.l. in the southern boundaries of the study area, above the glaciers. The Digital Elevation Model (DEM) is available with a resolution of 5 m x 5 m and corresponds to the year 2019 (Amt der Tiroler Landesregierung, 2019).

The Gepatsch reservoir, located downstream from the outlet of the catchment, is one of the most important reservoirs in the country used for hydropower production. It is able to store up to 138 Mio.m<sup>3</sup> of water within a surface of 2.6 km<sup>2</sup> and to generate up to 392 MW (TIWAG, 2023). Apart from the gauging station that records measurements of runoff at the outlet of the catchment, several meteorological stations are available within and near the area. A description of all the available and used data is presented in detail in Section 3.2.

## 3.2 Data

This section introduces the different input datasets used in the model simulations, like the land cover and glacier outlines. In addition, the datasets used during calibration and validation of the models (e.g. runoff) are also included.

### 3.2.1 Land cover and soil classification

The land cover and soil classification play a fundamental role in water balance modeling, affecting processes such as interception and water flow through the soils (i.e. baseflow, interflow). Hence, a correct representation of these variables should be ensured. Since the simulations are performed with a fully-distributed model, a high spatial resolution is also desired. Figure 3.2a shows the land cover, whereas Figure 3.2b shows the soil classification within the study area.

Due to its mountainous topography and location, the study area is predominately characterized by bare rocks and screes covered by perpetual snow and ice (80.2% of the total area). In the lower elevations and in the vicinity of the Gepatsch reservoir, forests and natural areas can be found, covering around 19.4% of the total area (representing forests only 2.8%). The land cover is adopted from the CORINE Land Cover 2018 of Europe (European Environment Agency, 2019), available at a 100 m x 100 m grid resolution (Figure 3.2a). As regards the soil classification, this is done according to the European Soil Data Centre (ESDAC), together with the soil profile analytical database 14 (SPADE 14) (Panagos et al., 2012, Figure 3.2b). In the southern part of the study area, in correspondence with the higher elevations and surfaces covered mainly by snow and ice, rock is the predominant soil type. When moving north towards lower elevations, the sand and loam content increases. Since these types of soils are characterized by a higher porosity compared to rocks, a higher content of water can be expected. Moreover, they are more fertile, allowing the growth of trees and other vegetation types in that area.

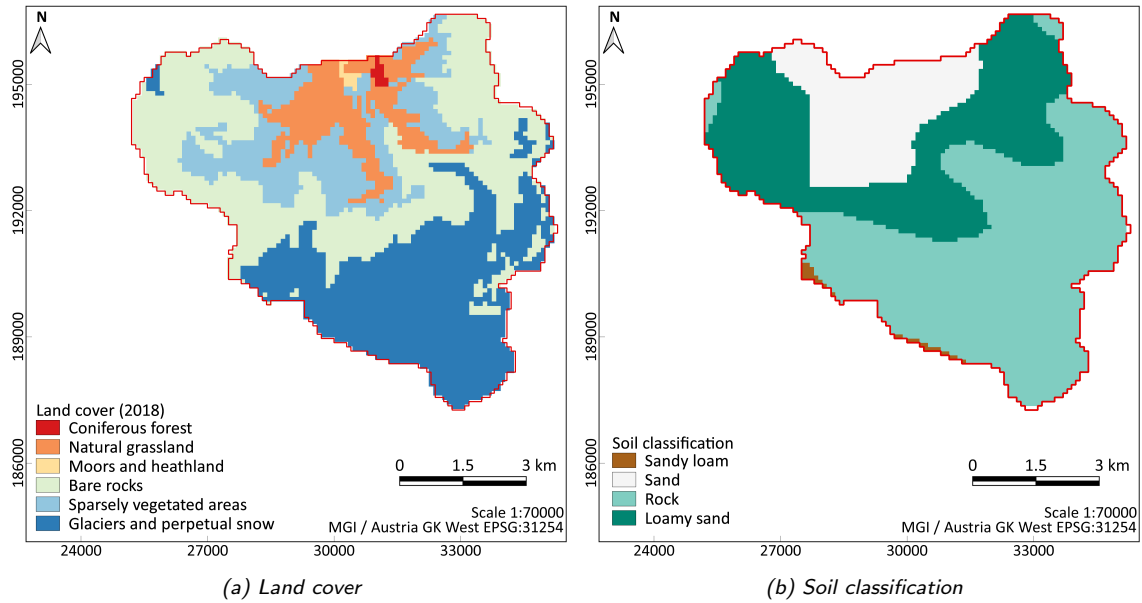


Figure 3.2: Land cover (adapted from European Environment Agency, 2019) and soil classification (adapted from Panagos et al., 2012) within the study area.

## 3.2.2 Glaciers

Since glaciers play a crucial role in the water balance of this type of regions, i.e. in the contribution to runoff generation, enough and reliable glaciers observations should be considered for performing model simulations, including calibration and validation of the model. On the one hand, glaciers' outlines can be accessed for specific years in the past, thus allowing a distributed representation of glaciers in space. On the other hand, continuous time series of mass balance are also available, though only for a few glaciers.

### 3.2.2.1 Glacier extents

The Austrian Glacier Inventory (AGI) offers four glacier outlines observed during the years: 1969 (Patzelt, 2013), 1998 (Kuhn et al., 2013), 2006 (Fischer et al., 2015b) and 2015 (Buckel and Otto, 2018). The latest versions are derived from high-resolution lidar DEMs and orthophotos (Fischer et al., 2015a). Furthermore, the Randolph Glacier Inventory (RGI) accounts for glacier outlines all over the world and the latest version is available for the year 2003 (RGI Consortium, 2017). Figure 3.3a depicts the glacier outlines according to the AGI and Figure 3.3b, the outlines according to the RGI. In addition, Figure 3.3b includes the elevation range at the tongue of the *Gepatschferner* (glacier ID RGI60-11.00746), for which measurements of the mass balance components at the tongue are also available (Section 3.2.2.2). The glacier outlines are utilized for (i) initializing the model in a certain year in the past and (ii) calibration and validation of the model.

### 3.2.2.2 Glacier mass balance

The World Glacier Monitoring Service (WGMS) has been collecting and disseminating data on glaciers fluctuations all over the world. In Central Europe, there are 15 glaciers that contain more than 30 years of measurements of the mass balance components (accumulation

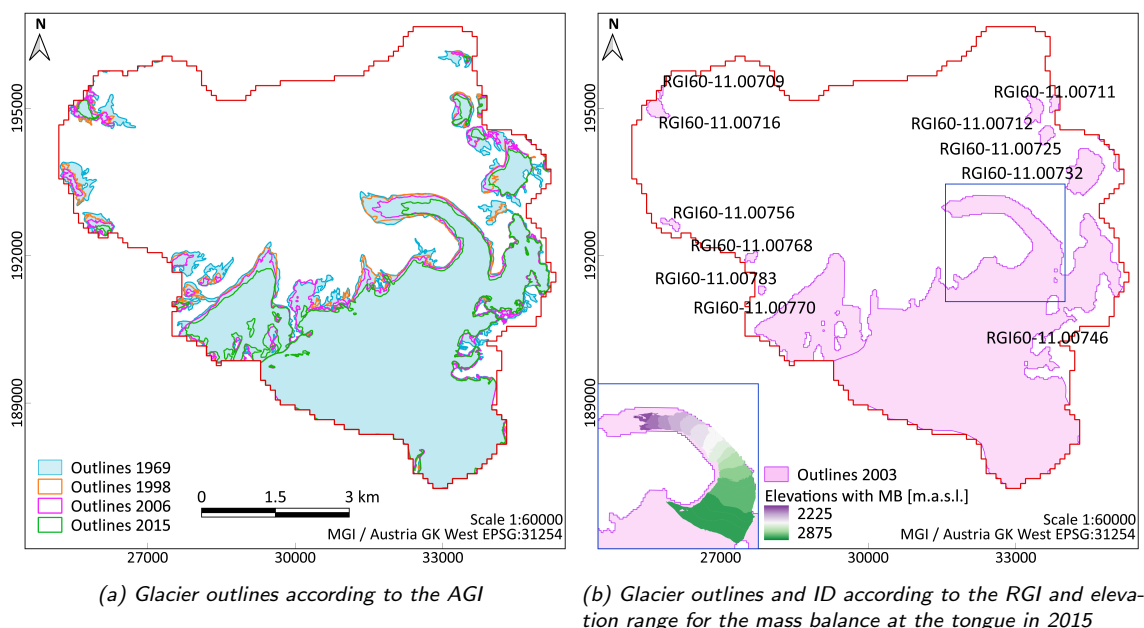


Figure 3.3: Glacier outlines for the years 1969, 1998, 2006 and 2015 (Patzelt, 2013; Kuhn et al., 2013; Fischer et al., 2015b; Buckel and Otto, 2018) and glacier ID and outlines for the year 2003 (RGI Consortium, 2017).

and ablation at different points (WGMS, 2022)), thus considered as reference glaciers. One of the main challenges regarding glacier modeling in this particular region is that none of the glaciers are included in the list of reference glaciers. Nonetheless, two latest datasets on mass balance observations may serve as a valuable tool for calibrating and validating the glacier model: (i) geodetic mass balances and (ii) mass balances at the tongue of a glacier. The techniques used in each of the methods were introduced in Section 2.2.3.

- (i) **Geodetic mass balance:** In this case, the mass balance components are derived from topographic changes. The latest dataset provided by Hugonnet et al., 2021, which covers the period between 2000 and 2020, offers the mean annual value of the geodetic mass balance for each glacier within the study area. Thus, these mean annual values are used for calibrating the glacier model.
- (ii) **Mass balance at the tongue:** A few gauges have been positioned since the year 2009 in the ablation zone of the main glacier in the study area, *Gepatschferner*, (RGI60-11.00746, Figure 3.3b), measuring melt and ice movement for the years 2012 to 2020. The measurements have been carried out for the elevation zones indicated in the figure and by Dr. Martin Stocker-Waldhuber at the Institut für Interdisziplinäre Gebirgsforschung der Österreichischen Akademie der Wissenschaften und Verein Gletscher und Klima. For more detailed information: Stocker-Waldhuber, 2019; Stocker-Waldhuber, 2020 and Appendix A.1.

### 3.2.2.3 Ice thickness

Between 1995 and 2014, point measurements of ice thickness were carried out on 66 glaciers in Austria by means of a Ground-penetrating radar (GPR, Section 2.2.3.5, Fischer and Kuhn, 2013; Fischer et al., 2015d). Within the study area, the three largest glaciers were

surveyed: *Gepatschferner* (RGI60-11.00746), *Östlicher Wannetferner* (RGI60-11.00732) and *Weißseeferner* (RGI60-11.00770), during the years 2001, 1996 and 2010, respectively. The mean thickness obtained from these measurements provides more insight into the accurate representation of the ice thickness obtained after performing OGGM's simulations, which is described in Sections 6.4.5 and 7.2.5. The location of the GPR points is shown in Figure A.2 in Appendix A.1.

### 3.2.3 Snow

Measurements of snow depth [m] and values of snow density [ $\text{kg m}^{-3}$ ] are available at a 15-min resolution for the period 10/2014 to 09/2018 at the Automatic Weather Station (AWS) located downstream the *Weißseeferner* glacier (RGI60-11.00770), as shown in Figure 3.1. The elevation at which the AWS is located is 2460 m a.s.l.. While snow depth is measured with two ultrasonic sensors, bulk snow density is calculated by means of the volumetric content of ice, water and air and snow depth, by using a Snow Pack Analyzer (SPA-2) (Schöber et al., 2019). Due to the short covered period of snow measurements, this dataset is not considered during calibration of the model, but is used during validation.

#### 3.2.3.1 Snow Water Equivalent

In hydrological modeling it is common to study the snow contribution to runoff generation by means of the snow water equivalent (SWE), given in mm of water equivalent. Since SWE is difficult to measure and often not directly available, SWE can be estimated from measured snow depth (SD) and bulk density ( $\rho_{snow}$ ) (Jonas et al., 2009).

From the averaged daily values of SD and  $\rho_{snow}$ , the SWE of the snowpack can be calculated using the following relationship according to Schattan et al., 2017:

$$SWE = \rho_{snow} \times SD \quad (3.1)$$

Where: SWE is the calculated snow water equivalent [ $\text{mm d}^{-1}$ ],  $\rho_{snow}$  is the bulk density [ $\text{kg m}^{-3}$ ] and SD is the snow depth, determined on a daily basis [m]. The relationship yields to  $\text{kg m}^{-2}$ , but knowing that the density of water is  $1 \text{ kg l}^{-1}$ , it is possible to express the SWE in mm.

#### 3.2.3.2 Snow coverage

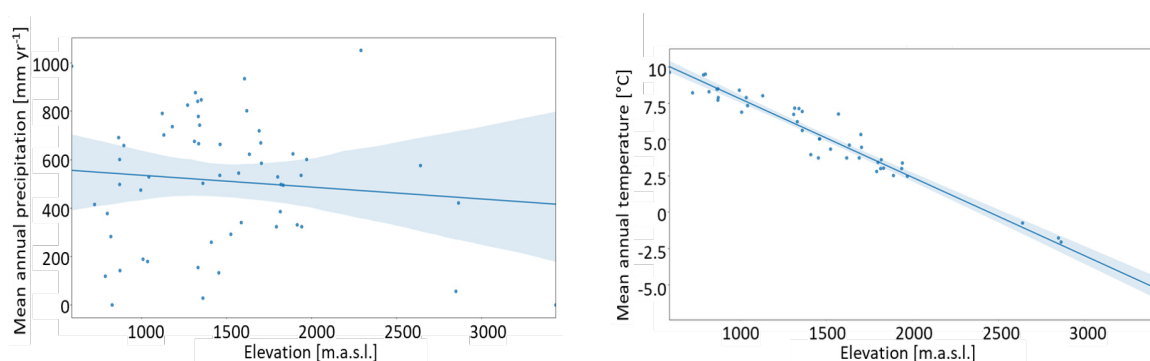
Apart from measurements of the snow depth (and consequent determination of the SWE) at certain points, it is possible to represent the distribution of snow over the catchment by means of snow cover maps. These products can provide, for example, the fraction of snow cover at the top of the canopy or on ground. The values are obtained through Sentinel-2 and Sentinel-1 data and are available thanks to the Copernicus Land Monitoring Service (European Environment Agency, 2020). The datasets are available with a spatial resolution of  $20 \text{ m} \times 20 \text{ m}$  and from the year 2016 onward. The snow cover maps can be used afterwards to complement the validation of the model by comparing them with simulated snow distribution, for selected days in which the sky is free from clouds.

### 3.2.4 Climate

The study area is characterized by a typical dry high-alpine climate (Groh and Blöthe, 2019; Hanzer et al., 2016), where the mean annual total precipitation recorded by two nearby stations (2640 and 1915 m a.s.l.) was 700 mm for the period 1990-1997, and the mean annual temperature for the same period was  $-1.2\text{ }^{\circ}\text{C}$ .

#### 3.2.4.1 Meteorological data

One of the main challenges in mountainous regions is the limited availability of meteorological stations. Within and around the modeled area (with a radius of approx. 30 km) more than 50 stations have been measuring both hourly and daily values of precipitation (P), temperature (T), relative humidity (RH), wind speed (WS) and global radiation (GR). However, only a few of them cover all variables and a period long enough for the simulation of glacier evolution. In addition, all variables require the extrapolation from the station's location to the center of the model grid cells, for which different methods can be applied (e.g. Inverse distance weight method (IWD), bilinear interpolation, etc.). The broad altitude range of the region, which varies from 1880 to 3495 m a.s.l. (Figure 3.1) is of major importance, since stations should be distributed along all different elevation zones for achieving an acceptable estimation of the extrapolated gridded values. More than 30% of the model grid cells are distributed within an altitude range of 3000 to 3500 m a.s.l., but only 16% of the stations are located above 3000 m a.s.l. Even though precipitation does not show a marked elevation dependence (Figure 3.4a), temperature is highly dependent on it (Figure 3.4b).



(a) Total (averaged) annual precipitation (1969-2006) vs. elevation (b) Mean (averaged) annual temperature (1969-2006) vs. elevation

Figure 3.4: Elevation dependency of total annual values of precipitation and mean annual values of temperature, for the period 1969 to 2006 and averaged over all available meteorological stations. The shaded area shows the confidence interval of the fitted regression line.

For the case of temperature, the extrapolation of point values to the model grid cells can be achieved by applying a lapse-rate, by assuming that temperature decreases with elevation. Many studies have successfully applied such method (e.g. Hanzer et al., 2016; Kormann et al., 2016; Stoll et al., 2020) in combination with other approaches, like the IDW method, for hydrological modeling. However, the determination of the lapse rate might be arduous. Although a unique and uniform value is usually adopted, this may not accurately represent reality. Therefore, monthly or seasonal values for lapse rates may serve as a suitable option. Moreover, identifying the terrain surrounding the stations is also crucial as

certain features, such as being situated above a glacier, can impact the local temperature (Minder et al., 2010).

Lately, there has been significant improvement on analysis or re-analysis datasets. These datasets can tackle the issue of having scarce meteorological stations, since a higher spatio-temporal representation of meteorological variables can be achieved (e.g. Förster et al., 2014). In this context, the Austrian Meteorological Service (Zentralanstalt für Meteorologie und Geodynamik, ZAMG) offers a multivariable analysis and nowcasting system, Integrated Nowcasting through Comprehensive Analysis system (INCA, Haiden et al., 2011), in which real-time observations and high-resolution topographic data are used to complement the model outputs of numerical weather predictors. Temperature, humidity and wind are analyzed and forecast in three dimensions, following three steps: (i) a first guess (interpolation of the weather forecast into INCA grid), (ii) observation correction and (iii) nowcast. For the case of precipitation, this is analyzed in two dimensions by (i) analysis (station data combined with radar observations) and (ii) nowcast (Haiden et al., 2011). Additionally, the impact of topography is taken into account for temperature and precipitation, with the latter also being obtained from a re-analysis dataset. Following the example of some successful applications of these datasets for hydrological modeling (e.g. Förster et al., 2018; Schöber et al., 2010), the INCA dataset is used in this study. The spatial resolution of a cell is 1 km x 1 km, whereas the variables are provided with a 1-hour time step (except precipitation, which is available at a 15-min resolution). The period covered by INCA spans from the year 2003 to present.

#### **3.2.4.2 Analogous downscaling method**

One drawback of the INCA dataset is its relatively short temporal coverage. For performing model simulations in the past, a dataset covering the entire simulation period must be available, including the initial year for which glacier outlines are at hand. In addition, when performing model simulations under future climatic conditions, a bias adjustment of the future climate model data is done based on reference datasets (usually observations). The reference dataset must be long enough to ensure the correct applicability of the methods. To overcome these limitations, an analogous downscaling approach is adopted to extend the dataset into the past (back to the year 1969). In this sense, a kNN (k-Nearest Neighbor, Lall and Sharma, 1996; Winter et al., 2019) re-sampling method was developed to automatically select appropriate days from station data. The extended INCA dataset with relatively short temporal coverage, allows long-term simulations given daily station data as a reference. Additional explanations of the method can be found in Appendix A.2 and the full description of the method is available in the Master Thesis developed by Philipp Schulte Overberg (Philipp Schulte Overberg, 2021).

#### **3.2.4.3 Future projections**

Climate projections are used as input data to run the models in the future. This allows not only to predict the catchment's hydrological and glaciological response until the end of the century, but also to evaluate the performance of the coupling scheme developed in this thesis. To achieve this, high-resolution regional climate model data provided by the EURO-CORDEX initiative (Jacob et al., 2014) is used. The regional climate model data comes at a horizontal resolution of 0.11 degrees and three different climate model

combinations are selected. These are composed of three Global Climate Models (GCM) and three Regional Climate Models (RCM) under different Representative Concentration Pathways (RCP 2.6, 4.5 and 8.5) which are summarized in Table 3.1. The reference period is taken from 01/1971 to 12/2000 and the data was bias adjusted following the Multi-scale bias AdjuStment (MidAS) tool (v0.2.1.), developed by Berg et al., 2022, using the developed INCA-kNN as reference dataset. The future projections were provided by Dr. Thomas Bosshard, project partner and colleague at the Swedish Meteorological and Hydrological Institute.

Table 3.1: GCMs and RCMs considered for the prediction of the catchment's response in the future.

GCM	RCM
ICHEC-EC-EARTH	SMHI-RCA4_v1a
MPI-M-MPI-ESM-LR	SMHI-RCA4_v1
MOHC-HadGEM2-ES	KNMI-RACMO22E_v2

### 3.2.5 Runoff

The main components of the runoff are snow and ice melt. This makes the runoff regime strongly dependent on seasonality, being its regime nivo-glacial (Förster et al., 2016; Hanzer et al., 2018). Runoff at the outlet of the Gepatschalm catchment is available since 1985, at an hourly resolution. The location of the gauge is shown in Figure 3.1. During the summer (June to August) of 2016 - 2018, between 327 to 527 mm month<sup>-1</sup> were registered, whereas the values decreased to 10 mm month<sup>-1</sup> during winter months (December to March) (BMLRT, 2021). The runoff, aggregated to a daily time step, is used as the main variable when calibrating and validating the water balance model and the coupling scheme.



# Chapter 4

## Water balance modeling

The water balance components are simulated using the **Water Flow and Balance Simulation Model**, **WaSiM** (Schulla, 1997; Schulla, 2021). WaSiM is a spatial fully-distributed model, capable of simulating the water cycle above and below the soil surface. WaSiM is available in two versions: (i) the Topmodel version, in which the soil is simulated following the conceptual approach based on variable saturation areas and (ii) the Richards version, in which detailed soil physical properties are used to simulate water transport in the soil. In this study, the WaSiM Richards version 10.06.04 (2021) for Windows is used.

The model structure followed by WaSiM is shown in Figure 4.1. For each time step (i.e. each day), a series of processes are carried out on each cell of the defined model grid. Different approaches are available for each of the processes described in the figure, which are also summarized in Table 4.1. In addition, a detailed description of each process is presented in the following sections. All of the descriptions refer to the model's documentation (Schulla, 2021).

Table 4.1: Summary of the main processes included in WaSiM.

Process	Approach
Precipitation correction	Based on threshold temperature and wind speed
Interpolation of meteorological data	Bilinear interpolation method
Radiation correction	Based on the impacts of topography
Potential evapotranspiration	Penman-Monteith
Real evapotranspiration	Richards equation
Interception	Bucket approach
Snow accumulation and melt	Energy balance with snow redistribution
Glacier model	Dynamic glacier model <sup>1</sup>
Soil model	Unsaturated zone with Richards equation
Discharge routing	Kinematic wave approach and single linear storage

<sup>1</sup> Described separately in Section 5.1.

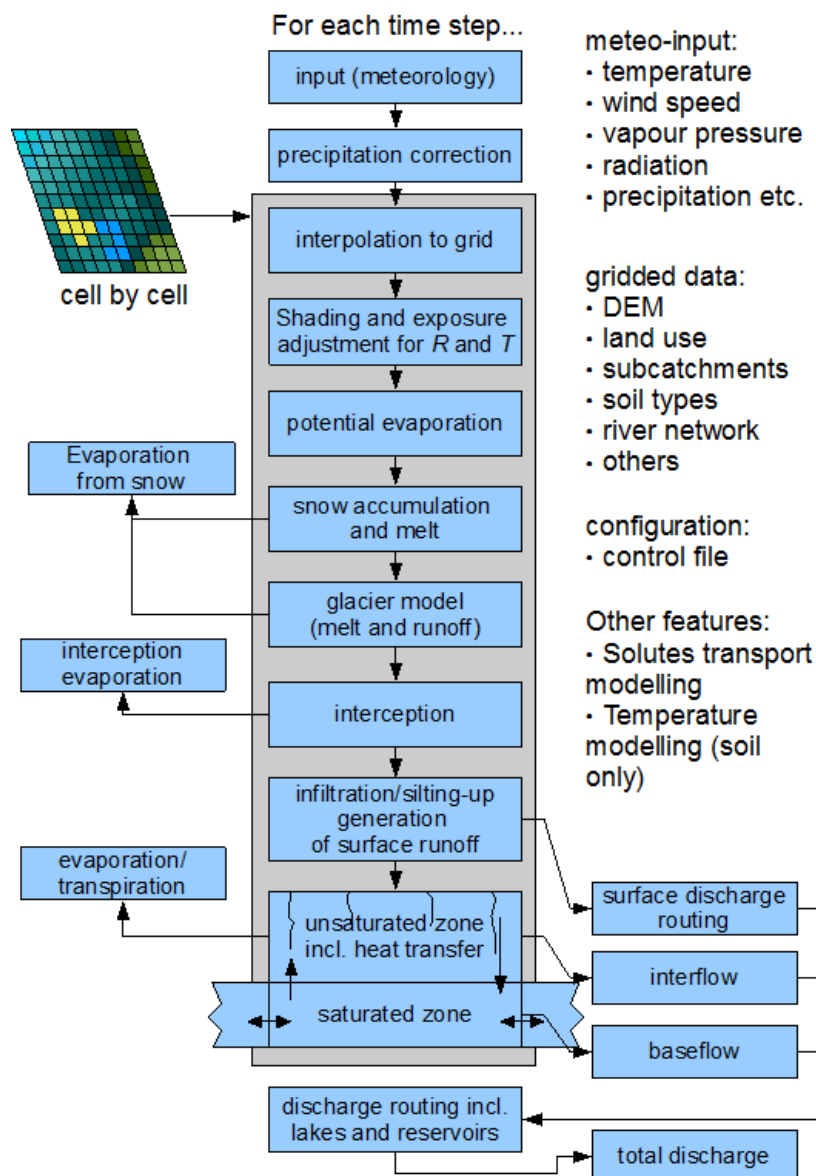


Figure 4.1: WaSiM model structure (Schulla, 2021).

## 4.1 Model resolution and simulation period

Even though the model is able to perform simulations on a minute-based resolution, a daily time step is adopted in this study. The reason of this choice is that the main focus of the simulations is given to the long-term water balance and study of glacier evolution. A finer temporal resolution could be well justified in other cases, such as for short-term simulations (floods), among others, but they are not the main aim of this study. Furthermore, WaSiM is a gridded-based model; thus the spatial resolution of the grid cells must be defined. In the case of Gepatschalm, model grid cells of 100 m  $\times$  100 m (area of a model cell = 0.01 km<sup>2</sup>) are adopted. Due to the high dependency of some variables to the altitudinal differences (high topography gradients, typical characteristic of mountainous regions, like depicted for temperature in Figure 3.4b), a coarser resolution might lead to more inaccurate results. Moreover, a more precise representation can be achieved by the selected spatial resolution, as glaciers tend to retreat faster along the tongue, which occupies a smaller area

than the total glacier. On the other hand, using a finer resolution to obtain more detailed information on simulation results might result in longer simulation times.

The model needs to be initialized with known glacier conditions. For this reason, and to study the glacier's evolution in the past years while maximizing the use of available observations, the year 1969 is selected as starting point for the simulations. For this year glacier outlines are available from the AGI, as described in Section 3.2.2. In this model run, where WaSiM is set up with its internal dynamic glacier model (no coupling scheme yet), the model runs in a continuous mode. Moreover and due to the extensive area covered by glaciers, the entire catchment is divided in subcatchments in order to analyze the evolution of the glaciers separately. Therefore, a new subcatchment is created for every glacier with a total covered area exceeding 1 km<sup>2</sup> (in 1969). This is particularly useful when studying the mass balance of the glaciers and comparing it with observations, if available.

Figure 4.2 shows the timeline used during WaSiM simulations. The model is initialized in 1969 and run continuously until 2018. Since observed runoff is available from 1985 to 2018, the period from 1985 until 2018 is selected for calibration and validation of the model. The total period is split into three parts: the period from 1969 to 1984 is used as warm-up, the period from 1990 to 2006 is used for calibration and the periods from 1985 to 1989 and from 2007 to 2018 are used for validation of the model. The break point in 2006 coincides with available glacier observations, thus it is a good chance to check the performance of the model regarding glaciers at the end of the calibration period. In addition, the available snow measurements at *Weißsee* station allows a comparison between observed and simulated SWE, for the period 2015 to 2018. The calibration and validation of the model is described in detail in Section 6.3.2 and the corresponding results are presented in Section 7.1.2.

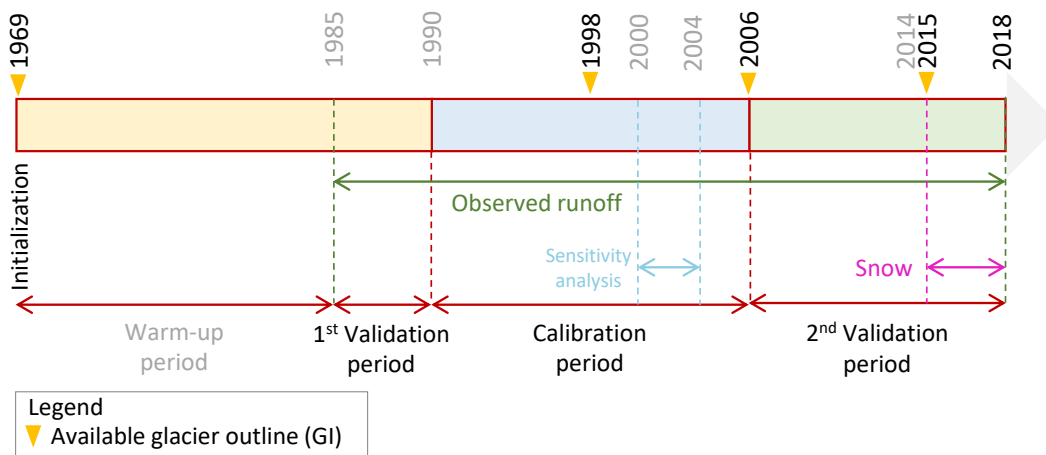


Figure 4.2: Simulation period selected for running WaSiM.

## 4.2 Precipitation correction

Before performing any simulation, precipitation input is corrected. This correction is done because solid precipitation is usually underestimated due to wind induced undercatch, wind

losses and evaporation losses (Sevruk, 1982; Hanzer et al., 2016). In this context, WaSiM performs the precipitation correction separately for rain and snow, based on a threshold temperature and the wind speed at each time step, according to Equation 4.1:

$$\begin{aligned} P_{corr} &= P \times (a_l + b_l \times u_w) & T \geq trs \\ P_{corr} &= P \times (a_s + b_s \times u_w) & T < trs \end{aligned} \quad (4.1)$$

Where:  $P_{corr}$  is the corrected precipitation [mm],  $P$  is the measured precipitation [mm],  $T$  is the measured air temperature [ $^{\circ}\text{C}$ ],  $tr_s$  is the threshold temperature that separates rain from snow [ $^{\circ}\text{C}$ ],  $u_w$  is the wind speed [ $\text{m s}^{-1}$ ],  $a_l$  [-] and  $b_l$  [ $\text{s m}^{-1}$ ] are correction parameters for rain (liquid precipitation), and  $a_s$  [-] and  $b_s$  [ $\text{s m}^{-1}$ ] are correction parameters for snow (solid precipitation).

The parameters involved in the correction of the precipitation are manually calibrated during a first step, where average annual precipitation values are compared to reference values provided by Hanzer et al., 2016, for the period 1997-2006. In that study, which also covers the Gepatschalm study area, precipitation was corrected twice: a second correction step was carried out after interpolation of the data and by applying a constant factor to the solid fraction of precipitation, ensuring that snowfall was not underestimated.

### 4.3 Interpolation of meteorological data

As presented in Section 3.2.4.1, the INCA-kNN dataset is used as meteorological input data. The variables are available with a spatial resolution of  $1 \text{ km}^2$ , whereas the model grid cells have a size of  $0.01 \text{ km}^2$ . Thus, an extrapolation to downscale the input dataset is required, so each cell in the model contains meteorological data, for each time step considered in the entire simulation period.

Following the recommendations from Dr. Schulla (model developer) and the hints given in the manual's documentation, a bilinear interpolation method is selected for all variables. Within this method and for each model cell, the next input stations are searched in the four quadrants, like the example shown in Figure 4.3.

A bilinear interpolation consists on two linear interpolations along the  $x$ -axis and one linear interpolation along the  $y$ -axis:

First, the auxiliary point  $z_j$  is defined as (linear interpolation along the  $x$ -axis):

$$z_j = z_3 \times \frac{(x_2 - x)}{(x_2 - x_1)} + z_4 \times \frac{(x - x_1)}{(x_2 - x_1)} \quad (4.2)$$

and the auxiliary point  $z_k$  is defined as (also linear interpolation along the  $x$ -axis):

$$z_k = z_2 \times \frac{(x_2 - x)}{(x_2 - x_1)} + z_1 \times \frac{(x - x_1)}{(x_2 - x_1)} \quad (4.3)$$

Then, the search point  $z_i$  can be written in terms of the previously defined  $z_j$  and  $z_k$  points (linear interpolation along the  $y$ -axis):

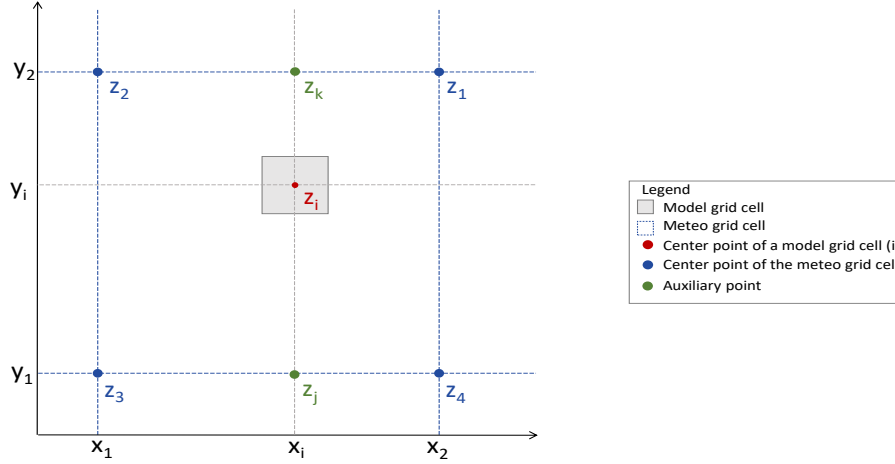


Figure 4.3: Example of a bilinear interpolation for point  $i$  from the meteorological input grid (Adapted from Schulla, 2021)

$$z_i = z_j \times \frac{(y_2 - y)}{(y_2 - y_1)} + z_k \times \frac{(y - y_1)}{(y_2 - y_1)} \quad (4.4)$$

If we consider that

$$u = \frac{(x - x_1)}{(x_2 - x_1)}; v = \frac{(y_2 - y)}{(y_2 - y_1)} \quad (4.5)$$

are the weights of the data in the stations used in the interpolation, then we can express the searched point  $z_i$  in terms of weights by using the following equation:

$$z_i = u \times (1 - v) \times z_1 + (1 - u) \times (1 - v) \times z_2 + (1 - u) \times v \times z_3 + u \times v \times z_4 \quad (4.6)$$

Where:  $z_i$  is the interpolated value of the meteorological variable at point  $i$ ;  $u$  and  $v$  are the weights of the data corresponding to the stations (Equation 4.5);  $z_{1-4}$  are the values observed at stations 1 to 4.

## 4.4 Radiation correction

The solar radiation is composed of *diffusive* and *direct-beam* short-wave radiation. In an idealized surface (i.e. extensive, flat and uniform), the behavior against solar radiation is equal at every point (Oke, 1987). However, if the surface presents varying topography, like in the case of Alpine catchments, the differences of slope and aspect interact with the incoming solar radiation and hence the behavior of the surface is different. In order to handle the effects of topography in the incoming solar radiation, WaSiM performs an adjustment based on the scheme developed by Oke, 1987. The corrected interpolated global radiation can be determined according to Equation 4.7:

$$RG_{eff} = RG \times \left( 1 + (1 - cr_0) \times SSD \times \left[ \frac{\cos \hat{\theta}}{\cos Z} - 1 \right] \right) \quad (4.7)$$

Where:  $RG$  is the interpolated global radiation [ $\text{Wh m}^{-2}$ ],  $cr_0$  is an empirical factor that considers the diffusive shortwave radiation [-],  $SSD$  is the interpolated relative sunshine duration (in this case computed by the model) [h],  $\hat{\theta}$  is the angle between the direction of the sun and the normal to a model cell [rad] and  $Z$  is the zenith angle [rad] (Schulla, 2021).

## 4.5 Evapotranspiration

Since the northern part of the study area contains different vegetation types (Figure 3.2a), transpiration and evaporation from plants might play a fundamental role in the water balance for this specific region. The potential evapotranspiration is determined after Penman-Monteith (Equation 4.8 Penman, 1978, the full set of equations can be found in the model's documentation Schulla, 2021), which is derived based on radiation and energy balances for a reference crop with unique properties. In order to extend the approach to the real vegetation and soil characteristics within the study area, the actual evapotranspiration is then determined based on some properties of the vegetation (e.g. minimum surface resistance of the plant, Leaf Area Index (LAI), etc.). Furthermore, the potential evapotranspiration is reduced according to the actual soil water content and capillary pressure, which are determined by the van Genuchten parameters (van Genuchten, 1980).

$$\lambda E = \frac{3.6 \times \frac{\Delta}{\gamma_p} \times (RN - G) + \frac{\rho \times c_p}{\gamma \times r_a} \times (e_s - e) \times t_i}{\frac{\Delta}{\gamma_p} + 1 + \frac{r_s}{r_a}} \quad (4.8)$$

Where:  $\lambda$  is the latent heat of vaporization [ $\text{KJ kg}^{-1}$ ],  $E$  is the latent heat flux [ $\text{kg m}^{-2}$ ],  $\Delta$  is the slope of the saturated vapor pressure curve [ $\text{hPa K}^{-1}$ ],  $\gamma_p$  is the psychrometric constant (as function of pressure and temperature) [ $\text{hPa K}^{-1}$ ],  $RN$  is the net radiation [ $\text{Wh m}^{-2}$ ],  $G$  is the soil heat flux [ $\text{Wh m}^{-2}$ ],  $\rho$  is the density of dry air [ $\text{kg m}^{-3}$ ],  $c_p$  is the specific heat capacity of dry air at constant pressure [ $\text{KJ (kg.K)}^{-1}$ ],  $e_s$  and  $e$  are the saturation and actual vapor pressure, respectively [ $\text{hPa}$ ],  $r_s$  and  $r_a$  are the bulk-surface and aerodynamic resistances, respectively [ $\text{s m}^{-1}$ ].

## 4.6 Interception

Rainfall that is intercepted by the canopy is determined based on the LAI, the vegetation coverage degree and the maximum height of water at the leafs, following a simple bucket approach (Schulla, 2021). With the most recent advances on the model, it is also possible to simulate the solid part of the precipitation that intercepts the canopy. The implementation of this canopy snow interception, which was developed by Förster et al., 2018, means a step forward for accurately representing the variability of snow in forest areas. In the present study, though, the canopy snow interception is not activated, since the proportion of coniferous forests is very small (less than 3%).

## 4.7 Snow accumulation and melt

In Alpine regions, snow is one of the determinant processes in the hydrology of the catchment. Snow that is accumulated will eventually turn into ice and therefore contributes to the mass gain of glaciers. Similarly, the part of the snow that melts, contributes to the runoff generation. There are different methods that can provide estimates of the amount of snow melt, like the T-index approach, or even physically-based methods, like an energy balance (similar to the glaciers, Section 2.3.2.1).

### 4.7.1 Snow accumulation

The total precipitation falling into the study area is separated into rain and snow. The accumulation of snow is then given by a fraction of the total precipitation ( $P_{total}$ ) that depends mainly on the air temperature, represented by Equation 4.9, which is valid for  $(T_{R/S} - T_{trans}) < T < (T_{R/S} + T_{trans})$ :

$$P_{snow} = P_{total} \times \frac{T_{R/S} + T_{trans} - T}{2 \times T_{trans}} \quad (4.9)$$

Where:  $P_{snow}$  is the snow precipitation [mm],  $T_{R/S}$  is the temperature at which 50% of the precipitation is falling as snow [°C],  $T_{trans}$  is half of the temperature-transition range from snow to rain [°C] and  $T$  is the air temperature [°C].

In the snow model, redistribution of snow is also considered. This can be explained by two mechanisms: (i) snow redistribution due to wind and (ii) snow redistribution due to gravitational slides. Both cases were implemented in WaSiM after Warscher et al., 2013 and selected within this study and are briefly explained in the next sections.

#### 4.7.1.1 Lateral wind driven snow redistribution

Snow can be redistributed throughout the catchment due to wind. It consists on increasing snow fall in the model grid cells that are sheltered from the main wind direction and decreasing it on wind-exposed model grid cells. The exposure of the grid cells can be determined with the directed sky view factor ( $SVF_{dir}$ , i.e. fraction of the overlying hemisphere occupied by sky, Oke, 1981) and the snow precipitation is corrected by means of Equation 4.10:

$$P_{snow} = P_{snow} + C_{wind} \times P_{snow} \quad (4.10)$$

Where:  $P_{snow}$  is the solid precipitation, previously determined according to Equation 4.9 [mm] and  $C_{wind}$  is the correction factor applied to each model grid cell and determined by Equation 4.11:

$$C_{wind} = E \times (D_{max} \times (1 - SVF_{dir}) - 1) + c_{min} \quad (4.11)$$

In this case,  $E$  represents a linear elevation weighting factor [-],  $D_{max}$  the maximum possible deposition [-] (recommended value: 2),  $SVF_{dir}$  the directed sky view factor [-] and

$c_{min}$  a minimum correction factor for shifting  $c_{wind}$  (recommended value: 0.2).

#### 4.7.1.2 Gravitational snow redistribution

This process originates at steep slopes and transports snow to lower areas, thus snow at one model grid cell might be transported to any neighboring cells with lower elevation. Many parameters describe this process, such as the minimum slope for creating a slide or the fraction of the snow pack that contributes to the slides. The procedure is based on the conservation of mass and flow propagation through multiple directions (Gruber, 2007; Warscher et al., 2013). The outflow from a cell [mm w.e.] is given by Equation 4.12:

$$M_{out} = \begin{cases} f_{erosion} \times SWE + M_{in} - D_{grav} & \text{if } i \geq i_{erosion} \text{ and } SWE > 0 \\ M_{in} - D_{grav} & \text{if } i \geq i_{erosion} \text{ and } SWE = 0 \\ M_{in} - D_{grav} & \text{if } i < i_{erosion} \end{cases} \quad (4.12)$$

Where:  $f_{erosion}$  is an erosion factor that depends on the simulation time step [-],  $SWE$  is the SWE in the considered model grid cell [mm w.e.],  $M_{in}$  is the inflow from neighboring cells [mm w.e.],  $i$  is the local slope [°],  $i_{erosion}$  is the lower inclination limit for snow erosion [°] (ranging from 0 to 90°) and  $D_{grav}$  is the deposition of snow in the considered model grid cell [mm w.e.] (Equation 4.13).

$$D_{grav} = \begin{cases} M_{in} & \text{if } M_{in} < D_{max,grav} \\ D_{max,grav} & \text{if } M_{in} \geq D_{max,grav} \end{cases} \quad (4.13)$$

Where  $D_{max,grav}$  [mm w.e.] and can be determined by Equation 4.14, being  $D_{lim}$  the maximum snow mass that could be deposited on a model grid cell (i.e. mass limit) [mm w.e.] and  $i_{lim}$  the upper slope limit [°] (i.e. the incoming sliding snow above this value will be transported downstream).

$$D_{max,grav} = \begin{cases} (1 - \frac{i}{i_{lim}}) \times D_{lim} & \text{if } i < i_{lim} \\ 0 & \text{if } i \geq i_{lim} \end{cases} \quad (4.14)$$

Due to the unknown nature of the involved parameters, they are considered in the calibration of the model and a precedent sensitivity analysis (Section 6.3.1). One of the main effects of the gravitational snow redistribution can be seen for example in the valleys, where a higher accumulation of snow is expected. As a result, a grid cell in that area might show a higher fraction of glacierization throughout the years, since snow is accumulated and then transformed into firn and finally into ice. This could result in an increase of the glacier areas and thus leading to a lower model performance in terms of glacier/snow.

#### 4.7.2 Snow melt

For the determination of snow melt, several approaches are available within WaSiM. In this study, an energy balance approach is chosen. The energy balance considers all fluxes into and out of the snow pack, like described by Equation 4.15:



$$Q + H + E + A + G + M = 0 \quad (4.15)$$

Where:  $Q$  accounts for the radiation balance between short and long wave radiation,  $H$  is the sensible heat flux,  $E$  is the latent heat flux,  $A$  is the advective heat flux by precipitation,  $G$  is the ground heat flux and  $M$  is the energy available for melting and/or sublimation, all given in  $[\text{W m}^{-2}]$ . The radiation balance ( $Q$ ) can be expressed by terms of Equation 4.16:

$$Q = (1 - \alpha) \times RG + LW_{in} + LW_{out} \quad (4.16)$$

Where:  $\alpha$  is the albedo (which varies between 0.5 and 0.9),  $RG$  is the global (short wave) radiation  $[\text{W m}^{-2}]$  and  $LW_{in}$  and  $LW_{out}$  are the incoming and outgoing long wave radiation  $[\text{W m}^{-2}]$ . The last two variables can be adjusted during calibration, for this reason, their sensitivity is tested a priori in a sensitivity analysis (Section 6.3.1).

In addition, the sensible heat flux ( $H$ ) and the latent heat flux ( $E$ ) are determined through empirical equations depending on the temperature and vapor pressures, respectively. The advective heat flux ( $A$ ) can be estimated by knowing the amount of solid/liquid precipitation, the air temperature and the specific heat capacity of water. The ground heat flux ( $G$ ) is set to  $2 \text{ W m}^{-2}$  (its value is smaller compared to the other fluxes). The respective equations can be found on the manual documentation (Schulla, 2021). Once the fluxes are determined, the remaining of the energy balance can be solved ( $M$ ), which can be either used for snow melt or sublimation, depending on the wet bulb temperature (temperature that results from evaporating as much water as required until saturation).

## 4.8 Soil model

The fluxes taking place within the soil are divided into two zones: (i) the unsaturated zone model and (ii) the saturated zone or groundwater model.

### 4.8.1 Unsaturated zone model

The fluxes within the unsaturated zone are modeled using the physically-based Richards equation, by considering a one-dimensional (vertical) direction through the soil with several layers. On the contrary, the lateral (horizontal) fluxes are represented by a conceptual approach. The general Richards equation is given by Equation 4.17 (Schulla, 2021):

$$\frac{\partial \theta}{\partial t} = \frac{\partial q}{\partial z} = \frac{\partial}{\partial z} \left( -k(\Theta) \times \frac{\partial \Psi(\Theta)}{\partial z} \right) \quad (4.17)$$

Where:  $\Theta$  is the water content  $[\text{m}^3 \text{ m}^{-3}]$ ,  $t$  is time  $[\text{s}]$ ,  $k$  is the hydraulic conductivity  $[\text{m s}^{-1}]$ ,  $\Psi$  is the hydraulic head as a sum of the suction head and geodetic altitude  $[\text{m}]$ ,  $q$  is the specific water flux  $[\text{m s}^{-1}]$  and  $z$  is the vertical coordinate  $[\text{m}]$ .

The model solves the discrete form of Equation 4.17 by applying the Van Genuchten method to parameterize the hydraulic properties of the soil (van Genuchten, 1980). The

fluxes along the vertical direction are composed by the interflow, drainage and infiltration from or exfiltration into rivers.

## 4.8.2 Groundwater model

WaSiM's unsaturated zone model can be coupled to any groundwater model, thus allowing the interaction between both zones through a bi-directional representation of the fluxes. However, in the Gepatschalm area, groundwater processes are not of great magnitude, since the predominant type of soil is extremely low permeable (i.e. rocky soils). In this case, the baseflow component can be represented through a conceptual approach (Equation 4.18, Schulla, 2021):

$$Q_B = Q_0 \times K_S \times e^{\frac{h_{GW} - h_{geo,0}}{k_B}} \quad (4.18)$$

Where:  $Q_B$  is the baseflow at each model grid cell [ $\text{m s}^{-1}$ ],  $Q_0$  is a scaling factor for baseflow [-],  $K_S$  is the saturated hydraulic conductivity [ $\text{m s}^{-1}$ ],  $h_{GW}$  and  $h_{geo,0}$  are the groundwater table from the unsaturated zone model and the geodetic altitude of the soil surface [m a.s.l.] and  $k_B$  is the recession constant for baseflow [m]. The parameters  $Q_0$  and  $k_B$  can be adjusted during calibration of the model.

## 4.9 Discharge routing

The routing through the channels is based on the kinematic wave approach and follows three main steps (Schulla, 2021):

- (i) **Translation within the channel:** The flow times are determined with the Manning-Strickler equation (e.g. Yen, 1992), which describes the flow through a channel that is assumed to be rectangular.
- (ii) **Retention:** After the translation of the flow wave through the channel is complete, the retention is considered (Equation 4.19). In this case, single linear reservoirs are applied for the main channel flow component and the flood plain flow component.

$$Q_{out,i} = Q_{i-1} \times e^{-\Delta t/k} + Q_i \times (1 - e^{-\Delta t/k}) \quad (4.19)$$

Where:  $Q_{out}$  is the outflow during time step  $i$  [mm],  $i$  is the time step,  $\Delta t$  is the length of the time step [h],  $k$  is the storage coefficient of the main channel or flood plains (e.g. for surface runoff, interflow, etc.) [h] and  $Q_i$  is the discharge in the main channel or flood plains [mm].

- (iii) **Superposition of discharges from different subcatchments:** Since the catchment is divided in several hydrological subcatchments, the discharges from each of them are superposed and routed to the outlet of the catchment. During this step, all routed discharges and the runoff from the catchment are superposed at the outlet weighted by their relative areas. If glaciers are present, the discharge generated from glacier melt is also superposed (depending if it comes from snow, firn and ice) to the final discharge of the catchment.

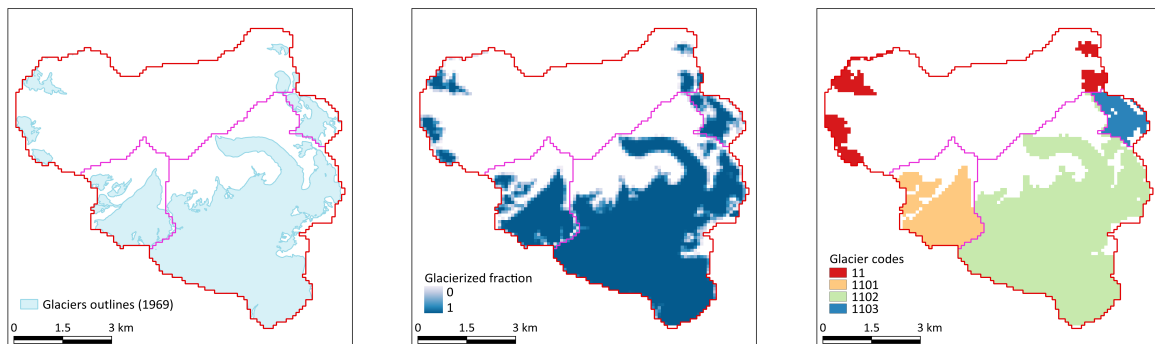
# Chapter 5

## Glacier modeling

### 5.1 WaSiM VA scaling glacier model

WaSiM provides two possibilities for modeling glaciers. On the one hand, the static model describes glacier melt and routing in a conceptual way and assumes that the geometry of the glacier remains unchanged throughout the simulations. On the other hand, the dynamic model allows to simulate not only the mass balance but also the changes in glacier geometry. Since in reality glaciers are dynamic entities which can advance and retreat, the consideration of a changing geometry is more adequate. For this reason, the dynamic glacier model is selected and used in this study. As an addition, this dynamic glacier model also includes a dynamic firn model, which considers the transformation from snow to firn and firn to ice (Schulla, 2021).

In order to initialize the dynamic glacier model in WaSiM, two glacier grids are required as input data. The first input grid contains the fraction of glacier coverage at each model cell. That means, that each cell can have a value that ranges between 0 (no glacier) and 1 (completely covered by glacier). For example, if a cell has a value of 0.35, that means that only 35% of the cell is covered by glaciers and this fraction will be used to determine the mass balance components and the new volume of the glacier. The second input grid contains glacier codes. These codes identify the subcatchment to which the glacierized cells (determined in the first input grid) belong. Figure 5.1 shows the procedure followed to determine the two input grids for activating the dynamic glacier model, starting from the available glacier outlines.



(a) Available data: AGI glacier outlines (1969, Fischer et al., 2015a)

(b) Fraction of glacier coverage for each cell, varying between 0 and 1

(c) Glacier codes, depending on the location within the subcatchments

Figure 5.1: Preparation of required glacier grids for running the dynamic glacier model (VA scaling approach) with WaSiM. The subcatchment' outlines are indicated in red.

### 5.1.1 Glacier mass balance

The mass balance of any glacier is determined following Section 2.2.2, in which a balance is done between the mass gained by the glacier (*accumulation*) and the mass lost by the glacier (*ablation*), after a certain period. In the dynamic model integrated in WaSiM, the accumulation counts for the amount of solid precipitation that falls over the glacierized area, the redistribution of snow (due to wind and gravitational slides) and the internal metamorphosis of snow to firn and then to ice. On the contrary, the melting component can be determined using the Temperature Index (T-index) method with or without accounting for radiation.

- (i) **Accumulation:** The amount of solid precipitation is determined at each time step considering the temperature threshold that separates rain from snow (Equation 4.1). All precipitation falling below this temperature threshold is considered snow and will be contributing to the mass gain of the glacier. Moreover, the change from snow to firn and from firn to ice also contributes as an internal process to the accumulation. If snow is not melted at the end of the mass balance period, then it becomes firn for the next period. This process occurs every period until firn turns into ice, which usually takes several years (e.g. seven years Schulla, 2021). As regards liquid precipitation (rain), it is generally treated as a loss to the system, although some complex models are able to consider re-freezing (Cogley et al., 2011).
- (ii) **Ablation:** The ablation accounts for the melt occurring in the glacierized areas. WaSiM calculates the melt based on the T-index method. The extended approach developed by Hock, 1999 considers also radiation as input variable. The melt rate is calculated with Equation 5.1:

$$M = \begin{cases} \left( MF + \alpha_{ice/firn/snow} \times I_0 \times \frac{G_s}{I_s} \right) \times (T - T_0) & T > T_0 \\ 0 & T \leq T_0 \end{cases} \quad (5.1)$$

Where:  $M$  is the melt rate [ $\text{mm d}^{-1}$ ],  $MF$  is the melt factor [ $\text{mm } ^\circ\text{C}^{-1} \text{d}^{-1}$ ],  $\alpha$  are empirical coefficients [ $\text{mm } ^\circ\text{C}^{-1} \text{d}^{-1}$ ],  $I_0$  and  $I_s$  are the potential direct incoming shortwave radiation at each model grid cell and at defined locations of meteorological stations, respectively [ $\text{Wh m}^{-2}$ ],  $G_s$  is the observed radiation at the same station [ $\text{Wh m}^{-2}$ ],  $T$  is the air temperature [ $^\circ\text{C}$ ] and  $T_0$  is the threshold temperature for melt [ $^\circ\text{C}$ ].

Even though radiation is available at a high temporal and spatial resolution, it is neglected during the determination of the melt rates. This choice is made to perform a more direct comparison between the results obtained by applying the VA scaling glacier model and the results from OGGM (Section 5.2.3), which does not include radiation in the determination of the glacier melt. To neglect radiation in Equation 5.1, the empirical coefficients  $\alpha$  are set to 0.

After *accumulation* and *ablation* are calculated, the mass balance of the glacier can be determined for each year by means of Equation 2.3.

### 5.1.2 Glacier retreat and advance

The dynamic glacier model integrated in WaSiM also allows to simulate the changes in the glacierized areas, that is, it considers the advance (growth) and retreat (shrinkage) of the glaciers. These changes are simulated with the Volume-Area (VA) scaling approach, based on the empirical relationship described by Chen and Ohmura, 1990a and physically validated by Bahr et al., 1997. This relationship is explained by Equation 5.2, which is an adaptation of the general Equation 2.7, introduced in Section 2.3.2.2:

$$V = b \times A^f \quad (5.2)$$

Where:  $V$  is the volume of the glacier [ $\text{m km}^2$ ],  $A$  is the area of the glacier [ $\text{km}^2$ ],  $b$  is an empiric factor that represents the mean ice thickness [ $\text{m}$ ] of a 1 [ $\text{km}^2$ ] glacier (default value  $b = 28.5 \text{ m}$ ) and  $f$  is the scaling factor [-] (default value  $f = 1.36$ ). The default values recommended by WaSiM correspond to the relationship found by Chen and Ohmura, 1990a for 63 mountain Alpine glaciers. Essentially, the general Equation 2.7 aims to express glacier volume ( $V$ ) [ $\text{L}^3$ ] by knowing the glacier area ( $S$ ) [ $\text{L}^2$ ] (represented by  $A$  in Equation 5.2). For consistency of units, the scaling parameter is expressed in [ $\text{L}^{3-2\gamma}$ ], with  $\gamma$  representing the scaling exponent (shown as  $f$  in Equation 5.2). Since this scaling parameter can be intuitively interpreted as the mean ice thickness per unit of glacier area (Grinsted, 2013), Equation 5.2 approximates  $b$  as the scaling parameter. The VA scaling approach, which seeks to describe the changes in volume due to a change in area for an idealized glacier, gives only an approximation. Therefore, utilizing  $b$  as a mean ice thickness to calculate glacier volume by means of Equation 5.2 may be appropriate.

In order to initialize the model, only the area of the glacier is required, hence no information about the glacier thickness or volume is provided. This is mainly related to the availability of the data, since glaciers' areas have been more readily at hand than ice thickness measurements or models, which became more popular later than the VA scaling method. WaSiM determines then the initial volume of the glacier based on the area and Equation 5.2 at the beginning of the simulation. Thus, it is important to initialize the model at a year for which known glacier geometries are available.

At the end of the first mass balance year, the mass balance of the glacier is converted into a volume by taking into account the ice density. Usually, for the Northern Hemisphere the mass balance year is considered between 1<sup>st</sup> October and 30<sup>th</sup> September. Knowing that  $V_{old}$  is the volume of the glacier at the beginning of the mass balance year and  $V_{new}$  is the newly calculated volume at the end of the first year of the simulation, the latter can be expressed as:

$$V_{new} = V_{old} + \frac{MB_{new}}{\rho_{ice}} \times ice_{value} \times cell_{size} \quad (5.3)$$

Where:  $V_{new}$  is the new calculated volume [ $\text{m km}^2$ ],  $V_{old}$  is the initial volume of the glacier [ $\text{m km}^2$ ],  $MB_{new}$  is the mass balance of the glacier at the end of the mass balance year (determined following Equations 2.3 and 5.1) [ $\text{mm w.e.}$ ] or [ $\text{kg m}^{-2}$ ],  $\rho_{ice}$  is the ice density [ $\text{kg m}^{-3}$ ],  $ice_{value}$  is the number of cells identified as glacierized cells and  $cell_{size}$  is the size of one model cell [ $\text{km}^2$ ].

Then, with the new volume (Equation 5.3), the new area of the glacier after the end of the mass balance year can be obtained by means of Equation 5.2:

$$A_{new} = \left( \frac{V_{new}}{b} \right)^{\frac{1}{f}} \quad (5.4)$$

With the new glacier area  $A_{new}$ , WaSiM estimates the number of cells that need to be added or subtracted (in case the mass balance is positive or negative, respectively) based on an iterative process. This process is done by dividing the glacier into elevation bands of equal elevation differences (Schulla, 2021).

### 5.1.3 Routing of melt components to the catchment outlet

Since the melting of the glacier is composed of ice, firn and snow, the routed runoff of the glacierized subcatchment is obtained after applying a set of parallel reservoirs. Each reservoir is described by its own storage coefficient, depending on the type of element (ice, firn or snow). The routed runoff is then added to the total runoff at the outlet of the subcatchment (like described in Section 4.9).

## 5.2 The Open Global Glacier Model

The **Open Global Glacier Model (OGGM)** is an open source modeling framework able to simulate past and future glacier evolution of almost any glacier in the world (Maussion et al., 2019). OGGM is a continuously developing up-to-date framework, written in Python and available for Linux and MacOS operating systems. The constantly updated repository (<https://github.com/OGGM/oggm>) allows to browse through all the capabilities of the model, as well as to contribute to it. In this study, the version v.1.6 is used in a Linux platform (Maussion et al., 2023). As already described in Section 2.3.2.3, OGGM follows the actual flow of ice along the flowlines to estimate glacier evolution.

### 5.2.1 General workflow

The workflow followed by almost any glacier simulation with OGGM is explained with an example. In this case, the *Gepatschferner* is chosen and the workflow is shown in Figure 5.2 and described in the following items (Maussion et al., 2019):

- (a) **Preprocessing:** During this first task, a glacier directory is created for each of the glaciers that are considered during the simulations. OGGM automatically downloads the outlines of the glaciers from the RGI, together with the corresponding topographical dataset (DEM). In this case, the RGI version 6.0, representing the glaciers outlines for the year 2003 (RGI Consortium, 2017) and the NASADEM digital elevation model (NASA JPL, 2020) are selected, based on the best available dataset for the studied glaciers. Moreover, reference datasets for model calibration are also downloaded, i.e. geodetic mass balance.
- (b) **Flowlines:** For each glacier, OGGM computes the centerlines based on the algorithm developed by Kienholz et al., 2014, in which the terminus of the glacier is searched (described in detail under Section 5.2.2).

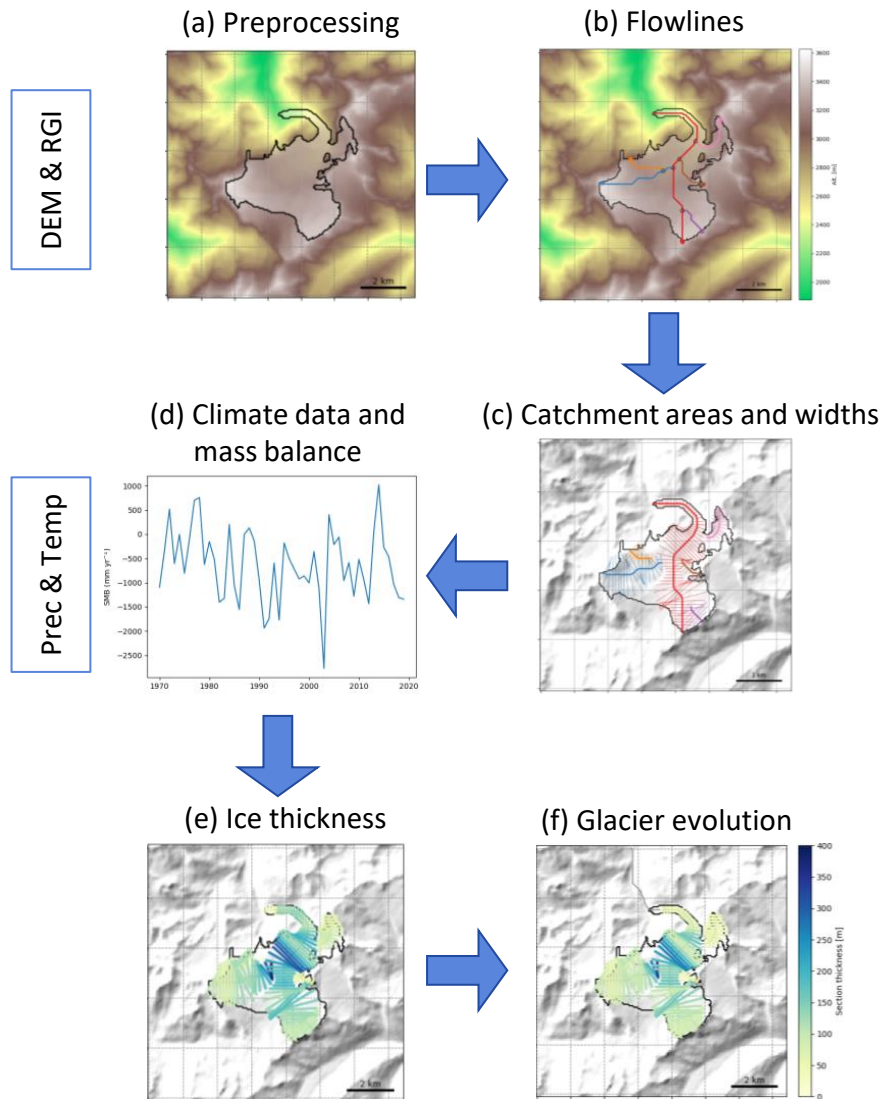


Figure 5.2: Example of the workflow followed in OGGM, applied to Gepatschferner (RGI60-11.00746).

- (c) **Catchment areas and widths:** A series of equally distributed points are selected along each of the flowlines and the corresponding widths are determined. This is simply done by intersecting the normals at each point with the glacier's outline. Furthermore, these widths are then corrected considering the actual area of each of the subcatchments defined within the glacier (for each of the flowlines, Section 5.2.2).
- (d) **Mass balances:** For each glacier, a historical time series of climate data (monthly values of precipitation and temperature) is created, for the center point of the glacier. Afterwards, the mass balance components of the glacier can be determined, by applying a calibrated T-index model (Section 5.2.3).
- (e) **Ice thickness inversion:** With the corresponding mass balance components of the glacier, considering conservation of mass and assuming a certain bed shape at each cross-section, the ice flow is computed for each point (Section 5.2.4).
- (f) **Glacier evolution:** Finally, a dynamic model simulation can be performed to see the evolution of the glacier under the given climatic conditions.

## 5.2.2 Glacier flowlines

In this section, a more detailed description on the determination of the glacier flowlines is presented. First of all, OGGM assumes that in each glacier, the ice flows only along the flowline. However, the geometrical width for each point along the flowline is known, hence the cross-sections of the flowline at those points can be determined. For this reason, the flowlines are then represented by a "1.5D" model, like in the example shown in Figure 5.3.



Figure 5.3: Example of the main glacier flowline along the tongue of Gepatschferner. The background image is from Stocker-Waldhuber, 2020 and the design of the flowline and cross-section was adapted from <https://docs.oggm.org/en/stable/flowlines.html>.

OGGM offers two possibilities for obtaining the "1.5D" flowlines: (i) via geometrical centerlines or (ii) via binned elevation band flowlines. In this study, the first method is selected, since it is recommended when simulating mountain glaciers (like in the Alps) and the geometry of the glacier matters. The geometrical centerlines are determined following the algorithm developed by Kienholz et al., 2014, which consists mainly of three steps:

1. **Identification of glacier terminus and local heads:** The glacier terminus is located in the grid cell with lower elevation value (lowest point). The local heads are identified along the glacier's outline and selected according to some restrictions.
2. **Determination of the grid-least-cost route:** For each defined grid cell on the glacier, a penalty value is determined, depending on the euclidean distance (from the cell to the closest edge) and the difference on elevation (from that cell to the minimum elevation). Then, a sum is carried out considering all penalty values from each head to the glacier terminus. Finally, the least-cost route is the one with the lowest penalty values and will be defined as the glacier centerline.
3. **Determination of branches and branch order:** All the defined centerlines are assigned with a geometric order, meaning that the longest centerline represents the main branch and the shortest, the lowest-order branch. The branch order increases with the number of contributing branches. Figure 5.4 shows the flowlines of the *Gepatschferner*, obtained after applying the algorithm. In this case, there are 6 flowlines and the longest one is identified with the highest number (5, since the numbering goes from 0 to 5).

Once the flowlines are determined, the catchment areas can be computed. Besides, by drawing a perpendicular line to the flowline for the points located along it, it is possible to obtain the geometrical widths. The widths are corrected afterwards, considering the altitude-area distribution. The determination of the corrected widths are of great interest within this study, since they are the basis for converting the "1.5D" to 2D geometry to obtain the glacier outlines that are used as input in the coupling scheme.



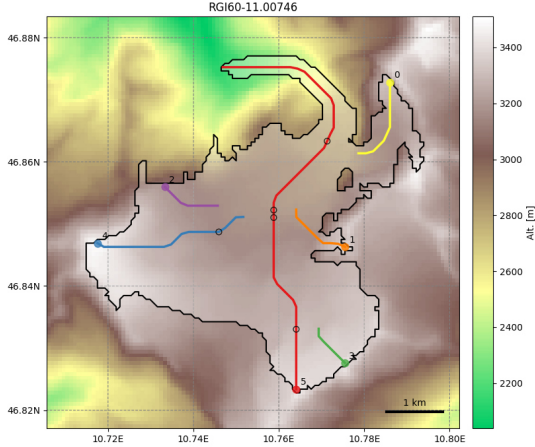


Figure 5.4: Example of the flowlines of Gepatschferner, with their identification number (from 0 to 5, being 5 the longest flowline). The empty circles indicate the connection with the tributaries, which are discontinued before touching the flowline they are tributary to (needed to improve glacier widths at junctions, Mausson et al., 2023).

### 5.2.3 Glacier mass balance

OGGM, similarly to WaSiM, uses a simple T-index model to determine monthly mass balances at every glacier (Equation 5.5). This model is calibrated based on geodetic mass balance observations (in this case and as a default, the Hugonnet et al., 2021 dataset is considered, Section 2.2.3.3):

$$B_i(z) = P_i^{solid}(z) - d_f \times \max(T_i(z) - T_{melt}, 0) \quad (5.5)$$

Where:  $B_i(z)$  is the monthly mass balance at elevation  $z$  [mm w.e. month<sup>-1</sup>],  $P_i^{solid}(z)$  is the monthly solid precipitation at elevation  $z$  [mm],  $T_i(z)$  is the monthly temperature at elevation  $z$  [°C],  $T_{melt}$  is the temperature threshold at which melt occurs [°C], and  $d_f$  indicates the temperature sensitivity of the glacier [mm month<sup>-1</sup> °C<sup>-1</sup>]. The fraction of  $P_i^{solid}(z)$  is determined from the total precipitation, being  $Temp\_all\_solid$  a lower and  $Temp\_all\_liquid$  an upper limit. For temperatures in between, a linear change is adopted. These two parameters are left with their default values (0 and 2 °C, respectively). Moreover, the total precipitation is adjusted by a precipitation factor  $prcp\_fac$  and the temperature is computed at the different altitudes  $z$  by considering a fixed lapse rate ( $Temp\_grad = -0.0065$  K m<sup>-1</sup>). Since some of these parameters need to be calibrated at a glacier basis, a description of the calibration procedure and the prior sensitivity analysis are explained in Sections 6.4.2 and 6.4.1.

### 5.2.4 Glacier ice thickness inversion

The ice thickness of the glacier is estimated through the ice that flows along the flowline. The evolution model used in OGGM is a depth-integrated flowline model, simplified by assuming shallow ice approximation (SIA, Section 2.3.2.3). By knowing the flux of ice  $q$ , the thickness  $h$  can be determined. This can be achieved by applying conservation of volume of a discrete element of ice (Figure 5.5), which means (Equation 5.6):

$$\frac{\partial S}{\partial t} = w\dot{m} - \nabla \cdot q \quad (5.6)$$

Where:  $S$  is the cross-section perpendicular to the flowline [m<sup>2</sup>],  $w$  is the width of the

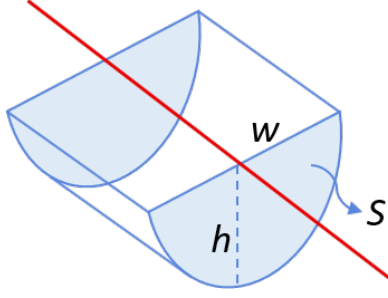


Figure 5.5: Example of a discrete volume of ice along a flowline (red) of a glacier.  $S$  is the cross-section perpendicular to the flowline with thickness  $h$  and width  $w$ . In this example, the cross-section has a parabolic shape.

cross-section [m],  $\dot{m}$  is the mass balance rate [m w.e. month<sup>-1</sup>] and  $q$  is the flux of ice [m<sup>3</sup> month<sup>-1</sup>]. The flux of ice  $q$  can be expressed in terms of the depth-integrated velocity  $u$  [m month<sup>-1</sup>] (Equation 5.7, Cuffey and Paterson, 2010):

$$q = uS = (f_d h \tau^n + f_s \frac{\tau^n}{h}) S \quad (5.7)$$

Where the first term of  $u$  refers to ice deformation and the second to basal sliding.  $\tau$  is the basal shear stress [kPa] and  $n$  is equal to 3.  $S$  depends on the type of bed shape. By assuming a parabolic bed shape (like in Figure 5.5),  $S = 2/3hw$  and Equation 5.7 could be solved for  $h$ .

In principle, OGGM numerically solves the second term on the right-hand side of Equation 5.6 ( $\nabla \cdot q$ ), and to compute the initial ice thickness, it follows the method developed by Farinotti et al., 2009 (briefly introduced in Section 2.3.2.3). Therefore,  $q$  is estimated by considering a point along the flowline and its upstream catchment area  $\Omega$ , as depicted in Equation 5.8, (which in fact follows Equation 5.6):

$$q = \int_{\Omega} (\dot{m} - \rho \frac{\partial h}{\partial t}) dA = \int_{\Omega} \tilde{m} dA \quad (5.8)$$

In this equation,  $\tilde{m}$  refers to the apparent mass balance defined by Farinotti et al., 2009, which is equal to the actual mass balance if the glacier were in steady state. To solve it, OGGM assumes that the glacier's geometry is in equilibrium by adding a residual to the mass balance profile. More information can be found in OGGM's documentation (Maussion et al., 2023).

In Figure 5.5 a parabolic bed shape is shown as an example. This type of shape is typically assumed for all glacier sections when using the geometrical centerlines approach. However, the shape changes to rectangular if the glacier section touches an ice-divide or a neighbor catchment and to trapezoidal, in case the parabolic shape gives unrealistic results (Maussion et al., 2019).

# Chapter 6

## WaSiM-OGGM coupling scheme

Not only the ability of performing simulations with daily (or even hourly) time steps, but also the possibility of representing all involved processes in a fully-distributed manner, make WaSiM a powerful model for simulating the water balance components in any region. Particularly in mountainous regions, where snow and glacier processes are of great importance, simulations carried out with WaSiM show to be successful (e.g. Klok et al., 2001; Kormann et al., 2016; Thornton et al., 2019; Verbunt et al., 2003). Still, for representing glacier evolution, WaSiM relies on the VA scaling approach. Even though good estimates can be obtained with this method (e.g. Radić et al., 2007; Kormann et al., 2016), an explicit representation of the ice flow dynamics is yet missing.

On the other hand, OGGM belongs to one of the latest generation of standalone global glacier models that provides glacier representations through the emergence of new global datasets (e.g. RGI) and novel approaches to quantify ice thickness. These properties, together with its open-source nature, make OGGM a flexible model to be adapted to any specific region in the world.

In this context, the WaSiM-OGGM coupling scheme aims to combine the capabilities of each separate model and complement their strengths, in order to improve glacier predictions while still focusing on all other involved processes (i.e. evapotranspiration, infiltration, etc). The main idea behind the coupling is to integrate the (annual) results provided by OGGM into a new run carried out with WaSiM, in which the glacier model is still activated but based on OGGM's results. To achieve this, input grids for WaSiM are required, which contain the areas and distributed ice thickness of the glaciers. The workflow of the coupling scheme is shown in Figure 6.1 and explained in detail in the following sections. The coupling of the models is developed completely in the Python programming language, in this case under version 3.9 (van Rossum and Drake, 2009).

### 6.1 Main capabilities of the models

As mentioned previously, the coupling scheme intends to take profit of the essential skills of each model and combine them together. The distinctive WaSiM's features can be summarized as:

- *Fully-distributed model*: Input and output data are available as grids, thus a spatial distribution of all variables is available. This is particularly important when looking at the meteorological variables, since altitudinal dependency is better represented due

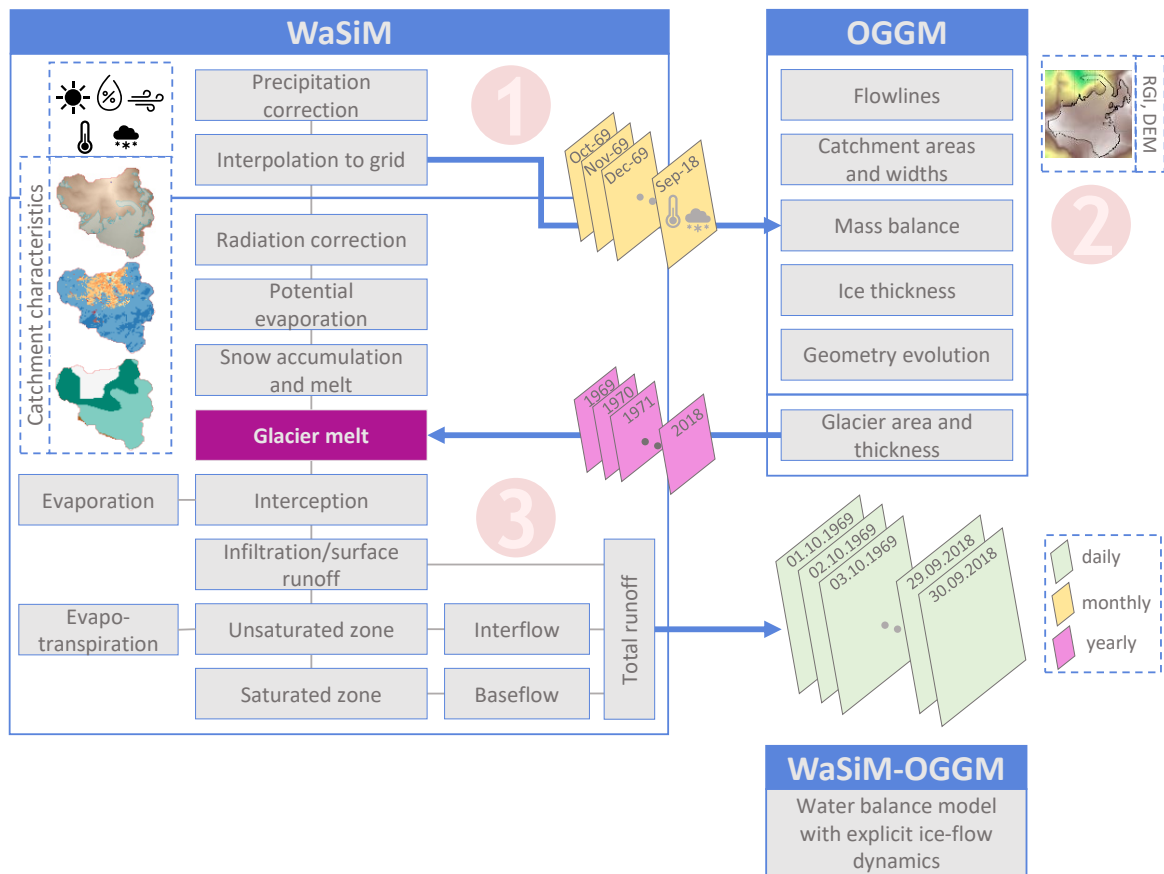


Figure 6.1: General workflow of the coupling scheme, including inputs/outputs from each model and corresponding time resolution.

to the finer resolution.

- **Hydrological processes:** Daily (and even sub-daily) time steps can be selected for representing all involved processes. Furthermore, most of the processes are physically-based, thus relying on real properties, such as soil water content or incoming solar radiation.
- **Melting from glaciers:** Since the melting from the glacierized parts of the catchment contributes greatly in the generation of runoff, a very good representation of this process is desired. WaSiM allows to calculate glacier melt at a daily (or sub-daily) time scale, with or without considering the influence of solar radiation based on the T-index method.
- **Free of charge:** WaSiM is available free of charge and can be easily adapted to any study case.

The main OGGM's features are:

- **Ice dynamics flowline model:** The default evolution model used in OGGM is a flowline model that represents the flow of ice along the glacier. Thus, the ice thickness can be determined at certain points along a flowline, together with the corresponding cross-section.

- *Open source and automated workflow*: The model evolves continuously, is fully automated and able to simulate almost any glacier in the world. This is of great interest particularly in regions where glaciers play a crucial role in the water resources management and face scarce data availability.

## 6.2 Assumptions

In order to benefit from the capabilities of each of the models and complement their strengths, the main features of each model are integrated into the coupling scheme. Since the assumptions and approaches behind the main core and processes that belong to each of the models are different, a straightforward coupling of the models is hardly possible. Furthermore, the spatio-temporal resolution varies between models, so variables cannot be directly transfer from one model to another. For these reasons, the following assumptions are made:

**Assumption 1:** An "offline" coupling scheme is adopted, where both models are run separately but with an update of their inputs/outputs to the other model.

**Assumption 2:** Since OGGM is an open-source framework that fully uses publicly available datasets, it is aimed to modify as little as possible the default options that OGGM has with it (e.g. the use of the RGI).

**Assumption 3:** The annual glacier outlines obtained from OGGM are an approximation: the flowline model in OGGM is a "1.5D" model, meaning that the glacier flows only in one direction along the flowline but each point along the line has a geometrical width (Maussion et al., 2019). Thus, when constructing a 2D geometry, parts of the actual area might be missing, especially specific features of the shape of the glacier itself.

**Assumption 4:** Another assumption is related to the volume of the glacier. The ice thickness determined by OGGM is also related to the points along the flowlines of the glaciers. When converting it from flowlines to grids, the distribution throughout the new glacier geometry is an approximation based on an interpolation to the desired model grid cell size.

**Assumption 5:** In order to integrate the ice volume of the glaciers determined by OGGM into WaSiM, the glacierized grids will not only contain the amount of glacierization at each cell, but also the thickness of ice at that cell. In this way, the "real" volume of the glacier is given at the beginning of the simulation and updated annually instead of calculating it with the empiric formulation of the VA scaling approach.

**Assumption 6:** The calibration of the mass balance model in OGGM is done at a glacier basis, thus each glacier has its own set of calibrated parameters. The multi-objective optimization of the coupling scheme can be performed considering the mass balance of all studied glaciers in average, or, like in this specific study case, the mass balance of the largest glacier (in this case *Gepatschferner*, which represents almost 80% of the total glacierized area).

### 6.3 First WaSiM run with resampling of climate data

The first step of the workflow consists of performing a continuous simulation with WaSiM with daily time steps, from which climate output datasets are produced for the consecutive step of the coupling. The processes involved in this simulation were already introduced in Chapter 4. All the tasks within this run can be summarized according to Figure 6.2 and are the main assignments required as first step for the coupling scheme.

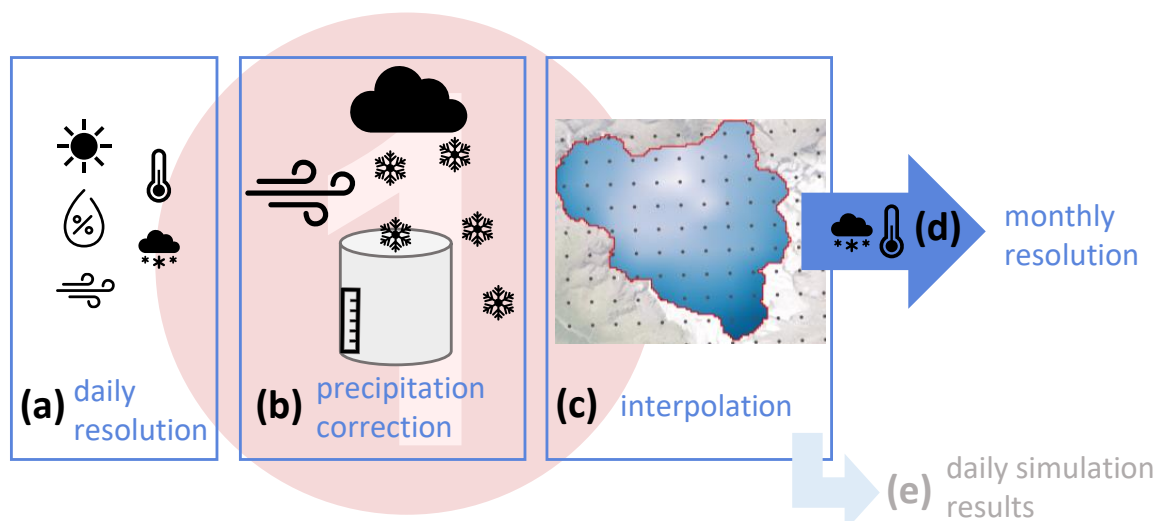


Figure 6.2: First step of the workflow of the coupling-scheme: WaSiM run with resampling of climate data (a) reading the climate datasets with daily resolution, (b) correction of precipitation due to e.g. wind undercatch, (c) interpolation to the model grid, (d) resampling of monthly mean temperature and monthly total precipitation to be used as input in OGGM and (e) achievement of simulation results on a daily basis, including VA scaling glacier model results.

In this first model run, the integrated VA scaling glacier model is activated, since not only the evolution of the glaciers but also the generation of runoff is strongly dependent on the glaciers' behavior. The model is calibrated and validated against observed data, as described in Section 6.3.2 and the results are used afterwards to compare the performance of the WaSiM VA scaling approach with the results from the WaSiM-OGGM coupling scheme (Section 7.4).

Nevertheless, if an intermediate evaluation of the model performance is not pursued (i.e. that the model user is not interested in the performance of the VA scaling glacier model or intermediate results), then the activation of the glacier model may be omitted. In this way, the main focus of the first WaSiM run is just given to the aggregation of the daily climate variables into monthly values that will be used for the coupling scheme. Moreover, the model does not need to be initialized in a year in which glacier outlines are available, which could be a huge advantage for study areas that do not rely on available observations (and also provide more freedom to the user on selecting the initial year for the simulations). Besides, the requirements of input data for running WaSiM (e.g. creation of grids with fraction of glacierization in each cell) are lower, thus reducing the workload demanded from the user.

### 6.3.1 Sensitivity analysis

All WaSiM processes are described by a wide variety of parameters. Many of these parameters can be defined separately for each subcatchment, such as the recession constant for describing interflow, among others. But a great number of parameters must be defined globally, thus the adjustment to each individual subcatchment cannot be easily performed. Examples of these parameters are the temperature threshold separating rain from snow or the melt factor that describes the melted water generated from glacierized areas.

Due to the large number of (unknown) parameters involved in WaSiM, a sensitivity analysis is performed a priori to identify non-influential parameters which can be disregarded during the calibration process and save computation times and reduce possible errors (Devak and Dhanya, 2017). For the sensitivity analysis, the **Statistical Parameter Optimization Tool for Python (SPOTPY)** (Houska et al., 2015) is used, in combination with the **Fourier Amplitude Sensitivity Test (FAST)** (e.g. Saltelli, 1999). SPOTPY could easily be linked to any model in order to perform uncertainty and sensitivity analysis or calibration, by selecting the most adequate algorithm and objective function on a wide variety of available options. Examples of other available algorithms are Monte Carlo, Maximum Likelihood Estimation, Simulated Annealing and much more. Regarding objective functions, Nash-Sutcliffe Efficiency (NSE, Nash and Sutcliffe, 1970), Kling-Gupta Efficiency (KGE, Gupta et al., 2009) and others are examples of the available options. Moreover, other objective functions can be defined and used by the modeler, due to the flexibility of the framework.

By applying FAST, which is suitable for nonlinear models, it is possible to determine how sensitive the parameters are based on the selected objective function (Saltelli, 1999). Moreover, the number of iterations must be defined, which depends directly on the number of parameters selected for the sensitivity analysis. After the analysis is finished, SPOTPY provides a database containing the sampled parameter sets and the corresponding simulation results and objective functions. In this study, and due to the high number of parameters involved in the model, the sensitivity analysis is performed in three steps, depending on the sub-model where they belong to. Furthermore, the sensitivity analysis is carried out for the period 01/2000 to 12/2004, being the model initialized in the year 1998 (two-year warm-up period), since for that year observed glacier outlines are available (Figure 4.2 in Section 4.1). The target variable is the simulated runoff at the outlet of the catchment and the selected objective function is the KGE. Appendix B contains a description of all performance measures used during sensitivity analysis, calibration and validation of the models within this thesis. Moreover, Table C.1 in Appendix C summarizes the three step analysis approach and the parameters involved in each of the steps, together with a description of the parameter and its range. The three processes and parameters selected during the sensitivity analysis are:

1. **Soil model:** In this case, the parameters describing the storage coefficients for the linear reservoirs (surface runoff, interflow and baseflow, Equation 4.19, Section 4.9) are selected, together with the scaling factor for the baseflow and the recession constant for the saturated hydraulic conductivity with increasing soil depth (Equation 4.18, Section 4.8).
2. **Glacier model:** The melt factor, the corresponding storage coefficients for the linear reservoirs for ice, firn and snow and the VA scaling parameters are chosen (Equations 5.1 and 5.2, Sections 5.1.1 and 5.1.2).

3. **Snow model:** Involved parameters of the energy balance model with gravitational slides and wind redistribution are selected during the sensitivity analysis (Equations 4.9, 4.12 and 4.16, Section 4.7).

As a summary, a total of twenty parameters are selected for the sensitivity analysis and the results are presented in Section 7.1.1. The results of the sensitivity analysis are a valuable help when performing the optimization of the coupling scheme, since the number of parameters to be adjusted is reduced to those who are more sensitive and consequently the required computational times might decrease.

### 6.3.2 Calibration and validation of the model

The calibration procedure in this section refers only to the calibration of WaSiM (with VA scaling) during the first step of the coupling scheme, in which the most sensitive parameters are adjusted against runoff and glaciers' observations. Although the coupling scheme is optimized afterwards following a multi-objective function (Section 6.5.1), this calibration step is simply needed to have an optimized WaSiM model to be used when comparing results to the coupling scheme, as introduced later in Section 7.4. Moreover, although the procedures mainly refer to Gepatschalm, they can be fully implemented in any other study case.

While the adjustment of subcatchment specific parameters can be done separately if observations are available at the outlet of each subcatchment, the calibration of global parameters can only be done by looking at the catchment as a whole. For calibrating those global parameters, one option is to use a multi-site approach, that is, calibrate all subcatchments together using all available runoff observations. If not enough observations or only one data set is available, then a one-site calibration can be performed. This is the case of Gepatschalm, where runoff observations correspond to the outlet of the catchment. As mentioned in Section 4.1, the simulation period is split in three parts:

1. **Warm-up period:** Like in every hydrological simulation, a warm-up period is required and refers to the time (usually from one to several years) in which the internal storages (i.e. soil moisture) reach an "ideal" state (Kim et al., 2018). In this study, the warm-up period starts at the year of initialization of the model (10/1969), for which glacier outlines are available.
2. **Calibration period:** The calibration period is based on the available runoff observations. The total period of available observations is split in two main parts, according to the split-sample test defined by Klemeš, 1986. Here, it is recommended that the period is distributed equally between calibration and validation (50/50). Therefore, the period from 01/1990 to 12/2006 (in total 17 years) is used for calibration of the model.
3. **Validation period:** The rest of the total period is assigned for validation of the model, according to the split-sample test (Klemeš, 1986). Thus, the remaining 17 years are divided into two validation periods: the first validation period spans from 01/1985 to 12/1989, just before the beginning of the calibration period and the second validation period spans from 01/2007 to 12/2018, right after the calibration period ends and coincident with the available glacier outlines for the year 2006.



During this validation period, simulated SWE and snow coverage are also compared to available observations.

To calibrate WaSiM, multiple criteria are taken into account, including available runoff observations at the catchment outlet and glacier outlines. These criteria are evaluated simultaneously, with the utmost attention given to setting the parameters that provide the most accurate representation of both simulated runoff and glacier outlines to closely reflect reality. Table 6.1 summarizes the criteria used for calibration of the model. In addition, Appendix B contains a description of the performance measures used within the calibration and validation of the models.

It is worth mentioning that snow is not included during calibration of the model due to the short period of available observations, which make it challenging to adjust model parameters while still focusing on long-term simulations. In addition, the response time of glaciers can take several years or decades (e.g. Cuffey and Paterson, 2010), thus affecting local hydrology even far beyond the short-term period (e.g. one year). For all these reasons and considering that the prime focus of this study is given to the evolution of glaciers and their impact on local/regional hydrology, snow observations are only considered during validation of the model but still parameters are adjusted during calibration.

Table 6.1: Criteria for evaluating the calibration and validation performance. All of them are used during the first run of WaSiM (including the VA scaling glacier approach), based on available runoff, glacier outlines and SWE (Appendix B).

Objective variable	Performance criteria	Comments
Runoff at the outlet of the catchment (Gepatschalm)	<i>NSE</i>	Nash-Sutcliffe Efficiency (Nash and Sutcliffe, 1970)
	<i>KGE</i>	Kling-Gupta Efficiency (Gupta et al., 2009)
	<i>BE</i>	Benchmark Efficiency (Schaefli and Gupta, 2007)
	<i>PBIAS</i>	Percentage bias
	<i>RMSE</i>	Root Mean Square Error
Glacier outlines	<i>POD</i>	Probability of detection (Kormann et al., 2016)
	<i>FAR</i>	False alarm rate (Kormann et al., 2016)
SWE at AWS Weißsee	<i>PBIAS</i>	Percentage bias
	<i>RMSE</i>	Root Mean Square Error

The evaluation of the calibration and validation model performances is done according to the performance ratings suggested by different authors, i.e. Moriasi et al., 2007; Thiemiig et al., 2013. The performance ratings are presented in Table B.1 (Appendix B).

### 6.3.3 Generation of monthly climate grids

While WaSiM runs at a daily time step, OGGM requires monthly input data of temperature and precipitation. For this reason, these climate variables need to be re-sampled to a

monthly time step while running WaSiM. For temperature, the average between all daily temperatures within that month is determined. For the case of precipitation, the daily values are aggregated to obtain the total sum for the month. The results are grids containing monthly values at each model grid cell. In the case of precipitation, the values have already been subjected to the correction (Section 4.2).

## 6.4 OGGM run and processing of glacier outputs

The second step of the workflow within the coupling scheme consists of performing the OGGM simulations. In this step, the monthly climate datasets of precipitation and temperature produced by WaSiM (aggregation from daily values, carried out during the first run) are used as input data for the model. Then, the outputs generated by OGGM are used again as input for the final run with WaSiM. The second step of the workflow is depicted in Figure 6.3 and described in the following sections.

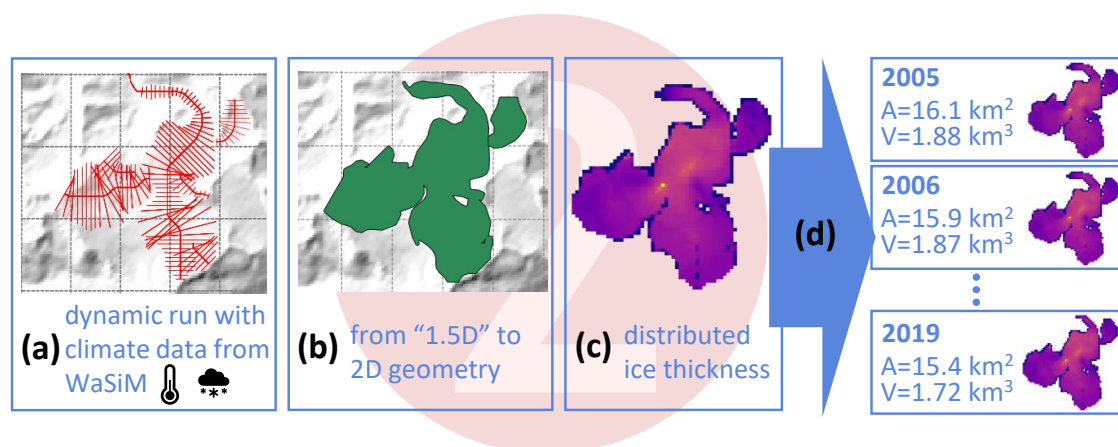


Figure 6.3: Second step of the workflow within the coupling-scheme: OGGM run with monthly climate data generated with WaSiM. (a) dynamic run with WaSiM climate datasets, (b) generation of 2D geometries (glacier outline) from "1.5D" geometries (flowlines and catchment widths), (c) distributed ice thickness for the previously generated 2D geometries (d) gridded input for WaSiM: annual glacier area, ice thickness distribution (and volume).

As mentioned in the workflow followed by OGGM (Section 5.2), the glacier outlines are automatically downloaded from the RGI, which per default correspond to the version 6.0 (year 2003). Although the user can change this option and work with any glacier outline that is available (and prepared accordingly to be used by OGGM), one of the assumptions of the coupling scheme is to modify as little as possible the default options that OGGM has with it. Therefore, in this study, the use of the available RGI v6.0 outlines is kept as a default for the simulations.

### 6.4.1 Calibration of the mass balance model

Despite the sensitivity analysis is carried out prior to the calibration of the mass balance model, in this particular study the calibration is described first to understand which parameters are kept as default (global parameters) and which parameters might require adjustment

(local parameters). In the results section, however, the results of the sensitivity analysis are shown prior to the calibration procedure. As shown in Section 5.2.3, the mass balance model used during OGGM's simulations is calibrated against geodetic mass balance data from Hugonnet et al., 2021. Even though the new calibration scheme (available from OGGM v1.6) is more flexible and adaptable to the user's needs, it is still the aim of this coupling scheme to reduce as much as possible the modifications into OGGM's default setup. Thus, a thorough analysis of the calibration procedure, parameters and analysis of results is performed in this study to finally determine the most adequate path to be followed in posterior applications of the coupling scheme.

The calibration of the monthly mass balance model (Equation 5.5) relies on several parameters. Some of them are considered as "global" parameters, hence they are the same for all glaciers and they are left with their default values. The rest of the parameters, so called "local", are adjusted at a glacier basis during the calibration. All parameters are summarized in Table 6.2.

Table 6.2: Global and local (glacier-based) parameters involved in the mass balance model. The global parameters are left as default, whereas the local parameters are calibrated against geodetic mass balance data. Each parameter includes a description with its default value and units and the range used during the calibration (Maussion et al., 2023).

Type	Parameter name	Description	Unit	Default value/range
Global	$T_{melt}$	Monthly mean threshold temperature for ice melt	°C	-1.0
	$Temp\_all\_solid$	Temperature limit for solid precipitation	°C	0.0
	$Temp\_all\_liquid$	Temperature limit for liquid precipitation	°C	2.0
	$Temp\_grad$	Gradient (i.e. lapse rate) for temperature calculation at different altitudes	K m <sup>-1</sup>	-0.0065
Local	$melt\_f$	Melt factor	kg m <sup>-2</sup> K <sup>-1</sup> d <sup>-1</sup>	1.5 - 17.0
	$temp\_bias$	Temperature bias	°C	-15.0 - 15.0
	$prcp\_fac$	Precipitation correction	-	0.1 - 10.0

From the global parameters,  $T_{melt}$  represents the temperature threshold at which melt occurs [°C].  $Temp\_grad$  refers to the lapse rate used to compute temperatures at different altitudes [K m<sup>-1</sup>] (OGGM's default is to keep this value fixed).  $Temp\_all\_solid$  and  $Temp\_all\_liquid$  are the upper and lower temperature limits for solid and liquid precipitation, respectively [°C]. In terms of local parameters,  $prcp\_fac$  [-] corrects precipitation to the altitude where the mass balance is calculated. For the total mass balance of the glacier, this point refers to the geometric center of the glacier. The parameter  $temp\_bias$  [°C] also involves downscaling temperature, which is adjusted by this bias to obtain the temperature values at the center of the glacier. Finally,  $melt\_f$  [kg m<sup>-2</sup> K<sup>-1</sup> d<sup>-1</sup>] is a degree-day (or melt) factor converted into a monthly value to simply represent  $d_f$  (temperature sensitivity of the glacier) as introduced in the mass balance equation (Equation 5.5).

The calibration is carried out based on the average geodetic annual mass balance for the period 01/2000 to 01/2020 (Hugonnet et al., 2021). This means that three parameters (*melt\_f*, *temp\_bias* and *prcp\_fac*) are adjusted for each glacier so that the average annual mass balance simulated with OGGM matches the average geodetic annual mass balance, for the considered period. But since three parameters are calibrated against only one available observation per glacier, the model is then overparameterized. In other words, different parameter combinations could yield to the same model results and therefore an unique solution is not possible (Mausson et al., 2023).

In order to reduce the number of parameters to be calibrated and avoid the equifinality problem (Beven and Freer, 2001, Section 2.3.4.1), a sensitivity analysis is performed prior to the calibration of the mass balance model. During this analysis, different parameter combinations are studied and simulated annual mass balances are compared to the geodetic observations. Moreover, the mass balance observations at the tongue of *Gepatschferner* are also included within the analysis, so that the inter-annual variability is contemplated.

Assuming there are other available observation for the glaciers, the calibration should be adapted to include the new target variable. For the case of reference glaciers (such as the neighboring glacier *Hintereisferner*), in-situ mass balance observations might definitely improve the calibration scheme, enabling more precise representation of not only the average mass balance but also the inter-annual variability. In both cases, calibration and sensitivity analysis of the parameters that describe the mass balance model in OGGM, simulations start in 2003 due to the known initial conditions (RGI outlines) and span until 2020. Once the mass balance model is calibrated, dynamic glacier runs can be performed, even starting at any year in the past (Section 6.4.3).

## 6.4.2 Sensitivity analysis of the mass balance model parameters

The sensitivity analysis is conducted on the "local" parameters, to see which of them will be adjusted during calibration of the mass balance model (the remaining parameters are fixed). During the sensitivity analysis, one parameter is selected as default ("*default parameter*") and its value is kept constant during the entire simulation period. A second parameter is selected within a predefined range ("*varying parameter*") whereas the third parameter is calibrated according to the two other parameters ("*calibrated parameter*"). Here, the term "calibrated" is used because this sensitivity analysis is performed manually, where the "calibrated" parameter is adjusted to test its influence on the simulation results, assuming the other parameters remain fixed. Table 6.3 summarizes the different runs performed during the sensitivity analysis with the corresponding parameter combinations. In all cases, the three local (glacier-based) parameters (*melt\_f*, *temp\_bias* and *prcp\_fac*) are considered.

For *melt\_f*, a default value of 5.0 and a range between 1.0 and 10.0 with increasing steps of 1.0 is selected [ $\text{kg m}^{-2} \text{K}^{-1} \text{d}^{-1}$ ]. For *temp\_bias*, the default value is set to 0.0, whereas a range between -5.0 and 5.0 and steps of 0.5 [ $^{\circ}\text{C}$ ] is chosen. Finally, for *prcp\_fac*, a default value of 1.0 and a range between 0.1 and 10.0 with steps of 0.5 [—] is used. The parameter ranges selected have been adapted from the OGGM's default configuration, with values ranging from 1.5 to 17.0 for *melt\_f*, -15.0 to 15.0 for *temp\_bias* and 0.1 to 10.0 for *prcp\_fac*. The *temp\_bias* range was additionally adjusted from the default configuration, since the range is quite large. Finally, the selected ranges are fairly consistent with the procedure defined by Schuster et al., 2023.

Table 6.3: Test runs performed during the sensitivity analysis and their parameter's combination, following the tutorial "A look into the new mass balance calibration in OGGM v1.6" from Maussion et al., 2023).

Test	Default	Varying	Calibrated
A	<i>melt_f</i>	<i>temp_bias</i>	<i>prcp_fac</i>
B	<i>melt_f</i>	<i>prcp_fac</i>	<i>temp_bias</i>
C	<i>temp_bias</i>	<i>prcp_fac</i>	<i>melt_f</i>
D	<i>temp_bias</i>	<i>melt_f</i>	<i>prcp_fac</i>
E	<i>prcp_fac</i>	<i>melt_f</i>	<i>temp_bias</i>
F	<i>prcp_fac</i>	<i>temp_bias</i>	<i>melt_f</i>

As mentioned in Section 6.4.1, the observed mass balances at the tongue of *Gepatschferner* for the period 2012 to 2019 are used to check the inter-annual variability of the mass balance. With the results from the sensitivity analysis, a decision can be made on which local parameters could be left with their default or fixed values while calibrating the third parameter. The results are presented in Section 7.2.1.

### 6.4.3 Dynamic runs

Two runs can be performed by OGGM for studying the evolution of the glaciers. On the one hand, the static run, which considers that the geometry of the glacier remains constant throughout the simulation period. On the other hand, the dynamic run considers the change in the glacier's geometry, so the area of the glacier differs from year to year. For long-term simulations, where the glacier geometry is expected to change, the dynamic run is more suitable. For this reason, the dynamic run is selected, in which the evolution of the glaciers is studied for a period of at least 50 years.

Although a fully-distributed representation of the climate variables (precipitation and temperature) is obtained from the first WaSiM run at a monthly time scale, OGGM computes the values at a glacier basis. This means that for each glacier, only the climate variables at one point (the geometrical center point) is considered when performing the simulations, hence an accurate representation for the entire glacier should be ensured. OGGM applies a correction to both precipitation and temperature to interpolate their values to the center point, as introduced in the mass balance equation (Section 5.5) to account for topography effects on such variables.

The model simulations, like with any other model, should be conducted with knowing initial conditions (i.e. known glacier outlines). Using the glacier outlines from the year 2003 (i.e. RGI v6.0), earlier simulations may pose a challenge as the glacier coverage is unknown. To overcome this issue and perform simulations in the past, two approaches (apart from the initialization at the outline's (RGI's) date) can be adopted:

- (a) **Run dynamic spinup for past simulations:** As mentioned before, if the model needs to be initialized in a date prior to the glaciers outline, then a dynamic spinup can be conducted. During this spinup, the model tries to find a glacier state in the past that matches the area (or volume) at the glacier outline's date. This procedure

is done iteratively, by adjusting a temperature bias until the areas (or volumes) match under a given precision error threshold.

- (b) **Run initialization method for past simulations (Eis et al., 2019; Eis et al., 2021)**: By selecting this approach, the model is initialized at any year in the past and the best candidate of all possible glacier states is selected. This selection is based on the minimum difference between the observed and simulated glacier area at the observed outline's date, considering a mass balance offset during simulations.
- (c) **Run OGGM starting from the outline's date**: This means that the model simulations are conducted from the glacier outlines's date onward. Hence, no results on the glacier's evolution for the past period (before the outline's date) is obtained. This option is useful if the model needs to be initialized in the recent past and used for predictions under future climate conditions.

Figure 6.4 schematizes the two initialization methods described previously. On the left (a), the workflow followed after selecting a dynamic spinup is presented, whereas on the right (b), the workflow followed by the initialization method proposed by Eis et al., 2019; Eis et al., 2021 is summarized.

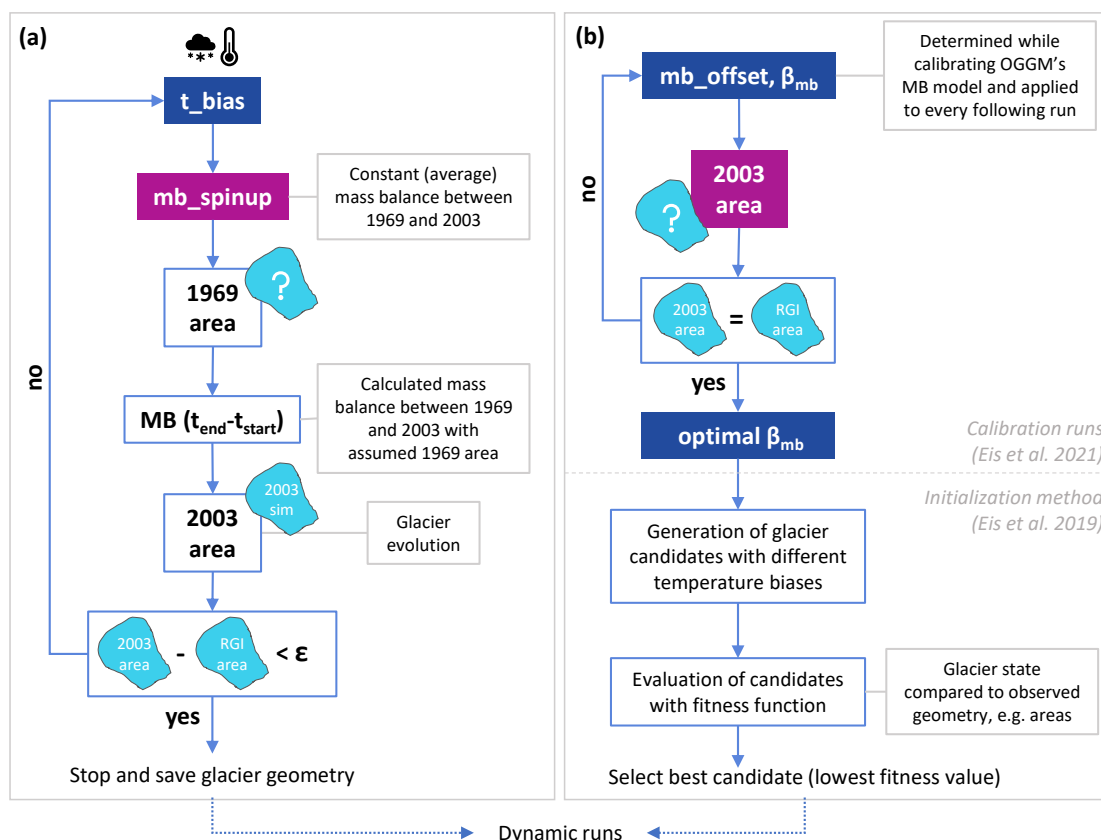


Figure 6.4: Workflow followed by two initialization methods in OGGM: (a) Dynamic spinup and (b) Initialization method after Eis et al., 2019; Eis et al., 2021.

The glacier outline's availability in the study area date from 1969 (Fischer et al., 2015a), hence WaSiM's simulations start from the same year. Additionally, the model could also be initialized in 1998, since another glacier outline is available for that year. In order to perform

the comparison of results between the integrated VA scaling glacier model in WaSiM and the coupling scheme, OGGM is also initialized in 1969. Due to the initialization of OGGM before the RGI's date, the dynamic spinup from 1969 to 2003 is carried out, where the simulated and observed glaciers' area in 2003 are compared and the temperature bias is adjusted until the difference between both areas is admissible (a). On the other hand, OGGM runs are also carried out from the RGI's date onward (c). The results are useful to compute the uncertainties on the selected initialization approach and how past predictions of glacier's evolution affect future simulations. As regards the initialization method developed by Eis et al., 2019 (b), the post-processing of OGGM's outputs yields to questionable results in terms of glacier geometry, when performing the conversion of "1.5D" to 2D geometries (as explained in the next Section, 6.4.4). For this reason, results of this method are not included in this thesis, but the corresponding code is available as an additional option within the coupling scheme, so this initialization method could still be selected in other case studies.

### 6.4.3.1 OGGM Default run

One of the key features of OGGM is that it comes with already pre-processed glacier directories, allowing the user to start the simulations at any step within the modeling workflow (described in Figure 5.2). These directories contain input data and results that resulted from using default parameters and input variables (Maussion et al., 2023). In order to further test the performance of the glacier simulations within the coupling scheme, an extra OGGM run with default values is also carried out (from now on called "Default run"). In other words, all parameters are kept with their default values, which were calibrated based on the default climate datasets that OGGM offers. The W5E5 re-analysis dataset is then selected for this default run. This dataset merges the WFDE5 over land with the ERA5 over the ocean (Lange, 2019).

### 6.4.4 From "1.5D" to 2D geometries

As described in Section 5.2.2, OGGM determines the ice thickness based on a flowline model. This means that the ice flow takes place only along the flowline, for which also the cross-section or bed shape can be determined. As a result, OGGM provides a "1.5D" geometry for the glaciers. This is, however, not sufficient for integrating OGGM's output into WaSiM's simulations. Since WaSiM is a fully-distributed model, a complete 2D geometry of the glaciers should be provided. For this reason, a conversion of the flowline model with "1.5D" geometry to a grid containing the glaciers outline is required. The core of the procedure is described in Figure 6.5, where only the case of *Gepatschferner* is illustrated as an example.

It is worth to mention that a modification into WaSiM's code is not carried out. Thus, the capabilities of the model are still exploited without any hidden changes and the input and control files are adapted so the outputs provided by OGGM can be integrated directly and without any extra configuration in WaSiM. The conversion from "1.5D" to 2D geometries is carried out based on the function

```
graphics.plot_catchment_width(gdirs)
```

that is included in the open-source code of OGGM (Maussion et al., 2023). In principle, the function is called after the dynamic run is performed, so that the flowlines for each of



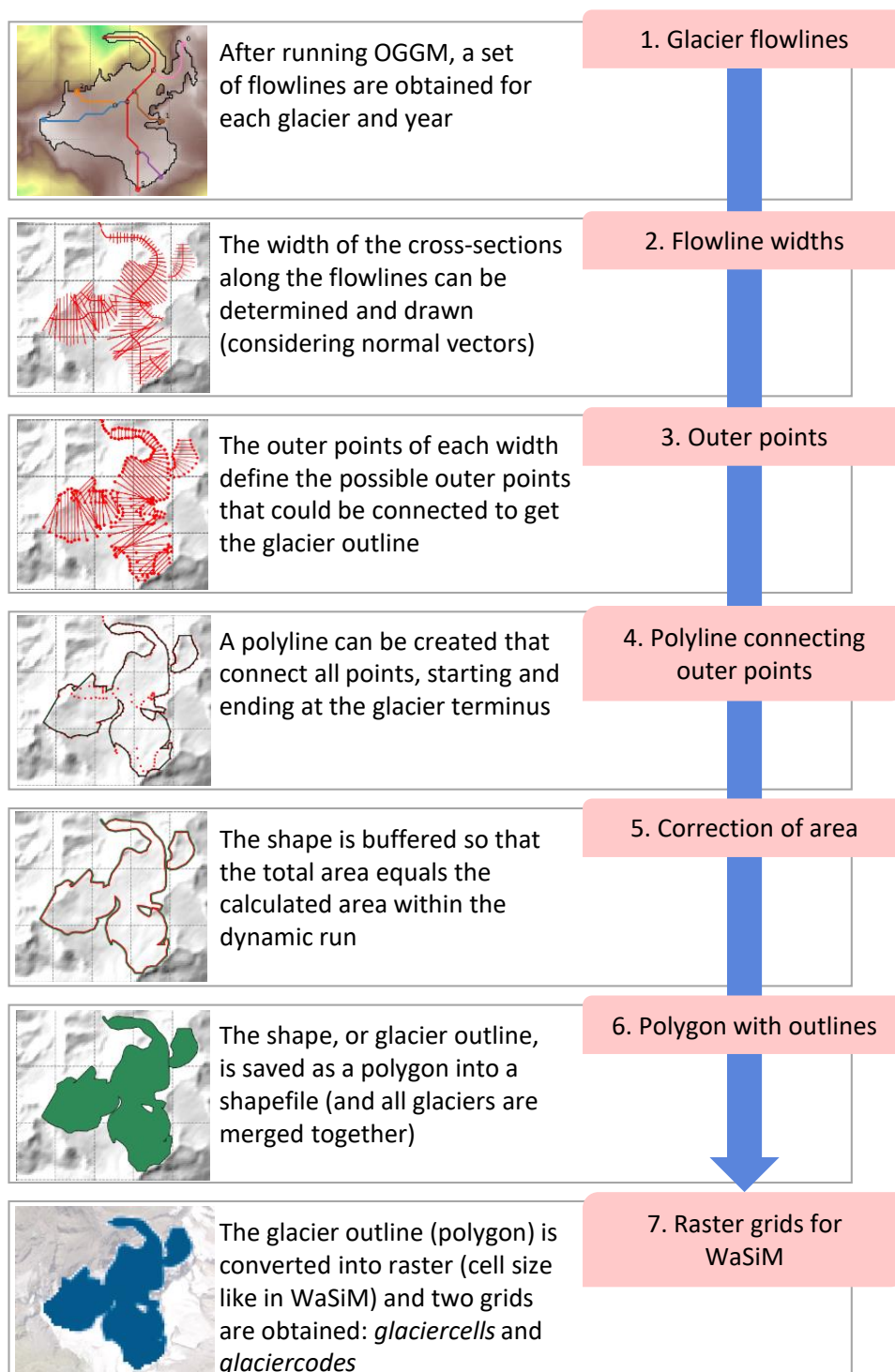


Figure 6.5: Procedure followed to convert the "1.5D" into 2D glacier geometries. The steps are applied for the case of Gepatschferner, but the procedure is carried out for all glaciers and all the years considered within the simulation period.

the years defined in the simulation period are used to determine the annual geometry of the glaciers. The procedure starts with the generation of the flowlines' widths for each of the points that OGGM identifies along them. Since each flowline is different and treated as an unique element, the number of points and distribution of them along the line are also



different. Nevertheless, this does not affect the method, since at the end only the outer shape of the glacier matters (**Step 2.** in Figure 6.5).

Once the flowline's widths are identified, the outer points are obtained. These points refer to the extremes of the widths, or cross-sections of each of the points along the flowlines (**Step 3.** in Figure 6.5). The connection of all outer points yield an approximation of the glacier's shape. However, not all outer points need to be included, but only the ones that define the smallest convex set that contains those points (also known as convex hull, Weisstein, 2023). As a result, a polyline (i.e. a continuous line connecting all selected outer points) is created, starting and ending at the glacier terminus (tongue) (**Step 4.** in Figure 6.5). At this stage, there are two main limitations of the procedure that cannot be ignored:

- (i) The connection of the outermost points does not precisely yield the glacier's outline. The reason is that the creation of the polygon is merely based on geometrical computations and does not include any additional topographical or physical information related to the glaciers. Hence, it is challenging to represent the exact geometry of the glacier. One possible solution to improve the delineation of the polygon is to use an *alpha shape*, which is a generalization of the convex hull. This tool can be implemented easily within the code (Bellock et al., 2021), where the alpha parameter, that regulates the fitting shape of the points, can be optimized.
  - However, the complex geometry and considerable number of outer points that ought to be connected makes the creation of the alpha shape arduous, especially near the points that form the tongue of the glacier.
  - Besides, although the alpha parameter can be automatically optimized, the created shape (i.e. polygon) should be visually verified. This might require a manual adjustment of the parameter and could turn into a tedious task if a great number of glaciers are included during the simulations.

Therefore, the simplest way of creating a polygon connecting all outermost points is selected at this stage.

- (ii) The total area covered by the resulting polygon that connects the outermost points might not exactly correspond to the value of the area obtained after performing the simulations. This is easily explained by the fact that the delineation of the glacier area is just an approximation resulting from the connection of the outermost points.
  - To maintain a coherence between the calculated area of the glacier and the area covered by the polygon, the latter is corrected (**Step 5.** in Figure 6.5).
  - For the correction, first the ratio between the simulated area and the area covered by the glacier is obtained, by applying Equation 6.1:

$$ratio = \frac{simulated\ area - polygon\ area}{polygon\ length} \quad (6.1)$$

Where: *simulated area* is the value of the area obtained after running the model [ $m^2$ ], *polygon area* is the value of the area contained within the polygon delineated from the outermost points [ $m^2$ ] and *polygon length* is the total length of the polyline that defines the polygon [m].

- Second, the polygon is buffered using the previously calculated ratio, so that the polygon area matches the value of the simulated area.

As a final step, the obtained polygon or glacier's outline is saved as a shapefile, that is, a file that stores all the geometrical information and attributes of the polygon (**Step 6.** in Figure 6.5). Moreover, all the polygons that define the glaciers outlines in the study area are merged together, since WaSiM requires only one input dataset containing the information for all present glaciers. Finally, the merged polygons (i.e. glaciers outlines) are converted into a raster, where the cell size coincides with the model cell size defined and used by WaSiM (**Step 7.** in Figure 6.5).

As described in Section 5.1, WaSiM requires two input grids containing the glacier's information. One is the grid with the fraction of glacierization for each of the cells, which varies between 0 (no glacier) and 1 (completely covered by glacier). This grid is called *glaciercells*. In addition, a grid containing the codes of the glaciers (*glaciercodes*) must also be provided. Hence, for each year considered within the simulation period, two grids are created from OGGM's outputs.

### 6.4.5 Distributed ice thickness

After applying the ice dynamics flowline model in OGGM, the ice thickness of the glaciers along the flowlines can be determined. In addition, OGGM provides a function that enables to obtain an approximation of the ice thickness distribution in the glacierized area. This is done by calling the function (Maussion et al., 2023)

```
graphics.plot_distributed_thickness(gdirs)
```

The procedure is schematized in Figure 6.6. The distribution of the ice thickness is performed by interpolating the thickness throughout the glacier mask (i.e. grid containing 1 for a cell that belongs to the glacier and 0 if the cell lies outside the glacier area, **Step 2.** in Figure 6.6). Originally, this function is only applied to get the distributed ice thickness in the glacier's outline corresponding to the RGI's date, which is the only known or observed outline.

Since the conversion of "1.5" to 2D glacier geometries enables to obtain glacier outlines for each year within the simulation period, an extension of the distributed ice thickness function is performed to obtain annual grids (**Step 3.** in Figure 6.6). This is simply done by updating yearly the glaciers outlines with the newly converted 2D geometries. A more detailed description on how the interpolation is carried out, based on the available function available in OGGM (Maussion et al., 2023), is summarized in Figure 6.7 and described in the following.

For each point along the flowline, the following attributes are available: altitude (i.e. elevation of the point above sea level), bed shape (e.g. parabolic), width, thickness, volume and flux (Figure 6.7 (a)). Additionally, grids containing the glacier mask and topography are available in the glacier directories, with their own model cell size (used internally by OGGM). For each cell, the topographic information, that is, the altitude of the center point at each grid cell (Figure 6.7 (b)) is available. Then, the interpolation of the thickness to each grid cell is carried out using the inverse distance weight (IDW) interpolation approach.

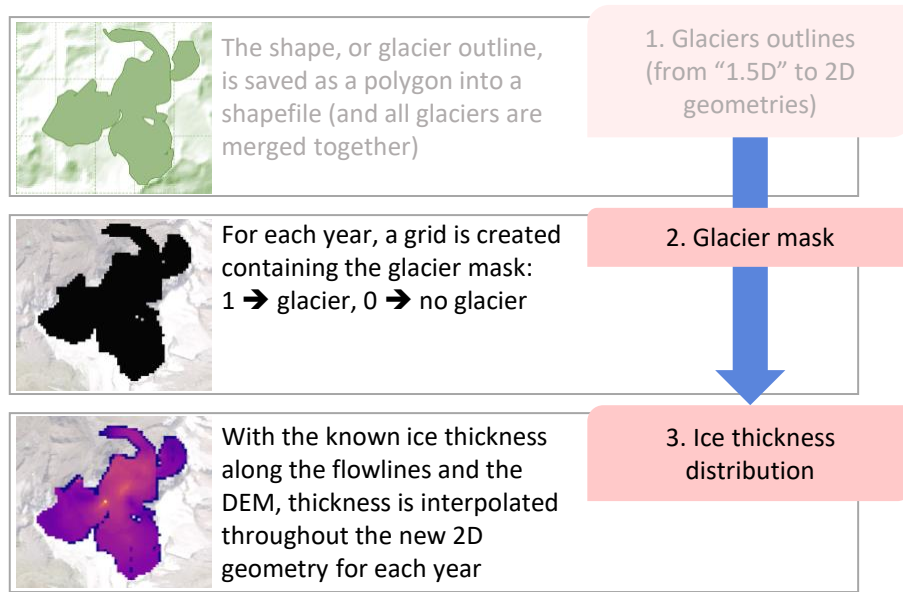


Figure 6.6: Procedure followed to get the distributed ice thickness for each of the 2D glacier geometries (outlines) determined in Section 6.4.4.

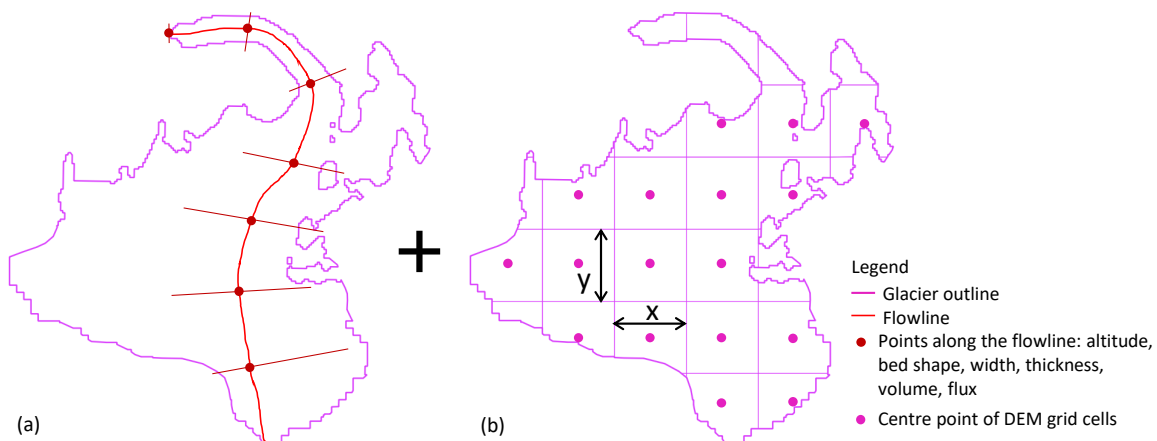


Figure 6.7: Procedure followed to interpolate the ice thickness, applied to the main flowline of Gepatschferner: (a) points along the main flowline of the glacier and (b) center points of the DEM grid cells, where the ice thickness is to be interpolated.

Finally, the results are saved in the same format as the 2D geometries so they can be used afterwards by WaSiM, together with the output grids defined in Section 6.4.4.

### 6.4.6 Glacier volumes

So far, the annual glacier outlines (2D geometries from flowlines) obtained after performing OGGM's simulations, satisfy WaSiM's requirements for running the integrated VA scaling glacier model. As already explained in Section 5.1, two input grids are needed by WaSiM, which are then used by the VA scaling approach to obtain the glacier's evolution throughout the modeling period.

Considering that a good approximation of the ice thickness distribution can be obtained for every glacier outline, the inclusion of this variable might reflect an improvement in the glacier modeling performed with WaSiM. In this way, not only the glacier area can be used as input, but also the glacier thickness, which together at the end yield the glacier volume. Figure 6.8 summarizes the steps needed to obtain the glacier volume starting from the glacier outlines and distributed ice thickness (i.e. the resulting outputs from the previous sections, 6.4.4 and 6.4.5).

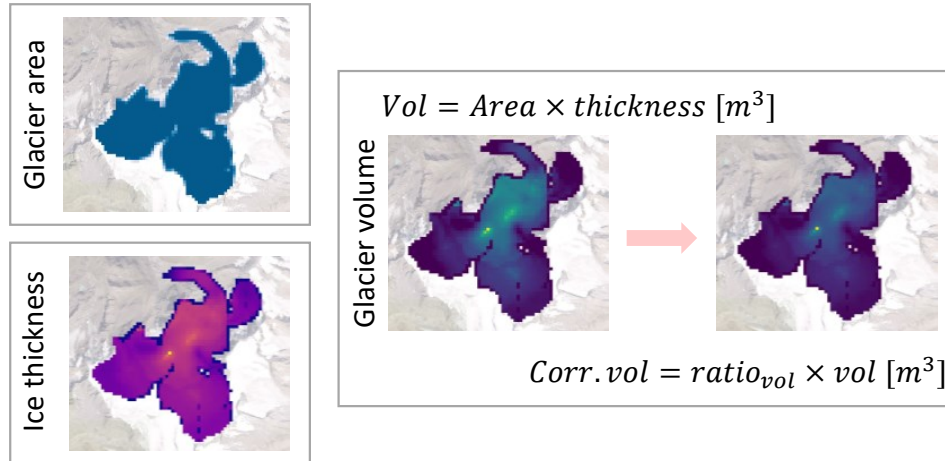


Figure 6.8: Determination of the (corrected) glacier volume, which serve as input for WaSiM, using the glacier area and distributed ice thickness obtained from sections 6.4.4 and 6.4.5.

The volume of the glaciers can be determined by simply multiplying the area covered by the glaciers and the thickness assigned to each of the cells that form the glacier area. This scheme can be adopted for every year, hence allowing to get annual volume grids for running WaSiM. Nevertheless, and similar as for when determining the glaciers area, there might be a mismatch between the total volume obtained after applying this procedure and the total volume calculated by OGGM, during the dynamic run. For this reason, a correction of the volume is performed at the end. In this step, the volume assigned to each grid cell is modified with a correction ratio, defined as (Equation 6.2):

$$ratio_{vol} = \frac{\text{simulated volume}}{\text{calculated volume}} \quad (6.2)$$

Where: *simulated volume* is the total annual volume obtained after the dynamic run with OGGM [ $m^3$ ] and *calculated volume* is the sum of the volume of each individual grid cell [ $m^3$ ], obtained from the glaciers areas [ $m^2$ ] and distributed ice thickness [ $m$ ].

## 6.5 Coupling the models: final WaSiM run with optimization

During the last step of the coupling scheme, the outputs generated from OGGM serve as input for re-running WaSiM. WaSiM's simulations are still carried out with a daily resolution but the glacier input grids are updated at an annual basis, since that is the time resolution of the outputs generated from OGGM. Moreover, in this run, the integrated VA scaling

approach in WaSiM is activated, but it is re-initialized at the beginning of each mass balance year (1<sup>st</sup> October for the Northern Hemisphere) with the outputs generated by OGGM, thus the internal calculations performed by the VA scaling are "replaced" by OGGM's results. Because of these reasons, and due to the rather slow movement of glaciers, an annual update of the glaciers' geometry is a conventional approach (e.g. Stoll et al., 2020).

As already mentioned, the modeling of glaciers with the VA scaling approach integrated in WaSiM requires as input only the area covered by the glaciers. Then, the volume of the glacier at the beginning of the simulation is calculated according to Equation 5.2, where the mean thickness of the glacier (represented by the parameter  $b$ ) is fixed for all the glaciers and the entire simulation period. At the end of the first year of the simulations, the new glacier area is calculated by means of Equation 5.4. By introducing the areas obtained from OGGM (from Section 6.4.4) at the beginning of each hydrological year, the new area calculated by WaSiM by Equation 5.4 is in a sense omitted, since the produced output is replaced by the new inputs generated from OGGM. As a result, a first connection between both models is established. In order to update the glacier areas at the beginning of each hydrological year, WaSiM is re-initialized every October. This re-initialization of the model denotes that the integrated VA scaling glacier model is also re-initialized every year, with the new OGGM's areas. Consequently, Equation 5.2 is solved each time the model is re-initialized, determining a new volume for each year.

By knowing the annual glacier areas and their corresponding ice thickness distribution, a volume distribution can also be approximated (Section 6.4.6). Considering that the yearly re-initialization of WaSiM yields to a newly calculated volume, a more robust connection between WaSiM and OGGM can be made by introducing also the ice thickness distribution, which is computed following the explicit ice-flow dynamics. The integration of the glacier thickness (and volumes) into the coupling scheme represents an improvement compared to existing coupling schemes, where only areas (e.g. Khadka et al., 2020; Stoll et al., 2020) or just the runoff from the glacierized parts of the catchment is included in the hydrological simulations (e.g. Wiersma et al., 2022). Figure 6.9 shows the general procedure followed in the third step of the workflow of the coupling scheme, in which WaSiM is re-initialized annually with OGGM's outputs.

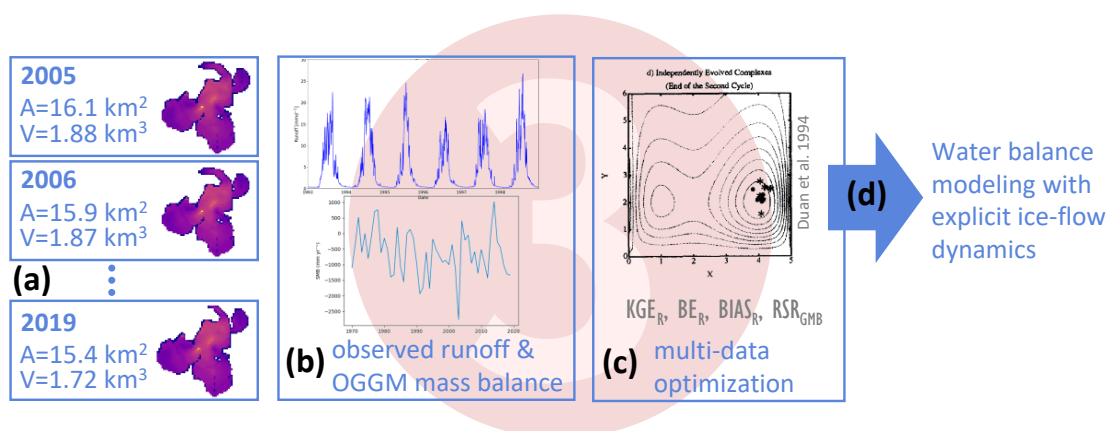


Figure 6.9: Third (last) step of the coupling-scheme: WaSiM continuous run with annual OGGM outputs and automatic multi-data optimization. (a) gridded input from OGGM run: annual glacier areas and ice thickness distributions (volumes), (b) observed runoff and glacier mass balance (OGGM) for running the (c) multi-data optimization, (d) final result: water balance modeling with explicit ice-flow dynamics.

Even though glacier areas, ice thickness distribution and volumes determined by OGGM serve as input for re-running WaSiM during the last step of the coupling scheme, both models calculate the glacier mass balance separately but based on the same T-index approach. On the one hand, WaSiM enables to obtain daily mass balances for each subcatchment (or each glacier), relying on the accumulation and ablation components that are determined after Section 5.1.1. On the other hand, OGGM determines the annual mass balance for each glacier by means of Equation 5.5 (Section 5.2.3). Therefore, a direct correspondence between both glacier mass balances must be made to ensure that the dynamics of the glaciers is correctly transferred from OGGM to WaSiM.

In this sense, one obvious solution might be the direct integration of OGGM mass balance into WaSiM, hence substituting the calculation of daily mass balance values. However, this cannot be easily done and a modification in the model's code is required. In some cases, the codes are not readily available for the user, or even if they are, a code's modification might work for the current WaSiM's version, but incompatibilities can be expected if another updated version is selected. Besides, in this study, WaSiM is chosen as the hydrological model, but the developed coupling might serve as a basis for coupling OGGM with any other similar model. Moreover, the potential of getting daily mass balance values would be unexploited and this is one of the main capabilities of WaSiM and a primary reason of using this model. As a consequence, another solution consists in using the glacier mass balance calculated by OGGM as a constraint when re-running WaSiM. This can be introduced through a multi-data optimization approach, in which the parameters describing the accumulation and ablation processes (among other parameters) in WaSiM are automatically adjusted by minimizing the differences between OGGM ("observed") and WaSiM (simulated) mass balances. The mass balances obtained from OGGM are considered as observed data, since no real measurements are available for the modeled glaciers (except the mass balances at the tongue of *Gepatschferner*) and also because it is used to constrain the integrated WaSiM's glacier model to match OGGM results. Figure 6.10 provides a summary of the considered simulation period within the coupling scheme, together with the intermediate steps required for running OGGM.

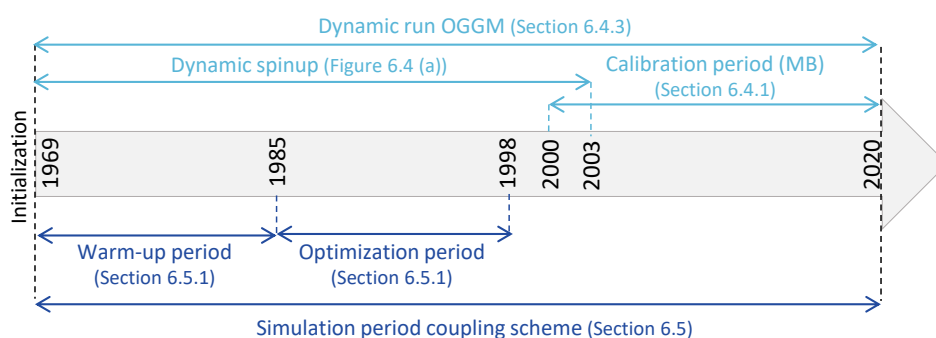


Figure 6.10: Simulation period selected for performing the simulations with the WaSiM-OGGM coupling scheme (dark blue). Additionally, the intermediate steps carried out by OGGM are also included (light blue).

### 6.5.1 Multi-data optimization

The general procedure is depicted in Figure 6.11 and refers to the main three steps that belong to the workflow followed in the coupling scheme. First of all, the term optimization

means obtaining the optimum parameter set adjusted during the calibration of the coupled model. All WaSiM sensitive parameters (determined from Section 6.3.1) are adjusted while minimizing the differences between observed and simulated data, which can be expressed in terms of an objective function. The parameter set that yields the smallest objective function is selected as optimum set. Second, the term multi-data refers to the use of more than one target variable for optimizing the model.

In this study, and considering that the glacier mass balance is used as a constraint for running the coupled model, two variables are selected during the optimization: (i) Runoff and (ii) Glacier mass balance. The choice of these two variables is also in line with the suggested way of calibrating hydrological models in glacierized catchments (e.g. Konz and Seibert, 2010; Tarasova et al., 2016; van Tiel et al., 2020).

- (i) **Runoff (R):** Data is available at a daily time step for the period covered between 01/1985 and 12/2019 and for the outlet of the catchment (Section 3.2 and Figure 3.1).
- (ii) **Glacier mass balance (GMB):** In this case, the glacier mass balance refer to the results obtained after running OGGM, since WaSiM's glacier simulations are constrained in a way that OGGM's results are closely represented. Thus, data is available at an annual scale and for each of the simulated glaciers. However, in this study, only the mass balance of *Gepatschferner* is used during optimization, since it is the main and biggest glacier within the study area.

The optimization is carried out at a daily time step for the period 01/1985 to 12/1998 and the model is initialized in 10/1969. However, two other optimization strategies are further adopted, in order to test different sources of uncertainties (model initialization and parameter uncertainties). Thus, the following schemes are developed:

- (a) Coupling initialized in **1969**. This corresponds to the current set up, and the optimization runs from 01/1985 to 12/1998. OGGM is initialized in 1969 with a dynamic spinup (Figure 6.4 (a)).
- (b) Coupling initialized in **1984**. In this case, the optimization is also carried out for the period between 01/1985 to 12/1998, but with a shorter warm-up period, to see whether the length of this period influences the final simulation results. OGGM is also initialized in 1969 with a dynamic spinup (same as (a)).
- (c) Coupling initialized in **2003**. The model is initialized in the same year for which the RGI glacier outlines are available, in order to study the uncertainties that might arise from the dynamic spinup of OGGM. In this case, OGGM is initialized in 2003 and no dynamic spinup is performed. The coupling is then optimized for the period 01/2006 to 12/2015.

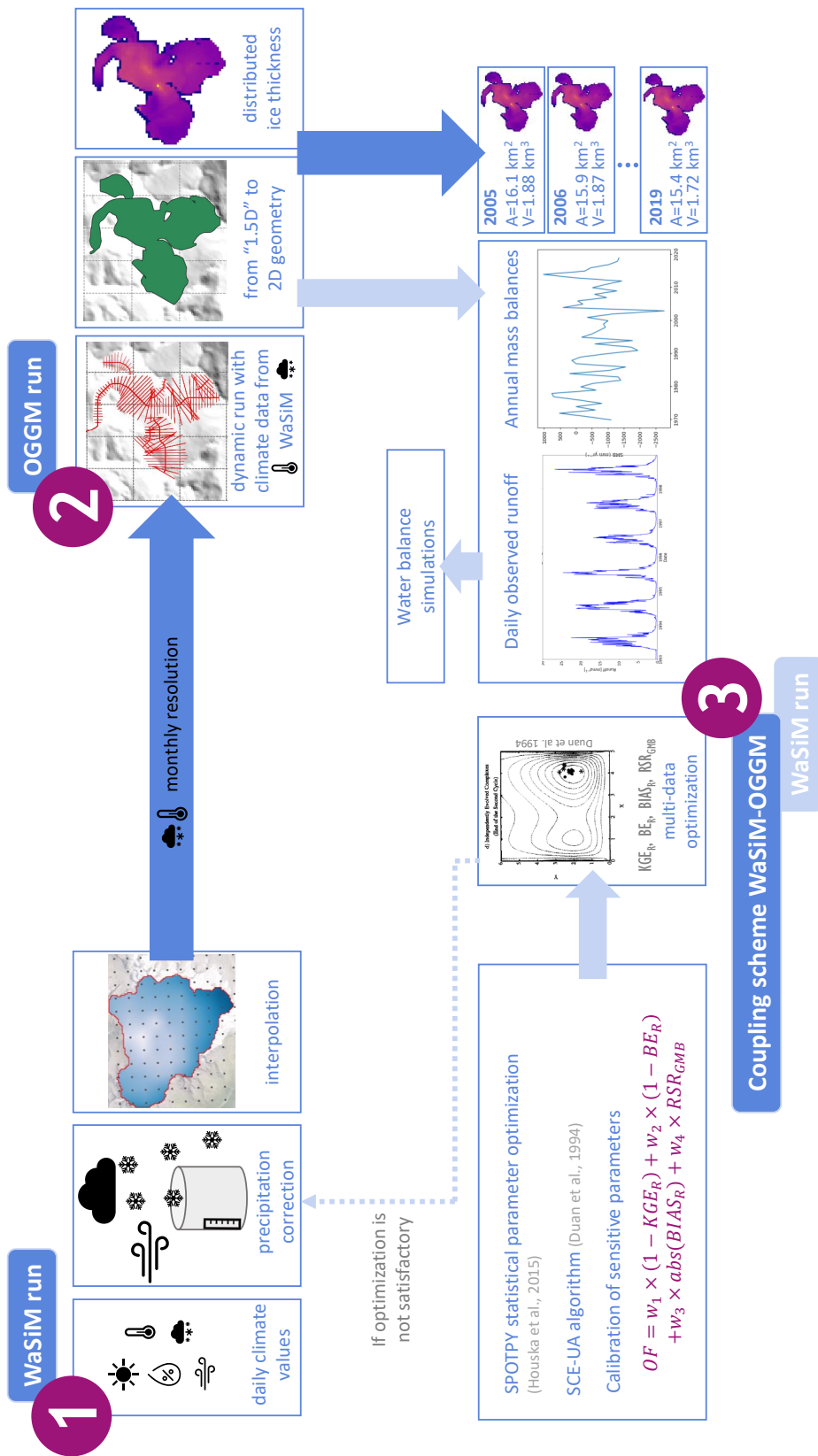


Figure 6.11: Detailed workflow of the coupling scheme with multi-data optimization.



The optimization period for the model setup (a) differs from the calibration period selected for the first WaSiM run with VA scaling (Section 6.3.2), although both models are initialized in the same year (1969). A few reasons explain this decision:

- Independent models: Despite that the first WaSiM run is needed to obtain the monthly climate datasets which serve as input to OGGM, the initial conditions of the glaciers are different in the coupling scheme. This means that the processes in each model (WaSiM with VA scaling and coupling scheme) are governed by different boundary conditions, so different parameter sets might be involved in the processes.
- Comparison of results: The first WaSiM run is calibrated in this study only to compare the results between WaSiM with VA scaling and the coupling scheme. As mentioned in Section 6.3.2, this calibration step could simply be ignored for any other applications of the coupling scheme.
- Computational times: While the required time to perform 1-year simulation with WaSiM (including VA scaling) is around 26 seconds, the coupling scheme takes almost 40 seconds. This means that the coupling scheme is computationally more expensive and that a continuous 50-year simulation takes approx. 33 minutes (almost 54% longer than the first WaSiM run). Thus, a shorter period is chosen while optimizing the coupling scheme.
- Warm-up period: By starting the optimization in 1985, the warm-up period can be reduced while still exploiting the available runoff observations, which start on that year. Besides, the ending year (1998) coincides with available glacier outlines.
- Number of iterations: The optimization algorithm requires several iterations until the minimum of the objective function is reached. Even by limiting the maximum number of iterations to 2000, 40 days are required to optimize the coupling scheme for the period 1985-1998 (initialized in 1969). This number could increase if a longer period is considered.

### 6.5.1.1 Multi-objective function

The consideration of two variables for the calibration of the model requires also the use of more than one objective function. Following the study of Tarasova et al., 2016, in which they developed a calibration strategy for a glacierized catchment in Asia, a similar strategy is used in this study. The multi-objective function ( $OF$ ) consists of four main components (Equation 6.3):

$$OF = w_1 \cdot (1 - KGE_R) + w_2 \cdot (1 - BE_R) + w_3 \cdot abs(BIAS_R) + w_4 \cdot RSR_{GMB} \quad (6.3)$$

Where:  $KGE_R$  is the Kling-Gupta efficiency (Gupta et al., 2009),  $BE_R$  is the Benchmark efficiency (Schaeffli and Gupta, 2007) and  $BIAS_R$  is the bias (according to Gupta et al., 1998), all of them calculated based on observed and simulated runoff (at a daily basis, see Table 6.1).  $RSR_{GMB}$  is the root mean square error standard deviation ratio between observed and simulated glacier mass balances (determined at an annual basis, Moriasi et al., 2007) (all measures are defined in Appendix B).  $w_1$  to  $w_4$  are the weights used to assign

the magnitude of the contribution of each performance measure into the total objective function. The sum of the weights is equal to 1 and similarly to the study carried out by Tarasova et al., 2016, the following values are adopted: 0.23, 0.4, 0.07 and 0.3 for  $w_1$ ,  $w_2$ ,  $w_3$  and  $w_4$ , respectively.  $w_1$ ,  $w_2$  and  $w_3$  make the multi-objective function more sensitive to the runoff behavior, representing 70% of the total weight. On the other hand,  $w_4$  suggests that the glacier mass balances represent a 30% of the total weight in the multi-objective function. This value is in the same order of magnitude as the ice melt contribution in the generation of the total runoff and similar to the value suggested by Tarasova et al., 2016.

### 6.5.1.2 Optimization algorithm

Similarly to the sensitivity analysis carried out during the first WaSiM run, the multi-data optimization is carried out automatically with the help of SPOTPY (Houska et al., 2015). Among the available optimization algorithms, the **Shuffled Complex Evolution - University of Arizona, SCE-UA** (Duan et al., 1994) is chosen in this study. It is one of the most used algorithms in hydrological and water balance modeling (e.g. Parajka et al., 2007; Tarasova et al., 2016) and searches the global improvement through competitive evolution (i.e. process of natural evolution) by applying a complex shuffling. While the term complex refers to a certain community of points that can evolve independently, the term shuffling alludes to the mixing of those communities (Duan et al., 1992; Duan et al., 1994). Since the algorithm requires a criterion to be minimized, an objective function should be defined beforehand. In this case, this is given by the multi-objective function expressed by Equation 6.3. Figure 6.12, which was taken from Duan et al., 1994, shows an example on how the SCE-UA optimization algorithm works.

The contour lines in Figure 6.12 represent a function with one global optimum ((a) located at  $x=4$ ,  $y=2$ ). The population contains in total ten points, which are separated in two complexes of five points each. As it can be seen in the figure, one complex converges towards the local optimum, whereas the other one, to the global optimum (b). After shuffling the complexes, the results are shown in (c) and finally, (d) shows the results at the end of the cycle, where all complexes converge towards the global optimum (Duan et al., 1994).

During the implementation of the SCE-UA algorithm, the selected parameter set is adjusted until the global optimum is reached. In other words, the algorithm stops when the objective function is minimized. Besides, the maximum number of iterations should be given, among other specific settings. In this case, the maximum number of iterations is limited to 3000.

## 6.5.2 Uncertainties

Among the different types of uncertainties inherent in modeling (Section 2.3.4.2), the uncertainties related to model initialization and parameters are analyzed in this study.

### 6.5.2.1 Uncertainties in model initialization

The uncertainties in model initialization refer particularly to the initialization of the glacier model. The accuracy of the simulation results relies on the initial glacier outlines, which

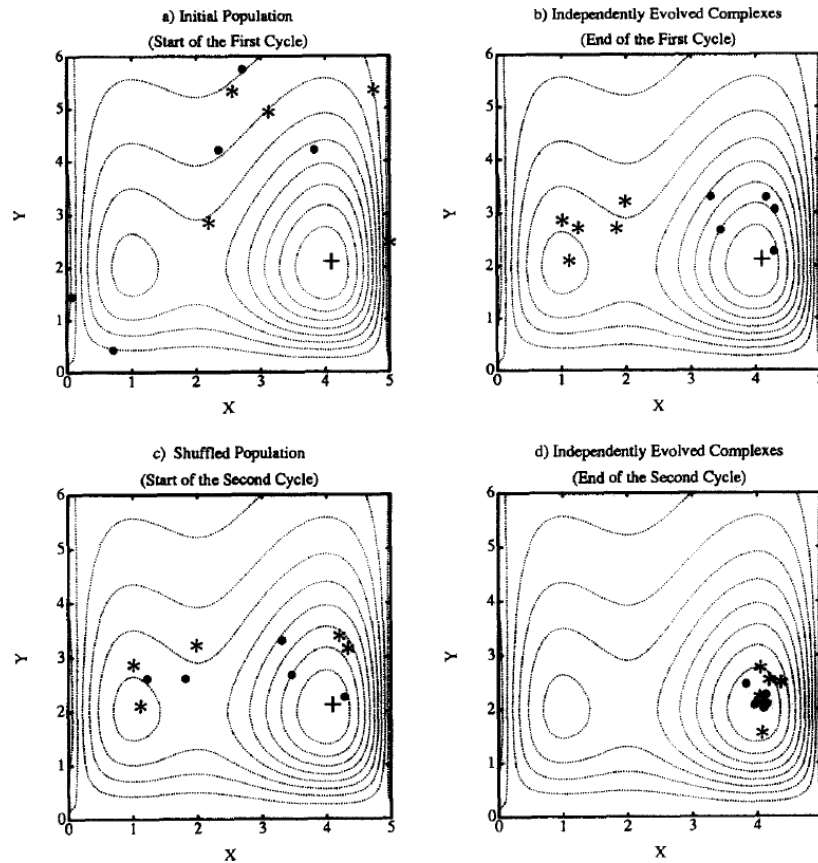


Figure 6.12: Example of the SCE-UA method, for a two-dimensional problem with one local and one global optimum. • denotes complex 1, whereas \* denotes complex 2 (each of them with 5 members, Duan et al., 1994).

might be unknown if past simulations are performed. Non-unique solutions on initial glacier states might be equally adequate for representing the present state under the current climatic conditions, making the initialization of the model a complex issue. One primary source of uncertainty is related to the derivation of the glacier outlines themselves. For example, Pfeffer et al., 2014 state that the uncertainty related to the RGI is about  $\pm 5\%$  since they are observed datasets and a misinterpretation of seasonal snow cover might lead to such discrepancies. Another source of uncertainty comes from the initialization method itself, being the uncertainties larger during the first years after initialization (Eis et al., 2021).

The initialization of the coupling scheme relies on the correct initialization of OGGM, which might include the above-mentioned uncertainties. In order to infer the magnitude of such uncertainties, different model simulations are performed (according to Section 6.4.3), in which the model is initialized in different years, spanning from 1969 to 2003, with intervals of 5 years. The initialization in the year 2003 corresponds to the OGGM model without dynamic spinup, hence overcoming the potential uncertainty related to the initialization method.

### 6.5.2.2 Parameter uncertainty

When optimizing a model, multiple parameter sets can yield to good performance, thus a unique solution might not be achieved (known as the equifinality problem, Beven and Freer,

2001; Beven, 2006). The robustness of the model can be estimated from the uncertainty of the model parameters in terms of stability and identifiability (Tarasova et al., 2016). Stability is the primary condition of robustness and can be inferred by analyzing parameter values over different optimization periods. Additionally, when considering different optimization periods, it is expected that the values of the parameters vary in the same narrow range, since they should not depend on the period or method used during optimization (identifiability). Following the studies by Stahl et al., 2008; Parajka et al., 2007; Tarasova et al., 2016, the results of different optimization periods are considered and evaluated to get the range of the parameters' uncertainties. Like described by Tarasova et al., 2016, parameter datasets that yield the lowest multi-objective function plus 10% of the function range are selected. For this analysis, the three model setups described in Section 6.5.1 are considered, which differ in their initialization and optimization periods.

### 6.5.3 Future projections

After calibration and validation of the individual models and optimization of the coupling scheme, simulations are also performed under future climatic conditions. This allows not only to evaluate the performance of each model in the future, but also to test whether the coupling scheme is able to predict a reliable catchment's response under changing climate. To achieve this, the three climate model combinations described in Section 3.2.4.3 are used as forcing datasets to run the three steps of the coupling scheme: (i) WaSiM run with VA scaling approach, (ii) OGGM run and (iii) final WaSiM run with OGGM outputs (i.e. WaSiM-OGGM coupling scheme). In all cases, two periods are distinguished: on the one hand, the historical simulations dating from 1970 to 2010 and on the other hand, future simulations from 2011 until 2100. The future simulations rely on the models that were set up and calibrated during the historical period.

For the first WaSiM run with the integrated VA scaling approach, the model starting in 1969 and calibrated during the period 1990-2006 is used. For OGGM's future simulations, the model with dynamic spinup is selected. Finally, the coupling scheme starting in 1969 is also selected. The results are presented altogether in Section 7.4, where a direct comparison between the WaSiM model with the integrated VA scaling approach and the WaSiM-OGGM coupling scheme is made.

# Chapter 7

## Results and discussion

This chapter includes the results of the coupling scheme and intermediate steps, following the structure of Chapter 6. In addition, Section 7.1.4 summarizes the main results of the glacier part, obtained after running WaSiM with the integrated VA scaling approach. These results serve as a reference for the comparison with the results from the coupling scheme, which is presented in Section 7.4. Here, the focus is not only given to the past simulations, but also to the behavior of both models under future climatic conditions. This enables to find support for answering the research questions introduced in Section 1.3. Finally, Section 7.5 shows the applicability of the coupling scheme in another catchment. For these simulations, the neighboring *Rofenache* catchment is considered due to the availability of the same INCA climate dataset and the presence of three reference glaciers. This allows to additionally include annual mass balance observations for the evaluation of the coupling scheme and to assess the performance of the coupling against more measurements.

### 7.1 First WaSiM run with resampling of climate data

This first run of the WaSiM model includes the dynamic VA scaling glacier approach (Section 5.1). Although the simulation results of this step are not required for running the coupling scheme (only the monthly climate grids are required after the first WaSiM run), they are used afterwards for the comparison with the results obtained from the coupling scheme. In this way, the simulation results in terms of glacier evolution and runoff gained by the integrated empirical VA scaling approach are directly compared to the results after introducing explicit ice-flow dynamics and determined with OGGM (Section 7.4).

#### 7.1.1 Sensitivity analysis

The results from the sensitivity analysis are depicted in terms of a sensitivity index. This index can vary between 0 and 1 and indicates the sensitivity of a parameter to the simulation results considering the interactions with other parameters (Saltelli et al., 1999; Xu and Gertner, 2011). A value close to 1 indicates that the parameter is very sensitive, whereas a value near 0 suggests that the parameter is not sensitive. Figure 7.1 shows the total sensitivity index for each of the parameters selected during the sensitivity analysis. Also, and for each of the sub-models, a threshold of three sensitive parameters is chosen. As it is feasible to see from the figure, it is clear that for the soil model (Figure 7.1a),  $k_d$  (storage coefficient for surface runoff),  $k_i$  (storage coefficient for interflow) and  $q_0$  (scaling factor for

baseflow) are the most sensitive parameters with a total sensitivity index between 0.3 and 0.4. Moreover, for the glacier model (Figure 7.1b), the most sensitive parameter is the melt factor,  $m_f$ , with a sensitivity index close to 1.0, whereas the two factors affecting the VA scaling equation ( $va_{scal}=b$  and  $va_{exp}=f$ , Equation 5.2) do not show any influence on the simulation results. The storage coefficients for ice ( $k_{ice}$ ), firn ( $k_{firn}$ ) and snow ( $k_{snow}$ ) show almost no sensitivity, compared to the melt factor. Finally, for the snow model (Figure 7.1c), the threshold temperature for snow melt,  $t_0$  is the most sensitive parameter, reaching a total sensitivity index of almost 0.8. The parameters  $min_{slope}$  (minimum slope for creating slides,  $i_{erosion}$  in Equation 4.12) and  $l_{wout}$  (correction factor for outcoming long wave radiation, affecting Equation 4.16) are also sensitive, but to a lesser extent.

In this sensitivity analysis, only the simulated runoff at the outlet of the catchment is considered as target variable. It might be expected that another set of parameters lead to higher total sensitivity indices if glacier mass balances or glacier outlines are selected as additional target variables. However, and since the main focus of the hydrological modeling is given to the simulated runoff, only this variable is analyzed at this stage and the resulting sensitive parameters can be used for the calibration of the model and optimization of the coupling scheme.

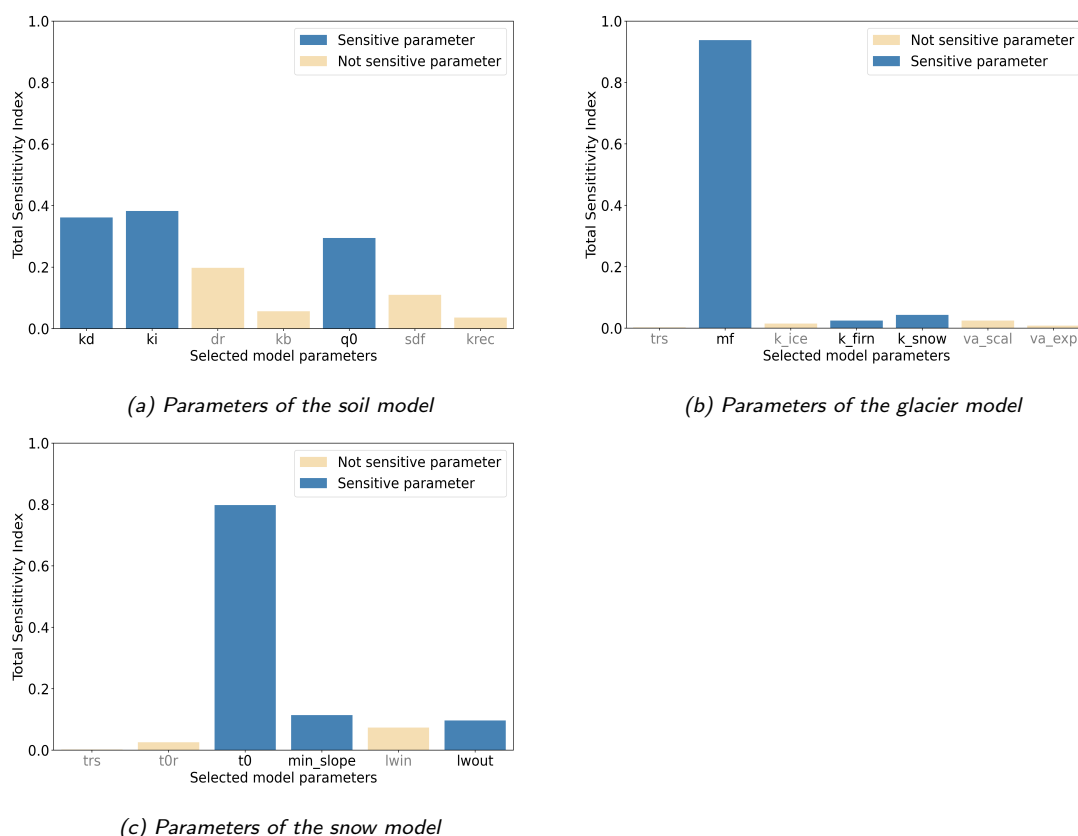


Figure 7.1: Results of the sensitivity analysis performed during the first WaSiM run. In each case, a threshold of three sensitive parameters is selected (following Houska et al., 2015).

## 7.1.2 Calibration and validation of the model

With the most sensitive parameters, a calibration of the model at a daily time step is performed. Apart from the runoff at the outlet of the catchment, the simulated glacier

areas for the years 1998 and 2006 are considered as target variables. Figure 7.2 illustrates the mean daily observed and simulated runoff at the outlet of Gepatschalm during the calibration period. The mean daily value refers to the average runoff of the same day during the entire simulation period. For example, if the simulation period consists of 17 years, the mean daily value for the 1<sup>st</sup> January is calculated as an average of 17 values. The figure also includes the simulated runoff component from ice melt and the performance measures during calibration. Additionally, Figure C.1 in the Appendix shows the daily observed and simulated values for the entire calibration period, whereas the calibrated parameter values are summarized in Table C.2.

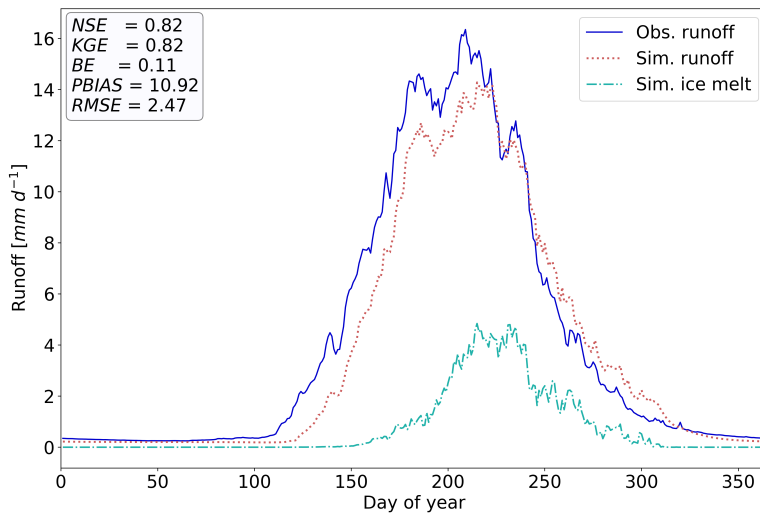


Figure 7.2: Mean daily observed and simulated runoff at the outlet of Gepatschalm during the calibration period (01/1990 - 12/2006), including simulated ice melt. Blue solid line: observed runoff, red dashed line: simulated runoff, light blue line: simulated melt from ice. The performance measures are defined in Section 6.3.2 and Appendix B.

As can be seen from Figure 7.2, observed and simulated values are in good agreement. The mean daily peak during summer is quite well represented, being  $16.4 \text{ mm d}^{-1}$  (end of July) and  $14.5 \text{ mm d}^{-1}$  (beginning of August) for observed and simulated runoff, respectively. In annual terms, the mean observed runoff is  $1588 \text{ mm yr}^{-1}$ , whereas the simulated value is  $1383 \text{ mm yr}^{-1}$ . The performance measures suggest that the calibration results are very good, since NSE and KGE are greater than 0.75 and PBIAS is almost 10%. Even though the BE is a bit low, this is in agreement with other studies carried out in similar regions (e.g. Hanzer et al., 2016), where seasonality plays a crucial role in runoff generation.

Nevertheless, there is an underestimation of the simulated values during late spring (approx. between mid May and mid June) and summer, and a small overestimation during autumn (mid September to mid November). On the one hand, snow melt is the predominant process for runoff generation during spring months. The adjustment of the parameters that describe snow processes is quite challenging, because they rely on mechanisms for snow redistribution and an energy balance approach, which are more complex compared to other methods (e.g. like the T-index method). Besides, snow measurements are not available during the calibration period, hence it is not possible to include snow as an additional target variable. For this reason, SWE is considered during the second validation period, for which the snow measurements are available. In addition, the determination of the melt rates in glacierized areas do not consider radiation, hence lower melt rates of snow/firn/ice during spring might be another reason of this underestimation. Furthermore, the wind and gravitational redistribution of snow might also play a role, since snow is redistributed to other areas, where the snow pack is not able to melt completely.

On the other hand, the contribution of the ice melt to the generation of runoff suggests that this is the main driver for the overestimation during the autumn months (September

to November), as shown in Figure 7.2. The parameters of the glacier model are adjusted globally considering not only runoff as a target variable but also glacier outlines during different years. The "disagreement" between observed and simulated runoff during autumn in the calibration period may be compensated with a more accurate representation of the glacier outlines, which are shown in Figures 7.3a for the year 1998 and 7.3b for the year 2006. Another important issue to mention is that the empirical factors that affect the VA scaling equation were not adjusted during calibration, since they showed to be not sensitive. In this case, the suggested values from literature are used. An exponential factor of  $f = 1.36$  and a mean ice thickness of  $b = 28.5$  m (Equation 5.2), are adopted for all glaciers and entire simulation period. However, this might not be completely accurate, since the mean ice thickness for all the glaciers in the catchment is close to 51 m (for example, Fischer and Kuhn, 2013). This issue is to be tackled in the third run of the coupling scheme, where the ice thicknesses and volumes calculated by OGGM are integrated into WaSiM, thus updating the factor not only at an annual scale, but also at a glacier (and model grid) basis.

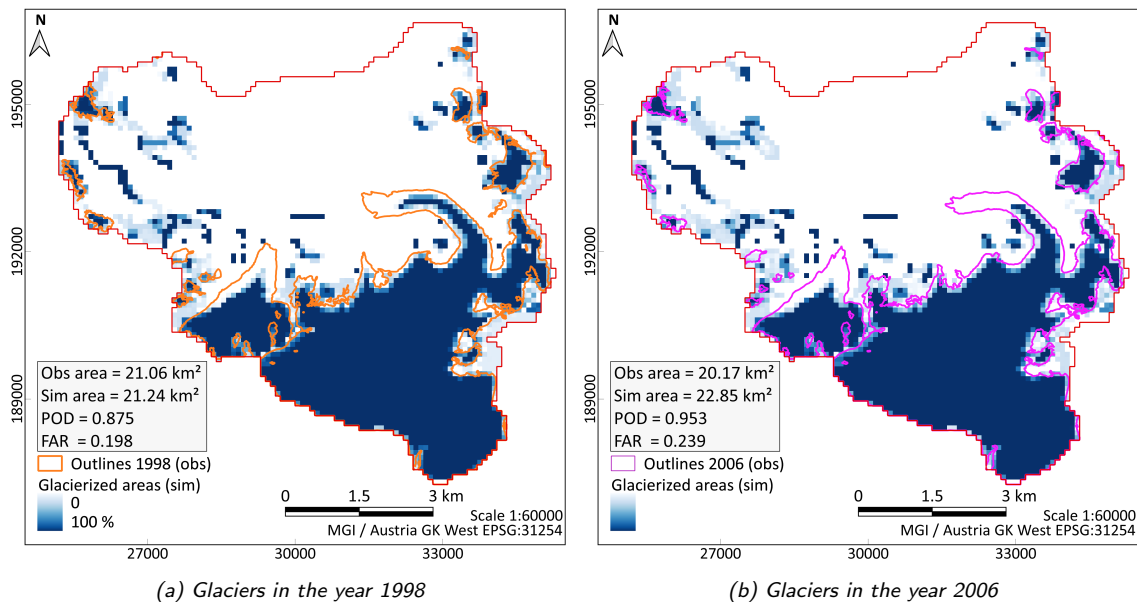


Figure 7.3: Observed and simulated glacier areas for the years 1998 and 2006. The outlines belong to the AGI (Section 3.2.2.1) and the performance measures are defined in Section 6.3.2 and Appendix B.

The dark blue color in Figures 7.3a (year 1998) and 7.3b (year 2006) stands for a completely glacierized cell (100%), whereas no color indicates that the cell does not contain any glacier (0%). For any color in between, the glacierization varies between 0 and 100%. The figures include the observed glacier area, provided by the AGI and the simulated area obtained from WaSiM, both given in  $\text{km}^2$ . Moreover, two performance measures are included, which follow the evaluation stated by Kormann et al., 2016. The Probability of Detection (POD) indicates the ability of the model to correctly predict glacierized cells. Similarly, the False Alarm Rate (FAR) indicates the model cells identified with glaciers by the simulation, but which do not contain any glacier component in the observation. Both measures range between 0 and 1, being 1 the optimum value for POD and 0 for FAR. The performance measures are defined in Appendix B.

For both years, there is a pretty accurate representation of the glacierized areas, especially for the two main glaciers, *Gepatschferner* and *Weißseeferner*. This can be inferred from the high POD values, which are close to 1. In the tongue of *Gepatschferner*, where



ice flow dynamics and mass balances rates are likely to be higher due to the lower altitudes compared to the rest of the glacier (Stocker-Waldhuber, 2019), there is a small underestimation. The presence of glacierized cells beyond the observed glacier outlines, together with the relatively large values of FAR, suggest that the model has some deficiencies in the accumulation component of the mass balance of the glaciers. One possible reason of this overestimation of glacierized cells may be related to the redistribution of snow due to wind and gravitational slides, as it was explained before.

To have a better understanding about the underestimation of runoff during spring months (contribution of snow melt), SWE is evaluated and shown in Figure 7.4, for the validation period. The purple solid line represents the observed (calculated after Equation 3.1 from observed SD and  $\rho_{snow}$ ) SWE, whereas the pink dashed line represents the simulated values at the outlet of the subcatchment where *Weißseeferner* is located. The period depicted in the figure spans from 01/2015 to 07/2018, where also the PBIAS and RMSE between observed and simulated values are indicated. In general, SWE increases steadily over the course of winter, reaching a maximum observed value of 628 mm, and a maximum simulated value of 754 mm. Seasonal differences result from the evolution of the snow bulk density, which is greater during the ablation than the accumulation period. Due to the accumulation and compaction of snow, the SWE of the snowpack is greatest at the end of winter, like shown in the figure (Schattan et al., 2017). Although there is a good correspondence between peaks, the simulated values are overall overestimated, except during the year 2017 (during this year, a PBIAS of 19% and RMSE of 90.7 mm are obtained).

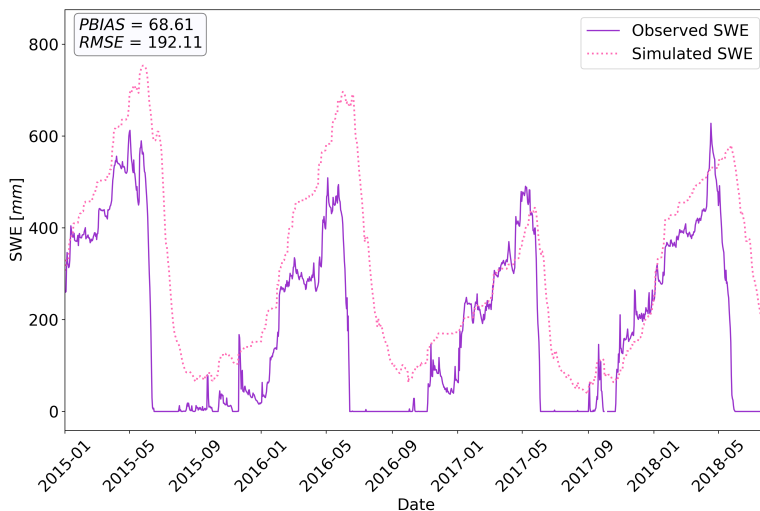


Figure 7.4: Observed (at AWS) and simulated (at the outlet of *Weißseeferner*) SWE during the period 01/2015 - 07/2018. Purple solid line: observed values, pink dashed line: simulated values. The performance measures are defined in Section 6.3.2 and Appendix B.

During summer months, observed SWE indicates that those months were mostly snow-free, when snow melted completely. However, the model seems to fail to represent SWE in those months, where minimum values of around 50 mm  $d^{-1}$  are obtained. The discrepancies might be attributed to different causes: on the one hand, observed SWE values are not directly measured values, but reconstructed from two other variables (SD and  $\rho_{snow}$ ), which results in expected uncertainties in the observed values. On the other hand, simulated SWE values are obtained at the center point of a model grid cell, and the location of the AWS (location showed in Figure 3.1), does not exactly correspond to this point. Hence, the incorrect representation of the surrounding terrain could also be another source of disagreement between values (e.g. Thornton et al., 2021). Additionally, although snow melt plays a fundamental role in the generation of runoff, the snow model was not calibrated against snow observations. The inability of the model to allow the melting of snow could be

explained by inaccuracies on the snow model, which in this case includes snow redistribution due to gravitational slides and wind. It could be possible, that the model grid cell in which the simulated values are evaluated, is directly influenced by those phenomenon. Moreover, in this model one single layer is used to represent the snowpack. By considering a multi-layered snow model, that is, modeling the snowpack with multiple layers, the temperature within the snowpack can be taken into account. In this way, the heat transfer processes through the snowpack might better represent the melting component and more accurate results could be achieved.

At this point, it is important to emphasize that the results obtained from this first WaSiM run are not required for running the coupling scheme. Only the aggregated monthly values of precipitation and temperature are needed, which serve as input for OGGM (see next Section). Nevertheless, the simulation results are still analyzed, since they are compared to the outcome of the coupling scheme. Appendix C.1 complement the results obtained during the sensitivity analysis, calibration and validation of the first WaSiM run.

### 7.1.3 Generation of monthly climate grids

As an example, Figure 7.5 shows the mean monthly temperature and total precipitation values for October 1998, result from the bilinear interpolation carried out in WaSiM. These monthly values are used as input for running OGGM during the second step of the coupling scheme. It is feasible to see the influence of the topography in both variables, since lower temperatures and higher precipitation amounts are expected in the southern boundaries of the catchment, where the elevations are higher. On the contrary, higher temperature and lower precipitation values can be seen at the lower elevations, in the vicinity of the Gepatsch reservoir. The figure also shows the location of the INCA points (grid size 1 km<sup>2</sup>). These points have a high density of "stations" which are used to interpolate the two variables.

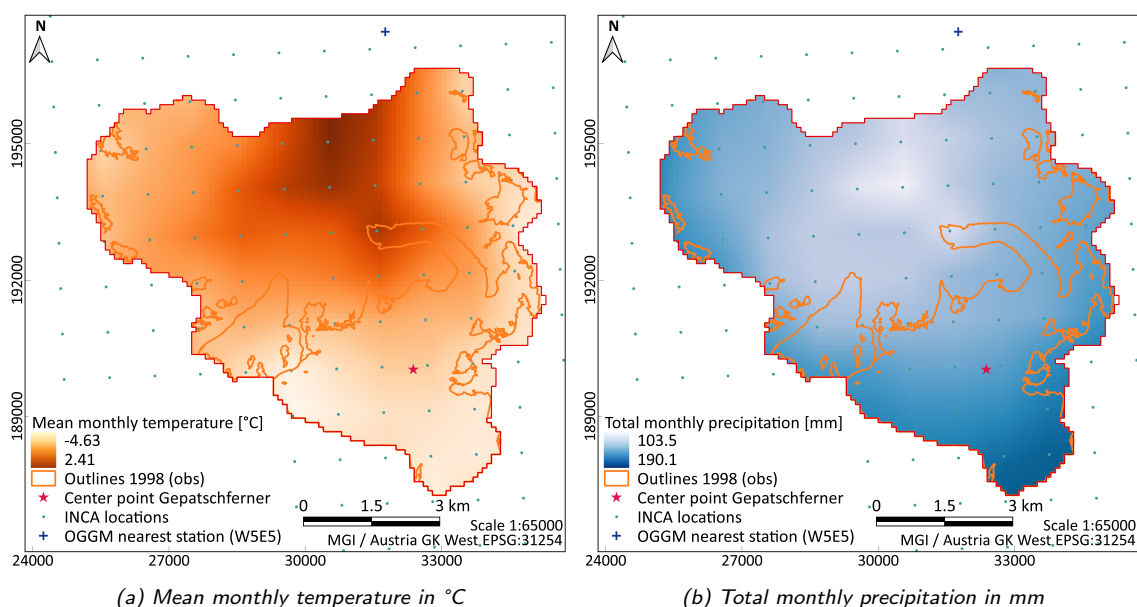


Figure 7.5: Aggregated interpolated temperature and precipitation values from INCA locations. The values correspond to October 1998. The observed glacier outlines for the year 1998 and the center point of the Gepatschferner are included in the figure, together with the OGGM's nearest station from the default dataset (W5E5).

Moreover, and to gain more insight into the next step of the coupling scheme, the center point of the *Gepatschferner* is included in the figure, which is the point used by OGGM for performing all internal climate computations related to this particular glacier (each glacier has its own center point). When performing OGGM calculations with its default climate dataset (W5E5 is the climate dataset used by OGGM per default), the nearest "station" to the glacier lies about 7 km away from the center of the glacier (north), as shown in the figure. The altitude at this point is nearly 2300 m a.s.l., whereas the altitude at the center of the glacier is 3010 m a.s.l. On the contrary, in case of the coupling scheme, the nearest "station" to the center of the glacier is taken from the INCA locations, which lie very close to it. This implies that the dense WaSiM climate grid (INCA) may provide more accurate input climate variables for the glacier, as the attitude dependence of such variables is accounted for by the nearest points.

### 7.1.4 WaSiM VA scaling glacier model

The results of the integrated VA scaling glacier model are analyzed in terms of glacier outlines and total glacier mass balance. For the first case, the glacierized cells for the years 1998 and 2006 together with the observed outlines were already shown and analyzed in Figure 7.3. The simulated annual mass balances are depicted in Figure 7.6a, where the dashed light blue line represents the annual mass balance only for *Gepatschferner* and the solid blue line represents the annual mass balance as a total average for all the glaciers within the study area. Moreover, the horizontal line indicates an annual mass balance of 0, meaning that the amount of accumulation equals the amount of ablation. In this case, the values are always below the horizontal line of 0, suggesting that the glaciers have been decreasing their volume and size throughout the simulation period (negative mass balance values).

Besides, Figure 7.6b shows the cumulative mass balance (this value is obtained by integrating annual mass balance values over time) for *Gepatschferner* and the total average of the glaciers. The figure confirms that for the analyzed period, the glaciers have been losing mass, reaching a total mass loss of approx. 35 m w.e. after almost 50 years considered during the simulations. Unfortunately, since there are no available measurements of the mass balance components for these glaciers, it is not so straightforward to evaluate the performance of the glacier model in terms of mass balance/volumes. Nevertheless, the comparison between the simulated and observed glacier areas already gives an idea of the accurate representation of glacierized cells within the area, but information on the volume of ice is still missing. Yet, it is possible to estimate an average of this volume by simply scaling the area of the glaciers, following Equation 5.3. More insight on these results are presented in Section 7.4.

## 7.2 OGGM run and processing of glacier outputs

This section contains the results from the second step of the coupling scheme, which includes all the simulation runs with OGGM. Moreover, the results include the conversion of OGGM's outputs into the required input for running WaSiM during the last step of the coupling scheme.

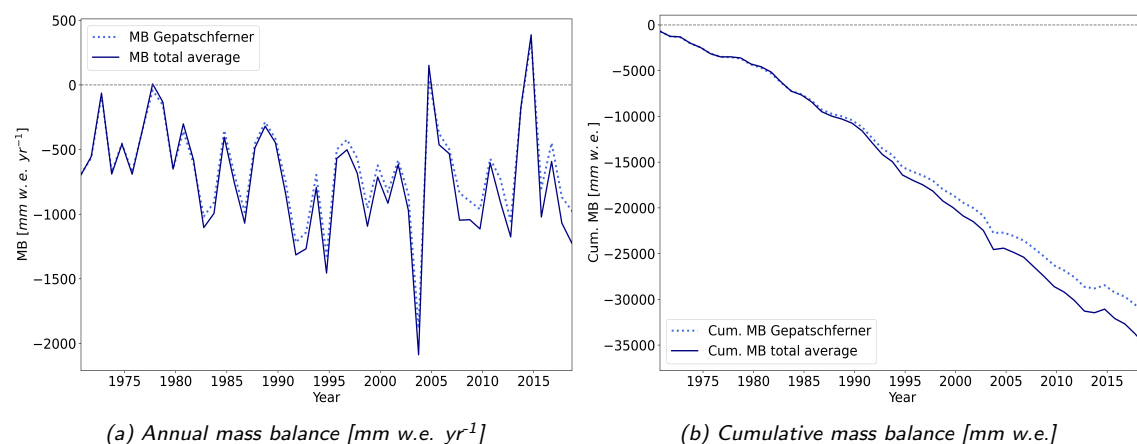


Figure 7.6: Annual and cumulative mass balance obtained with the VA scaling glacier model in WaSiM, for Gepatschferner (dashed light blue line) and the total average of all the glaciers within the catchment (solid blue line).

## 7.2.1 Sensitivity analysis of the mass balance model parameters

Even though the sensitivity analysis is performed for all glaciers within the study area, the focus is given solely to *Gepatschferner* (glacier ID: RGI60-11.00746) due to its mass balance observations at the tongue and because it is the largest glacier in the area. Figures 7.7 to 7.11 show the results for the different test runs, which were introduced in Table 6.3. From the six different parameter combinations, only five are presented, since one yields unrealistic simulation results. Results for two other glaciers (*Weißseeferner* and *Östlicher Wannetferner*) can be found in Appendix C.2.

Figures 7.7a to 7.11a (figures on the left) show a set of annual mass balance simulations for *Gepatschferner* during the period 2000 to 2020, in which one parameter is fixed with its default value and a second parameter is calibrated while varying the third parameter. Each simulation result is represented by a single line. In all the figures, the horizontal gray dashed line indicates the value of the mean annual geodetic mass balance measurement for that glacier (value used by OGGM for the calibration of the mass balance model), according to Hugonnet et al., 2021.

Furthermore, Figures 7.7b to 7.11b (figures on the right) show the mean mass balance at the tongue of *Gepatschferner*, following the corresponding parameter combinations depicted in Figures 7.7a to 7.11a. In each figure, the red dashed line represents the observations, available for the period 2012 to 2019 and as an averaged value over all heights (Section 3.2.2.2). Moreover, the set of simulated annual mass balance is represented with individual gray lines, as an average of all heights. The average value of those simulations is also included in the figures (blue dark line), together with the three best simulation results (light blue lines). The selection of these three runs is based on the smallest errors between simulation and observations, in terms of Mean Bias Error (MBE, e.g. Eis et al., 2021) and Root Mean Square Error (RMSE) (both measures defined in Appendix B). The distribution of these errors among all considered cases is shown in Figure 7.12.

Figure 7.7 shows the results for test A, in which the default parameter is *melt\_f*, whereas *prec\_fac* is calibrated for a given range of *temp\_bias* values (varying parameter). In general, the inter-annual variability of the mean mass balance at the tongue is represented quite well for all parameter combinations (Figure 7.7b). The mean value is in line with the

observations, even though the spread of the simulation results is quite high.

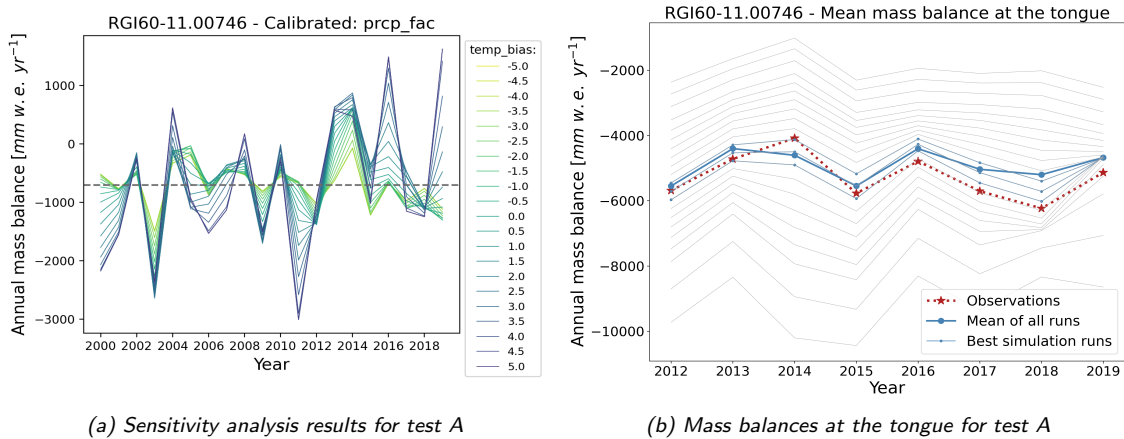


Figure 7.7: Results of the sensitivity analysis for test A (according to Table 6.3). Default: *melt\_f*, varying: *temp\_bias*, calibrated: *prcp\_fac*.

Figure 7.8 shows the results for test B. In this case, the default parameter is also *melt\_f* but *temp\_bias* is calibrated for a given range of *prcp\_fac* values. As expected, the inter-annual variability of the total mass balance (Figure 7.8a) is very close to the results obtained for test A, since the same *melt\_f* is used. Although the mean mass balance simulations at the tongue (Figure 7.8b) behave similar to the simulations results from test A, a narrower spread can be observed.

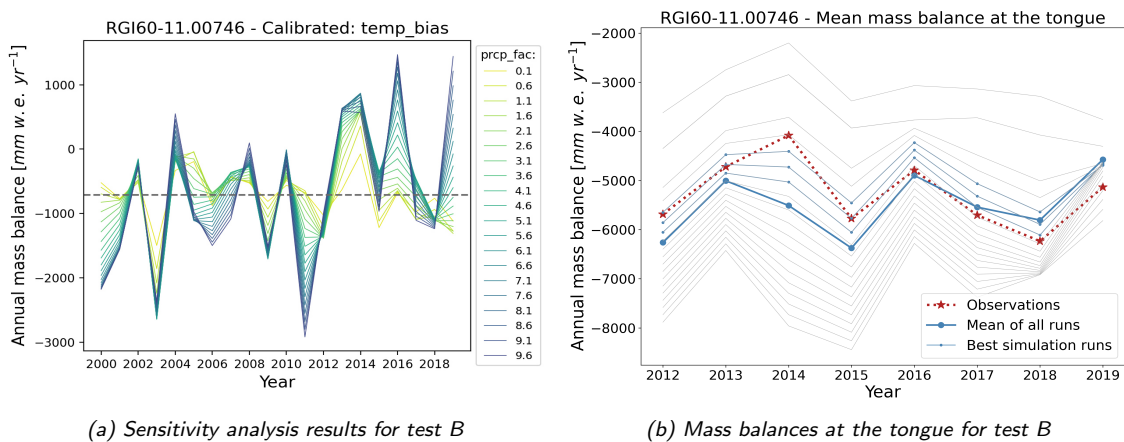


Figure 7.8: Results of the sensitivity analysis for test B (according to Table 6.3). Default: *melt\_f*, varying: *prcp\_fac*, calibrated: *temp\_bias*.

During test C, *temp\_bias* is left with its default value and *melt\_f* is calibrated for different *prcp\_fac* values. The simulation results are shown in Figure 7.9. In this case, a higher variation on the *melt\_f* values is achieved. For the case in which *prcp\_fac* is equal to its lower limit (0.1), the calibrated value of the *melt\_f* is 1.5, whereas a value of 17 is obtained when considering the higher limit of the *prcp\_fac* (10.0). In contrast to the previous test results (test A and B), higher absolute maximum values are observed for the annual mass balances, with higher variations between simulation runs (Figure 7.9a). In addition, a wider spread of simulation results is obtained for the mean annual mass balance at the tongue. Figure 7.9b shows that for some of the runs, greater negative values are obtained compared to the annual observations. These results correspond to the higher values of *melt\_f*, in which the glacier is losing too much mass. The mean of all runs also

suggests that, in general, the simulation results overestimate the loss of mass at the tongue, since the values are always below observations. Nevertheless, the three best simulation runs are very close to the observations, representing quite well the inter-annual variability of the mass balance.

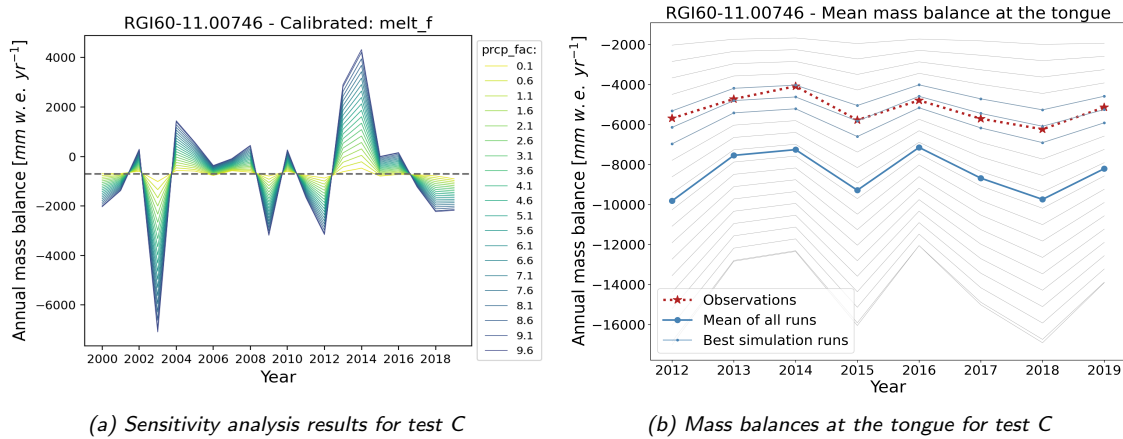


Figure 7.9: Results of the sensitivity analysis for test C (according to Table 6.3). Default: *temp\_bias*, varying: *prcp\_fac*, calibrated: *melt\_f*.

For the sensitivity test E, *prcp\_fac* was left with its default value. Then, *temp\_bias* is calibrated for different *melt\_f* values. From Figure 7.10a it is feasible to see that after the year 2016, the annual mass balances at the glacier are decreasing for almost all simulation runs. These results differ from the results obtained from test A and B, in which a positive mass balance was also observed for some runs. In contrast, the mean annual mass balance observations shown in Figure 7.10b, suggest an increase of the mean mass balance at the tongue between the years 2018 and 2019. Hence, the majority of the simulation runs from test E (including the mean of all runs and the best three simulation results) fail to represent this behavior, even though the results are quite good for the first part of the period (between years 2012 to 2016).

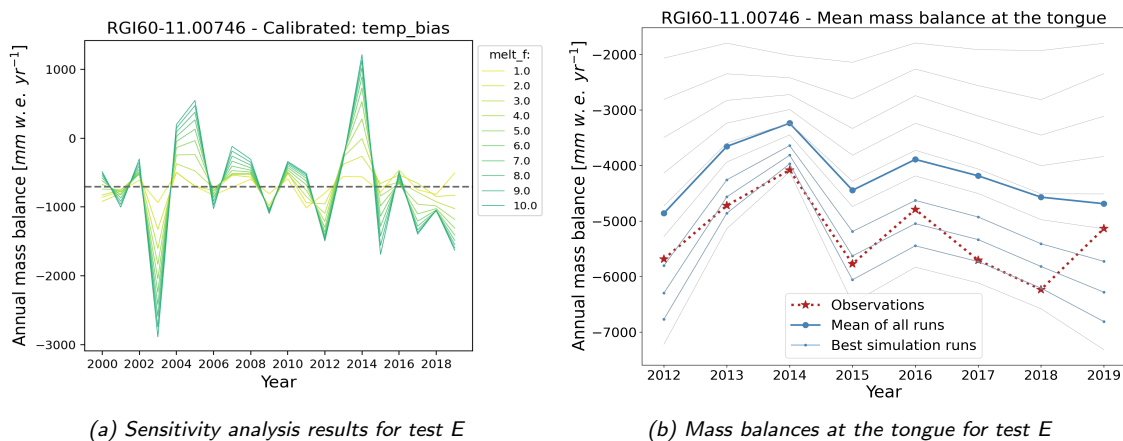


Figure 7.10: Results of the sensitivity analysis for test E (according to Table 6.3). Default: *prcp\_fac*, varying: *melt\_f*, calibrated: *temp\_bias*.

Finally, Figures 7.11a and 7.11b show the results for sensitivity test F. In this case, *prcp\_fac* is left as default, whereas *melt\_f* is calibrated for different *temp\_bias* values. As expected, a similar behavior to the results from test E is observed, since the same parameter was left as default.



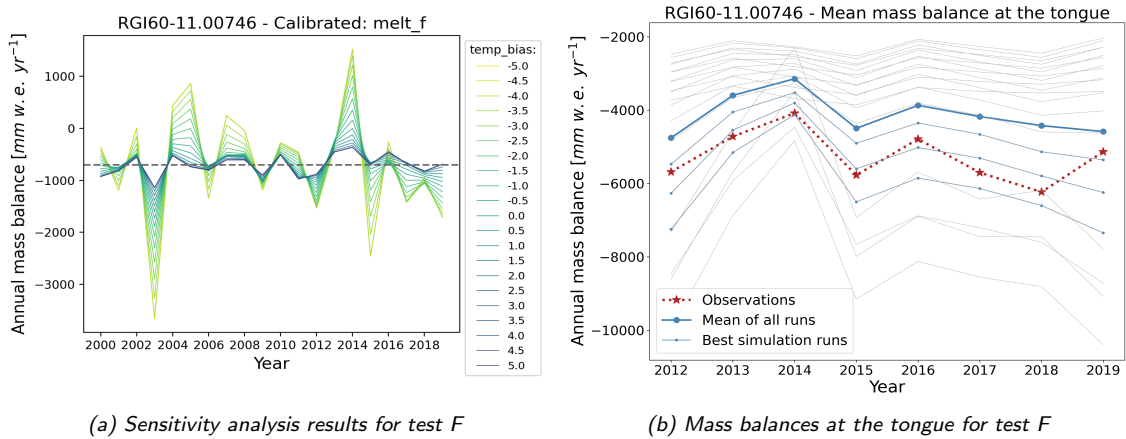


Figure 7.11: Results of the sensitivity analysis for test F (according to Table 6.3). Default: *prec\_fac*, varying: *temp\_bias*, calibrated: *melt\_f*.

Results from test case D are not included in the analysis, since the model was not able to calibrate the value of the *prec\_fac* for the given default *temp\_bias* and range of *melt\_f* (the model stopped since calibration could not be carried out). It appears that the average annual geodetic mass balance of the glacier cannot be matched with a *prec\_fac* within the given climatic conditions and fixed parameters. This suggests that a factor higher than the upper limit ( $>10.0$ ) would be required, which is rather unrealistic.

To summarize and better interpret the results from the sensitivity test, Figure 7.12 shows the ranges of MBE and RMSE for the different test runs (A, B, C, E and F). The horizontal gray line in each box plot indicates the mean value, whereas the orange line indicates the median. In addition, the optimal error value of 0 is indicated by the horizontal dashed line.

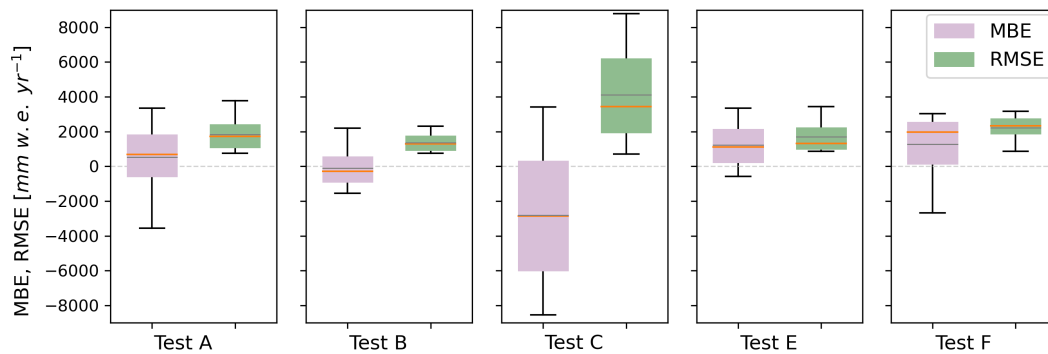


Figure 7.12: MBE and RMSE [mm w. e. yr<sup>-1</sup>] of the mass balance simulations as an average over all elevations for the different sensitivity test runs and for the given period. The mean of the error values is indicated in gray, while the median is indicated in orange.

From all test cases, C shows the largest dispersion in both errors, MBE and RMSE. Moreover, the mean and median values are farther away to the optimal value, compared to the rest of the test cases. This is in line with the results shown in Figure 7.9, where this test case showed the wider spread of simulation results. On the other hand, when looking at the rest of the test cases, the errors' ranges lay within the same limits and the mean and median values are closer to 0. This might be explained by the overall narrower spread between simulation runs and the closest distance between the mean of the runs and observations, achieved during each test case.

In general, the mean value of MBE and RMSE for test cases A and B are closest to 0 and the inter-annual variability of the mean annual mass balance at the tongue is better represented. This suggests that one of these two model configurations (test A or B) may be used during calibration of the model. Thus, the parameter *melt\_f* might be left with its default value of  $5.0 \text{ kg m}^{-2} \text{ K}^{-1} \text{ d}^{-1}$ , whereas *prcp\_fac* or *temp\_bias* should be calibrated. According to the different calibration studies carried out by Schuster et al., 2023, *prcp\_fac* at a glacier scale affects inter-annual variability of the mass balance more than *temp\_bias*. For all these reasons, *prcp\_fac* is selected as calibration parameter while *temp\_bias* is fixed with a value of  $0.5 \text{ }^{\circ}\text{C}$ , since this value was obtained for the best simulation runs during test A and B.

## 7.2.2 Calibration of the mass balance model

With the calibration strategy defined from the sensitivity analysis, *prcp\_fac* is calibrated at a glacier basis while leaving *melt\_f* and *temp\_bias* as constant parameters. Figure 7.13 shows the observed (red dashed line) and simulated (blue solid line) annual mass balance at the tongue of *Gepatschferner* for different elevations, from 2175 to 2875 m a.s.l., in increasing steps of 50 m (from bottom to top and from left to right). Overall, a very good match between observations and simulations is achieved for elevations above 2425 and below 2675 m a.s.l. For lower elevations, simulated values are a bit underestimated until the year 2015 and overestimated afterwards, whereas for the highest elevations, the model tends to underestimate the loss of mass at the tongue of the glacier. In all cases, however, the errors are below 1200 mm w.e., being the minimum  $\text{MBE} = 54$  and  $\text{RMSE} = 219$  mm w.e. for the elevation of 2575 m a.s.l. For the case of *Gepatschferner*, the value of *prcp\_fac* obtained after calibration is 2.74, being close to the default value used by OGGM (2.5). The values of the calibrated parameters for all glaciers are included in Appendix C.2.

As with any model, discrepancies between observed and simulated values are to be expected. One possible explanation for this may be related to the observed values themselves, as they are obtained through extrapolation after performing glaciological measurements at certain points along the glacier tongue. The extrapolation of these measurements to the entire glacier, as explained in Section 2.2.3.1, is one of the main sources of uncertainty for this method. Moreover, there may be errors inherent in the measuring devices or in the reading of values. Finally, the contour lines that illustrate the distribution of elevations on the tongue could vary between observations and the model due to the use of different DEMs for observation and simulation.

## 7.2.3 Dynamic runs

Once the mass balance model is calibrated, a dynamic run can be performed. The aim of this run is to obtain the ice thickness along the flowlines after applying the depth-integrated flowline model (Section 5.2.4). The results of the dynamic run can be summarized in terms of glacier's volumes, areas, lengths and mass balance. The run includes a dynamic spinup period starting in 1969 and finishing before the year 2003, in which the areas are compared to the RGI available outlines. Afterwards, the simulations are performed until the year 2019. The simulated glacier volumes and areas can be seen in Figures 7.14a and 7.14b, respectively (in green). The dashed lines indicate the simulation results during the spinup



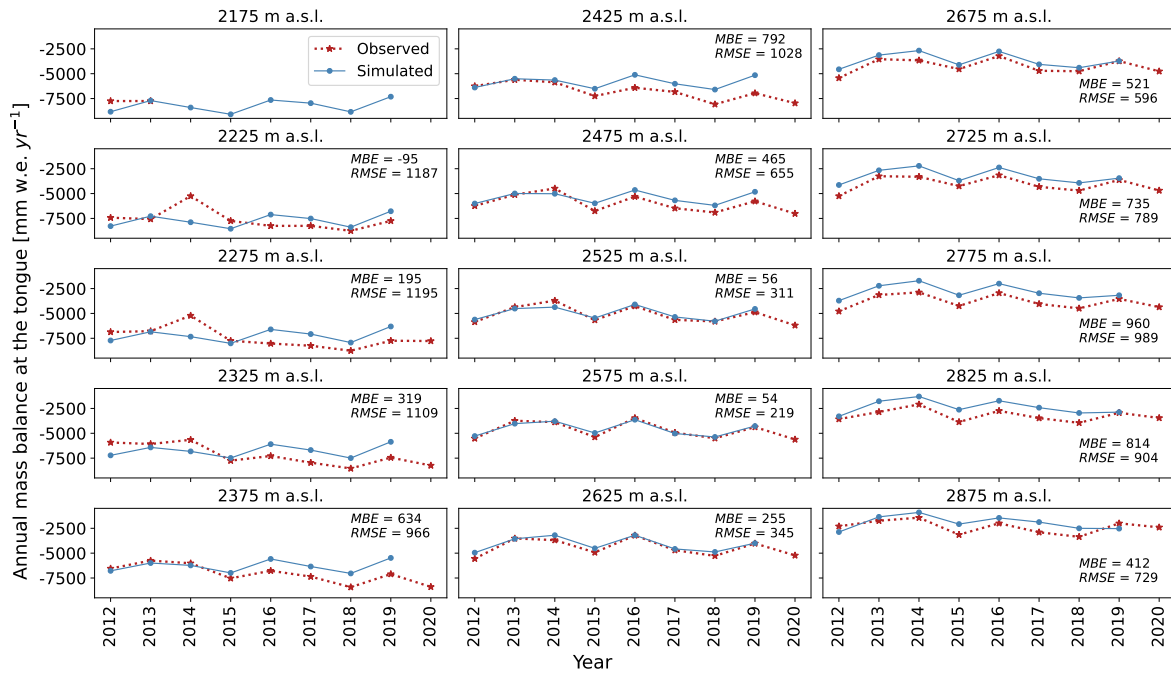


Figure 7.13: Observed (red dashed line with \*) and simulated (blue solid line with ●) mass balance at the tongue of Gepatschferner for different elevations. Simulated values were calibrated with *prcp\_fac*. The parameters *melt\_f* and *temp\_bias* are fixed with a value of  $5.0 \text{ kg m}^{-2} \text{ K}^{-1} \text{ d}^{-1}$  and  $0.5 \text{ }^\circ\text{C}$ , respectively. The errors MBE and RMSE [mm w.e.  $\text{yr}^{-1}$ ] between observed and simulated values are indicated for each elevation.

period (1969–2002), whereas the solid lines represent the simulation results afterwards (2003–2019). Moreover, the "Default run" is also included, which uses W5E5, the default's OGGM climate dataset, as input climate (purple lines, described in Section 6.4.3.1).

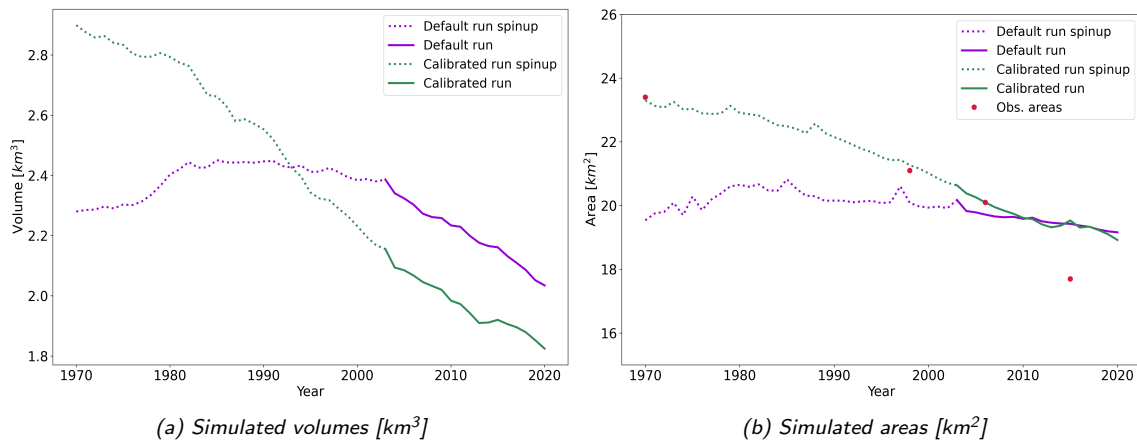


Figure 7.14: Simulation results of the dynamic runs: calibrated run in green, default run (with default's OGGM climate dataset) in purple. The dashed lines indicate the simulation results during the spinup period, whereas the solid lines indicate the results from 2003 onward. The red points indicate the observed areas, considering only glaciers that are included in the RGI (year 2003).

From Figure 7.14, it is possible to see that the simulated areas from the calibrated run are in close proximity to the observed values. It is worth to mention, however, that the observed areas here only refer to the glaciers that belong to the RGI outline, since OGGM is not able to create new glaciers in the past. Hence the real areas in 1969 and 1998 are greater than the values plotted here, but they are still useful for comparison purposes. Another

key aspect shown in the figure is that the initial volume simulated from the calibrated run is  $2.9 \text{ km}^3$ , being approx. 21% higher than the initial volume simulated from the default run. Moreover, the calibrated run shows a declining tendency throughout the entire simulation period, whereas the results of the default run suggest an increase in the volume during the spinup period with a posterior decrease. After the end of the spinup period, in 2003, both models perform similarly, showing the same rate in the volume decrease. This similarity can also be observed in the simulated areas, since again, after 2003, there are only small differences between both model results. The closer representation of areas from the calibrated run might be related to the finer spatial resolution provided by the WaSiM-INCA dataset, compared to the coarser resolution given by the default climate dataset W5E5 (according to Figure 7.5). Finally, Figure 7.14 confirms the need of an adequate initialization of the glacier model, since volumes can be very different and as a result the mass balance components may be wrong. For this reason, the uncertainties of the model initialization (Section 6.5.2) are investigated and presented in Section 7.3.2.

#### 7.2.4 From "1.5D" to 2D geometries

For each glacier within the study area, an outline is created by connecting the outer points of the widths which have been defined along the flowlines. This procedure is performed annually during the simulation period and based on an approximation, resulting in some discrepancies with observations. However, since the glacier outline is then transferred to a  $100 \text{ m} \times 100 \text{ m}$  grid, its accuracy is slightly reduced. Moreover, during the dynamic spinup period, the glaciers are likely to have grown in the past to reach their current geometry (for the given climatic conditions). Since OGGM is not a fully-distributed model, glaciers can only encounter growth along their flowlines. This results in an extension of the glacier tongues, like for the year 1969 which is shown in Figure 7.15a, where for three of the glaciers (including *Gepatschferner*), the tongue exceeds the observed geometry. This phenomenon is less critical for posterior years, when the glaciers continue to lose mass and therefore the tongues become smaller. For example, Figure 7.15b shows the obtained glacier geometries for the year 2015, where a better representation of the tongue is achieved, compared to the year 1969. Similar to the results analyzed in Section 7.1.4, dark blue colors indicate that a model cell is 100% covered by glaciers, whereas no color indicate that the cell is glacier-free.

Figure 7.15a also depicts one weakness of the model, in which glaciers cannot be created during the dynamic spinup period, or in other words, the model cannot simulate glaciers that existed and completely melted before the RGI's date. This yields to a lower total glacier area, but seems to be resolved during the following years, like in 2015 (Figure 7.15b). At the beginning of the simulations (in 1969), the POD reaches a value of 0.771. This indicates that the 2D glacier geometries obtained after running OGGM are captured with 77% of confidence. The value becomes higher after 46 years of simulations, being  $\text{POD} = 0.909$  for the year 2015. Even though a complete representation of the initial glacierized area is not ensured from the 2D conversion, the annual update of the glacierized areas is expected to bring significant improvement in the long-term representation of the glaciers and its contribution to runoff generation.

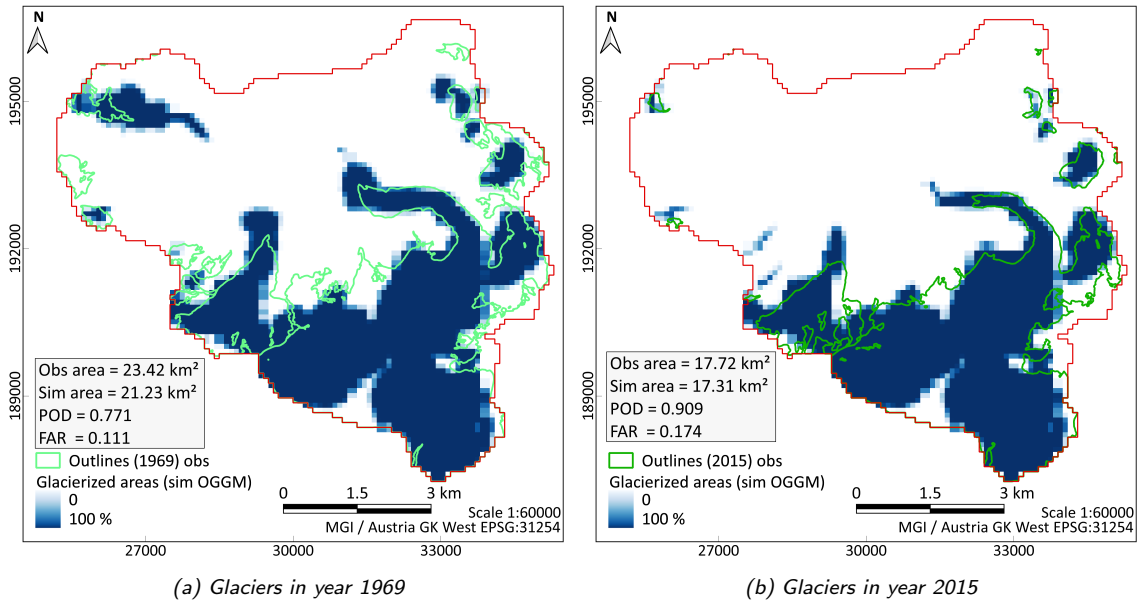


Figure 7.15: Observed and converted 2D glacier areas for the years 1969 and 2015, after performing the OGGM runs, with dynamic spinup. The observed outlines belong to the AGI (Section 3.2.2.1) and the performance measures are defined in Section 6.3.2 and Appendix B.

## 7.2.5 Distributed ice thickness

With the resulting glacier geometries, both at an annual and glacier basis, the distributed ice thickness is obtained. Figures 7.16a and 7.16b show the simulation results for the years 1969 and 2015, respectively (thickness values increase from dark to light colors). The first evident outcome from the figure is that the glaciers experience a general reduction on their thickness, from 1969 to 2015. This result aligns with the decrease in glacier areas. In 1969, the maximum simulated ice thickness at a model cell near the center of *Gepatschferner* was 493 m, but by 2015, this had decreased to 344 m. Moreover, the mean simulated ice thickness of all glaciers is 65 m in 1969 and 49 m in 2015. This indicates that the glaciers underwent a 25% decrease over a period of nearly 50 years, wherein *Gepatschferner* had the largest contribution with a 30% reduction in mean ice thickness.

There are, however, some deficiencies on the representation of the distributed ice thickness. First of all, the thickness value at each model cell is obtained through a simple interpolation from the values along the glaciers' flowlines, hence some information might be missed when transferring it to a 2D geometry (similar to the conversion of glacier areas). Second, since the glacier areas and distribution of the ice thicknesses are determined at a glacier basis, a smooth transition between neighboring glaciers might not be achieved. This results in a "jump" of values between neighboring glaciers, which in this study area is only visible for the case of *Gepatschferner* and *Weißseeferner*. Finally, along the outlines of each glacier, the minimum thickness is assigned to those cells. This is simply required to overcome mathematical complications in case an active cell has a value of zero when transferring it to the final WaSiM run.

Simulated values are compared with GPR point measurements of ice thickness at specific locations (Fischer et al., 2015d, Section 3.2.2.3) on three glaciers within the catchment, as shown in Figure 7.17. The measurements are available for different years: 2001 for *Gepatschferner*, 2010 for *Östlicher Wannetferner* and 1996 for *Weißseeferner*. The figure

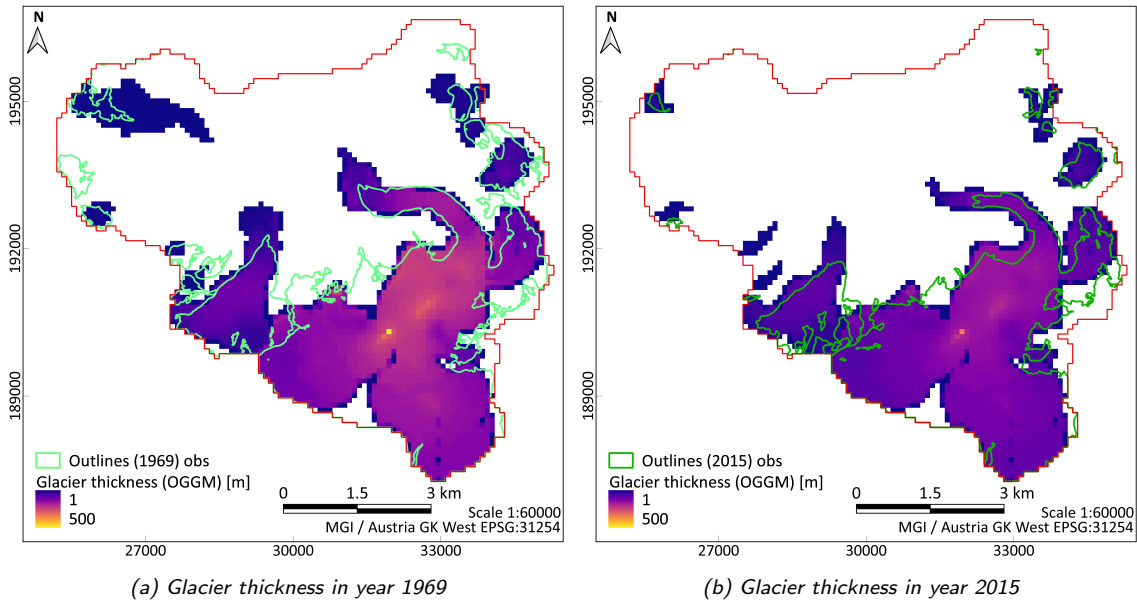


Figure 7.16: Observed glacier outlines and simulated distributed glacier ice thickness for the years 1969 and 2015, after performing the OGGM runs, with dynamic spinup. The outlines belong to the AGI (Section 3.2.2.1).

displays the distribution of the ice thickness that was simulated in those particular years. The mean values (both observed and simulated) for each glacier are also indicated [m].

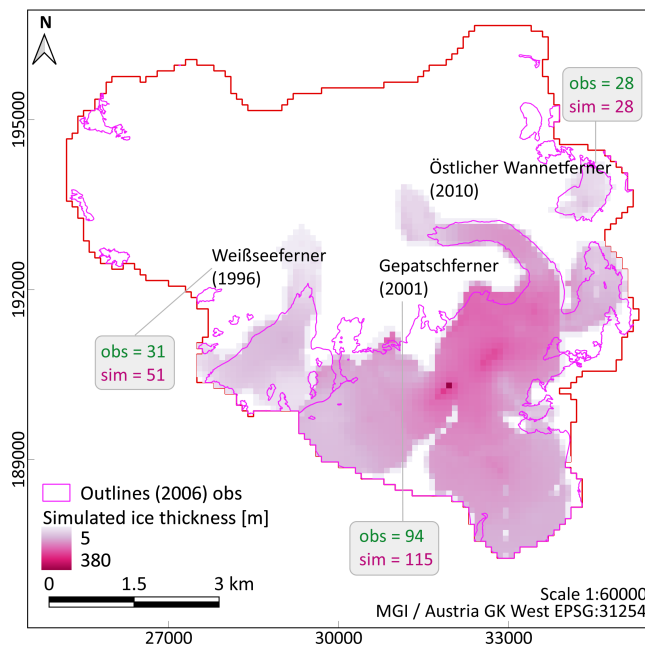


Figure 7.17: Simulated ice thickness for three glaciers: Gepatschferner, Östlicher Wannetferner and Weißseeferner at years in which point observations are available (years are indicated in brackets). The observed and simulated values given for each glacier refer to the mean value during the corresponding year. The observed outlines belong to the AGI (Section 3.2.2.1).

For the case of *Gepatschferner*, the mean simulated ice thickness is overestimated in approx. 22%, whereas the error is higher for *Weißseeferner* (63%). On the contrary, the ice thickness is very well simulated for the smallest glacier, the *Östlicher Wannetferner*, where the mean value matches the mean of the measurements. As with any observed dataset, there are uncertainty sources that might explain the discrepancies with simulation results. For the case of the GPR, the ice thickness is derived from the measured time signal in the glacier. Hence, uncertainties related to the conversion from this value to the ice thickness are expected. Moreover, the accuracy on the reading and misinterpretation of multiple re-

flections play a significant role (Fischer and Kuhn, 2013). In terms of simulations, expected uncertainties are related to the approximation method described before to obtain the distributed ice thickness and to the initialization of the model (i.e. dynamic spinup). This last point might be especially important for *Gepatschferner* and *Weißseeferner*, since the analyzed years belong to the dynamic spinup (they are before the RGI's year). Nevertheless, the mean values (observed and simulated) are in good agreement and provide additional confidence on the integration of the ice thickness into the coupling scheme. Additional results including minimum and maximum values and other years are provided in Appendix C.2.

## 7.2.6 Glacier volumes

The combination of the glacier areas together with the ice thickness distribution yield to the volume of the glaciers. The distribution of the volume follows the same pattern as the ice thickness and the results are adjusted so that the total values match the total values determined by OGGM after performing the dynamic run (Section 6.2 and Figure 7.14a). During the year 1969, when the model is initialized, a total glacier volume of  $2.9 \text{ km}^3$  is obtained. This value is an equivalent of 50 m of ice distributed all over the Gepatschalm catchment (entire area, inclusive non-glacierized parts). For the year 2015, however, the total volume is reduced to almost  $1.9 \text{ km}^3$ , or its equivalent of 33 m of ice.

## 7.3 Coupling the models: final WaSiM run with optimization

The last step of the coupling scheme integrates the post-processed results obtained from OGGM (glacier area, thickness and volume) into the final WaSiM run. In this step, WaSiM runs with daily time steps but every year, on 1<sup>st</sup> October, the glacier grids are updated with OGGM's outputs, while simultaneously optimizing the most sensitive parameters. Besides, the mass balances from OGGM are used as additional constraints while performing the optimization. The results of the coupling scheme are shown in terms of runoff and glacier mass balances. Afterwards, in Section 7.4, a detailed comparison is carried out between the results from the coupling scheme and the original WaSiM model with the integrated VA scaling approach.

### 7.3.1 Multi-data optimization

Figure 7.18 shows the convergence of the multi-objective function during optimization of the coupling scheme with the SCE-UA algorithm. Although the maximum number of iterations was set to 3000, the convergence was achieved after 1218 iterations. The value of the multi-objective function in this case is 0.547 (Equation 6.3) and corresponds to the global minimum.

Table 7.1 summarizes the parameters adjusted during optimization, with their corresponding value and selected range (in red for the model initialized in 1969 and optimized during 1985-1998). In order to compare the influence of the different initialization years and

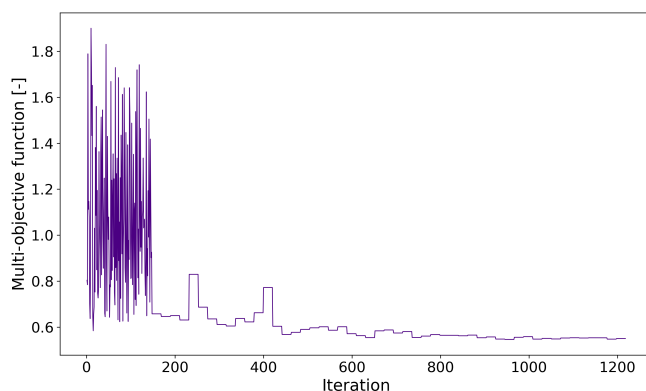


Figure 7.18: Convergence of the multi-objective function during the optimization with the SCE-UA algorithm, for the coupling scheme initialized in the year 1969.

optimization periods, the adjusted parameter values for the other two model configurations are also included in the table (these model configurations were introduced in Section 6.5.1).

Table 7.1: Parameters adjusted during optimization of the coupling scheme, including their values and ranges. The columns refer to the different model configurations used during optimization, depending on the initial year (given in brackets) and optimization period.

Param.	Unit	Range	Coupling (1969) 1985- 1998	Coupling (2003) 2006- 2015	Coupling (1984) 1985- 1998
$k_d$	h	5 - 300	174.9	105.3	155.0
$k_i$	h	5 - 300	177.4	131.3	186.3
$q_0$	mm h <sup>-1</sup>	0.01 - 1	0.28	0.37	0.53
$t_0$	°C	-1.0 - 2.0	0.33	1.09	-0.02
$min_{slope}$	grad	0 - 90	27	48	71
$lw_{out}$	-	0.8 - 1.2	0.98	0.91	1.03
$mf$	mm °C <sup>-1</sup> d <sup>-1</sup>	1.2 - 4.0	3.8	3.7	3.8
$k_{ice}$	h	1 - 20	15.4	11.9	19.3
$k_{firm}$	h	100 - 1000	202.6	311.4	115.8
$k_{snow}$	h	10 - 100	69.7	61.6	74.5

The values in the table indicate that the model parameters depend not only on the initialization year of the model, but also on the optimization period chosen. For example, the recession constant for surface runoff ( $k_d$ ) has a similar value in all model configurations, indicating a rather low recession limb for the hydrograph. The same can be concluded for the recession constant for interflow ( $k_i$ ). When comparing the values of the threshold temperature separating rain from snow ( $t_0$ ), lower values are obtained for the model configurations that include a dynamic spinup of the glaciers (coupling initialized in 1969 and 1984). This might indicate that the model attempts to generate more solid precipitation to expand the glacier's accumulation area and hence increase the glacierized area for the past climatic conditions. On the contrary, almost identical values are obtained for the melt factor in all model configurations. This suggests that WaSiM tends to adjust the accumulation rather than the ablation component of the mass balance model and that a more robust representation of the latter can be achieved. The remaining parameters show comparable behavior among the various configurations.

Table 7.2 summarizes some of the performance measures achieved during the optimization period, for the different model configurations. Here, it is already feasible to see that the coupling scheme performs better when initializing the model in 2003, rather than in 1969. This might be attributed to the more reliable initial glacier areas and volumes, since they correspond to the RGI and do not depend on the dynamic spinup. Thus, the glaciers that existed and completely melted before 2003, do not play any role on the evaluation of the model and the uncertainties might be reduced. Additionally, the values indicate that there are not much variations on the performance of the model if the coupling scheme is initialized in 1984, instead of 1969. Hence, a shorter warm-up period (one year against fifteen years) may be long enough for the model to reach ideal state conditions. This finding is fairly advantageous if the computation times are quite long or if past simulations are not to be analyzed.

Table 7.2: Performance measures obtained after optimization, for the different model configurations, following the optimum parameter set defined in Table 7.1.

Measure	Coupling (1969) 1985- 1998	Coupling (2003) 2006- 2015	Coupling (1984) 1985- 1998
$KGE_R$	0.88	0.93	0.88
$BE_R$	0.25	0.42	0.24
$PBIAS_R$	6.1	0.46	5.6
$POD_{2015}$	0.91	0.92	0.91
$FAR_{2015}$	0.17	0.24	0.17
$RSR_{GMB}$	0.72	0.75	0.72

The simulation results obtained with the optimized parameter set (red column in Table 7.1) are shown in Figure 7.19. The results refer to the model that is initialized in 10/1969 and optimized at a daily time step during the period 01/1985 to 12/1998 (Figure 6.10). On the one hand, Figure 7.19a shows the mean daily observed and simulated runoff, together with the simulated ice melt component. From the performance measures, it is feasible to conclude that the results are very good, since NSE and KGE are above 0.75 and PBIAS is smaller than 10%. On the other hand, Figure 7.19b shows the cumulative mass balances for *Gepatschferner*: the solid green line shows the simulation results from OGGM (used to constrain the optimization of the coupling scheme), and the blue dashed line, the results obtained from the coupling scheme. Although a complete match between both curves is not achieved, the MBE suggests that in average, the mass balance rates are overestimated by less than 40 mm w.e. per year.

It is worth to mention that the weight assigned to the glacier mass balance component in the multi-objective function is 0.3. The selection of a higher weight would increase the importance of the glacier component in the multi-objective function, thus a more accurate representation of the mass balances could be achieved. Nevertheless, and considering that the curves are very similar and that the MBE and RMSE are still low, the assigned weight of 0.3 is kept and considered acceptable. Additional results are depicted in Section 7.4 and in Appendix C.3.

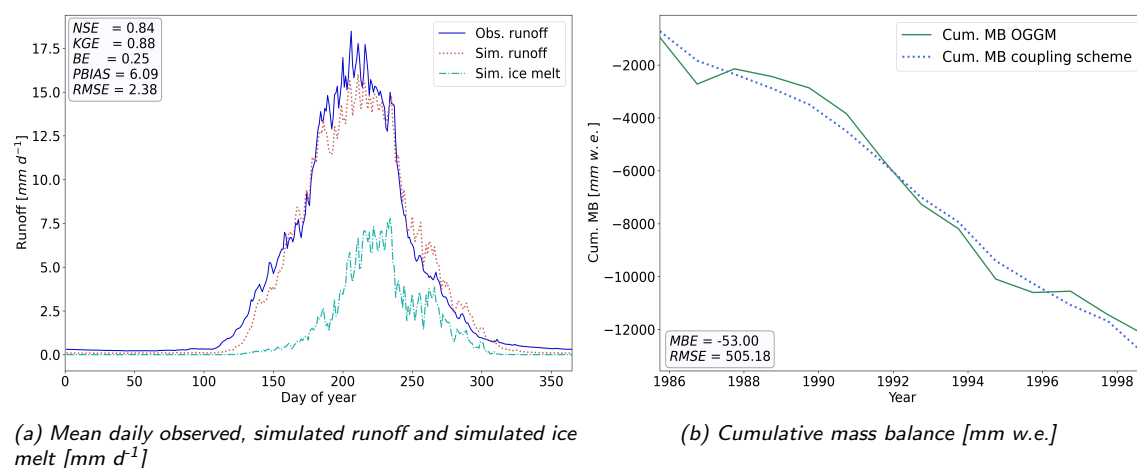


Figure 7.19: (a) Mean daily observed (blue solid line) and simulated runoff (red dashed line) at the outlet of Gepatschalm, including the mean daily simulated ice melt component (light blue line), obtained from the optimized coupling scheme, for the period 01/1985 to 12/1998. (b) Cumulative mass balance of Gepatschferner simulated with OGGM (green solid line) and with the optimized coupling scheme (blue dashed line). The performance measures are defined in Section 6.3.2 and Appendix B.

## 7.3.2 Uncertainties

The uncertainties in (glacier) model initialization and parameters of the coupling scheme are presented and discussed in the following sections.

### 7.3.2.1 Uncertainties in model initialization

The performance of the coupling scheme varies depending on the year chosen for initializing the glacier model. (Table 7.2). As mentioned before, this can be attributed to the selection of a dynamic spinup in OGGM or by starting the simulations from the RGI's date onward. On the contrary, when considering the same initialization year in OGGM (same dynamic spinup length) but different warm-up periods within the coupling scheme, similar results are obtained from the simulations. This suggests that the coupling scheme is quite independent from the length of the warm-up period and that the main source of uncertainty might originate from the initialization method chosen for running OGGM.

To infer the magnitude of such uncertainties, several dynamic runs are performed with OGGM considering different initialization years. The initialization year influences the length of the dynamic spinup, which is changed at intervals of 5 years. Figures 7.20a and 7.20b show the evolution of the glaciers in terms of volume and area, respectively, while considering different initialization years. The simulation results are distinguished by color. The dashed lines represent the dynamic spinup period, the length of which is given in brackets next to the initial year, while the solid lines represent the results after 2003. Moreover, 7.20b also includes the observed areas, as was already depicted in Figure 7.14b.

As it can be seen in Figure 7.20, the length of the dynamic spinup clearly affects the evolution of the glaciers after 2003. For the areas, results have a relatively narrow spread, with the largest difference being 1 km<sup>2</sup> for the year 2019. This value represents only 5% of the simulated area in 2003. On the contrary, when looking at volumes, the spread of simulation results widens. The largest difference between runs is 0.43 km<sup>3</sup> for the year 2019, which represents approx. 20% of the volume obtained in 2003. Since the dynamic



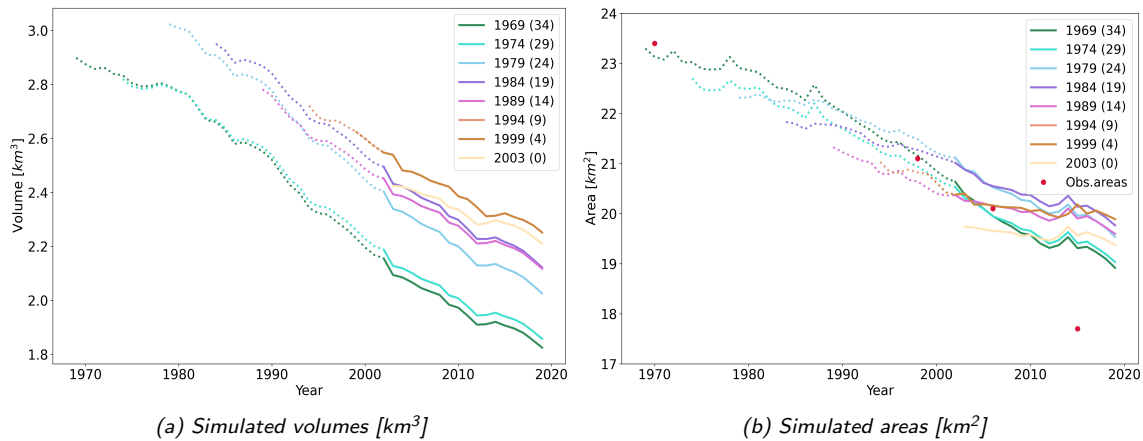


Figure 7.20: Simulation results of the OGGM dynamic runs with different initialization years: (a) volumes and (b) areas. The dashed lines indicate the spinup period, whereas the solid lines indicate the dynamic run from 2003 onward. The red points indicate the observed areas, considering only glaciers that are included in the RGI.

spinup aims to minimize the difference between observed and simulated areas (as illustrated in Section 6.4.3), this might explain the thinner spread in results, compared to the volumes. From this analysis it is possible to conclude that the models' initialization and the length of the dynamic spinup play a crucial role on future glacier simulations. Nevertheless, in this particular study case, the level of uncertainty aligns with the approximate 5% identified in the RGI outlines, assuming that the is area targeted for error minimization during the dynamic spinup. However, it may be worthwhile to conduct a similar analysis for other catchments, as every glacier reacts differently to the given climatic conditions and model configuration, leading to diverse outcomes (and hence, more uncertainties).

### 7.3.2.2 Parameter uncertainty

Figure 7.21 illustrates the normalized parameter range for the three different coupling configurations, which are initialized in different years (1969, 2003 and 1984) and optimized during different periods (1985-1998, 2006-2015 and 1985-1998, respectively). The parameters refer to the best parameter set, which aims to minimize the multi-objective function given by Equation 6.3. In the figure, the parameter set that yields the lowest multi-objective function plus 10% of the function range, is included. In all cases, the values are normalized, which means that the values are divided into their corresponding range. Besides, the mean (gray) and median (orange) values of each parameter set are included.

The first row in Figure 7.21 shows the normalized range for the parameters belonging to the soil model:  $k_d$ ,  $k_i$  and  $q_0$ . All of them seem to be stable as similar values are obtained for the different periods. The exception is  $k_i$  for the model initialized in 1969, where higher values are sought. The second row in the figure shows the normalized range for some of the parameters that describe the snow model. In this case, the minimum slope for creating slides,  $min_{slope}$ , and the correction factor for outgoing long wave radiation,  $lw_{out}$ , seem to be stable over the three periods. The same can be concluded for the threshold temperature separating rain from snow,  $t_0$ , except for the 1969 model, in which the parameter range lies within higher values. Finally, the third row depicts the normalized range for some of the parameters that characterize the glacier model. The values of the two storage coefficients for ice and firn,  $k_{ice}$  and  $k_{firn}$ , are similar throughout the different periods, thus showing

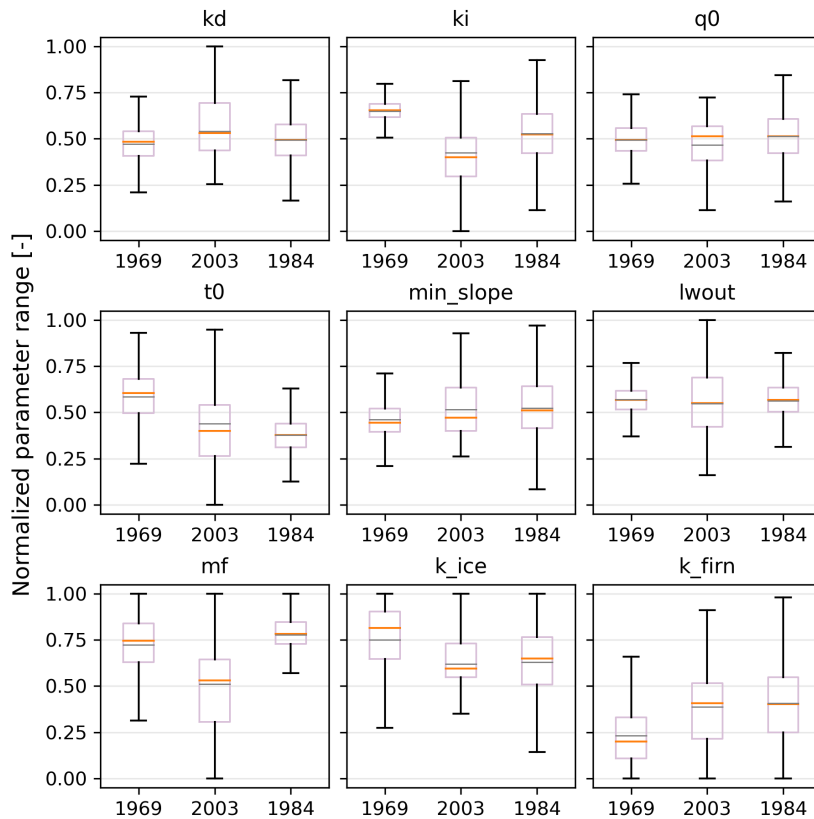


Figure 7.21: Normalized parameter range of 10% of the best parameter set adjusted during optimization of the different model configurations, that depend on the initialization year and optimization period. 1969, 2003 and 1984 indicate the initial model year chosen to start the simulations with the coupling scheme. The mean of the parameter values is indicated in gray, while the median is indicated in orange.

also some stability. However, the melt factor  $m_f$  seems to be less stable. This parameter's high sensitivity, as identified during the sensitivity analysis (Section 7.1.1), possibly explains this instability. The same could be inferred for the parameter  $t_0$ , as it also showed to be very sensitive and less stable than the remaining parameters. Nevertheless, optimized values are comparable between the different configurations for  $m_f$  (Table 7.1). This may also be related to the narrower range of variation possible for the parameter during the optimization process.

Overall, the mean value of each parameter seems to be quite close when considering the different periods. Only for the parameters describing the glacier model and the temperature threshold ( $t_0$ ), a lower stability is observed. Another aspect to analyze is the identifiability of the parameters. This can be described by a narrow parameter range across various optimization periods (Tarasova et al., 2016). In general, all studied parameters show varying ranges, with a wider range for the coupling initialized in 2003, for most of the parameters. This issue might be related to the initialization of the model, the length of the periods and the number of iterations achieved during the optimization. For example, the models initialized in 1969 and 1984 were optimized during the period 1985 to 1998, hence they both have the same length. However, for the model initialized in 2003, a shorter period was considered (2006-2015). What is more, although the same limit was set in all optimization periods, more iterations were required for the model initialized in 1969 (1218), whereas the models initialized in 1984 and 2003 required 882 and 483 iterations to reach the optimum minimum, respectively. These findings indicate that, for long-term water balance

simulations, a sufficient period of time for model optimization may be necessary, since less stable parameters are those which have a major impact on snow and glacier processes (like  $m_f$ ). Moreover, the robustness of the model could be improved by incorporating additional datasets during optimization, such as snow measurements.

## 7.4 Comparison: WaSiM VA scaling vs. WaSiM-OGGM coupling scheme

In this section, a close comparison between the results obtained by the first WaSiM run with integrated VA scaling (first step of the coupling, Section 7.1) and the WaSiM-OGGM coupling scheme itself (third step of the coupling, Section 7.3) is drawn. This comparison may allow to justify whether the inclusion of explicit ice-flow dynamics into the water balance model improves the prediction of glacier's evolution and runoff in glacierized catchments compared to the empirical VA scaling approach, as introduced in the two key research questions of this thesis (Section 1.3). The results are part of an original research article (submitted on 18<sup>th</sup> September 2023 and published on 20<sup>th</sup> December 2023), as part of the Research Topic *Water and Hazards in Mountainous Regions in a Changing Climate*:

*Pesci, M.H., Schulte Overberg, P., Bosshard, T. and Förster, K. (2023): "From global glacier modeling to catchment hydrology: bridging the gap with the WaSiM-OGGM coupling scheme". Frontiers in Water 5, Article 1296344, doi.org/10.3389/frwa.2023.1296344.*

*The co-authors involved in the article were mainly responsible for the preparation of climate data. While Philipp Schulte Overberg developed the analogous downscaling kNN-method applied to the INCA dataset (Section 3.2.4.2), Thomas Bosshard provided the bias-adjusted climate projections (Section 3.2.4.3). Then, and as indicated in this thesis, María Herminia Pesci developed the methodology of the coupling scheme, performed all simulations, elaborated results and created the Github repository for the coupling. Finally, Kristian Förster as main supervisor, developed the original research idea, applied for funding and supervised the work.*

The comparison is made between the first WaSiM run with VA scaling (named later on just "VA scaling") and the coupling scheme initialized in the year 1969 and optimized during the period 1985-1998 (set up (a) in Section 6.5.1, later on referred to as "Coupling scheme"). The results of the comparison refer to the Gepatschalm study case and are split into two sections. First, simulation results from the historical period (1971-2010) are presented in Section 7.4.1 in terms of water balance components, emphasizing the behavior of runoff. Then, the future behavior of the models (2011-2100) are shown in Section 7.4.2, where runoff and glacier evolution are analyzed.

### 7.4.1 Historical period

The simulations carried out during the historical period span from 1971 to 2010, being both models initialized in the year 1969. Figure 7.22 shows the simulated runoff as a result from the VA scaling (gray solid line) and the coupling scheme (green solid line), together with their contribution from ice melt (dashed lines). Moreover, the figure includes the observed runoff (blue solid line) and corresponding performance measures (observed vs. simulated

values). Since observations are only available after 1985, the measures are calculated during the period 01/1985 to 12/2010, just before the future simulations begin.

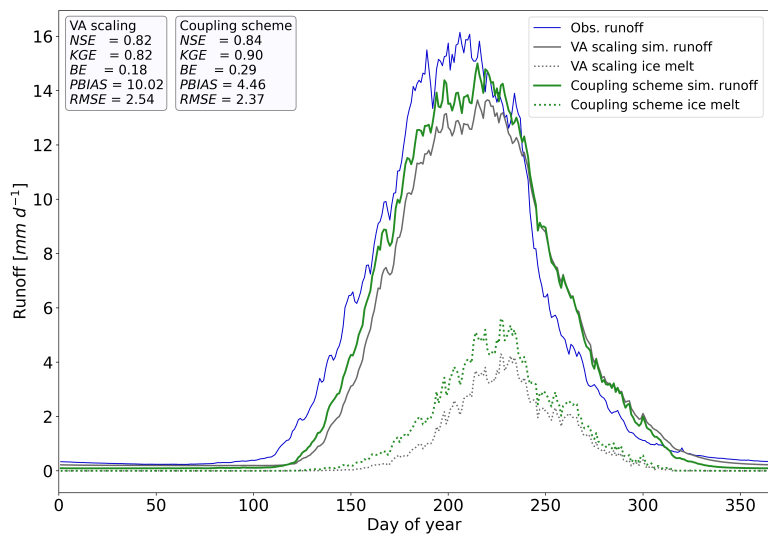


Figure 7.22: Comparison between observed (blue solid line) and simulated runoff, result from the WaSiM with VA scaling approach ("VA scaling", gray solid line) and WaSiM-OGGM coupling scheme ("Coupling scheme", green solid line), during the historical period (1971-2010). The simulated ice melt component is also included in the figure (dashed lines).

Similar to the results obtained during the calibration period for each individual model (Sections 7.1.2 and 7.3), an underestimation of runoff is observed during spring and summer months, possibly related to the snow model. Another reason might be explained by the glacier model itself. In both cases, the T-index approach without radiation is used to calculate melt, which might result in lower melting rates than explicitly including radiation into the T-index equation. During autumn and winter months, both models behave very similar. This indicates that the major differences arise from the processes that involve glacier and snow melting. To have a deeper understanding of such comparisons, Table 7.3 summarizes the mean water balance components for the historical period and for both models.

Following Equation 2.1, the main components of the water balance are determined as the annual average during the historical period, including their standard deviation. Total runoff,  $R$ , is split into two fundamental components: runoff from unglacierized and glacierized areas. On the one hand, the first term includes surface runoff, interflow and baseflow, which seem to be quite similar between both models. The exception can be seen for the baseflow, since the coupling scheme predicts a rather low value. In both models, a conceptual approach is selected for representing this process and a correct evaluation of this particular component is quite challenging. Besides, the values represent only 8 and 3% of the runoff from unglacierized catchments, respectively, thus being negligible compared to the remaining components. On the other hand, the runoff from glacierized areas includes the melting from ice, firn and snow. Here, the main differences arise from the simulation of ice melt, due to the differences in input glacier data and equations involved.

Regarding the rest of the water balance components, only minor discrepancies can be observed. As expected, the mean annual precipitation ( $P$ ) is identical in both cases, since the same climate input data and interpolation methods are used in both models (in fact, the data is transferred from the first WaSiM run (with VA scaling) to OGGM and finally to the coupling scheme). Evapotranspiration ( $ET$ ) shows small differences, being the values higher in the coupling scheme. These differences may be traced back to divergences in glacierized areas between the models, while the remaining land cover remains mostly unaffected. Specifically, the coupling scheme may exhibit a greater proportion of bare soils

Table 7.3: Mean annual water balance components [ $\text{mm yr}^{-1}$ ] (and standard deviation) during the historical period (1971-2010) for the Gepatschalm catchment, determined from the two models: WaSiM with VA scaling and WaSiM-OGGM coupling scheme.

Component [ $\text{mm yr}^{-1}$ ]	WaSiM with VA scaling	WaSiM-OGGM coupling scheme
<i>Surface runoff</i>	237 $\pm$ 66	254 $\pm$ 65
<i>Interflow</i>	336 $\pm$ 62	327 $\pm$ 66
<i>Baseflow</i>	49 $\pm$ 0	16 $\pm$ 5
Runoff from unglacierized areas	621 $\pm$ 127	597 $\pm$ 130
<i>Ice melt</i>	248 $\pm$ 102	353 $\pm$ 115
<i>Firn melt</i>	180 $\pm$ 107	131 $\pm$ 86
<i>Snow melt</i>	341 $\pm$ 109	324 $\pm$ 93
Glacier runoff	769 $\pm$ 110	808 $\pm$ 111
<b>Total runoff, R</b>	1390 $\pm$ 196	1405 $\pm$ 196
<b>Precipitation, P</b>	1279 $\pm$ 221	1279 $\pm$ 221
<b>Evapotranspiration, ET</b>	35 $\pm$ 8	59 $\pm$ 12
<b>Storage change, <math>\Delta S</math></b>	-189 $\pm$ 163	-186 $\pm$ 176

(not covered by glaciers) compared to the VA scaling model, thereby leading to an increase in *ET* values. Finally, the change in storage ( $\Delta S$ ) is practically the same in both cases. The evolution of the glaciers from the historical period up to the future is presented in the next section, together with the behavior of runoff until the end of the century.

## 7.4.2 Future projections

The first outcome of the simulation results from the historical period is that, although the coupling scheme delivers improved representation of runoff compared to the VA scaling, the results still look very alike. At this stage, it is hard to state which model behaves more adequate in the past. However, the focus of the comparison is given to the accurate prediction of future runoff in glacierized catchments and to conclude which model is more robust and reliable to achieve this goal.

For this reason, runoff and glacier evolution (mass balances, areas and volumes) are investigated under three future climate GCM/RCMs combinations and for three different RCPs: 2.6, 4.5 and 8.5, according to the climate input data introduced in Section 3.2.4.3. The results for runoff are shown in Figure 7.23, where the left column represents the results from the VA scaling (Sub-figures a<sub>1</sub> to a<sub>4</sub>) and the right column represents the results from the coupling scheme (Sub-figures b<sub>1</sub> to b<sub>4</sub>). In all cases, the mean monthly runoff for the reference and three different future periods are included (rows, from bottom to top: 1971-2010, 2011-2040, 2041-2070 and 2071-2100). The results are depicted as an ensemble mean and for the three RCPs (blue for RCP2.6, green for RCP4.5 and red for RCP8.5), with their corresponding spread. In addition, the simulated mean monthly runoff for the historical period (1971-2010, gray dashed line) from each model is also included in each sub-figure.

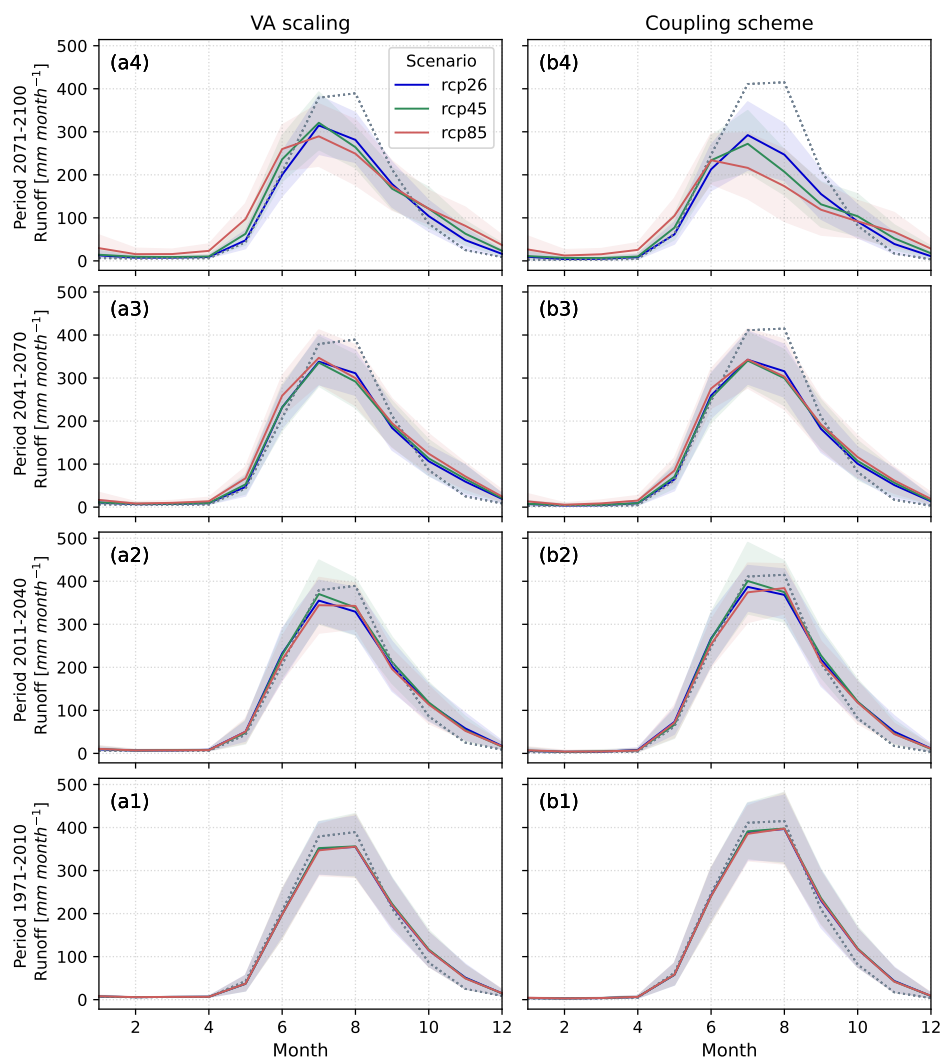


Figure 7.23: Mean monthly runoff for the reference and three different future periods (rows, from bottom to top: 1971-2010, 2011-2040, 2041-2070, 2071-2100) and for the two models: on the left (a<sub>1</sub> to a<sub>4</sub>) WaSiM with VA scaling and on the right (b<sub>1</sub> to b<sub>4</sub>) WaSiM-OGGM coupling scheme. The values represent the ensemble mean of the three GCM/RCMs combinations and for RCP2.6 (blue), RCP4.5 (green) and RCP8.5 (red). The gray dashed line indicates the simulated mean monthly value during the historical period.

During the reference period (first row, 1971-2010, Sub-figures a<sub>1</sub> and b<sub>1</sub>), almost no differences can be observed between simulation results. The models behave similarly under the different RCPs and the results closely align with the historical simulations. Like the results shown in Figure 7.22, the VA scaling seems to slightly underestimate the peak runoff, compared to the coupling scheme. For the near future (period 2011-2040, second row, Sub-figures a<sub>2</sub> and b<sub>2</sub>), both models behave similarly and there are only small differences between simulation results under the different RCPs. The mean monthly peak is slightly reduced and remains in August for RCP8.5 but is shifted to July for RCP2.6 and 4.5 in both models. Moreover, there is an increase on the winter flows, between September and December. This increase can also be seen when analyzing the middle period 2041-2070 (third row, Sub-figures a<sub>3</sub> and b<sub>3</sub>). In addition, for both models and for all RCPs, the mean monthly peak already shifts to July, suggesting that the runoff of the catchment changes from a glacial/glacionival to a nivo-glacial regime (Hanzer et al., 2018). When comparing the results from both models, it is feasible to see that the reduction of the monthly peak

is stronger in the coupling scheme, whereas higher runoff values are observed during spring in the VA scaling model, particularly for RCP8.5.

Comparable results are observed during the last period 2071-2100 (upper row, Sub-figures a<sub>4</sub> and b<sub>4</sub>), where the mean monthly peak is reduced and shifted to July. However, the results of the coupling scheme for RCP8.5 suggest that the peak might be further shifted to June while experiencing a more substantial reduction (44% decrease of the peak as compared to the historical period). Again, simulated winter runoff increases in both models, most importantly for RCP8.5. During spring months, the VA scaling shows an increase in the monthly values compared to the coupling scheme. The mean annual runoff during this last period and for RCP8.5 is 1393 mm for the VA scaling and 1108 mm for the coupling scheme. This suggests that the simulated runoff from the coupling scheme is approx. 20% lower than the results from the VA scaling, so the increased spring values do not compensate the strong reduction of runoff during summer. Similarly, 8% and 14% lower values are obtained from the coupling scheme for RCP2.6 and RCP4.5, respectively.

To better understand the relatively diverse response between both models when simulating runoff under future climate projections, glacier evolution in terms of mass balances, volumes and areas are analyzed in detail in Figure 7.24. Similarly to the case of runoff, the left column refers to the results from the VA scaling, whereas the right column indicates the results from the coupling scheme. The lower row (Sub-figures a<sub>1</sub> and b<sub>1</sub>) depicts the evolution of the glaciers' volume, given in km<sup>3</sup>. The middle row (Sub-figures a<sub>2</sub> and b<sub>2</sub>) contains the evolution of the glaciers' area, given in km<sup>2</sup>, where also observed areas are indicated (red dots). Finally, the upper row (Sub-figures a<sub>3</sub> and b<sub>3</sub>) show the evolution of the glaciers' mass balance, as an average for all the glaciers within the study area, given in m w.e. yr<sup>-1</sup>. From 1971 to 2010, the results correspond to the historical period and are represented by the gray solid line. From 2011 onward, results under different RCPs are shown, following the same representation used for runoff.

From Sub-figures a<sub>3</sub> and b<sub>3</sub> in Figure 7.24, it is clear that the models behave quite similar during the historical period, where a mean annual mass balance of -0.71 m w.e. and -0.82 m w.e. is obtained from the VA scaling and coupling scheme, respectively. During the period 2000-2020, the mean annual observed value is -0.74 m w.e., calculated as a weighted average from all the glaciers within the area (according to Hugonnet et al., 2021). As for RCP2.6, a much higher inter-annual variability is observed from the VA scaling results, where at the end of the century, a total average cumulative mass loss of approx. 142 m w.e. is expected (this value is obtained by integrating annual mass balance values over time). On the other hand, the results from the coupling scheme suggests that only 124 m w.e. will be lost by 2100 (thus, the mass loss obtained from the VA scaling is 13% higher than from the coupling scheme). From the simulation results under RCP4.5 and 8.5, higher losses are expected. By the end of the century under RCP4.5, the total average mass loss is approx. 214 m w.e. for the VA scaling and 144 m w.e. for the coupling scheme. The greatest difference between simulation results, however, appears under RCP8.5. In this case, the VA scaling indicates that the study area may experience a total average mass loss of almost 390 m w.e. by 2100, whereas the results obtained with the coupling scheme are nearly halved (198 m w.e.). The peculiar VA scaling behavior under RCP8.5 could be linked to the very small glacierized areas that still prevail on the region at the end of the century. As the mass balance definition involves changes in mass per unit area, even very small areas could result in substantial mass balance values.



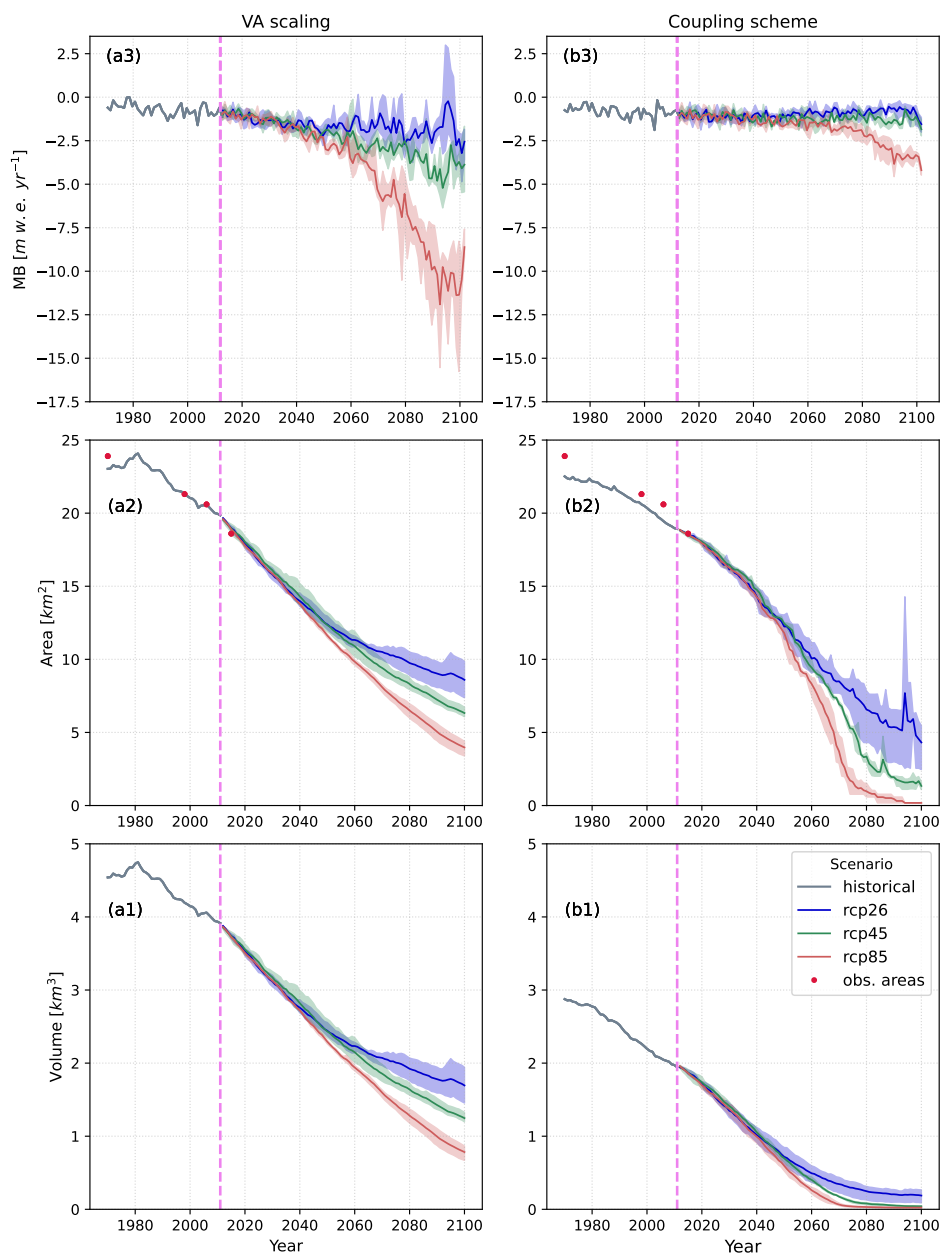


Figure 7.24: Volumes ( $a_1$  and  $b_1$ ), areas ( $a_2$  and  $b_2$ ) and annual mass balance ( $a_3$  and  $b_3$ ), as a total average (i.e. considering all glaciers within the study area). On the left, results from the WaSiM model with VA scaling and on the right, results from the WaSiM-OGGM coupling scheme. The values represent the ensemble mean of the three GCM/RCMs combinations and for RCP2.6 (blue), RCP4.5 (green) and RCP8.5 (red). The gray line indicates the results obtained during the historical period.

When looking at the evolution of the glacier areas (Sub-figures  $a_2$  and  $b_2$ ) throughout the historical period, it becomes clear that both models behave quite similarly. Even though the coupling scheme seems to underestimate the areas in the past, both models reach a similar value at the end of the period. In 2010, the total area simulated using the VA scaling is  $19.9 \text{ km}^2$ , whereas a value of  $19.0 \text{ km}^2$  is obtained from the coupling scheme. This similar behavior between models can still be perceived until 2040 and for all RCPs, where results differ only in 2% (glacier area of  $14.0$  and  $14.3 \text{ km}^2$  for the VA scaling and coupling scheme, respectively). After 2040, greater deviations between models in terms of areas are expected. For example, by the end of the century and for RCP2.6, the VA scaling



predicts a total glacier coverage of 8.6 km<sup>2</sup>, whereas this value is 4.3 km<sup>2</sup> when considering the coupling scheme. That means that by the year 2100, 77% of the glaciers will melt according to the coupling scheme, but only 57% according to the VA scaling, compared to the areas in 2010. For RCP4.5, these numbers increase up to 93% and 68%, and they become extreme for RCP8.5, where a total area loss of 99% and 80% is expected by the coupling scheme and the VA scaling, respectively.

In terms of volumes (Sub-figures a<sub>1</sub> and b<sub>1</sub>), the discrepancies between model results are much larger. At the beginning of the simulations, the total volume expected from the VA scaling is 4.5 km<sup>3</sup>, which is equivalent to a mean ice thickness of almost 80 m distributed all over the area (i.e. total study area, including unglacierized parts). As for the coupling scheme, this value is 2.9 km<sup>3</sup> or likewise, 50 m of ice thickness. The initial volume clearly affects the evolution of the glaciers in the future. For the VA scaling, glacier volumes of 1.7, 1.3 and 0.8 km<sup>3</sup> are expected by 2100 for RCP2.6, 4.5 and 8.5, respectively. These values are much more optimistic than the values predicted by the coupling scheme, where almost all glaciers would have disappeared by the end of the century and under all RCPs (0.19, 0.04 and 0.02 km<sup>3</sup> for RCP2.6, 4.5 and 8.5, respectively). The results from the coupling scheme share more affinity with other studies carried out in the European Alps. One example can be found in Zekollari et al., 2019, where the authors conclude that the projected volume loss for the European Alps by 2100 under a strong warming (RCP8.5) is around 94%.

The discrepancies between both simulation results could be explained by two main arguments. On the one hand, the initial volume within WaSiM simulations is determined direct and empirically with the VA scaling equation (Equation 5.2), where only the glacier area is known. On the other hand, the coupling scheme relies on the area and ice thickness distribution determined by OGGM, which are based on the ice-flow dynamics. Moreover, the annual update of the glacier volumes is performed differently in each model. In the case of WaSiM with VA scaling, the same relation between volume and area is maintained over the years, since the empirical factors affecting Equation 5.2 do not change in time. On the contrary, the feedback from OGGM is integrated annually into the coupling scheme, hence trusting the evolution of the ice dynamics. Another point to consider is the spatial representation of the parameters involved. The VA scaling approach describes volume's evolution using "global" parameters (i.e. parameters that are the same across the entire catchment and cannot be adjusted on a glacier basis), which means that all glaciers within the study area are affected by the same mean thickness (represented by the parameter  $b$  in Equation 5.2). This, however, is hardly the case, due to the diversity in size and shape of glaciers throughout the catchment (also depicted in Figure 7.17). The coupling scheme is able to deal with this issue due to the annual update of the glaciers' geometries, including the ice thickness distribution at a glacier basis.

As shown in Section 7.1.1, the parameters involved in the VA scaling approach seem to be not sensitive in terms of runoff during the historical period. This may suggest that different values would yield to similar results. However, this might not be the case when looking into the future. As an example, an extra simulation with a different value of  $b$  is performed (the default value is 28.5 m) under RCP4.5. For this purpose, new model simulations with  $b = 60$  m are carried out, since this is a mean ice thickness representative for the glaciers within the study area (Section 3.2.2.3). Figure 7.25 displays the results with the new  $b$  parameter (blue point-dashed lines), together with the results by using the default value of 28.5 m (red dashed lines). Additionally, the results from the coupling

scheme are also included in the figure (green solid lines).

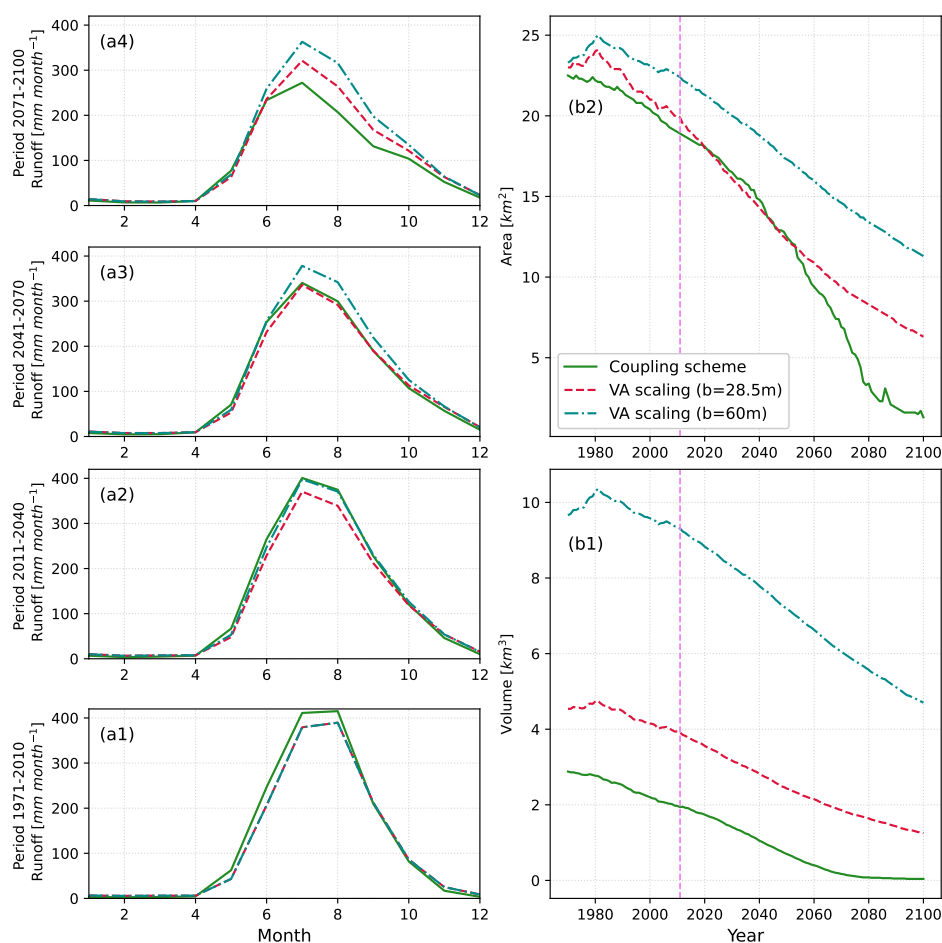


Figure 7.25: Influence of the "b" parameter from the VA scaling approach in the simulation results. On the left ( $a_1$  to  $a_4$ ) runoff at the outlet of Gepatschalm, for the reference and three different future periods ( $a_1$ :1971-2010,  $a_2$ :2011-2040,  $a_3$ :2041-2070,  $a_4$ :2071-2100). On the right, volumes ( $b_1$ ) and areas ( $b_2$ ). The red dashed lines refer to the default parameter  $b=28.5$ , whereas the blue point-dashed line, to a higher value,  $b=60$  m. Moreover, the results from the coupling scheme are also included (green solid line).

Sub-figures  $a_1$  to  $a_4$  show the mean monthly runoff at the outlet of Gepatschalm for the reference and three future periods, similar to the results depicted in Figure 7.23. It is evident that the value of  $b$  does not influence the results in terms of runoff during the reference period (Sub-figure  $a_1$ ), since both VA scaling outcomes are identical. This discovery, which confirms the findings from the sensitivity analysis, may lead to wrong interpretations when looking into the future. For example, for the near future (Sub-figure  $a_2$ , period 2011-2040), different values of  $b$  still deliver similar results in terms of runoff, but it is already feasible to see that a higher value ( $b = 60$  m) results in higher peaks. Interestingly, this model setup behaves almost identical to the coupling scheme. This might be explained by the fact that, at the beginning of the simulations, the mean ice thickness is 65 m when using the coupling scheme (obtained from OGGM), and as an average across all glaciers.

However, when looking into the second half of the century (2041-2070 and 2071-2100, Sub-figures  $a_3$  and  $a_4$ , respectively), the models behave differently. On the one hand, the coupling scheme still yields lower values of runoff by the end of the century, compared to the VA scaling. On the other hand, a higher value of  $b$  result in much higher peaks, compared to the default value. While the peak in July reaches a value of  $321 \text{ mm month}^{-1}$  with  $b$

$= 28.5$  m, a value of  $363 \text{ mm month}^{-1}$  is expected with  $b = 60$  m. Even though the peak runoff is overestimated by 13% with a larger value of  $b$ , larger discrepancies are expected in terms of glacier areas and volumes. The findings can be seen in Sub-figures  $b_1$  and  $b_2$ , where the evolution of glacier volume and area are presented, respectively.

In terms of areas, a higher value of  $b$  result in larger glacierized areas. This is represented by the upper curve in Sub-figure  $b_2$ . By the end of the century, a value of  $b = 60$  m suggests that still 48% of the glaciers will remain in the area. This value is much more optimistic than the results obtained with  $b = 28.5$ , where only 27% will be covered by glaciers. In both cases, though, simulated values still exceed predictions from the coupling scheme. The discrepancies are even more dramatic when analyzing the volume's evolution. As shown in Figure 7.24, the coupling scheme yields to smaller values compared to the VA scaling with  $b = 28.5$  m, which is estimated by knowing the glacierized area and after applying Equation 5.3. Thus, the same approximation can be done when considering  $b = 60$  m and the results will look quite similar but scaled in more than 200%. Although different scaling parameters in Equation 5.2 yield to similar results under past conditions, the models behave clearly contrastingly in the future and a robust estimation of such parameters is hardly possible. These findings arise more doubts about the applicability of empirical models when predicting future evolution of glaciers and encourage the introduction or more physically-based approaches, like ice-flow dynamics.

With focus on the potential impacts of glacier mass loss on water availability in the future, the evolution of annual runoff at the outlet of the catchment is analyzed. As introduced in Section 1.1 (Figure 1.1), the runoff from glacierized catchments increases along with the loss of glacier mass until it reaches a maximum, after which it decreases due to the reduced glacier volume. This maximum (*peak water*), is a critical point beyond which water availability can become critical and potentially lead to water shortage in the future. Many glaciers in the European Alps have already reached this peak or is expected to be reached in the next decade, showing a growing concern for water availability in the regions that depend on glacier runoff (Farinotti et al., 2012; Huss and Hock, 2018). Since peak water could serve as a valuable indicator for analyzing water availability among hydrologists, the evolution of runoff and corresponding peak water is estimated for Gepatschalm, under the different scenarios. Results are shown in Figure 7.26. The two upper rows (Sub-figures  $a_4$  and  $a_3$ ) show the total annual precipitation and mean annual temperature, respectively, as an average for the entire catchment. The two lower rows (Sub-figures  $a_2$  and  $a_1$ ) depict the evolution of annual runoff at the outlet of Gepatschalm, determined by WaSiM with VA scaling and with the coupling scheme, respectively. In all cases, the thick lines represent the ensemble mean as a 10-year moving average, whereas the thinner lines show the annual variability, for the three RCPs (blue for RCP2.6, green for RCP4.5 and red for RCP8.5). Moreover, the annual average value of the observed runoff during the period 1985-2010 and the annual average value of the simulated runoff during the historical period (1971-2010) are also indicated (horizontal lines) in Sub-figures  $a_1$  and  $a_2$ .

The evolution of runoff under RCPs 2.6 and 4.5 show a similar behavior. In both cases, VA scaling and coupling scheme, the peak water is awaited around the year 2030. However, after this peak is reached, the results from the VA scaling model show a gentle decline, compared to the results from the coupling scheme. Similarly, the runoff evolution under RCP8.5 indicates that the peak water is expected by the year 2056 with the coupling scheme, but no clear peak is observed from the VA scaling results. The continuous increase temperature values under RCP8.5 leads to higher melt rates that might compensate the

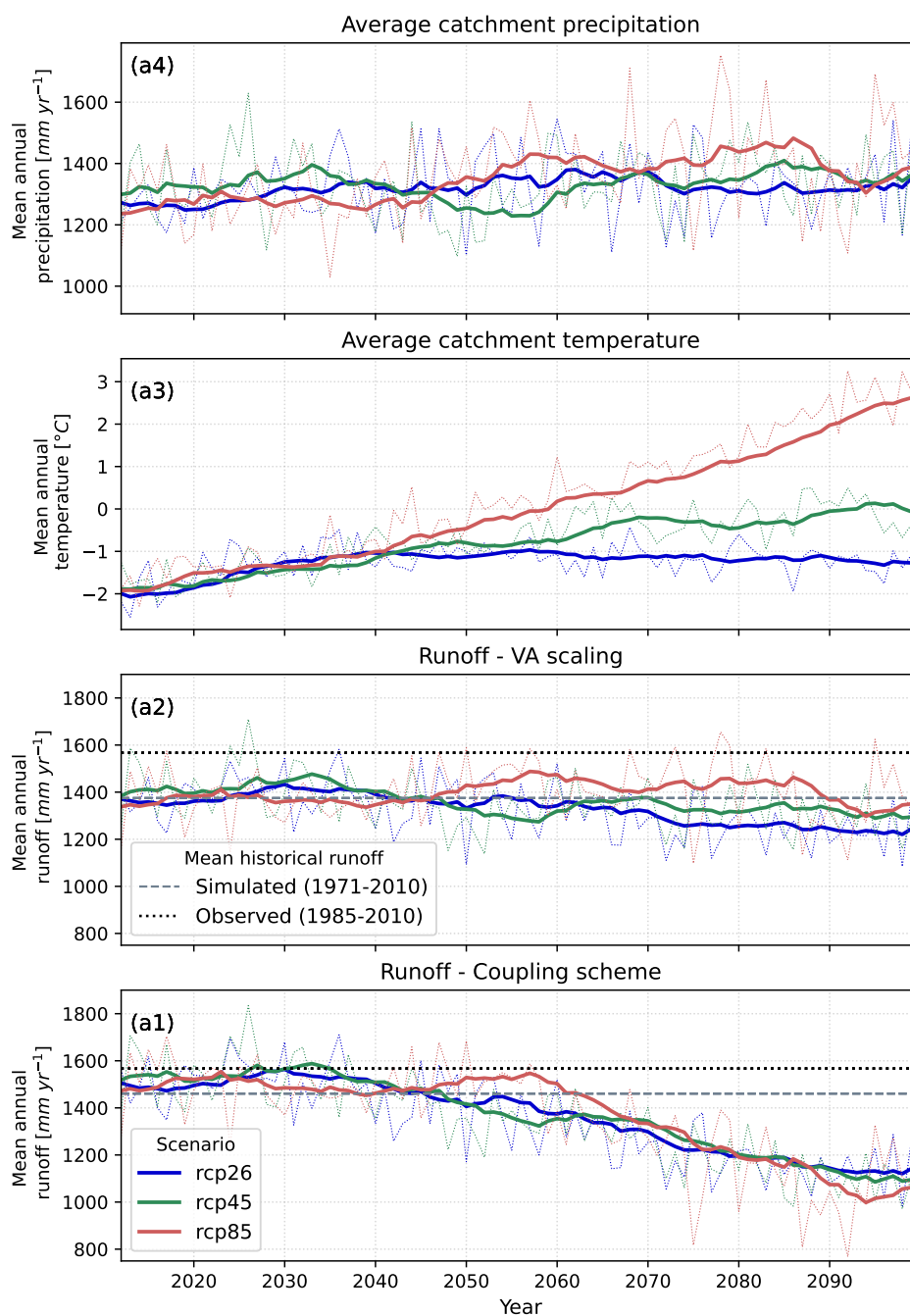


Figure 7.26: Future evolution of (a<sub>4</sub>) total annual precipitation and (a<sub>3</sub>) mean annual temperature values, computed as an average for the entire Gepatschalm catchment. a<sub>2</sub> and a<sub>1</sub> show the evolution of annual runoff at the outlet of the catchment, obtained from the WaSiM with VA scaling model and coupling scheme, respectively. The thick lines represent the ensemble mean of the three GCM/RCMs combinations and for RCP2.6 (blue), RCP4.5 (green) and RCP8.5 (red) as a 10-year moving average. The gray dashed line in sub-figures a<sub>2</sub> and a<sub>1</sub> indicates the mean annual runoff simulated by each model during the period 1971-2010, whereas the black point line indicates the mean annual observed runoff during the period 1985-2010.

reduction on the glacier area, thus delaying the peak (Huss and Hock, 2018), compared to the other two scenarios. Moreover, and although the glaciers get smaller, runoff is still possible due to the increase in rainfall (as shown in Sub-figure a<sub>4</sub>). By the year 2100, the annual runoff under RCP8.5 is expected to decrease by nearly 44% with the coupling scheme, in comparison to the mean value observed from 1985-2010. This reduction only

represents 16% for the VA scaling. Once more, the results from WaSiM with VA scaling approach show a more optimistic prognosis, whereas the results from the coupling scheme emphasizes the possibility of facing water shortage in the future. Appendix C.3 complements these findings with additional results.

To summarize Section 7.4, the comparison of simulation results between the WaSiM with VA scaling model and the WaSiM-OGGM coupling scheme, shows quite a contrasting behavior of runoff and glacier evolution within the study area under future projections. These results express more concerns about applying the VA scaling approach for estimating runoff in high glacierized catchments and places more trust in the use of global glacier models with explicit ice-flow dynamics, like OGGM.

## 7.5 Application of the coupling scheme in another catchment

So far, the coupling scheme was developed and applied to the Gepatschalm catchment, where one of the main challenges lies on the limited observations in terms of glaciers. As mentioned in Section 3.2.2.2, none of the glaciers in the study area are reference glaciers, hence no mass balance measurements (as a total value for the entire glacier) are available for them. Although OGGM (second step of the coupling scheme, Section 7.2) seems to succeed even with a few constraints (i.e. calibration was done only considering annual average geodetic mass balance and mass balance at the tongue of *Gepatschferner*), it would be interesting to see whether the coupling scheme is able to replicate the total mass balance of the glaciers for the considered simulation period.

For this reason, and also to test the performance of the coupling scheme in another study area, the coupling scheme is applied to a neighboring catchment, which is shown in Figure 7.27. The Rofenache study area covers a total surface of 97.2 km<sup>2</sup> and contains three reference glaciers: *Hintereisferner* (HEF), *Kasselwandferner* (KWF) and *Vernagtferner* (VEF). Thus, annual mass balance measurements are available for each of them, starting before 1969 and up to date (WGMS, 2022).

Similar to the Gepatschalm study case, the INCA-kNN climate dataset (Section 3.2.4.1) is used as input and the same spatio-temporal resolution is adopted for running the models. As regards observed runoff, this is available for the period 01/1967 to 12/2018 at the outlet of the catchment (Bundesministerium Land- und Forstwirtschaft, Regionen und Wasserwirtschaft, 2023). The workflow explained in Chapter 6 and shown in Figure 6.11 is followed and the corresponding assumptions and results are introduced in the following sections.

### 7.5.1 First WaSiM run with resampling of climate data

Like for the Gepatschalm study case, a continuous WaSiM run is carried out with daily resolution to obtain mean monthly values of temperature and total monthly values of precipitation (interpolated to the model grid, also with a 100 m × 100 m resolution). Since a comparison with the VA scaling approach is not pursued in this case, the calibration of the first WaSiM run is omitted (Section 6.3.2). During the third step of the coupling scheme,

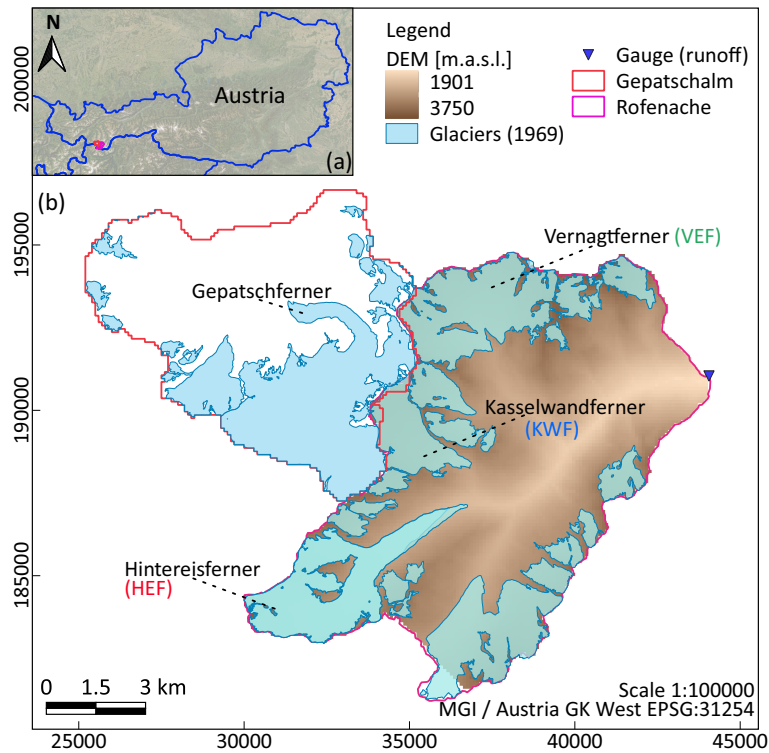


Figure 7.27: Rofenache catchment: (a) location within Austria and (b) subcatchments' division with Digital Elevation Model (DEM), glacier coverage for the year 1969 (AGI, Section 3.2.2.1), available gauging station for runoff and reference glaciers.

the model is optimized anyway, by selecting the most sensitive parameters (resulting from Section 7.1.1).

## 7.5.2 OGGM run and processing of glacier outputs

Following the sensitivity analysis performed in Section 6.4.2 and the corresponding results in Section 7.2.1, the same procedure is adopted for the Rofenache catchment. Thus, the parameters *melt\_f* and *temp\_bias* are kept with their default or fixed values ( $5.0 \text{ kg m}^{-2} \text{ K}^{-1} \text{ d}^{-1}$  and  $0.5 \text{ }^\circ\text{C}$ , respectively) while *prcp\_fac* is calibrated at a glacier basis based on average geodetic mass balance measurements (Hugonnet et al., 2021). Although total mass balances are available for the reference glaciers, these datasets are not considered during the calibration. This choice aims to follow the general workflow as described in Chapter 6, hence to test the applicability of the developed coupling scheme. OGGM is initialized in 1969, which means that a dynamic spinup of 34 years is performed.

## 7.5.3 Coupling the models: final WaSiM run with optimization

During the third step, WaSiM runs continuously at a daily time step from 1969 to 2020, while the glacier inputs are updated annually according to the outputs generated from OGGM. The optimization, which is carried out between 01/1985 and 12/1998, aims to minimize the multi-objective function described by Equation 6.3. The same weighting factors and objective functions are employed and the results are presented in the following section.

## 7.5.4 Results of the coupling scheme in Rofenache

First, the applicability of the coupling scheme in terms of runoff prediction is assessed. The results are depicted in Figure 7.28, where mean daily observed and simulated runoff are displayed for the period considered during optimization (1985-1998). Moreover, the contribution of ice melt and the performance measures are also included.

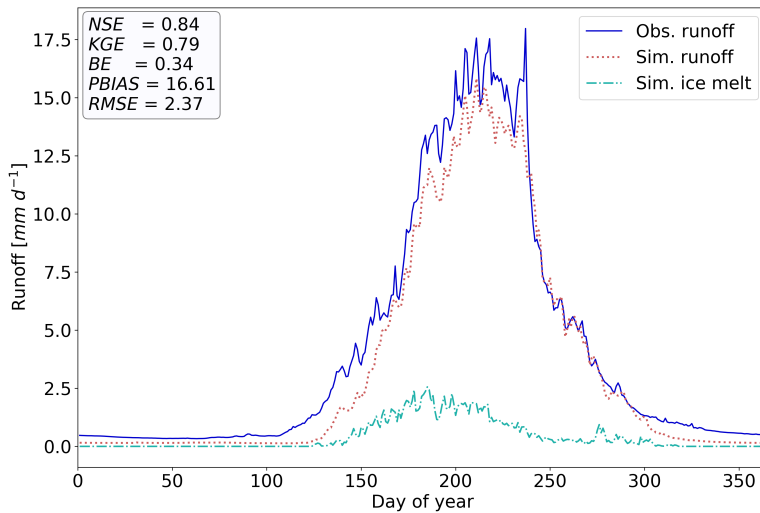


Figure 7.28: Mean daily observed and simulated runoff at the outlet of Rofenache during the optimization period (01/1985 - 12/1998). Blue solid line: observed runoff, red dashed line: simulated runoff, light blue line: simulated melt from ice. The performance measures are defined in Section 6.3.2 and Appendix B.

The coupling scheme performs very well when representing runoff during the optimization period, which can be observed by the very good performance measures. However, the model seems to underestimate runoff during spring and summer months, probably related to the snow melt, since this is the main contributor to runoff generation. Similar to the Gepatschalm study case, this issue could be related to the snow model, ratifying once again the need to include snow measurements for model calibration, if available. In terms of glaciers, Figure 7.29 shows the obtained 2D geometries after converting the "1.5D" flowlines from OGGM, like the procedure described in Section 6.4.4.

While Figure 7.29a shows the glaciers at the beginning of the simulations (year 1969), Figure 7.29b depicts the geometry of the glaciers after 46 years of simulations (year 2015). As described by Maussion, 2018, the release of the RGI v6.0 came with some complications for a few glaciers, including *Hintereisferner* and *Vernagtferner*. Although they should be divided into several entities, the RGI's outline considers them as single glaciers, as they used to be decades ago. Efforts have been carried out to divide these entities and the results can be seen for example, for *Hintereisferner*. At first glance, it seems that the coupling failed to capture part of the glacier in the north, but this is done intentionally, since it is considered that this part is an independent entity and hence do not contribute to the main flowline of the glacier (Maussion et al., 2023). The tongue is adequately represented at the beginning of the simulations, contrary to the case of *Gepatschferner*, but it is still overestimated at the year 2015.

When looking at *Vernagtferner*, however, a larger mismatch originates between observed and simulated areas. Besides, it seems that the glacier does not experience large changes in its geometry after 46 years, even though the observed values suggest a decrease of approx. 23% during that period. The results of the OGGM dynamic run show that in 2015, a reduction of only 4% is predicted, compared to the area in 1969. Nevertheless, a reduction of 22% in volume is simulated, which indicates that the discrepancy of the results might come from the conversion of "1.5D" to 2D geometries. To have a deeper insight into



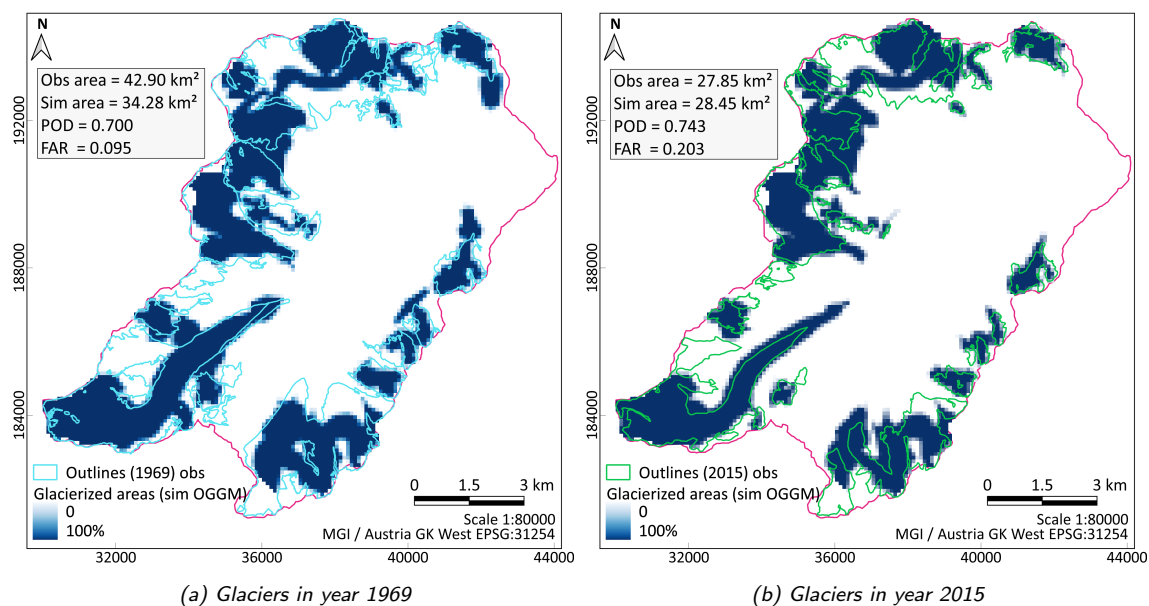


Figure 7.29: Observed and converted 2D glacier areas for the years 1969 (initialization of the model) and 2015, after performing the OGGM runs, with dynamic spinup. The observed outlines belong to the AGI (Section 3.2.2.1) and the performance measures are defined in Section 6.3.2 and Appendix B.

this issue, Figure 7.30 shows the three main flowlines of the glacier, which are considered by OGGM. This suggests that the longest flowline (red line) flows from north-east (A) to south-west (B), being the latter point the terminus of the glacier. However, the current glacier outline and topography might indicate the presence of a glacier divide (yellow dashed line), which may lead to a break of the longest flowline. This break point (C) will generate another glacier terminus and the possible split of the glacier into two entities, being the result closer to the observed areas in 2015.

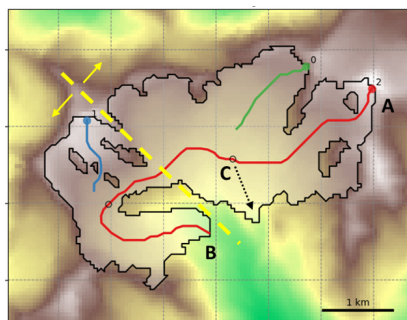


Figure 7.30: The three main flowlines of Vernagtferner, determined by OGGM. The longest flowline (red) flows from north-east (A) to south-west (B), but the current glacier geometry and topography might indicate the presence of a glacier divide (yellow dashed line) which may lead to a break of this flowline (C).

This analysis reveals that there are still some deficiencies in representing glacier areas (2D geometries), but it seems that this deviation comes explicitly from OGGM (flowlines) and not from the coupling scheme (conversion of "1.5D" to 2D geometries, Section 6.4.4).

Regarding the remaining glaciers, in general a good representation is achieved, which can be seen by the low FAR values. Still, the model underestimates the total area during the first year of the simulations (lower POD), due to the issues explained before and because OGGM is not yet able to create glaciers that existed and melted completely before the RGI's date. Similarly, the quite complex nature of the glaciers in this catchment makes the prediction of areas a difficult task. In terms of thickness, simulated values show to be larger than mean observed values, particularly for *Hintereisferner* and *Vernagtferner*. Since the simulated areas are underestimated, the higher thickness might explain that OGGM tries



to conserve volumes (and mass balances). A verification of the ice thickness is shown in Appendix C.5.

Finally, Figure 7.31 shows the annual mass balance (left) and cumulative values (right) for the three reference glaciers (rows, from top to bottom): *Hintereisferner* (HEF), *Kasselerwandferner* (KWF), *Vernagtferner* (VEF) and the weighted average. The values correspond to the period 1989-2019, so a part of the dynamic spinup is included. The dashed lines refer to the observed annual mass balances according to WGMS, 2022, the thin solid lines are the results obtained from OGGM after calibration of the mass balance model and performing the dynamic run, following Section 7.5.2. The thick solid lines reflect the results from the coupling scheme, after performing the optimization (according to Section 6.5.1). The horizontal gray dashed line on the left diagrams indicates the average geodetic mass balance used during calibration of the OGGM's mass balance model, for each of the glaciers. Moreover, the average MBE and RMSE [mm w.e. yr<sup>-1</sup>] between observed datasets and simulated values from OGGM are included in each case.

The first outcome after looking at Figure 7.31 is that, although each individual glacier behaves differently, the inter-annual variability of the mass balances is well captured, especially when considering the weighted average of the three glaciers (Sub-figure a<sub>1</sub>). In addition, the peaks are in close agreement and the huge loss in thickness caused by the extreme warm and dry conditions during the summer of 2003 (UNEP, 2004), seems to be very well captured. The cumulative curves shown in Sub-figures b<sub>1</sub> to b<sub>4</sub> indicate that both values, simulated by OGGM and the coupling scheme, overestimate the mass loss, except for *Vernagtferner*, where the coupling scheme performs very close to the observations.

Sub-figure b<sub>1</sub> suggests that the observed weighted average mass loss by the year 2019 accumulated since the year 1989 is 24.4 m w.e, being 30.4 and 26.7 m w.e. for OGGM and the coupling scheme, respectively. The differences between OGGM and the coupling scheme simulations are to be expected, since OGGM's mass balances are only used as an additional constraint when optimizing the coupling scheme. Therefore, a perfect match can be hardly obtained. Nevertheless, the results of the coupling scheme are very encouraging, since not only the evolution of glaciers can be well represented, but also the prediction of runoff is reasonable accurate. All complementary results can be found in Appendix C.5.

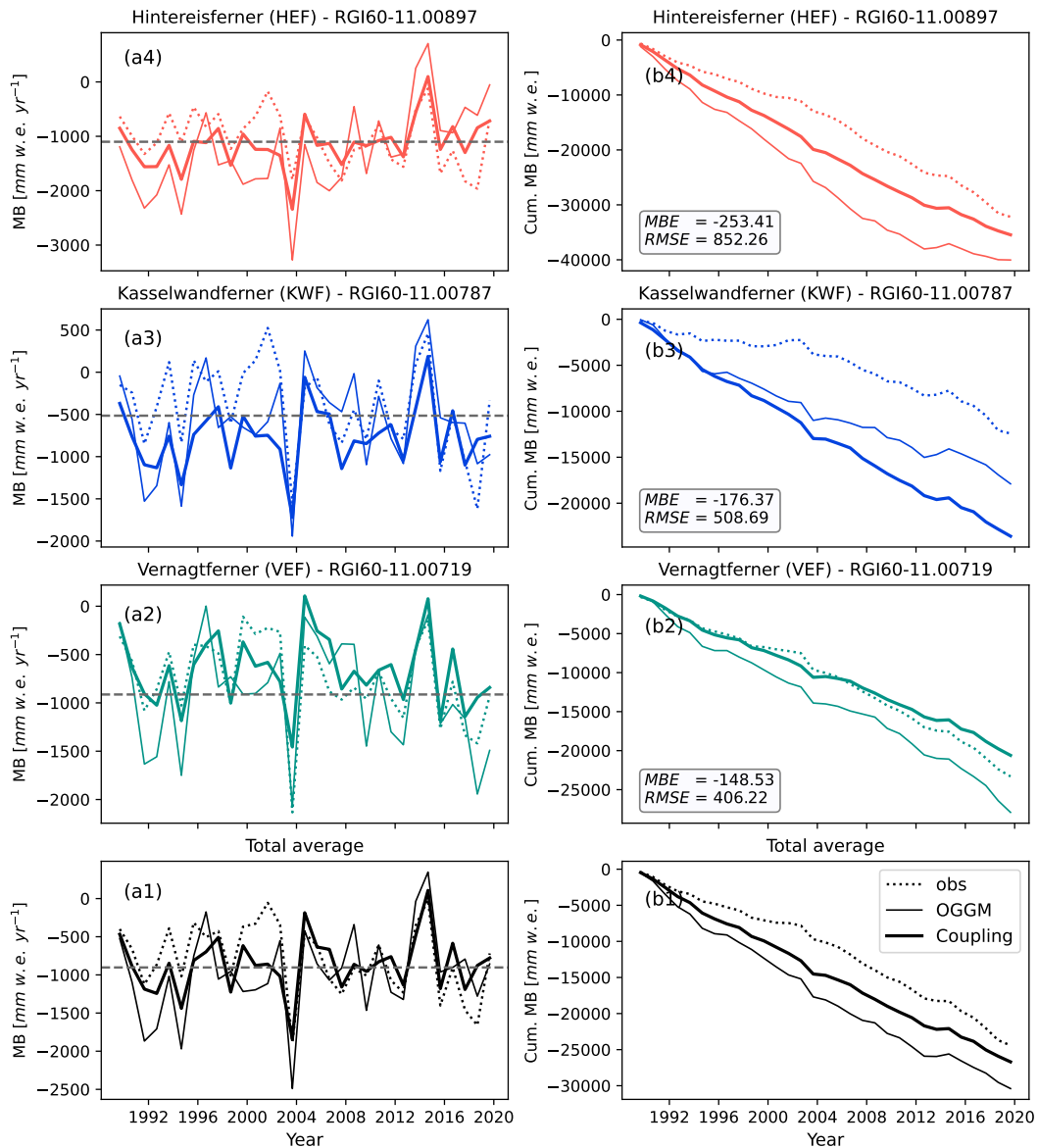


Figure 7.31: Mass balances for the three reference glaciers in the Rofenache catchment (rows, from top to bottom): Hintereisferner (HEF), Kasselwandferner (KWF), Vernagtferner (VEF) and the (area) weighted average, for the period 1989-2019. The dashed lines refer to the observed mass balances (WGMS, 2022) and the thin solid lines are the results obtained from OGGM after calibration of the mass balance model and performing the dynamic run. The thick solid lines are the results from the coupling scheme, after performing the optimization. The diagrams on the left refer to the annual mass balances, where the horizontal gray dashed line indicates the average geodetic mass balance used during calibration of the OGGM's mass balance model. The diagrams on the right depict the cumulative values. MBE and RMSE are calculated between observations and OGGM simulation results.

# Chapter 8

## Conclusions and outlook

### 8.1 Conclusions

The prediction of runoff in highly glacierized catchments is a challenging task. Even though the retreat of glaciers is considered to be rather a slow movement (from a few years to centuries), glaciers are capable of altering the hydrological cycle of a catchment at a much shorter time scale. Glaciers store water during winter due to precipitation in form of snow, firn and ice and then release it during summer by melting, being the latter the major contributor to runoff generation. Thus, the runoff of such catchments shows a very high seasonality, with low flows during winter and peak flows during summer (November - March and July - August, respectively, in the Northern Hemisphere). However, projected adverse climatic conditions (e.g. increasing temperatures) might profoundly impact the hydrological response of glacierized catchments in the European Alps, where summer runoff is expected to decrease whilst increasing in spring, suggesting that the runoff regime may change from glacial/glacionival to nivo-glacial (e.g. Hanzer et al., 2018). Furthermore, the continuous retreat of the glaciers will ultimately reach a maximum contribution to runoff, beyond that it begins to decrease due to the reduction of the glacier's volume. This maximum, which is known as *peak water* (Huss and Hock, 2018), has already been reached for most of the glaciers in the European Alps or is closed to be reached. For the case of the glaciers in the Gepatschalm catchment, for example, the *peak water* could be expected in a few years under RCPs 2.6 and 4.5, whereas under strong warming conditions (RCP8.5) the peak is expected for the year 2056, followed by a stronger decline in runoff.

An accurate prediction of glacier processes and runoff generation is therefore essential to evaluate water availability and the immediate consequences that the reliant areas may face. Since the changes in glacier's geometry are based on complex mechanisms, the modeling of glaciers is not an easy task. Many hydrological models rely on empirical approaches to estimate glacier evolution, thus neglecting the physics behind the processes. In this sense, the VA scaling approach integrated in WaSiM allows the estimation of the glacier's volume by simply scaling the glacier's area. One of the main advantages of this method is the low requirement of input data, since only the glacier's area at the beginning of the simulations is required. Moreover, a sensitivity analysis on the empirical parameters involved in the VA scaling approach showed that they are not sensitive, i.e. different parameter values yield to the same runoff result. These findings suggest that the VA-parameters are independent of the glacier's size and geometry and a representative value could be adopted for all glaciers within the catchment, making it quite a robust method. The application of the WaSiM model with VA scaling in the Gepatschalm study area confirms the suitability and simplicity

of this method for determining runoff, at least for simulations during past periods (Sections 7.1.2 and 7.1.4).

On the other hand, and to account for the physical processes behind glacier evolution, OGGM enables the simulation of glaciers based on explicit ice-flow dynamics. Even though the required input data and methods are more sophisticated compared to the VA scaling approach, a more detailed representation can be obtained in terms of area, thickness and volume for each studied glacier. Moreover, the constant update and improvement of its code and the use of publicly available datasets, make OGGM a versatile model that can be adapted and applied to any catchment in the world, even without catchment-wise observations. The only drawback can be related to the initialization of the model, since simulations performed before the glacier outline's date (RGI's date) require special attention (i.e. performing a dynamic spinup). Besides, through the incorporation of additional measurements on ice thickness and mass balances at the tongue of one glacier, the calibration of the mass balance model parameters was improved, and the application of OGGM for the glaciers in the Gepatschalm study area shows encouraging results (Sections 7.2.2 and 7.2.3).

Consequently, the WaSiM-OGGM coupling scheme was developed in this thesis to benefit from each model's capabilities and complement their strengths, while making it a useful tool for predicting glacier evolution and runoff in glacierized catchments. This coupling scheme, which is based on an *offline* coupling, grants the feedback between both independent models in a way that the outputs generated by one model serve as input for the subsequent model. More specifically, the feedback between models is ensured by three steps: (i) the driven precipitation input is corrected (e.g. due to wind-undercatch) and together with temperature values are extrapolated to WaSiM's model grid, aggregated to monthly values and transferred to OGGM (Sections 6.3 and 7.1). Then, during the second step (ii) OGGM applies additional internal calculations to the climate data provided by WaSiM and after calibrating the mass balance model parameters, a dynamic run is performed (with dynamic spinup, if the model is initialized before the RGI's date). At the end of each hydrological year (30<sup>th</sup> September for the Northern Hemisphere), the "1.5D" flowline geometries are converted into a 2D grid, containing information about the area, ice thickness and volume for each glacier within the study area (Sections 6.4 and 7.2). Finally, during the last step (iii), the 2D resulting grids, together with the annual mass balances of the glaciers estimated by OGGM, are used for performing the hydrological simulations with WaSiM, whilst optimizing the most sensitive parameters in terms of runoff and glaciers. During this last step, in which WaSiM runs at a daily time step, the outputs from OGGM (glacier areas and volumes) are integrated at the beginning of each hydrological year (Sections 6.5 and 7.3). The success of the WaSiM-OGGM coupling scheme is guaranteed not only by the results obtained in the Gepatschalm study case, but also by demonstrating the applicability of the coupling to the neighboring Rofenache catchment.

Coming back to the key research questions of this thesis (Section 1.3), it is possible to address them by analyzing the results described in Section 7.4, in which a comparison between WaSiM with VA scaling approach and the WaSiM-OGGM coupling scheme (with explicit ice-flow dynamics) is drawn:

1

Does the inclusion of ice-flow dynamics yield a more realistic glacier representation at a catchment scale?

Although the results referring to the glacier areas seem to be more accurate for the WaSiM run with empirical VA scaling approach (higher POD values), a less erroneous prediction of glacierized cells is obtained from the coupling scheme (lower FAR values). In addition, the distributed ice thickness throughout each glacier (obtained from OGGM and introduced into the coupling scheme) enables a more accurate estimation of the glacier volume. This finding can be clearly seen in Figure 7.25, where a different  $b$  parameter in the VA scaling equation (Equation 5.2) can yield to very contrasting volumes, especially at the beginning of the simulation. Interestingly, this parameter showed to be not sensitive in terms of runoff, but it exerts a great influence on the prediction of glacier volumes. Moreover, its value as a global parameter remains constant throughout the simulation period. In this sense, the coupling scheme (i.e. OGGM), which relies on the ice-flow dynamics to estimate the ice thickness, is able to deal with this rough representation of the glacier volume, providing an annual- and glacier basis update of each glacier's attributes. Additionally, the simulation results under different climate scenarios show different glacier behavior for the coupling scheme, compared to the VA scaling approach (e.g. Figure 7.24, Pesci et al., 2023b). Although the future behavior of glaciers is unknown, similar studies carried out in the European Alps (e.g. Hanzer et al., 2018; Stoll et al., 2020; Zekollari et al., 2019) show an analogy with the coupling scheme results. For this reason, more realistic outcomes in terms of glacier evolution could be expected with the inclusion of ice-flow dynamics at the catchment scale.

2

Does the inclusion of ice-flow dynamics improve the prediction of runoff in glacierized catchments?

At first glance, this question is not easy to answer. Simulations during the historical period show similar results in terms of runoff, both from WaSiM with VA scaling approach and the coupling scheme. This may suggest that the inclusion of ice-flow dynamics for estimating glacier runoff does not exert any changes and that a rather simple and empirical approach (like the VA scaling), would be suitable for predicting the hydrological response of glacierized catchments. However, when looking into the future, more precisely after the year 2040, marked discrepancies arise between simulation results (e.g. Figure 7.23). This goes in line with the predicted glacier evolution, as explained before. The more detailed representation provided by OGGM (and therefore the coupling scheme) gives more confidence when estimating runoff in the future.

In summary, it is feasible to conclude that:

1. The empirical VA scaling approach is suitable for considering glacier evolution when performing hydrological simulations in the past, but more reliable results are expected with the inclusion of ice-flow dynamics, especially for simulations over a century.
2. The empirical VA scaling approach might become more convenient when simulating hundreds of glaciers simultaneously, therefore other methods should be employed when working at the catchment scale.

3. The WaSiM-OGGM coupling scheme allows a physically-based, fully-distributed representation of hydrological processes, placing emphasis on glacier evolution.
4. The WaSiM-OGGM coupling scheme can be applied to any catchment with no available glacier observations and be initialized at any desired year.
5. The WaSiM-OGGM coupling scheme can be used as valuable tool when predicting the future hydrological response of glacierized catchments under changing climatic conditions, without increasing the required glaciological expertise.

## 8.2 Limitations and Outlook

There are some limitations of the coupling scheme that cannot be evaded, either because of the simplifications made during its development or simply because the applicability is restricted to certain cases. Nevertheless, an outlook on feasible solutions and future research is provided for each of these limitations.

1. **OGGM is not a fully-distributed model:** The conversion of "1.5D" to 2D geometries is a merely geometrical approximation. The connection between the outermost points could be improved by introducing, for example, the bedrock topography. In addition, a new function is already available in OGGM, which is able to provide an approximated extrapolation of the glacier into a 2D grid, by a *redistribution* process (however, only working from the RGI's date onward). This new function could be adopted within the coupling, by replacing the conversion from "1.5D" to 2D geometries, but only when performing future simulations.
2. **Initialization of OGGM:**
  - The initialization of the model with a dynamic spinup is restricted to approximately 30 years in the past. For simulations starting earlier back in time, another method has to be chosen (e.g. the method developed by Eis et al., 2019). Additionally, a new feature of OGGM allows to calibrate the parameter *melt\_f* simultaneously when performing a dynamic spinup, hence considering a changing glacier geometry (and not a fixed one, as it is assumed during the default calibration of this parameter) (OGGM, 28/08/2023).
  - Even though for the Gepatschalm study case rather low uncertainties were obtained from the model initialization, other study cases could yield higher uncertainties. However, additional constraints may reduce these uncertainties. For example, instead of only minimizing the error between simulated and observed RGI's areas (in the year 2003), observed areas in another year (e.g. the observed areas during the year 1969 could be used for the case of Austrian glaciers) could be considered.
  - In this coupling scheme, the choice of working with the RGI was made in order to leave OGGM's settings with their defaults, whenever possible. This aims to increase the applicability of the model to any catchment, since the RGI covers all glaciers in the world. However, in some cases (like in Gepatschalm), other observed outlines are available, which might be more suitable. These datasets

can be adapted accordingly (i.e. the dataset should contain the same attributes as the RGI) and OGGM could be initialized with the given glacier outline, thus evading the need of a dynamic spinup or any other initialization method.

- During the initialization period (e.g. dynamic spinup), when the glaciers were normally larger than today, the model attempts to grow the glacier so that after the spinup is finished, it has the same area (or volume) as today, for the given past climatic conditions. However, this expansion of the glacier can only take place along the flowlines, due to the nature of OGGM. This can result in exaggerated terminus (or tongues), like for some of the glaciers in the Gepatschalm catchment.
- Glaciers that existed and melted completely before the RGI's date are not included in the simulations, since OGGM is not yet able to "create" glaciers in the past. This can result in an underestimation of the total glacier area. This issue combined with the limitation mentioned before, do not intervene when performing future simulations, since they usually start after the RGI's date (for instance, after the year 2010) and no initialization method is further required.

### 3. Glacier mass balance:

- The glacier mass balance calculated by OGGM is not directly transferred to WaSiM in the last step of the coupling scheme. This could have been achieved by modifying WaSiM's code, so that the model reads the results from OGGM and avoids internal calculations. However, this was not adopted because: (i) this could work for the current version of WaSiM, but the continuous update on the models' versions may lead to incompatibilities if another version is then used; (ii) WaSiM was chosen as the hydrological model, but the developed coupling scheme may serve as a basis for coupling OGGM with any other similar hydrological model; (iii) OGGM provides monthly or annual mass balances, whereas WaSiM is able to produce daily outputs. Regarding this latter point, the OGGM community is working towards producing daily outputs as well. Hence, another possibility might be to include daily mass balances into the coupling scheme (OGGM, 23/10/2023; Schuster et al., 2023).
- WaSiM relies on a more detailed representation of snow accumulation processes (with gravitational slides and wind redistribution), whereas OGGM accounts for avalanches and wind-blown snow just under the precipitation factor. Nevertheless, in this coupling scheme it is ensured that both models are driven with the same precipitation (and temperature) data to perform similarly to an *online* coupling.
- Currently, the melting of glacierized areas does not account for radiation. WaSiM already offers the possibility to include this variable into its calculations, so it would be interesting to extend the T-index method in OGGM to also include this variable. By doing so, a compatibility between both models can be ensured when calculating melting from glaciers considering radiation.
- Even though WaSiM is already capable of determining snow melt from glaciers based on an energy balance approach, firn and ice are still handled differently (with the T-index method). Further research should be carried out to extend the energy balance to firn and ice states as well, so melting from glaciers can be

determined equally with this approach, like for example the model AMUNDSEN (Hanzer et al., 2016). Moreover, OGGM still relies on the T-index method, so additional developments on an energy balance approach to account for glacier melt are also encouraged. In this context, however, one of the latest developments allows the inclusion of the standalone model PyGEM (Rounce et al., 2020a) into OGGM, which considers refreezing as an additional component of the mass balance. The adoption of an energy balance approach to describe ablation processes could potentially improve model simulations and the accuracy of glacier evolution estimations.

- In WaSiM, snow is modeled considering only one single layer to form the snow-pack. The possibility of integrating a layered-snow model might, however, improve simulation results, as explained in Section 7.1.2
4. **Glacier runoff:** Within this coupling scheme, the runoff from the glacierized areas is calculated with the hydrological model WaSiM. Latest developments on OGGM enable to produce monthly hydrological outputs which could be used as feedback between models in the coupling. This may be an alternative to the integration of the OGGM's glaciers area and ice thickness into WaSiM, hence only glacier runoff is used as input for the third run of the coupling scheme. However, the outcomes of the coupling scheme will then be limited to a monthly time step. As mentioned before, though, current research on producing daily outputs of glacier mass balance could potentially overcome this problem and allow for simulations at a daily time step.
  5. **Optimization of the coupling scheme:** In this study, the SCE-UA algorithm was selected for optimizing the model parameters as it is one of the most used algorithms in the field of hydrology. But it can be changed and adapted to any modeler's need, since the coupling scheme is open-source and SPOTPY is a pretty flexible tool. For example, if uncertainty is to be inferred together with the optimum value of the parameters, the Markov Chain Monte Carlo version of the Differential Evolution algorithm could be used (DE-MC, Braak, 2006). Similarly, the multi-objective function and its weights might be changed. For example, if snow measurements are available during the considered optimization period, it would be meaningful to include this variable as well.
  6. **Uncertainties:** In this thesis, the uncertainties associated with the initialization of the glacier model and model parameters of the coupling scheme were examined. On the one hand, uncertainties related to model initialization are relatively low for the case of Gepatschalm, as the values are in the same order of magnitude as the inherent uncertainty in observed glacier outlines. On the other hand, uncertainties concerning model parameters were investigated in terms of their stability across various simulation periods, which suggested that the parameters are quite stable. However, such uncertainties may potentially increase in other study cases, or there may be additional sources of uncertainty that need to be examined. These could be related to the models' structure or the input data, such as the climate data. Especially when predicting the future response of glacierized catchments, emission scenarios can introduce the primary source of uncertainty (Marzeion et al., 2020). Therefore, further research should be conducted to understand other sources of uncertainty and how they affect simulation results.



Overall, the developed WaSiM-OGGM coupling scheme can be considered as a valuable and versatile tool for predicting the hydrological response of glacierized catchments with low or even no available glacier observations. Compared to other existing (*offline*) coupled models, the WaSiM-OGGM coupling scheme shows more consistency in terms of feedback between the independent models, since both of them, WaSiM and OGGM, are driven with the same input climate dataset. Additionally, it goes beyond the common procedure in which only one variable (output) is transferred from one model to the other (usually glacier areas or glacier runoff, e.g. Khadka et al., 2020; Stoll et al., 2020; Wiersma et al., 2022), as not only glacier areas but also the ice thickness distribution and glacier mass balances are foreseen as feedback between models.

The proposed future research might help to facilitate and hopefully improve the applicability of the coupling scheme in other case studies. Since the coupling scheme is available as open-source, it could be used and adapted to any other catchment, even by choosing other optimization algorithms and objective functions. This coupling scheme might serve as a basis for further developments in the field, and to raise awareness among hydrological modelers about the need to include glacier dynamics when predicting the catchment's hydrological response. Finally, the WaSiM-OGGM coupling scheme and the findings presented in this thesis might represent a modest contribution to the possible solutions for the current problems in hydrology and the effective management of water resources in face of a changing climate.



# GitHub Repository and code availability

The WaSiM-OGGM coupling scheme was entirely developed based on freely available models. On the one hand, the WaSiM Richards version 10.06.04 for Windows, and on the other hand, the OGGM version 1.6 for Linux were adopted. The coupling of the models was performed 100% in the Python programming language and the code is available as open-source in the GitHub repository mariapesci/WaSiM-OGGM (Figure 8.1, Pesci, 2023). For further uses of the coupling scheme with other model versions, an update of the code might be required. Moreover, this is an *offline* coupling, so the feedback between both models is not continuously and automatically done during the model simulations. This expects a reasonable level of interaction with the user.

The theory behind the coupling scheme was described in Chapter 6 and the results of its applicability to the Gepatschalm study case were presented in Chapter 7, where also the application to the neighboring Rofenache catchment was shown. The repository leans on several scripts containing different steps for reading input data, converting them into required formats and finally running the models, including the optimization of the coupling itself.

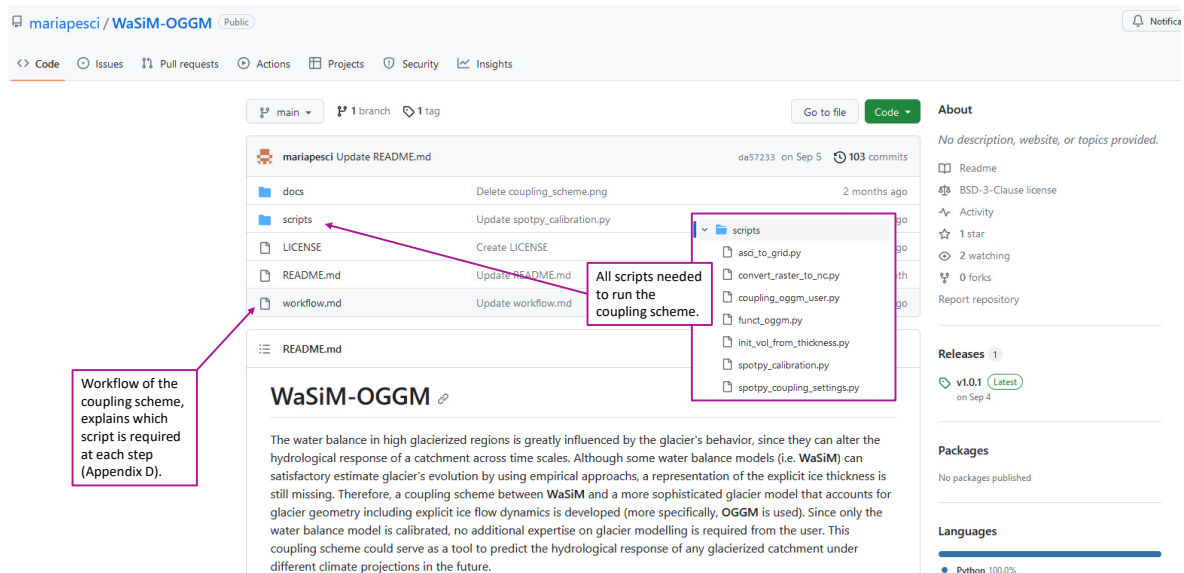


Figure 8.1: Screenshot of the GitHub repository with a few explanations (Pesci, 2023).

Appendix D includes a detailed description of the workflow that should be carried out to perform the coupling, with an overview of the needed scripts to achieve it. Moreover, an example of the required inputs and outputs (prepared by the user or produced by the different models) is also included in the Appendix.



## Bibliography

- Abdollahi, K., Bazargan, A., and McKay, G. (2019). "Water Balance Models in Environmental Modeling". In: *Handbook of Environmental Materials Management*. Springer, Cham, pp. 1961–1976. DOI: 10.1007/978-3-319-73645-7\_{\text{underscore}}119. URL: [https://link.springer.com/referenceworkentry/10.1007/978-3-319-73645-7\\_119](https://link.springer.com/referenceworkentry/10.1007/978-3-319-73645-7_119).
- Amt der Tiroler Landesregierung (2019). *DEM*.
- Andermann, C., Longuevergne, L., Bonnet, S., Crave, A., Davy, P., and Gloaguen, R. (2012). "Impact of transient groundwater storage on the discharge of Himalayan rivers". In: *Nature Geoscience* 5.2, pp. 127–132. ISSN: 1752-0894. DOI: 10.1038/ngeo1356.
- AntarcticGlaciers.org (3/07/2023). *Antarctic Glaciers*. URL: <https://www.antarcticglaciers.org/>.
- (22/06/2020). *Moraine formation - AntarcticGlaciers.org*. URL: <https://www.antarcticglaciers.org/glacial-geology/glacial-landforms/glacial-depositional-landforms/moraine-formation/>.
- Arnold, J., Srinivasan, R., Muttiah, R., and Williams, J. (1998). "Large area hydrologic modeling and assessment part I: model development". In: *Journal of the American Water Resources Association* 34.1, pp. 73–89. ISSN: 1093-474X. DOI: 10.1111/j.1752-1688.1998.tb05961.x.
- Bahr, D., Meier, M., and Peckham, S. (1997). "The physical basis of glacier volume-area scaling". In: *Journal of Geophysical Research Atmospheres* 102.B9, pp. 20355–20362. ISSN: 0148-0227. DOI: 10.1029/97JB01696. URL: [https://www.researchgate.net/publication/254890728\\_The\\_Physical\\_Basis\\_of\\_Glacier\\_Volume-Area\\_Scaling](https://www.researchgate.net/publication/254890728_The_Physical_Basis_of_Glacier_Volume-Area_Scaling).
- Bahr, D. B., Pfeffer, W. T., and Kaser, G. (2015). "A review of volume-area scaling of glaciers". In: *Reviews of geophysics (Washington, D.C. : 1985)* 53.1, pp. 95–140. ISSN: 8755-1209. DOI: 10.1002/2014RG000470.
- Barnett, T. P., Adam, J. C., and Lettenmaier, D. P. (2005). "Potential impacts of a warming climate on water availability in snow-dominated regions". In: *Nature* 438.7066, pp. 303–309. ISSN: 1476-4687. DOI: 10.1038/nature04141. URL: <https://www.nature.com/articles/nature04141>.
- Baumgartner, A. and Liebscher, H.-J. (1996). *Lehrbuch der Hydrologie: Quantitative Hydrologie*. 2. Aufl. Vol. Band 1. Lehrbuch der Hydrologie / hrsg. von Hans-Jürgen Liebscher. Stuttgart: Hirt. ISBN: 3443300022.
- Bellock, K., Godber, N., and Kahn, P. (2021). *bellockk/alphashape: v1.3.1 Release*. DOI: 10.5281/ZENODO.4603210.
- Benn, D. I. and Evans, D. J. A. (2010). *Glaciers & glaciation*. 2nd ed. London: Hodder Education. ISBN: 978-0-340-90579-1.
- Berg, P., Bosshard, T., Yang, W., and Zimmermann, K. (2022). *MIdAS—Multi-scale bias Adjustment*. DOI: 10.5194/gmd-2022-6.

- Bergström, S. and Forsman, A. (1973). "Development of a conceptual deterministic rainfall-runoff model". In: *Nord. Hydrol* 4, pp. 240–253.
- Berthier, E., Floriciou, D., Gardner, A. S., Gourmelen, N., Jakob, L., Paul, F., Treichler, D., Wouters, B., Belart, J. M. C., Dehecq, A., Dussaillant, I., Hugonnet, R., Käab, A., Krieger, L., Pálsson, F., and Zemp, M. (2023). "Measuring glacier mass changes from space—a review". In: *Reports on progress in physics. Physical Society (Great Britain)* 86.3. DOI: 10.1088/1361-6633/acaf8e.
- Beven, K. J. (2012). *Rainfall-runoff modelling: The primer / Keith Beven*. 2nd ed. Chichester, West Sussex and Hoboken, NJ: Wiley-Blackwell. ISBN: 978-0-470-71459-1.
- Beven, K. (2006). "A manifesto for the equifinality thesis". In: *Journal of Hydrology* 320.1-2, pp. 18–36. ISSN: 00221694. DOI: 10.1016/j.jhydro.2005.07.007. URL: <https://www.sciencedirect.com/science/article/pii/S002216940500332X>.
- Beven, K. and Binley, A. (2014). "GLUE: 20 years on". In: *Hydrological Processes* 28.24, pp. 5897–5918. ISSN: 08856087. DOI: 10.1002/hyp.10082.
- Beven, K. and Freer, J. (2001). "Equifinality, data assimilation, and uncertainty estimation in mechanistic modelling of complex environmental systems using the GLUE methodology". In: *Journal of Hydrology* 249.1-4, pp. 11–29. ISSN: 00221694. DOI: 10.1016/S0022-1694(01)00421-8. URL: <https://www.sciencedirect.com/science/article/pii/S0022169401004218>.
- Beven, K. and Lamb, R. (2017). "The uncertainty cascade in model fusion". In: *Geological Society, London, Special Publications* 408.1, pp. 255–266. ISSN: 0305-8719. DOI: 10.1144/SP408.3.
- Bindschadler, R., Harrison, W. D., Raymond, C. F., and Crosson, R. (1977). "Geometry and Dynamics of a Surge-type Glacier". In: *Journal of Glaciology* 18.79, pp. 181–194. ISSN: 0022-1430. DOI: 10.3189/S0022143000021298. URL: <https://www.cambridge.org/core/journals/journal-of-glaciology/article/geometry-and-dynamics-of-a-surgetype-glacier/F49B97479F520E215741CA9E10EBD259>.
- Blöschl, G. et al. (2019). "Twenty-three unsolved problems in hydrology (UPH) – a community perspective". In: *Hydrological Sciences Journal* 64.10, pp. 1141–1158. ISSN: 0262-6667. DOI: 10.1080/02626667.2019.1620507.
- BMLRT (2021). *Hydrographisches Jahrbuch von Österreich 2018*. URL: <https://info.bml.gv.at/themen/wasser/wasser-oesterreich/hydrographie/der-weg-zu-den-daten/jahrbuch2018.html>.
- Bolch, T., Duethmann, D., Wortmann, M., Liu, S., and Disse, M. (2022). "Declining glaciers endanger sustainable development of the oases along the Aksu-Tarim River (Central Asia)". In: *International Journal of Sustainable Development & World Ecology* 29.3, pp. 209–218. ISSN: 1350-4509. DOI: 10.1080/13504509.2021.1943723.
- Bonfils, C., Santer, B. D., Pierce, D. W., Hidalgo, H. G., Bala, G., Das, T., Barnett, T. P., Cayan, D. R., Doutriaux, C., Wood, A. W., Mirin, A., and Nozawa, T. (2008). "Detection and Attribution of Temperature Changes in the Mountainous Western United States". In: *Journal of Climate* 21.23, pp. 6404–6424. ISSN: 0894-8755. DOI: 10.1175/2008JCLI2397.1.
- Braak, C. J. F. ter (2006). "A Markov Chain Monte Carlo version of the genetic algorithm Differential Evolution: easy Bayesian computing for real parameter spaces". In: *Statistics and Computing* 16.3, pp. 239–249. ISSN: 0960-3174. DOI: 10.1007/s11222-006-8769-1.

- Braithwaite, R. J. and Raper, S. C. (2002). "Glaciers and their contribution to sea level change". In: *Physics and Chemistry of the Earth, Parts A/B/C* 27.32-34, pp. 1445–1454. ISSN: 14747065. DOI: 10.1016/S1474-7065(02)28020-8.
- Buckel, J. and Otto, J.-C. (2018). *The Austrian Glacier Inventory GI 4 (2015) in ArcGIS (shapefile) format, supplement to: Buckel, Johannes; Otto, Jan-Christoph; Prasicek, Günther; Keuschnig, Markus (2018): Glacial lakes in Austria - Distribution and formation since the Little Ice Age. Global and Planetary Change, 164, 39-51.* DOI: 10.1594/PANGAEA.887415.
- Bundesministerium Land- und Forstwirtschaft, Regionen und Wasserwirtschaft (2023). *eHYD – der Zugang zu hydrographischen Daten Österreichs*. URL: <https://ehyd.gv.at/>.
- Chen, J. and Ohmura, A. (1990a). "Estimation of Alpine glacier water resources and their changes since the 1870s". In: vol. 193. IAHS.
- (1990b). "On the influence of Alpine glaciers on runoff". In: vol. 193. IAHS.
- Chen, X., Di Long, Hong, Y., Zeng, C., and Yan, D. (2017a). "Improved modeling of snow and glacier melting by a progressive two-stage calibration strategy with GRACE and multisource data: How snow and glacier meltwater contributes to the runoff of the Upper Brahmaputra River basin?" In: *Water Resources Research* 53.3, pp. 2431–2466. ISSN: 1944-7973. DOI: 10.1002/2016WR019656.
- Chen, Y., Li, W., Fang, G., and Li, Z. (2017b). "Review article: Hydrological modeling in glacierized catchments of central Asia – status and challenges". In: *Hydrology and Earth System Sciences* 21.2, pp. 669–684. DOI: 10.5194/hess-21-669-2017.
- Church, J. A., Gregory, J. M., Huybrechts, P., Kuhn, M., Lambeck, K., Nhuan, M. T., Qin, D., and Woodworth, P. L. (2001). "Changes in sea level". In: *Climate change 2001: the scientific basis*. Ed. by Intergovernmental Panel on Climate Change. Cambridge: Cambridge University Press, pp. 641–684. ISBN: 0521 80767 0.
- Clason, C., Rangecroft, S., Owens, P. N., Łokas, E., Baccolo, G., Selmes, N., Beard, D., Kitch, J., Dextre, R. M., Morera, S., and Blake, W. (2022). "Contribution of glaciers to water, energy and food security in mountain regions: current perspectives and future priorities". In: *Annals of Glaciology* 63.87-89, pp. 73–78. ISSN: 0260-3055. DOI: 10.1017/aog.2023.14. URL: <https://www.cambridge.org/core/journals/annals-of-glaciology/article/contribution-of-glaciers-to-water-energy-and-food-security-in-mountain-regions-current-perspectives-and-future-priorities/2D6CB36C24CC5F26F9A9FEE789D119AF>.
- Cochand, M., Christe, P., Ornstein, P., and Hunkeler, D. (2019). "Groundwater Storage in High Alpine Catchments and Its Contribution to Streamflow". In: *Water Resources Research* 55.4, pp. 2613–2630. ISSN: 1944-7973. DOI: 10.1029/2018WR022989.
- Cogley, J. G., Hock, R., Rasmussen, B., Arendt, A., Bauder, A., Braithwaite, R. J., Jansson, P., Kaser, G., Moller, M., Nicholson, L., and Zemp, M. (2011). *Glossary of glacier mass balance and related terms*. Vol. 2. Paris.
- Compagno, L., Eggs, S., Huss, M., Zekollari, H., and Farinotti, D. (2021). "Brief communication: Do 1.0, 1.5, or 2.0 °C matter for the future evolution of Alpine glaciers?" In: *The Cryosphere* 15.6, pp. 2593–2599. DOI: 10.5194/tc-15-2593-2021.
- Cuffey, K. M. and Paterson, W. S. B. (2010). *The physics of glaciers*. 4th rev. ed. Amsterdam and London: Butterworth-Heinemann. ISBN: 978-0-12-369461-4.
- Devak, M. and Dhanya, C. T. (2017). "Sensitivity analysis of hydrological models: review and way forward". In: *Journal of Water and Climate Change* 8.4, pp. 557–575. ISSN: 2040-2244. DOI: 10.2166/wcc.2017.149.

- Duan, Q., Sorooshian, S., and Gupta, V. (1992). "Effective and efficient global optimization for conceptual rainfall-runoff models". In: *Water Resources Research* 28.4, pp. 1015–1031. ISSN: 00431397. DOI: 10.1029/91WR02985.
- Duan, Q., Sorooshian, S., and Gupta, V. K. (1994). "Optimal use of the SCE-UA global optimization method for calibrating watershed models". In: *Journal of Hydrology* 158.3-4, pp. 265–284. ISSN: 00221694. DOI: 10.1016/0022-1694(94)90057-4. URL: <http://www.sciencedirect.com/science/article/pii/0022169494900574>.
- Duethmann, D., Menz, C., Jiang, T., and Vorogushyn, S. (2016). "Projections for headwater catchments of the Tarim River reveal glacier retreat and decreasing surface water availability but uncertainties are large". In: *Environmental Research Letters* 11.5, p. 054024. DOI: 10.1088/1748-9326/11/5/054024.
- Eis, J., Maussion, F., and Marzeion, B. (2019). "Initialization of a global glacier model based on present-day glacier geometry and past climate information: an ensemble approach". In: *The Cryosphere* 13.12, pp. 3317–3335. DOI: 10.5194/tc-13-3317-2019.
- Eis, J., van der Laan, L., Maussion, F., and Marzeion, B. (2021). "Reconstruction of Past Glacier Changes with an Ice-Flow Glacier Model: Proof of Concept and Validation". In: *Frontiers in Earth Science* 9. DOI: 10.3389/feart.2021.595755.
- Encyclopedia Britannica (20/10/2023). *Sedimentary rock - Evaporites, Deposits, Minerals*. URL: <https://www.britannica.com/science/sedimentary-rock/Evaporites>.
- European Commission (2015). *Guidance document on the application of water balances for supporting the implementation of the WFD: Final : version 6.1-18/05/2015*. Vol. 2015, 090. Technical Report. Luxembourg: Publications Office. ISBN: 978-92-79-52021-1.
- European Environment Agency (2019). *Corine Land Cover (CLC) 2018, Version 20*. URL: <https://land.copernicus.eu/pan-european/corine-land-cover/clc2018>.
- (2020). *Copernicus High Resolution Snow and Ice Monitoring: Fractional Snow Cover (FSC) 20 m*. DOI: 10.2909/3e2b4b7b-a460-41dd-a373-962d032795f3. URL: <https://land.copernicus.eu/pan-european/biophysical-parameters/high-resolution-snow-and-ice-monitoring>.
- Eyring, V., Bony, S., Meehl, G. A., Senior, C. A., Stevens, B., Stouffer, R. J., and Taylor, K. E. (2016). "Overview of the Coupled Model Intercomparison Project Phase 6 (CMIP6) experimental design and organization". In: *Geoscientific Model Development* 9.5, pp. 1937–1958. DOI: 10.5194/gmd-9-1937-2016.
- Farinotti, D. and Huss, M. (2013). "An upper-bound estimate for the accuracy of glacier volume–area scaling". In: *The Cryosphere* 7.6, pp. 1707–1720. DOI: 10.5194/tc-7-1707-2013.
- Farinotti, D., Huss, M., Bauder, A., Funk, M., and Truffer, M. (2009). "A method to estimate the ice volume and ice-thickness distribution of alpine glaciers". In: *Journal of Glaciology* 55.191, pp. 422–430. ISSN: 0022-1430. DOI: 10.3189/002214309788816759. URL: <https://www.cambridge.org/core/journals/journal-of-glaciology/article/method-to-estimate-the-ice-volume-and-icethickness-distribution-of-alpine-glaciers/40D2B92744F6512E8DEC142DE6BEA471>.
- Farinotti, D., Usselman, S., Huss, M., Bauder, A., and Funk, M. (2012). "Runoff evolution in the Swiss Alps: projections for selected high–alpine catchments based on ensembles scenarios". In: *Hydrological Processes* 26.13, pp. 1909–1924. ISSN: 08856087. DOI: 10.1002/hyp.8276.
- Fischer, A. (2010). *Comparison of direct and geodetic mass balances on a multi-annual time scale*. DOI: 10.5194/tcd-4-1151-2010.



- (2011). “Comparison of direct and geodetic mass balances on a multi-annual time scale”. In: *The Cryosphere* 5.1, pp. 107–124. DOI: 10.5194/tc-5-107-2011.
- Fischer, A., Seiser, B., Stocker-Waldhuber, M., Mitterer, C., and Abermann, J. (2015a). “Tracing glacier changes in Austria from the Little Ice Age to the present using a lidar-based high-resolution glacier inventory in Austria”. In: *The Cryosphere* 9.2, pp. 753–766. DOI: 10.5194/tc-9-753-2015.
- Fischer, A. and Kuhn, M. (2013). “Ground-penetrating radar measurements of 64 Austrian glaciers between 1995 and 2010”. In: *Annals of Glaciology* 54.64, pp. 179–188. ISSN: 0260-3055. DOI: 10.3189/2013AoG64A108. URL: <https://www.cambridge.org/core/journals/annals-of-glaciology/article/groundpenetrating-radar-measurements-of-64-austrian-glaciers-between-1995-and-2010/27F001E11BA6AC163A3D31F5C1448853>.
- Fischer, A., Seiser, B., Stocker-Waldhuber, M., and Abermann, J. (2015b). *The Austrian Glacier Inventory GI 3, 2006, in ArcGIS (shapefile) format*. DOI: 10.1594/PANGAEA.844985.
- Fischer, A., Seiser, B., Stocker-Waldhuber, M., Mitterer, C., and Abermann, J. (2015c). *The Austrian Glacier Inventories GI 1 (1969), GI 2 (1998), GI 3 (2006), and GI LIA in ArcGIS (shapefile) format, supplement to: Fischer, Andrea; Seiser, Bernd; Stocker-Waldhuber, Martin; Mitterer, Christian; Abermann, Jakob (2015): Tracing glacier changes in Austria from the Little Ice Age to the present using a lidar-based high-resolution glacier inventory in Austria. The Cryosphere, 9(2), 753-766*. DOI: 10.1594/PANGAEA.844988.
- Fischer, A., Span, N., Kuhn, M., Helfricht, K., Stocker-Waldhuber, M., Seiser, B., Massimo, M., and Butschek, M. (2015d). *Ground-penetrating radar (GPR) point measurements of ice thickness in Austria*. DOI: 10.1594/PANGAEA.849497.
- Förster, K. (2013). “Detaillierte Nachbildung von Schneeprozessen in der hydrologischen Modellierung”. Dissertation. Technischen Universität Carolo-Wilhelmina Braunschweig. URL: [https://leopard.tu-braunschweig.de/servlets/MCRFileNodeServlet/dbbs\\_derivate\\_00031181/diss\\_kf.pdf](https://leopard.tu-braunschweig.de/servlets/MCRFileNodeServlet/dbbs_derivate_00031181/diss_kf.pdf).
- Förster, K., Meon, G., Marke, T., and Strasser, U. (2014). “Effect of meteorological forcing and snow model complexity on hydrological simulations in the Sieber catchment (Harz Mountains, Germany)”. In: *Hydrology and Earth System Sciences* 18.11, pp. 4703–4720. DOI: 10.5194/hess-18-4703-2014.
- Förster, K., Garvelmann, J., Meißl, G., and Strasser, U. (2018). “Modelling forest snow processes with a new version of WaSiM”. In: *Hydrological Sciences Journal* 63.10, pp. 1540–1557. ISSN: 0262-6667. DOI: 10.1080/02626667.2018.1518626.
- Förster, K., Oesterle, F., Hanzer, F., Schöber, J., Huttenlau, M., and Strasser, U. (2016). “A snow and ice melt seasonal prediction modelling system for Alpine reservoirs”. In: *Proceedings of the International Association of Hydrological Sciences* 374, pp. 143–150. DOI: 10.5194/piahs-374-143-2016.
- Freudiger, D., Kohn, I., Seibert, J., Stahl, K., and Weiler, M. (2017). “Snow redistribution for the hydrological modeling of alpine catchments”. In: *WIREs Water* 4.5. ISSN: 2049-1948. DOI: 10.1002/wat2.1232.
- Gardner, A. S., Moholdt, G., Cogley, J. G., Wouters, B., Arendt, A. A., Wahr, J., Berthier, E., Hock, R., Pfeffer, W. T., Kaser, G., Ligtenberg, S. R. M., Bolch, T., Sharp, M. J., Hagen, J. O., van den Broeke, M. R., and Paul, F. (2013). “A reconciled estimate of glacier contributions to sea level rise: 2003 to 2009”. In: *Science (New York, N.Y.)* 340.6134, pp. 852–857. DOI: 10.1126/science.1234532.

- Gelleszun, M., Kreye, P., and Meon, G. (2017). "Representative parameter estimation for hydrological models using a lexicographic calibration strategy". In: *Journal of Hydrology* 553, pp. 722–734. ISSN: 00221694. DOI: 10.1016/j.jhydrol.2017.08.015.
- Goodison, B. E., Louie, P., and Yang, D. (1998). *WMO solid precipitation measurement intercomparison: Tech. Rep. WMO/TD 872*. Geneva. URL: <https://library.wmo.int/idurl/4/28336>.
- Grinsted, A. (2013). "An estimate of global glacier volume". In: *The Cryosphere* 7.1, pp. 141–151. DOI: 10.5194/tc-7-141-2013.
- Groh, T. and Blöthe, J. H. (2019). "Rock Glacier Kinematics in the Kaunertal, Ötztal Alps, Austria". In: *Geosciences* 9.9, p. 373. DOI: 10.3390/geosciences9090373.
- Gruber, S. (2007). "A mass-conserving fast algorithm to parameterize gravitational transport and deposition using digital elevation models". In: *Water Resources Research* 43.6. ISSN: 00431397. DOI: 10.1029/2006WR004868.
- Gupta, H. V., Beven, K. J., and Wagener, T. (2005). "Model Calibration and Uncertainty Estimation". In: *Encyclopedia of hydrological sciences*. Ed. by M. G. Anderson. Chichester: Wiley. ISBN: 9780471491033. DOI: 10.1002/0470848944.hsa138.
- Gupta, H. V., Kling, H., Yilmaz, K. K., and Martinez, G. F. (2009). "Decomposition of the mean squared error and NSE performance criteria: Implications for improving hydrological modelling". In: *Journal of Hydrology* 377.1-2, pp. 80–91. ISSN: 00221694. DOI: 10.1016/j.jhydrol.2009.08.003.
- Gupta, H. V., Sorooshian, S., and Yapo, P. O. (1998). "Toward improved calibration of hydrologic models: Multiple and noncommensurable measures of information". In: *Water Resources Research* 34.4, pp. 751–763. ISSN: 00431397. DOI: 10.1029/97WR03495.
- Hagg, W. J., Braun, L. N., Uvarov, V. N., and Makarevich, K. G. (2004). "A comparison of three methods of mass-balance determination in the Tuyuksu glacier region, Tien Shan, Central Asia". In: *Journal of Glaciology* 50.171, pp. 505–510. ISSN: 0022-1430. DOI: 10.3189/172756504781829783.
- Haggreén, H., Mayer, C., Nuikka, M., Braun, L., Rentsch, H., and Peipe, J. (2007). "Processing of old terrestrial photography for verifying the 1907 digital elevation model of Hochjochferner glacier". In: *Zeitschrift für Gletscherkunde und Glazialgeologie* 41, pp. 29–53.
- Haiden, T., Kann, A., Wittmann, C., Pistotnik, G., Bica, B., and Gruber, C. (2011). "The Integrated Nowcasting through Comprehensive Analysis (INCA) System and Its Validation over the Eastern Alpine Region". In: *Weather and Forecasting* 26.2, pp. 166–183. ISSN: 0882-8156. DOI: 10.1175/2010WAF2222451.1.
- Hanzer, F., Förster, K., Nemeč, J., and Strasser, U. (2018). "Projected cryospheric and hydrological impacts of 21st century climate change in the Ötztal Alps (Austria) simulated using a physically based approach". In: *Hydrology and Earth System Sciences* 22.2, pp. 1593–1614. DOI: 10.5194/hess-22-1593-2018.
- Hanzer, F., Helfricht, K., Marke, T., and Strasser, U. (2016). "Multilevel spatiotemporal validation of snow/ice mass balance and runoff modeling in glacierized catchments". In: *The Cryosphere* 10.4, pp. 1859–1881. DOI: 10.5194/tc-10-1859-2016.
- Healy, R. W. and Scanlon, B. R. (2018). *Estimating groundwater recharge*. 1st ed. Cambridge: Cambridge University Press. ISBN: 9780511780745. DOI: 10.1017/cbo9780511780745.
- Hock, R., Rasul, G., Adler, C., Cáceres, B., Gruber, S., Hirabayashi, Y., Jackson, M., Kääh, A., Kang, J., Kutuzov, S., Milner, A., Molau, U., Morin, S., Orlove, B., and Steltzer, H. (2019). "High Mountain Areas: Special Report on the Ocean and Cryosphere in a

- Changing Climate". In: *Ocean and Cryosphere in a changing climate*. Ed. by I. P. O. C. C. (IPCC). [Place of publication not identified]: CAMBRIDGE UNIV Press, pp. 131–202. ISBN: 9781009157964. DOI: 10.1017/9781009157964.004.
- Hock, R. (1999). "A distributed temperature-index ice- and snowmelt model including potential direct solar radiation". In: *Journal of Glaciology* 45.149, pp. 101–111. ISSN: 0022-1430. DOI: 10.3189/S0022143000003087.
- Hofmeister, F., Arias-Rodriguez, L. F., Premier, V., Marin, C., Notarnicola, C., Disse, M., and Chiogna, G. (2022). "Intercomparison of Sentinel-2 and modelled snow cover maps in a high-elevation Alpine catchment". In: *Journal of Hydrology X* 15, p. 100123. ISSN: 2589-9155. DOI: 10.1016/j.hydroa.2022.100123. URL: <https://www.sciencedirect.com/science/article/pii/S2589915522000050>.
- Hofmeister, F., Graziano, F., Marcolini, G., Willems, W., Disse, M., and Chiogna, G. (2023). "Quality assessment of hydrometeorological observational data and their influence on hydrological model results in Alpine catchments". In: *Hydrological Sciences Journal* 68.4, pp. 552–571. ISSN: 0262-6667. DOI: 10.1080/02626667.2023.2172335.
- Hooke, R. L. (2020). *Principles of glacier mechanics*. Third edition. Cambridge: Cambridge University Press. ISBN: 978-1-108-42734-0.
- Houska, T., Kraft, P., Chamorro-Chavez, A., and Breuer, L. (2015). "SPOTting Model Parameters Using a Ready-Made Python Package". In: *PLOS ONE* 10.12, e0145180. DOI: 10.1371/journal.pone.0145180.
- Hugonnet, R., McNabb, R., Berthier, E., Menounos, B., Nuth, C., Girod, L., Farinotti, D., Huss, M., Dussailant, I., Brun, F., and Käab, A. (2021). "Accelerated global glacier mass loss in the early twenty-first century". In: *Nature* 592.7856, pp. 726–731. DOI: 10.1038/s41586-021-03436-z.
- Huss, M., Juvet, G., Farinotti, D., and Bauder, A. (2010). "Future high-mountain hydrology: a new parameterization of glacier retreat". In: *Hydrology and Earth System Sciences* 14.5, pp. 815–829. DOI: 10.5194/hess-14-815-2010.
- Huss, M. and Farinotti, D. (2012). "Distributed ice thickness and volume of all glaciers around the globe". In: *Journal of Geophysical Research: Atmospheres* 117.F4, n/a–n/a. ISSN: 01480227. DOI: 10.1029/2012JF002523.
- Huss, M., Farinotti, D., Bauder, A., and Funk, M. (2008). "Modelling runoff from highly glacierized alpine drainage basins in a changing climate". In: *Hydrological Processes* 22.19, pp. 3888–3902. ISSN: 08856087. DOI: 10.1002/hyp.7055.
- Huss, M. and Hock, R. (2015). "A new model for global glacier change and sea-level rise". In: *Frontiers in Earth Science* 3. DOI: 10.3389/feart.2015.00054.
- (2018). "Global-scale hydrological response to future glacier mass loss". In: *Nature Climate Change* 8.2, pp. 135–140. ISSN: 1758-678X. DOI: 10.1038/s41558-017-0049-x.
- Hutter, K. (1983). *Theoretical Glaciology*. Dordrecht: Springer Netherlands. ISBN: 978-94-015-1169-8. DOI: 10.1007/978-94-015-1167-4.
- Immerzeel, W. W. et al. (2020). "Importance and vulnerability of the world's water towers". In: *Nature* 577.7790, pp. 364–369. ISSN: 1476-4687. DOI: 10.1038/s41586-019-1822-y. URL: <https://www.nature.com/articles/s41586-019-1822-y>.
- Immerzeel, W. W., van Beek, L. P. H., Konz, M., Shrestha, A. B., and Bierkens, M. F. P. (2012). "Hydrological response to climate change in a glacierized catchment in the Himalayas". In: *Climatic change* 110.3-4, pp. 721–736. ISSN: 0165-0009. DOI: 10.1007/s10584-011-0143-4.

- Intergovernmental Panel on Climate Change (2023). "Ocean, Cryosphere and Sea Level Change". In: *Climate Change 2021 – The Physical Science Basis: Working Group I Contribution to the Sixth Assessment Report of the Intergovernmental Panel on Climate Change*. Cambridge University Press, pp. 1211–1362. DOI: 10.1017/9781009157896.011. URL: <https://www.cambridge.org/core/books/climate-change-2021-the-physical-science-basis/ocean-cryosphere-and-sea-level-change/F61263910A16BD9FDE86921E85E1E4D5>.
- Jacob, D. et al. (2014). "EURO-CORDEX: new high-resolution climate change projections for European impact research". In: *Regional Environmental Change* 14.2, pp. 563–578. ISSN: 1436-3798. DOI: 10.1007/s10113-013-0499-2.
- Jansson, P., Hock, R., and Schneider, T. (2003). "The concept of glacier storage: a review". In: *Journal of Hydrology* 282.1-4, pp. 116–129. ISSN: 00221694. DOI: 10.1016/S0022-1694(03)00258-0. URL: <https://www.sciencedirect.com/science/article/pii/S0022169403002580>.
- Jonas, T., Marty, C., and Magnusson, J. (2009). "Estimating the snow water equivalent from snow depth measurements in the Swiss Alps". In: *Journal of Hydrology* 378.1-2, pp. 161–167. ISSN: 00221694. DOI: 10.1016/j.jhydro1.2009.09.021.
- Kalcic, M., I. Chaubey, and J. Frankenberger, eds. (2015). *Defining Soil and Water Assessment Tool (SWAT) hydrologic response units (HRUs) by field boundaries*. Vol. 8, pp. 69–80.
- Kaser, G., Cogley, J. G., Dyurgerov, M. B., Meier, M. F., and Ohmura, A. (2006). "Mass balance of glaciers and ice caps: Consensus estimates for 1961–2004". In: *Geophysical Research Letters* 33.19. ISSN: 0094-8276. DOI: 10.1029/2006GL027511.
- Kaser, G., Grosshauser, M., and Marzeion, B. (2010). "Contribution potential of glaciers to water availability in different climate regimes". In: *Proceedings of the National Academy of Sciences of the United States of America* 107.47, pp. 20223–20227. DOI: 10.1073/pnas.1008162107.
- Khadka, M., Kayastha, R. B., and Kayastha, R. (2020). "Future projection of cryospheric and hydrologic regimes in Koshi River basin, Central Himalaya, using coupled glacier dynamics and glacio-hydrological models". In: *Journal of Glaciology* 66.259, pp. 831–845. ISSN: 0022-1430. DOI: 10.1017/jog.2020.51.
- Kienholz, C., Rich, J. L., Arendt, A. A., and Hock, R. (2014). "A new method for deriving glacier centerlines applied to glaciers in Alaska and northwest Canada". In: *The Cryosphere* 8.2, pp. 503–519. DOI: 10.5194/tc-8-503-2014.
- Killingtveit, Å., Petterson, L.-E., and Sand, K. (2003). "Water balance investigations in Svalbard". In: *Polar Research* 22.2, pp. 161–174. ISSN: 0800-0395. DOI: 10.1111/j.1751-8369.2003.tb00105.x.
- Kim, K. B., Kwon, H.-H., and Han, D. (2018). "Exploration of warm-up period in conceptual hydrological modelling". In: *Journal of Hydrology* 556, pp. 197–210. ISSN: 00221694. DOI: 10.1016/j.jhydro1.2017.11.015. URL: [https://research-information.bris.ac.uk/files/135959620/Exploration\\_of\\_warm\\_up\\_period\\_in\\_conceptual\\_hydrological\\_modelling.pdf](https://research-information.bris.ac.uk/files/135959620/Exploration_of_warm_up_period_in_conceptual_hydrological_modelling.pdf).
- Kingston, D. G., Thompson, J. R., and Kite, G. (2011). "Uncertainty in climate change projections of discharge for the Mekong River Basin". In: *Hydrology and Earth System Sciences* 15.5, pp. 1459–1471. DOI: 10.5194/hess-15-1459-2011.
- Klemeš, V. (1986). "Operational testing of hydrological simulation models". In: *Hydrological Sciences Journal* 31.1, pp. 13–24. ISSN: 0262-6667. DOI: 10.1080/02626668609491024. URL: <https://www.tandfonline.com/doi/pdf/10.1080/02626668609491024>.

- Klok, E. J., Jasper, K., Roelofsma, K. P., Gurtz, J., and Badoux, A. (2001). "Distributed hydrological modelling of a heavily glaciated Alpine river basin". In: *Hydrological Sciences Journal* 46.4, pp. 553–570. ISSN: 0262-6667. DOI: 10.1080/02626660109492850.
- Klok, E. J. and Oerlemans, J. (2002). "Model study of the spatial distribution of the energy and mass balance of Morteratschgletscher, Switzerland". In: *Journal of Glaciology* 48.163, pp. 505–518. ISSN: 0022-1430. DOI: 10.3189/172756502781831133. URL: <https://www.cambridge.org/core/journals/journal-of-glaciology/article/model-study-of-the-spatial-distribution-of-the-energy-and-mass-balance-of-morteratschgletscher-switzerland/4F4C0CA013582E1EF9470E4A7FC9CDD9>.
- Knoben, W. J. M., Freer, J. E., and Woods, R. A. (2019). "Technical note: Inherent benchmark or not? Comparing Nash–Sutcliffe and Kling–Gupta efficiency scores". In: *Hydrology and Earth System Sciences* 23.10, pp. 4323–4331. DOI: 10.5194/hess-23-4323-2019.
- Koboltschnig, G. R. and Schöner, W. (2011). "The relevance of glacier melt in the water cycle of the Alps: the example of Austria". In: *Hydrology and Earth System Sciences* 15.6, pp. 2039–2048. DOI: 10.5194/hess-15-2039-2011.
- Konz, M. and Seibert, J. (2010). "On the value of glacier mass balances for hydrological model calibration". In: *Journal of Hydrology* 385.1-4, pp. 238–246. ISSN: 00221694. DOI: 10.1016/j.jhydrol.2010.02.025. URL: <https://www.sciencedirect.com/science/article/pii/S0022169410000958>.
- Kormann, C., Bronstert, A., Francke, T., Recknagel, T., and Graeff, T. (2016). "Model-Based Attribution of High-Resolution Streamflow Trends in Two Alpine Basins of Western Austria". In: *Hydrology* 3.1, p. 7. DOI: 10.3390/hydrology3010007.
- Krampe, D., Arndt, A., and Schneider, C. (2022). "Energy and glacier mass balance of Fúrkeleferner, Italy: past, present, and future". In: *Frontiers in Earth Science* 10. DOI: 10.3389/feart.2022.814027.
- Kruss, P. and Smith, J. (1982). "Numerical modelling of the Vernagtferner and its fluctuations". In: *Zeitschrift für Gletscherkunde und Glazialgeologie* 1.18, pp. 93–106.
- Kuhn, M., Lambrecht, A., and Abermann, J. (2013). *Austrian glacier inventory 1998 (GI II)*. DOI: 10.1594/PANGAEA.809196.
- Lall, U. and Sharma, A. (1996). "A Nearest Neighbor Bootstrap For Resampling Hydrologic Time Series". In: *Water Resources Research* 32.3, pp. 679–693. ISSN: 00431397. DOI: 10.1029/95WR02966.
- Lambrecht, A. and Kuhn, M. (2007). "Glacier changes in the Austrian Alps during the last three decades, derived from the new Austrian glacier inventory". In: *Annals of Glaciology* 46, pp. 177–184. ISSN: 0260-3055. DOI: 10.3189/172756407782871341.
- Lange, S. (2019). *WFDE5 over land merged with ERA5 over the ocean (W5E5)*. DOI: 10.5880/pik.2019.023.
- Lange, S., Quesada-Chacón, D., and Büchner, M. (2023). *Secondary ISIMIP3b bias-adjusted atmospheric climate input data*. DOI: 10.48364/ISIMIP.581124.2.
- Le Meur, E., Gerbaux, M., Schäfer, M., and Vincent, C. (2007). "Disappearance of an Alpine glacier over the 21st Century simulated from modeling its future surface mass balance". In: *Earth and Planetary Science Letters* 261.3-4, pp. 367–374. ISSN: 0012-821X. DOI: 10.1016/j.epsl.2007.07.022. URL: <https://www.sciencedirect.com/science/article/pii/S0012821X07004372>.
- Lee, H. et al. (2023). *IPCC, 2023: Climate Change 2023: Synthesis Report. Contribution of Working Groups I, II and III to the Sixth Assessment Report of the Intergovernmental*

- Panel on Climate Change [Core Writing Team, H. Lee and J. Romero (eds.)]. IPCC, Geneva, Switzerland. DOI: 10.59327/IPCC/AR6-9789291691647.
- Li, H., Beldring, S., Xu, C.-Y., Huss, M., Melvold, K., and Jain, S. K. (2015). "Integrating a glacier retreat model into a hydrological model – Case studies of three glacierised catchments in Norway and Himalayan region". In: *Journal of Hydrology* 527, pp. 656–667. ISSN: 00221694. DOI: 10.1016/j.jhydro.2015.05.017.
- Liu, H., Tolson, B. A., Newman, A. J., and Wood, A. W. (2021). "Leveraging ensemble meteorological forcing data to improve parameter estimation of hydrologic models". In: *Hydrological Processes* 35.11. ISSN: 08856087. DOI: 10.1002/hyp.14410.
- Liu, Y. and Gupta, H. V. (2007). "Uncertainty in hydrologic modeling: Toward an integrated data assimilation framework". In: *Water Resources Research* 43.7. ISSN: 1944-7973. DOI: 10.1029/2006WR005756.
- Machguth, H., Paul, F., Hoelzle, M., and Haeblerli, W. (2006). "Distributed glacier mass-balance modelling as an important component of modern multi-level glacier monitoring". In: *Annals of Glaciology* 43, pp. 335–343. ISSN: 0260-3055. DOI: 10.3189/172756406781812285. URL: <https://www.cambridge.org/core/journals/annals-of-glaciology/article/distributed-glacier-massbalance-modelling-as-an-important-component-of-modern-multilevel-glacier-monitoring/88B848F3560F0D4FADB9D62F6B4741D5>.
- Mackay, J. D., Barrand, N. E., Hannah, D. M., Krause, S., Jackson, C. R., Everest, J., and Aalgeirsdóttir, G. (2018). "Glacio-hydrological melt and run-off modelling: application of a limits of acceptability framework for model comparison and selection". In: *The Cryosphere* 12.7, pp. 2175–2210. DOI: 10.5194/tc-12-2175-2018.
- Maidment, D. R. (1993). *Handbook of hydrology*. New York: McGraw-Hill. ISBN: 0-07-039732-5.
- Marzeion, B., Cogley, J. G., Richter, K., and Parkes, D. (2014). "Glaciers. Attribution of global glacier mass loss to anthropogenic and natural causes". In: *Science (New York, N.Y.)* 345.6199, pp. 919–921. DOI: 10.1126/science.1254702.
- Marzeion, B., Hock, R., Anderson, B., Bliss, A., Champollion, N., Fujita, K., Huss, M., Immerzeel, W. W., Kraaijenbrink, P., Malles, J.-H., Maussion, F., Radić, V., Rounce, D. R., Sakai, A., Shannon, S., van de Wal, R., and Zekollari, H. (2020). "Partitioning the Uncertainty of Ensemble Projections of Global Glacier Mass Change". In: *Earth's Future* 8.7. ISSN: 2328-4277. DOI: 10.1029/2019EF001470.
- Marzeion, B., Jarosch, A. H., and Hofer, M. (2012). "Past and future sea-level change from the surface mass balance of glaciers". In: *The Cryosphere* 6.6, pp. 1295–1322. DOI: 10.5194/tc-6-1295-2012.
- Maussion, F. (2018). *A (not so) realistic wishlist for the RGI*. URL: <https://oggm.org/2018/12/09/RGI-wishlist/>.
- Maussion, F., Butenko, A., Champollion, N., Dusch, M., Eis, J., Fourteau, K., Gregor, P., Jarosch, A. H., Landmann, J., Oesterle, F., Recinos, B., Rothenpieler, T., Vlug, A., Wild, C. T., and Marzeion, B. (2019). "The Open Global Glacier Model (OGGM) v1.1". In: *Geoscientific Model Development* 12.3, pp. 909–931. DOI: 10.5194/gmd-12-909-2019.
- Maussion, F., Rothenpieler, T., Dusch, M., Schmitt, P., Vlug, A., Schuster, L., Champollion, N., Li, F., Marzeion, B., Oberrauch, M., Eis, J., Landmann, J., Jarosch, A., Alexander, F., Iuzpaz, Hanus, S., Rounce, D., Matteo, C., L., B. S., Samar, M., bowenbelongstonature, Chris, M., Otto, D., David, L., Lizz, U., Schmitt, T., anton-ub, Philipp, G., and zhaohongyu (2023). *OGGM/oggm: v1.6.0*. DOI: 10.5281/ZENODO.7718476.

- McIntyre, N., Wheeler, H., and Lees, M. (2002). "Estimation and propagation of parametric uncertainty in environmental models". In: *Journal of Hydroinformatics* 4.3, pp. 177–198. ISSN: 1464-7141. DOI: 10.2166/hydro.2002.0018.
- Minder, J. R., Mote, P. W., and Lundquist, J. D. (2010). "Surface temperature lapse rates over complex terrain: Lessons from the Cascade Mountains". In: *Journal of Geophysical Research: Atmospheres* 115.D14. ISSN: 01480227. DOI: 10.1029/2009JD013493.
- Moges, E., Demissie, Y., Larsen, L., and Yassin, F. (2021). "Review: Sources of Hydrological Model Uncertainties and Advances in Their Analysis". In: *Water* 13.1, p. 28. DOI: 10.3390/w13010028.
- Mohajerani, H., Zema, D. A., Lucas-Borja, M. E., and Casper, M. (2021). "Chapter 9 - Understanding the water balance and its estimation methods". In: *Precipitation*. Ed. by J. Rodrigo-Comino. Amsterdam: Elsevier, pp. 193–221. ISBN: 978-0-12-822699-5. DOI: 10.1016/B978-0-12-822699-5.00019-7. URL: <https://www.sciencedirect.com/science/article/pii/B9780128226995000197>.
- Moriasi, D. N., Arnold, J. G., van Liew, M. W., Bingner, R. L., Harmel, R. D., and Veith, T. L. (2007). "Model Evaluation Guidelines for Systematic Quantification of Accuracy in Watershed Simulations". In: *Transactions of the ASABE* 50.3, pp. 885–900. DOI: 10.13031/2013.23153.
- Mulvaney, T. J. (1851). *On the use of self-registering rain and flood gauges in making observations of the relations of rainfall and flood discharges in a given catchment*. Ed. by Proceedings of the Institute Civil Engineers. Dublin.
- Muñoz, R., Huggel, C., Drenkhan, F., Vis, M., and Viviroli, D. (2021). "Comparing model complexity for glacio-hydrological simulation in the data-scarce Peruvian Andes". In: *Journal of Hydrology: Regional Studies* 37, p. 100932. ISSN: 2214-5818. DOI: 10.1016/j.ejrh.2021.100932. URL: <https://www.sciencedirect.com/science/article/pii/S2214581821001610>.
- Mutz, S. G. and Aschauer, J. (2022). "Empirical glacier mass-balance models for South America". In: *Journal of Glaciology* 68.271, pp. 1–15. ISSN: 0022-1430. DOI: 10.1017/jog.2022.6. URL: <https://www.cambridge.org/core/journals/journal-of-glaciology/article/empirical-glacier-massbalance-models-for-south-america/5858720EDDF9D02938D728114E408764>.
- NASA JPL (2020). *NASADEM Merged DEM Global 1 arc second V001*. DOI: 10.5067/MEASURES/NASADEM/NASADEM{\textunderscore}HGT.001.
- Nash, J. E. and Sutcliffe, J. V. (1970). "River flow forecasting through conceptual models part I — A discussion of principles". In: *Journal of Hydrology* 10.3, pp. 282–290. ISSN: 00221694. DOI: 10.1016/0022-1694(70)90255-6.
- Naz, B. S., Frans, C. D., Clarke, G. K. C., Burns, P., and Lettenmaier, D. P. (2014). "Modeling the effect of glacier recession on streamflow response using a coupled glacio-hydrological model". In: *Hydrology and Earth System Sciences* 18.2, pp. 787–802. DOI: 10.5194/hess-18-787-2014.
- Oerlemans, J., Anderson, B., Hubbard, A., Huybrechts, P., Jóhannesson, T., Knap, W. H., Schmeits, M., Stroeven, A. P., van de Wal, R. S. W., Wallinga, J., and Zuo, Z. (1998). "Modelling the response of glaciers to climate warming". In: *Climate Dynamics* 14.4, pp. 267–274. ISSN: 1432-0894. DOI: 10.1007/s003820050222. URL: <https://link.springer.com/article/10.1007/s003820050222>.
- Oerlemans, J., Dyurgerov, M., and van de Wal, R. S. W. (2007). "Reconstructing the glacier contribution to sea-level rise back to 1850". In: *The Cryosphere* 1.1, pp. 59–65. DOI: 10.5194/TC-1-59-2007.

- OGGM (2023). *Dynamic spinup*. URL: [https://oggm.org/tutorials/stable/notebooks/advanced/dynamical\\_spinup.html](https://oggm.org/tutorials/stable/notebooks/advanced/dynamical_spinup.html).
- (28/08/2023). *Dynamic spinup and dynamic melt\_f calibration for past simulations — OGGM tutorials*. URL: [https://oggm.org/tutorials/stable/notebooks/advanced/dynamical\\_spinup.html](https://oggm.org/tutorials/stable/notebooks/advanced/dynamical_spinup.html).
- (23/10/2023). *OGGM/massbalance-sandbox: New generation of OGGM mass-balance models*. URL: <https://github.com/OGGM/massbalance-sandbox>.
- Ohmura, A. (2001). “Physical Basis for the Temperature-Based Melt-Index Method”. In: *Journal of Applied Meteorology* 40.4, pp. 753–761. ISSN: 0894-8763. DOI: 10.1175/1520-0450(2001)040<0753:PBFTTB>2.0.CO;2.
- Oke, T. R. (1981). “Canyon geometry and the nocturnal urban heat island: Comparison of scale model and field observations”. In: *Journal of Climatology* 1.3, pp. 237–254. ISSN: 01961748. DOI: 10.1002/joc.3370010304. URL: <https://rmets.onlinelibrary.wiley.com/doi/10.1002/joc.3370010304>.
- (1987). *Boundary layer climates*. 2nd ed. London: Methuen & Co. ISBN: 9781134951345. DOI: 10.4324/9780203407219. URL: <https://bayanbox.ir/view/6693893538424427706/T.-R.-Oke-Boundary-Layer-Climates-Second-Editio-BookFi.org.pdf>.
- Panagos, P., van Liedekerke, M., Jones, A., and Montanarella, L. (2012). “European Soil Data Centre: Response to European policy support and public data requirements”. In: *Land Use Policy* 29.2, pp. 329–338. ISSN: 02648377. DOI: 10.1016/j.landusepol.2011.07.003.
- Parajka, J., Merz, R., and Blöschl, G. (2007). “Uncertainty and multiple objective calibration in regional water balance modelling: case study in 320 Austrian catchments”. In: *Hydrological Processes* 21.4, pp. 435–446. ISSN: 08856087. DOI: 10.1002/hyp.6253.
- Patzelt, G. (2013). *Austrian glacier inventory 1969 (G I)*. PANGAEA. DOI: 10.1594/PANGAEA.807098.
- Pechlivanidis, I., Jackson, B., McIntyre, N., and Wheeler, H. (2011). “Catchment scale hydrological modelling: a review of model types, calibration approaches and uncertainty analysis methods in the context of recent developments in technology and applications”. In: *Global Nest Journal*. URL: <https://www.semanticscholar.org/paper/Catchment-scale-hydrological-modelling%3A-a-review-of-Pechlivanidis-Jackson/a41953b14383e793c87bce4457c4d3f13bee0c51>.
- Penman, H. L. (1978). “Vegetation and the Atmosphere. Ed. J. L. Monteith. London: Academic Press (1975) Vol.1; principles pp. 298, £10; Vol. 2; Case Studies pp. 459, £15”. In: *Experimental Agriculture* 14.2, p. 178. ISSN: 0014-4797. DOI: 10.1017/S0014479700008607.
- Pepin, N. C., Arnone, E., Gobiet, A., Haslinger, K., Kotlarski, S., Notarnicola, C., Palazzi, E., Seibert, P., Serafin, S., Schöner, W., Terzago, S., Thornton, J. M., Vuille, M., and Adler, C. (2022). “Climate Changes and Their Elevational Patterns in the Mountains of the World”. In: *Reviews of geophysics (Washington, D.C. : 1985)* 60.1. ISSN: 8755-1209. DOI: 10.1029/2020RG000730.
- Perico, R., Brunner, P., Frattini, P., and Crosta, G. B. (2022). “Water Balance in Alpine Catchments by Sentinel Data”. In: *Water Resources Research* 58.11. ISSN: 1944-7973. DOI: 10.1029/2021WR031355.
- Perrin, C., Michel, C., and Andréassian, V. (2003). “Improvement of a parsimonious model for streamflow simulation”. In: *Journal of Hydrology* 279.1-4, pp. 275–289. ISSN: 00221694.



- DOI: 10.1016/S0022-1694(03)00225-7. URL: <https://www.sciencedirect.com/science/article/pii/S0022169403002257>.
- Pesci, M. H. (2023). *WaSiM-OGGM: v1.0.1*. DOI: 10.5281/ZENODO.8315508.
- Pesci, M. H., Mouris, K., Haun, S., and Förster, K. (2023a). "Assessment of uncertainties in a complex modeling chain for predicting reservoir sedimentation under changing climate". In: *Modeling Earth Systems and Environment* 9.4, pp. 3777–3793. ISSN: 2363-6203. DOI: 10.1007/s40808-023-01705-6.
- Pesci, M. H., Schulte Overberg, P., Bosshard, T., and Förster, K. (2023b). "From global glacier modeling to catchment hydrology: bridging the gap with the WaSiM-OGGM coupling scheme". In: *Frontiers in Water* 5. DOI: 10.3389/frwa.2023.1296344.
- Pfeffer, W. T., Arendt, A. A., Bliss, A., Bolch, T., Cogley, J. G., Gardner, A. S., Hagen, J.-O., Hock, R., Kaser, G., Kienholz, C., Miles, E. S., Moholdt, G., Mölg, N., Paul, F., Radić, V., Rastner, P., Raup, B. H., Rich, J., and Sharp, M. J. (2014). "The Randolph Glacier Inventory: a globally complete inventory of glaciers". In: *Journal of Glaciology* 60.221, pp. 537–552. ISSN: 0022-1430. DOI: 10.3189/2014JoG13J176.
- Philipp Schulte Overberg (2021). "Prozessbasierte Wasserhaushaltsmodellierung im Hochgebirge unter Verwendung verschiedener meteorologischer Datensätze". Master of Science. Hannover: Leibniz Universität Hannover.
- Psenner, R. (2007). *The water balance of the Alps: What do we need to protect the water resources of the Alps ? : proceedings of the conference held at Innsbruck University, 28 - 29 September 2006 Roland Psenner ... (Hg.)* 1. Aufl. Alpine space 3. ISBN: 978-3-902571-33-5.
- Radić, V. and Hock, R. (2011). "Regionally differentiated contribution of mountain glaciers and ice caps to future sea-level rise". In: *Nature Geoscience* 4.2, pp. 91–94. ISSN: 1752-0894. DOI: 10.1038/ngeo1052.
- (2014). "Glaciers in the Earth's Hydrological Cycle: Assessments of Glacier Mass and Runoff Changes on Global and Regional Scales". In: *Surveys in Geophysics* 35.3, pp. 813–837. ISSN: 0169-3298. DOI: 10.1007/s10712-013-9262-y.
- Radić, V., Hock, R., and Oerlemans, J. (2007). "Volume–area scaling vs flowline modelling in glacier volume projections". In: *Annals of Glaciology* 46, pp. 234–240. ISSN: 0260-3055. DOI: 10.3189/172756407782871288.
- RGI Consortium (2017). *Randolph Glacier Inventory 6.0*. DOI: 10.7265/N5-RGI-60. URL: <https://www.glims.org/RGI/>.
- Rounce, D. R., Hock, R., and Shean, D. E. (2020a). "Glacier Mass Change in High Mountain Asia Through 2100 Using the Open-Source Python Glacier Evolution Model (PyGEM)". In: *Frontiers in Earth Science* 7. DOI: 10.3389/feart.2019.00331.
- Rounce, D. R., Khurana, T., Short, M. B., Hock, R., Shean, D. E., and Brinkerhoff, D. J. (2020b). "Quantifying parameter uncertainty in a large-scale glacier evolution model using Bayesian inference: application to High Mountain Asia". In: *Journal of Glaciology* 66.256, pp. 175–187. ISSN: 0022-1430. DOI: 10.1017/jog.2019.91. URL: <https://www.cambridge.org/core/journals/journal-of-glaciology/article/quantifying-parameter-uncertainty-in-a-largescale-glacier-evolution-model-using-bayesian-inference-application-to-high-mountain-asia/61D8956E9A6C27CC1A5AEBFCDADC0432>.
- Saltelli, A. (1999). "Sensitivity analysis: Could better methods be used?" In: *Journal of Geophysical Research: Atmospheres* 104.D3, pp. 3789–3793. ISSN: 01480227. DOI: 10.1029/1998JD100042.

- Saltelli, A., Tarantola, S., and Chan, K.-S. (1999). "A quantitative model-independent method for global sensitivity analysis of model output". In: *Technometrics* 41.1, pp. 39–56.
- Savenije, H., A. Viglione, T. Wagener, M. Sivapalan, and G. Blöeschl, eds. (2013). *Runoff Prediction in Ungauged Basins: Synthesis across Processes, Places and Scales*. Cambridge: Cambridge University Press. ISBN: 9781139235761. DOI: 10.1017/CB09781139235761.
- Schaefli, B., Hingray, B., Niggli, M., and Musy, A. (2005). "A conceptual glacio-hydrological model for high mountainous catchments". In: *Hydrology and Earth System Sciences* 9.1/2, pp. 95–109. DOI: 10.5194/hess-9-95-2005.
- Schaefli, B. and Gupta, H. V. (2007). "Do Nash values have value?" In: *Hydrological Processes* 21.15, pp. 2075–2080. ISSN: 08856087. DOI: 10.1002/hyp.6825.
- Schattan, P., Baroni, G., Oswald, S. E., Schöber, J., Fey, C., Kormann, C., Huttenlau, M., and Achleitner, S. (2017). "Continuous monitoring of snowpack dynamics in alpine terrain by aboveground neutron sensing". In: *Water Resources Research* 53.5, pp. 3615–3634. ISSN: 00431397. DOI: 10.1002/2016WR020234.
- Schattan, P., Schwaizer, G., Schöber, J., and Achleitner, S. (2020). "The complementary value of cosmic-ray neutron sensing and snow covered area products for snow hydrological modelling". In: *Remote Sensing of Environment* 239, p. 111603. ISSN: 00344257. DOI: 10.1016/j.rse.2019.111603.
- Schmidt, L. K., Francke, T., Rottler, E., Blume, T., Schöber, J., and Bronstert, A. (2022). "Suspended sediment and discharge dynamics in a glaciated alpine environment: identifying crucial areas and time periods on several spatial and temporal scales in the Ötztal, Austria". In: *Earth Surface Dynamics* 10.3, pp. 653–669. DOI: 10.5194/esurf-10-653-2022.
- Schöber, J., Achleitner, S., Kirnbauer, R., Schöberl, F., and Schönlaub, H. (2010). "Hydrological modelling of glacierized catchments focussing on the validation of simulated snow patterns – applications within the flood forecasting system of the Tyrolean river Inn". In: *Advances in Geosciences* 27, pp. 99–109. DOI: 10.5194/adgeo-27-99-2010.
- Schöber, J., Klebelsberg, A., Schattan, P., Helfricht, K., and Fey, C. (2019). *Automatic weather station data from Weisssee snow research site (2014–2018)*. DOI: 10.1594/PANGAEA.898217.
- Schöber, J., Schneider, K., Helfricht, K., Schattan, P., Achleitner, S., Schöberl, F., and Kirnbauer, R. (2014). "Snow cover characteristics in a glacierized catchment in the Tyrolean Alps - Improved spatially distributed modelling by usage of Lidar data". In: *Journal of Hydrology* 519, pp. 3492–3510. ISSN: 00221694. DOI: 10.1016/j.jhydro.2013.12.054. URL: <https://www.sciencedirect.com/science/article/pii/S002216941400016X>.
- Schulla, J. (1997). "Hydrologische Modellierung von Flussgebieten zur Abschätzung der Folgen von Klimaänderungen". Dissertation. Zurich: ETH. URL: [http://www.wasim.ch/downloads/doku/wasim/schulla\\_1997.pdf](http://www.wasim.ch/downloads/doku/wasim/schulla_1997.pdf).
- (2021). *Model Description WaSiM*. URL: [http://www.wasim.ch/downloads/doku/wasim/wasim\\_2021\\_en.pdf](http://www.wasim.ch/downloads/doku/wasim/wasim_2021_en.pdf).
- Schuster, L., Rounce, D., and Maussion, F. (2023). *Glacier projections sensitivity to temperature-index model choices and calibration strategies*. DOI: 10.31223/X5C65S.
- Seibert, J. and Bergström, S. (2022). "A retrospective on hydrological catchment modelling based on half a century with the HBV model". In: *Hydrology and Earth System Sciences* 26.5, pp. 1371–1388. DOI: 10.5194/hess-26-1371-2022.

- Seibert, J., Vis, M. J. P., Kohn, I., Weiler, M., and Stahl, K. (2018). "Technical note: Representing glacier geometry changes in a semi-distributed hydrological model". In: *Hydrology and Earth System Sciences* 22.4, pp. 2211–2224. DOI: 10.5194/hess-22-2211-2018.
- Sevruk, B. (1982). *Methods of correction for systematic errors in point precipitation measurement for operational use*. Switzerland.
- Singh, P. and Jain, S. K. (2002). "Snow and glacier melt in the Satluj River at Bhakra Dam in the western Himalayan region". In: *Hydrological Sciences Journal* 47.1, pp. 93–106. ISSN: 0262-6667. DOI: 10.1080/02626660209492910.
- Singh, V. P. (2018). "Hydrologic modeling: progress and future directions". In: *Geoscience Letters* 5.1, pp. 1–18. ISSN: 2196-4092. DOI: 10.1186/s40562-018-0113-z. URL: <https://geoscienceletters.springeropen.com/articles/10.1186/s40562-018-0113-z#Sec25>.
- Somers, L. D. and McKenzie, J. M. (2020). "A review of groundwater in high mountain environments". In: *WIREs Water* 7.6. ISSN: 2049-1948. DOI: 10.1002/wat2.1475.
- Stahl, K., Moore, R. D., Shea, J. M., Hutchinson, D., and Cannon, A. J. (2008). "Coupled modelling of glacier and streamflow response to future climate scenarios". In: *Water Resources Research* 44.2. ISSN: 00431397. DOI: 10.1029/2007WR005956.
- Stephen, J. T. and Rafferty, J. P. (2023). *Little Ice Age*. Ed. by Encyclopedia Britannica. URL: <https://www.britannica.com/science/Little-Ice-Age>.
- Stocker-Waldhuber, M. (2019). "Multi-Method Investigation of Dynamic Processes in Rapidly Changing Alpine Glaciers". Dissertation. Eichstätt-Ingolstadt: Katholische Universität Eichstätt-Ingolstadt.
- (2020). *Projektbericht Gepatschferner und Weißseeferner: Ablations- und Geschwindigkeitmessungen 2019/2020*. Innsbruck.
- Stoll, E., Hanzer, F., Oesterle, F., Nemeč, J., Schöber, J., Huttenlau, M., and Förster, K. (2020). "What Can We Learn from Comparing Glacio-Hydrological Models?" In: *Atmosphere* 11.9, p. 981. DOI: 10.3390/atmos11090981.
- Strasser, U., Bernhardt, M., Weber, M., Liston, G. E., and Mauser, W. (2008). "Is snow sublimation important in the alpine water balance?" In: *The Cryosphere* 2.1, pp. 53–66. DOI: 10.5194/tc-2-53-2008.
- Tarasova, L., Knoche, M., Dietrich, J., and Merz, R. (2016). "Effects of input discretization, model complexity, and calibration strategy on model performance in a data-scarce glacierized catchment in Central Asia". In: *Water Resources Research* 52.6, pp. 4674–4699. ISSN: 00431397. DOI: 10.1002/2015WR018551.
- Thiemig, V., Rojas, R., Zambrano-Bigiarini, M., and Roo, A. de (2013). "Hydrological evaluation of satellite-based rainfall estimates over the Volta and Baro-Akobo Basin". In: *Journal of Hydrology* 499, pp. 324–338. ISSN: 00221694. DOI: 10.1016/j.jhydro.2013.07.012.
- Thornton, J. M., Brauchli, T., Mariethoz, G., and Brunner, P. (2021). "Efficient multi-objective calibration and uncertainty analysis of distributed snow simulations in rugged alpine terrain". In: *Journal of Hydrology* 598, p. 126241. ISSN: 00221694. DOI: 10.1016/j.jhydro.2021.126241.
- Thornton, J. M., Mariethoz, G., Brauchli, T. J., and Brunner, P. (2019). *Efficient multi-objective calibration and uncertainty analysis of distributed snow simulations in rugged alpine terrain*. DOI: 10.5194/tc-2019-181.
- TIWAG (2023). *Kraftwerk Kanuertal*. URL: <https://www.tiwag.at/unternehmen/unsere-kraftwerke/kraftwerk/kraftwerk-kaunertal/>.

- UNEP (2004). "Impacts of summer 2003 heat wave in Europe". In: *Environment Alert Bulletin*.
- van Genuchten, M. T. (1980). "A Closed-form Equation for Predicting the Hydraulic Conductivity of Unsaturated Soils". In: *Soil Science Society of America Journal* 44.5, pp. 892–898. ISSN: 03615995. DOI: 10.2136/sssaj1980.03615995004400050002x.
- van Rossum, G. and Drake, F. L. (2009). *Python*.
- van Tiel, M., Stahl, K., Freudiger, D., and Seibert, J. (2020). "Glacio–hydrological model calibration and evaluation". In: *WIREs Water* 66.3, p. 249. ISSN: 2049-1948. DOI: 10.1002/wat2.1483.
- van Tricht, L., Zekollari, H., Huss, M., Farinotti, D., and Huybrechts, P. (2023). *Global vs local glacier modelling: a comparison in the Tien Shan*. DOI: 10.5194/tc-2023-87.
- Verbunt, M., GURTZ, J., JASPER, K., Lang, H., Warmerdam, P., and Zappa, M. (2003). "The hydrological role of snow and glaciers in alpine river basins and their distributed modeling". In: *Journal of Hydrology* 282.1-4, pp. 36–55. ISSN: 00221694. DOI: 10.1016/S0022-1694(03)00251-8.
- Viviroli, D., Archer, D. R., Buytaert, W., Fowler, H. J., Greenwood, G. B., Hamlet, A. F., Huang, Y., Koboltschnig, G., Litaor, M. I., López-Moreno, J. I., Lorentz, S., Schädler, B., Schreier, H., Schwaiger, K., Vuille, M., and Woods, R. (2011). "Climate change and mountain water resources: overview and recommendations for research, management and policy". In: *Hydrology and Earth System Sciences* 15.2, pp. 471–504. DOI: 10.5194/hess-15-471-2011.
- Viviroli, D., Dürr, H. H., Messerli, B., Meybeck, M., and Weingartner, R. (2007). "Mountains of the world, water towers for humanity: Typology, mapping, and global significance". In: *Water Resources Research* 43.7. ISSN: 1944-7973. DOI: 10.1029/2006WR005653.
- Viviroli, D., Kummu, M., Meybeck, M., Kallio, M., and Wada, Y. (2020). "Increasing dependence of lowland populations on mountain water resources". In: *Nature Sustainability* 3.11, pp. 917–928. ISSN: 2398-9629. DOI: 10.1038/s41893-020-0559-9. URL: <https://www.nature.com/articles/s41893-020-0559-9>.
- Voordendag, A. (19.9.2023). "Glacier Loss Day indicates record breaking glacier melt". In: *Phys.org*. URL: <https://phys.org/news/2023-09-glacier-loss-day.html>.
- Wagner, T., Themeßl, M., Schüppel, A., Gobiet, A., Stigler, H., and Birk, S. (2017). "Impacts of climate change on stream flow and hydro power generation in the Alpine region". In: *Environmental Earth Sciences* 76.1, pp. 1–22. ISSN: 1866-6299. DOI: 10.1007/s12665-016-6318-6. URL: <https://link.springer.com/article/10.1007/s12665-016-6318-6>.
- Warscher, M., Strasser, U., Kraller, G., Marke, T., Franz, H., and Kunstmann, H. (2013). "Performance of complex snow cover descriptions in a distributed hydrological model system: A case study for the high Alpine terrain of the Berchtesgaden Alps". In: *Water Resources Research* 49.5, pp. 2619–2637. ISSN: 00431397. DOI: 10.1002/wrcr.20219.
- Weingartner, R., Viviroli, D., and Schädler, B. (2007). "Water resources in mountain regions: a methodological approach to assess the water balance in a highland-lowland-system". In: *Hydrological Processes* 21.5, pp. 578–585. ISSN: 08856087. DOI: 10.1002/hyp.6268.
- Weisstein, E. (2023). *Convex hull*. URL: <https://mathworld.wolfram.com/ConvexHull1.html>.
- WGMS (2022). *Reference glaciers for mass balance*. URL: [https://wgms.ch/products\\_ref\\_glaciers/](https://wgms.ch/products_ref_glaciers/).

- Wiersma, P., Aerts, J., Zekollari, H., Hrachowitz, M., Drost, N., Huss, M., Sutanudjaja, E. H., and Hut, R. (2022). "Coupling a global glacier model to a global hydrological model prevents underestimation of glacier runoff". In: *Hydrology and Earth System Sciences* 26.23, pp. 5971–5986. DOI: 10.5194/hess-26-5971-2022.
- Winter, B., Schneeberger, K., Dung, N. V., Huttenlau, M., Achleitner, S., Stötter, J., Merz, B., and Vorogushyn, S. (2019). "A continuous modelling approach for design flood estimation on sub-daily time scale". In: *Hydrological Sciences Journal* 64.5, pp. 539–554. ISSN: 0262-6667. DOI: 10.1080/02626667.2019.1593419.
- Wortmann, M., Bolch, T., Su, B., and Krysanova, V. (2019). "An efficient representation of glacier dynamics in a semi-distributed hydrological model to bridge glacier and river catchment scales". In: *Journal of Hydrology* 573, pp. 136–152. ISSN: 00221694. DOI: 10.1016/j.jhydrol.2019.03.006. URL: <https://www.sciencedirect.com/science/article/pii/S0022169419302549>.
- Xu, C. and Gertner, G. (2011). "Understanding and comparisons of different sampling approaches for the Fourier Amplitudes Sensitivity Test (FAST)". In: *Computational Statistics Data Analysis* 55.1, pp. 184–198. ISSN: 0167-9473. DOI: <https://doi.org/10.1016/j.csda.2010.06.028>. URL: <https://www.sciencedirect.com/science/article/pii/S0167947310002756>.
- Yen, B. C. (1992). "Dimensionally Homogeneous Manning's Formula". In: *Journal of Hydraulic Engineering* 118.9, pp. 1326–1332. ISSN: 0733-9429. DOI: 10.1061/(ASCE)0733-9429(1992)118:9(1326).
- Yevjevich, V. (1987). "Stochastic models in hydrology". In: *Stochastic Hydrology and Hydraulics* 1.1, pp. 17–36. ISSN: 1435-151X. DOI: 10.1007/BF01543907. URL: <https://link.springer.com/article/10.1007/BF01543907>.
- Yu, D., Yang, J., Shi, L., Zhang, Q., Huang, K., Fang, Y., and Zha, Y. (2019). "On the uncertainty of initial condition and initialization approaches in variably saturated flow modeling". In: *Hydrology and Earth System Sciences* 23.7, pp. 2897–2914. DOI: 10.5194/hess-23-2897-2019. URL: <https://hess.copernicus.org/articles/23/2897/2019/>.
- Zekollari, H., Huss, M., Farinotti, D., and Lhermitte, S. (2022). "Ice-Dynamical Glacier Evolution Modeling—A Review". In: *Reviews of geophysics (Washington, D.C. : 1985)* 60.2. ISSN: 8755-1209. DOI: 10.1029/2021RG000754.
- Zekollari, H., Fürst, J. J., and Huybrechts, P. (2014). "Modelling the evolution of Vadret da Morteratsch, Switzerland, since the Little Ice Age and into the future". In: *Journal of Glaciology* 60.224, pp. 1155–1168. ISSN: 0022-1430. DOI: 10.3189/2014JoG14J053. URL: <https://www.cambridge.org/core/journals/journal-of-glaciology/article/modelling-the-evolution-of-vadret-da-morteratsch-switzerland-since-the-little-ice-age-and-into-the-future/BDBEB7196196DAE2801317EE12BE4FAA>.
- Zekollari, H., Huss, M., and Farinotti, D. (2019). "Modelling the future evolution of glaciers in the European Alps under the EURO-CORDEX RCM ensemble". In: *The Cryosphere* 13.4, pp. 1125–1146. DOI: 10.5194/tc-13-1125-2019.
- Zemp, M., Hoelzle, M., and Haeberli, W. (2009). "Six decades of glacier mass-balance observations: a review of the worldwide monitoring network". In: *Annals of Glaciology* 50.50, pp. 101–111. ISSN: 0260-3055. DOI: 10.3189/172756409787769591.
- Zemp, M., Huss, M., Thibert, E., Eckert, N., McNabb, R., Huber, J., Barandun, M., Machguth, H., Nussbaumer, S. U., Gärtner-Roer, I., Thomson, L., Paul, F., Mausson, F., Kutuzov, S., and Cogley, J. G. (2019). "Global glacier mass changes and their

- contributions to sea-level rise from 1961 to 2016". In: *Nature* 568.7752, pp. 382–386. ISSN: 1476-4687. DOI: 10.1038/s41586-019-1071-0. URL: <https://www.nature.com/articles/s41586-019-1071-0>.
- Zemp, M., Paul, F., Hoelzle, M., and Haeberli, W. (2008). *Glacier fluctuations in the European Alps, 1850–2000: an overview and spatio-temporal analysis of available data*. DOI: 10.5167/uzh-9024.
- Zhang, S., Ye, B., Liu, S., Zhang, X., and Hagemann, S. (2012). "A modified monthly degree-day model for evaluating glacier runoff changes in China. Part I: model development". In: *Hydrological Processes* 26.11, pp. 1686–1696. ISSN: 08856087. DOI: 10.1002/hyp.8286. URL: <https://onlinelibrary.wiley.com/doi/full/10.1002/hyp.8286>.
- Zhao, Q., Ding, Y., Wang, J., Gao, H., Zhang, S., Zhao, C., Xu, J., Han, H., and Shang-guan, D. (2019). "Projecting climate change impacts on hydrological processes on the Tibetan Plateau with model calibration against the glacier inventory data and observed streamflow". In: *Journal of Hydrology* 573, pp. 60–81. ISSN: 00221694. DOI: 10.1016/j.jhydrol.2019.03.043. URL: <https://www.sciencedirect.com/science/article/pii/S0022169419302434>.

# Appendix A

## Observed data

### A.1 Glaciers

Interpolated values of the glaciological measurements of mass balance components at the tongue of *Gepatschferner* for the years 2012 to 2019 are shown in Figure A.1. Figure A.2 indicates the location of the Ground-penetrating radar (GPR) measurements for three glaciers in the study area.

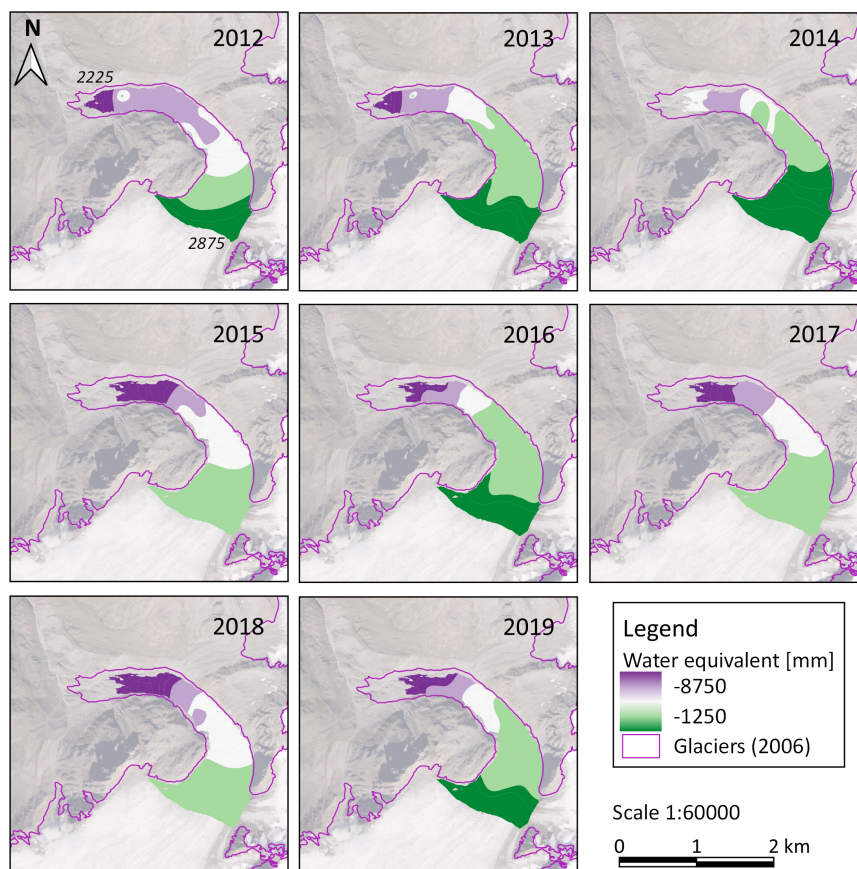


Figure A.1: Mass balance at the tongue of the Gepatschferner (expressed in water equivalent height [mm]). The elevations at the tongue vary between 2225 to 2875 m.a.s.l. In addition, observed glacier outlines for the year 2006 are included (Fischer et al., 2015b). Adapted from Stocker-Waldhuber, 2020

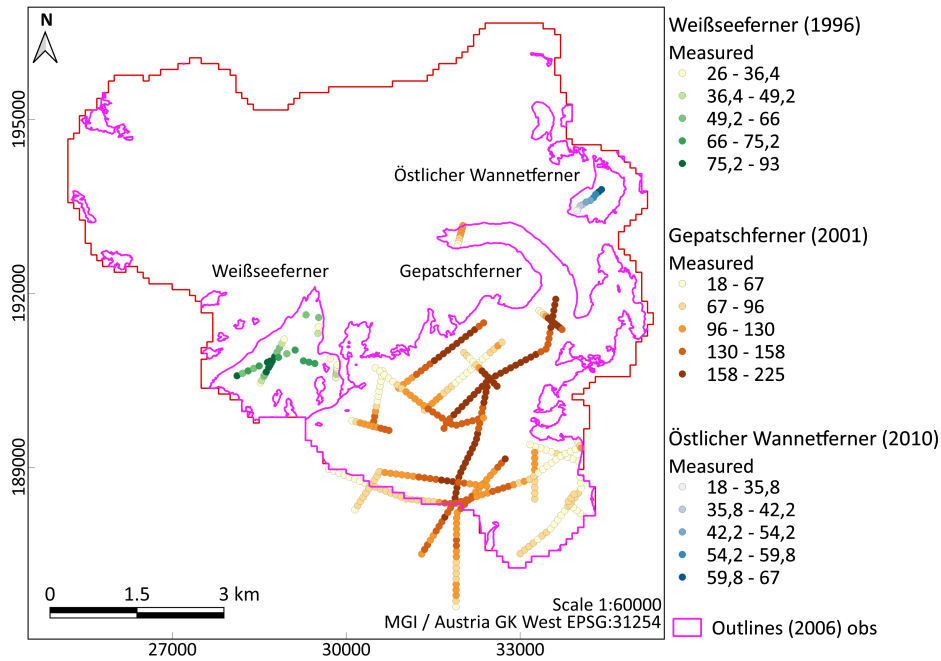


Figure A.2: Ground-penetrating radar (GPR) point measurements of ice thickness in Gepatschferner (2001), Östlicher Wannetferner (2010) and Weißseeferner (1996) (adapted from Fischer et al., 2015d). In addition, observed glacier outlines for the year 2006 are included (Fischer et al., 2015b).

## A.2 Climate

The analogous downscaling method used to extend the INCA dataset into the past is based on a **k Nearest Neighbor** bootstrap for resampling (**kNN**, Lall and Sharma, 1996; Winter et al., 2019). The objective is to reconstruct the period 1969-2003 by resampling (with replacement) from nearest neighbors (NN). NN refer to the days in a *Database* (dataset with observations, period 2003-2014) for which the observation is closest to that same day in the kNN-time series (1969-2003). Then, the NN with the smallest euclidean distance is selected. When considering all stations simultaneously, the match-day is selected from the minimum average from all station values.

Day	$P_{st}$	$P_{INCA}$
1	2,5	
2	3,2	
3	4,0	
4	3,5	3,6
5	2,8	2,4
6	0,8	1,2

KNN-time series (Days 1-3) and Database (Days 4-6)

Day	$P_{st}$	$\Delta P_{st,1}-P_{st,4}$	$\Delta P_{st,1}-P_{st,5}$	$\Delta P_{st,1}-P_{st,6}$	$P_{INCA,new}$
1	2,5	1,0	0,3	0,7	2,4
2	3,2	0,3	0,4	0,4	3,6
3	4,0	0,5	1,2	3,2	3,6

Figure A.3: Example of the application of the kNN method to get new values of precipitation ( $P$ ).  $P_{st}$  refers to the observed precipitation value from station data, whereas  $P_{INCA}$  refers to the observed value from INCA. The days 1-3 belong to the kNN-time series and the days 4-6, to the Database. The smallest euclidean distances for each day (1-3) are indicated with a green frame, and the new values for the  $P_{INCA}$  in the kNN-time series, in orange.

The mean daily values of precipitation, temperature, solar radiation, wind speed and



relative humidity as an average of the entire catchment are shown in Figure A.4. In all cases, the solid lines indicate the values from the stations, whereas the dashed lines, the values from the INCA dataset. The diagrams on the left considers the kNN-time series period (1969–2003), while the right diagrams, the Database period (2003–2014).

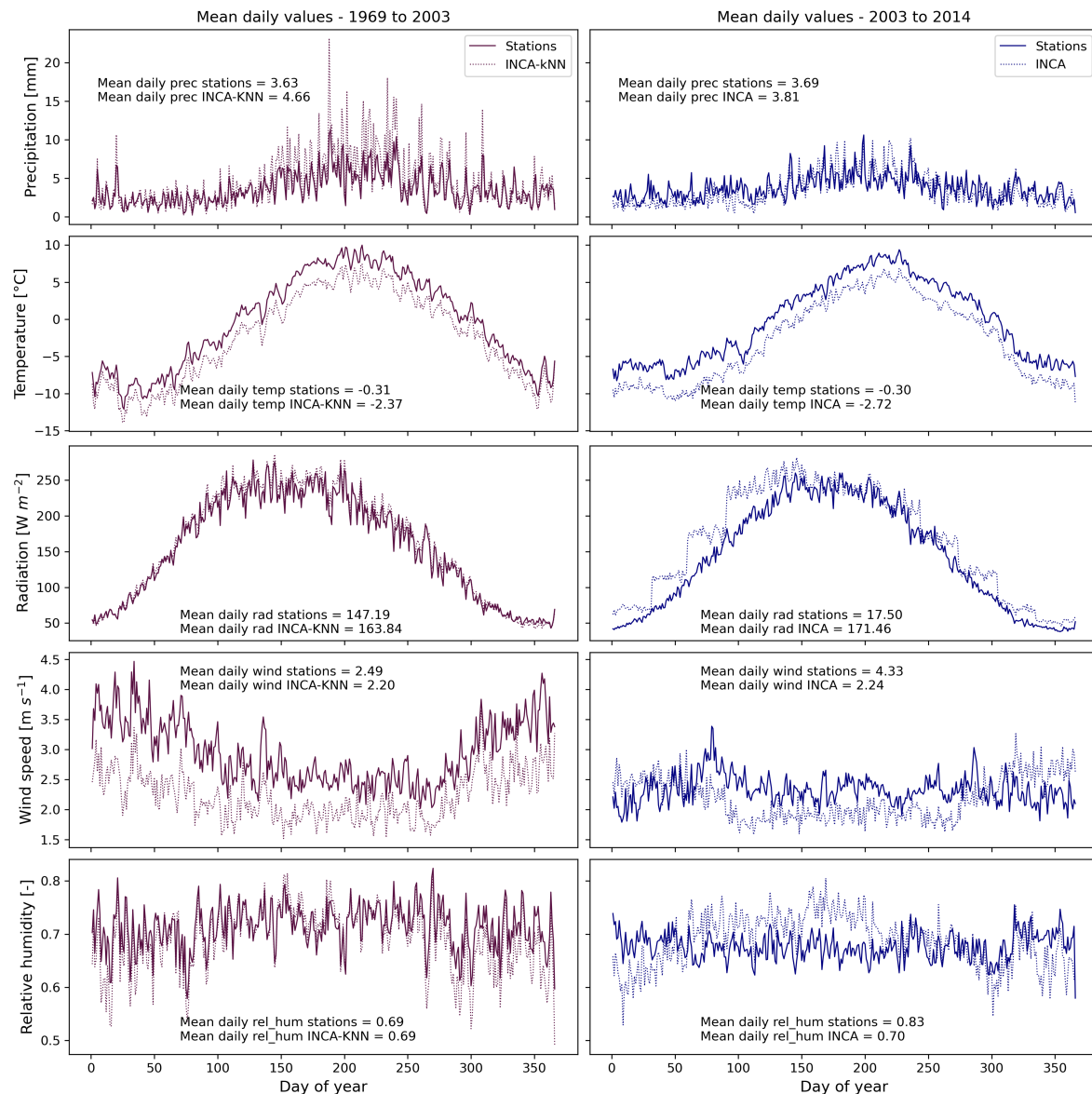


Figure A.4: Mean daily values of precipitation, temperature, solar radiation, wind speed and relative humidity as an average of the entire catchment. The solid lines indicate the values from the stations, whereas the dashed lines, the values from the INCA dataset.

# Appendix B

## Performance measures

1. ***NSE*, Nash-Sutcliffe Efficiency:** The *NSE* is one of the most used criteria when evaluating the performance of hydrological models. It was first derived by Nash and Sutcliffe, 1970 and can be computed according to Equation B.1. *NSE* can vary between  $-\infty$  and 1: a value of 1 indicates that there is a perfect correspondence between observed and simulated values, whereas a value of 0 indicates that the model performs similar as when using the mean observed value. A value of *NSE*  $< 0$  indicates a bad performance of the model (Schaepli and Gupta, 2007; Knoben et al., 2019).

$$NSE = 1 - \frac{\sum_{t=1}^N [q_{obs}(t) - q_{sim}(t)]^2}{\sum_{t=1}^N [q_{obs}(t) - \bar{q}_{obs}]^2} \quad (\text{B.1})$$

Where:  $q_{obs}$  is the observed variable (e.g. runoff) at time step  $t$ ,  $q_{sim}$  is the simulated variable (e.g. runoff) at time step  $t$  and  $\bar{q}$  is the mean observed variable (e.g. runoff) over the entire simulation period of length  $N$ .

2. ***KGE*, Kling-Gupta Efficiency:** The *KGE* is a decomposition of *NSE* which can be used as an alternative criteria for hydrological model calibration. Developed by Gupta et al., 2009, it can be computed as follow:

$$KGE = 1 - \sqrt{(r - 1)^2 + (\alpha - 1)^2 + (\beta - 1)^2} \quad (\text{B.2})$$

Where:  $r$  is the ratio between the covariance (simulated and observed values) and the product of standard deviations (simulated and observed values),  $\alpha$  is the ratio between standard deviation of simulated and observed values and  $\beta$  is the ratio between mean simulated and observed values. Like *NSE*, the range of *KGE* is between  $-\infty$  and 1, indicating 1 a perfect correspondence between observed and simulated values.

3. ***BE*, Benchmark Efficiency:** In catchments showing a strong seasonality (e.g. snow- and ice melt dominated catchments), *NSE* can be misleading, since very good values are obtained with the use of the mean observed value. For predictions at a daily time step a benchmark model might be suitable. Schaepli and Gupta, 2007 suggests the *BE*, in which the mean observed value for each calendar day is used ( $q_b(t)$  i.e. 365 values are used as benchmark), instead of the mean observed value for the entire period. Like *NSE* and *KGE*, the range of *BE* lies between  $-\infty$  and 1, indicating 1 a perfect correspondence between observed and simulated values:

$$BE = 1 - \frac{\sum_{t=1}^N [q_{obs}(t) - q_{sim}(t)]^2}{\sum_{t=1}^N [q_{obs}(t) - \bar{q}_b(t)]^2} \quad (\text{B.3})$$

4. **PBIAS, Percentage bias:** Computes the absolute volume error of the simulated time series given observations as reference (given in percentage, e.g. Moriasi et al., 2007), being its optimal value equal to 0:

$$PBIAS = \frac{\sum_{t=1}^N [q_{obs}(t) - q_{sim}(t)]}{\sum_{t=1}^N [q_{obs}(t)]} \times 100 \quad (B.4)$$

5. **RMSE, Root Mean Square Error:** Computes the root mean square error of the simulated time series given observations as reference, being its optimal value equal to 0:

$$RMSE = \sqrt{\frac{\sum_{t=1}^N [q_{obs}(t) - q_{sim}(t)]^2}{n}} \quad (B.5)$$

Where  $n$  represents the number of time steps (or length of given time series).

6. **POD, Probability of detection:** Indicates the ability of the model to correctly predict a variable within a cell (e.g. glacierization, Kormann et al., 2016). This measure, together with *FAR* are useful when comparing gridded values, like the example shown in Figure B.1. The optimal value of POD is 1.
7. **FAR, False Alarm Rate:** Indicates the model cells identified with a variable by the simulations (e.g. glacierization), but which do not contain any observed value in the reference dataset (Kormann et al., 2016). The optimal value of FAR is 0.

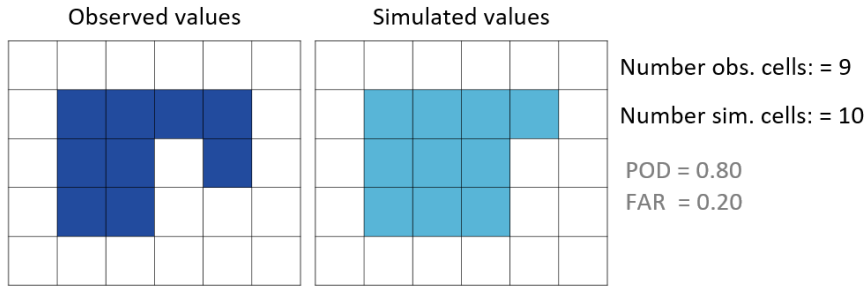


Figure B.1: Example of POD and FAR determination, considering observed and simulated cell values.

8. **MBE, Mean Bias Error:** It is used for estimating the bias in terms of glacier mass balance (Eis et al., 2021) between observed ( $MB_{obs}$ ) and simulated ( $MB_{sim}$ ) values, being its optimal value 0:

$$MBE = \frac{\sum_{t=1}^N [MB_{sim}(t) - MB_{obs}(t)]}{n} \quad (B.6)$$

Where  $n$  is the number of time steps (or length of the time series, e.g. number of years with mass balance measurements).

9. **RSR, Root Mean Square Error Standard Deviation Ratio:** It is determined as the ratio between *RMSE* (Equation B.5) and the standard deviation of the observed dataset (Moriasi et al., 2007), being its optimal value 0:

$$RSR = \frac{RMSE}{STDEV_{obs}} = \frac{\sqrt{\sum_{t=1}^N [q_{obs}(t) - q_{sim}(t)]^2}}{\sqrt{\sum_{t=1}^N [q_{obs}(t) - \bar{q}_{obs}]^2}} \quad (B.7)$$

Table B.1: Classification of the model performance according to the different evaluation criteria during calibration and validation of the models (e.g. Moriasi et al., 2007; Thiemiig et al., 2013)

Performance rating	NSE	KGE	PBIAS	RSR
Very good	$0.75 < NSE \leq 1.00$		$PBIAS \leq \pm 10$	$0.00 \leq RSR \leq 0.50$
Good	$0.65 < NSE \leq 0.75$	$KGE \geq 0.75$	$\pm 10 \leq PBIAS < \pm 15$	$0.50 \leq RSR \leq 0.60$
Satisfactory	$0.50 < NSE \leq 0.65$	$0.50 < KGE \leq 0.75$	$\pm 15 \leq PBIAS < \pm 25$	$0.60 \leq RSR \leq 0.70$
Unsatisfactory	$0.00 < NSE \leq 0.50$	$0.00 < KGE \leq 0.50$	$PBIAS \geq \pm 25$	$RSR > 0.70$
Bad performance	$NSE \leq 0.00$	$KGE \leq 0.00$		

# Appendix C

## Model runs

In this Appendix, additional results to the different steps within the coupling scheme are included.

### C.1 Additional results: first WaSiM run with resampling of climate data

These results complement Section 7.1. Table C.1 summarizes the parameters used during the sensitivity analysis performed with WaSiM (with VA scaling), their description, units and range. Table C.2 summarizes the values of the parameters adjusted during calibration of the WaSiM model. Figure C.1 shows observed and simulated runoff values during the calibration period, at the outlet of Gepatschalm. In addition, Figures C.2a and C.2b present the mean daily observed and simulated runoff during the first and second validation periods, respectively.

Figures C.3 and C.4 show the fraction of snow coverage (FSC, European Environment Agency, 2020) ranging from 0 (no coverage) to 100 (completely covered by snow) and the simulated snow storage, given in mm of water equivalent (SWE), for the days 12.28.2016 and 19.04.2018, respectively. Since WaSiM provides SWE, a direct comparison cannot be ensured. However, it was assumed that all model cells with values of  $SWE < 30$  mm, are not covered by snow.

Table C.1: Selected parameters during the sensitivity analysis for the first WaSiM model run. The table also includes a description of each parameter, the unit and the selected range.

WaSiM sub-process	Parameter	Description	Unit	Range
Soil model	$k_d$	storage coefficient for surface runoff	$h$	5 - 300
	$k_i$	storage coefficient for interflow	$h$	5 - 300
	$d_r$	drainage density for interflow	$m^{-1}$	0 - 80
	$k_b$	recession constant for baseflow	$m$	0 - 10
	$Q_0$	scaling factor for baseflow	$mm\ h^{-1}$	0.01 - 1
	$k_{rec}$	recession constant for hydraulic conductivity	–	0 - 1
Glacier model	$MF$	melt factor	$mm\ ^\circ C^{-1}\ d^{-1}$	1.2 - 6
	$trs$	threshold temperature separating rain and snow	$^\circ C$	-1.0 - 2.0
	$k_{ice}$	storage coefficient for ice	$h$	1 - 20
	$k_{firm}$	storage coefficient for firn	$h$	100 - 1000
	$k_{snow}$	storage coefficient for snow	$h$	10 - 100
	$VA_{scal}$	empiric factor representing thickness of the glacier ( $b$ )	$m$	20 - 100
	$VA_{exp}$	exponential factor ( $f$ )	-	1.2 - 1.4
Snow model	$trs$	threshold temperature separating rain and snow	$^\circ C$	-1.0 - 2.0
	$t_{0r}$	temperature limit for rain	$^\circ C$	-1.0 - 2.0
	$t_0$	temperature limit for snow melt	$^\circ C$	-1.0 - 2.0
	$min_{slope}$	minimum slope for creating slides	$grad$	0 - 90
	$lw_{in}$	correction factor for incoming long wave radiation	–	0.8 - 1.2
	$lw_{out}$	correction factor for outgoing long wave radiation	–	0.8 - 1.2

Table C.2: Parameters adjusted during calibration of the first WaSiM model run, including their calibrated value. The column "Calibrated value 1969" refers to the parameters values for the model initialized in the year 1969 whereas column "Calibrated value 2003" refers to the initialization in the year 2003.

Parameter	Calibrated value 1969	Calibrated value 2003
$k_d$	270	227
$k_i$	210	15.7
$q_0$	1.0	0.32
$MF$	2.9	2.0
$t_0$	0.0	-0.9

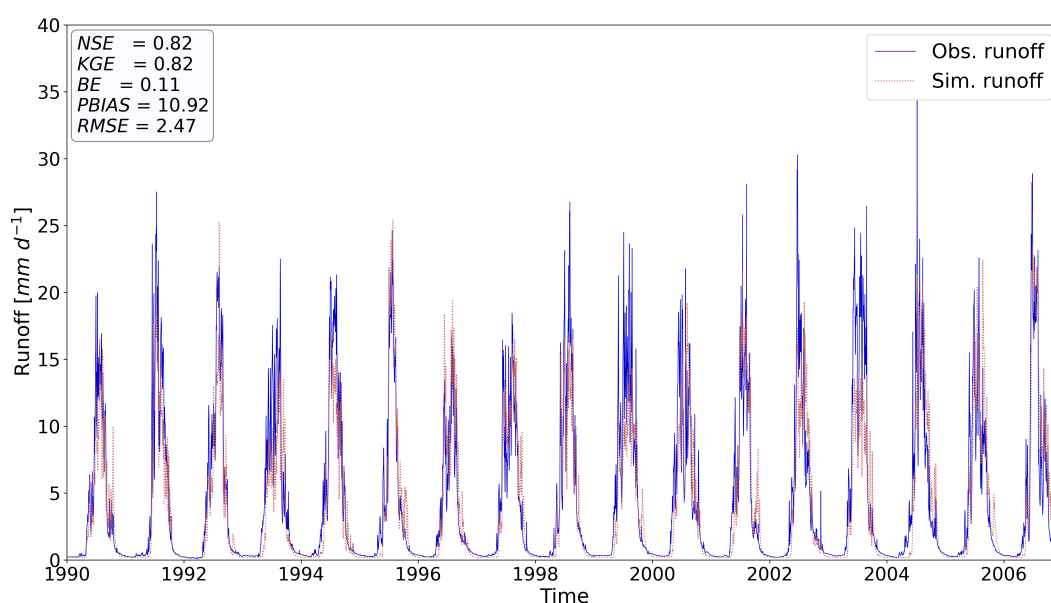


Figure C.1: Observed and simulated runoff at the outlet of Gepatschalm during the calibration period (01/1990 - 12/2006) obtained from the first WaSiM run. Blue solid line: observed runoff, red dashed line: simulated runoff.

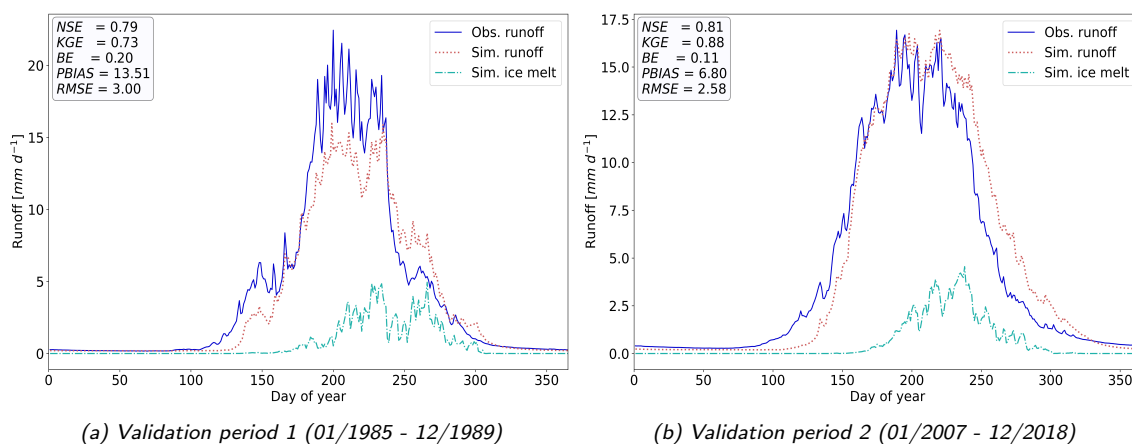


Figure C.2: Mean daily observed and simulated runoff at the outlet of Gepatschalm during the two validation periods. Blue solid line: observed runoff, red dashed line: simulated runoff, light blue line: simulated melt from ice.

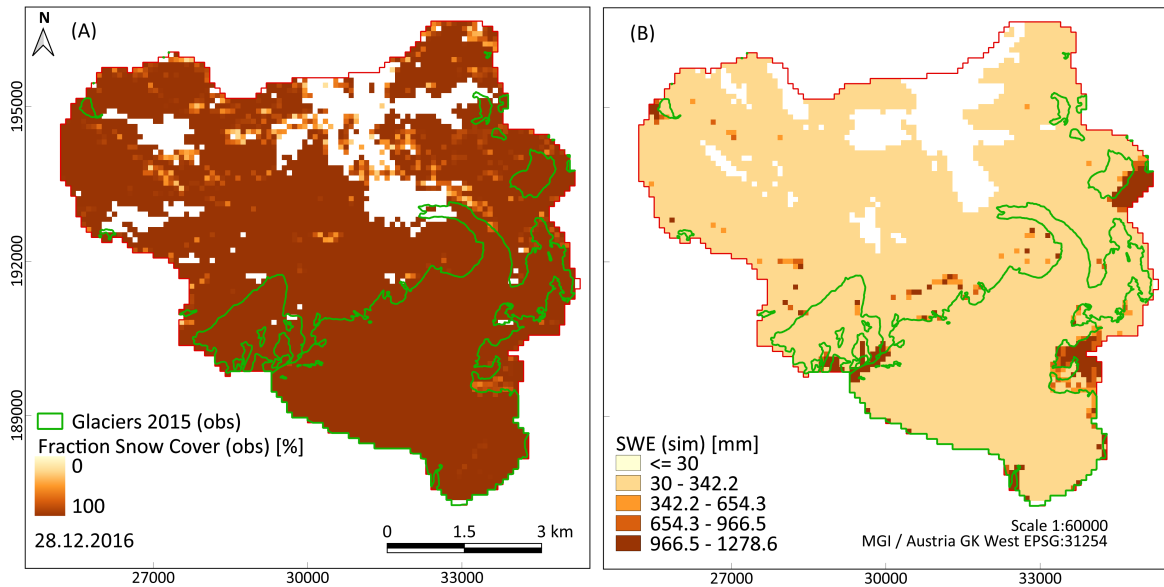


Figure C.3: Observed FSC (fraction of snow coverage) and simulated snow storage, given in SWE, for the day 28.12.2016.

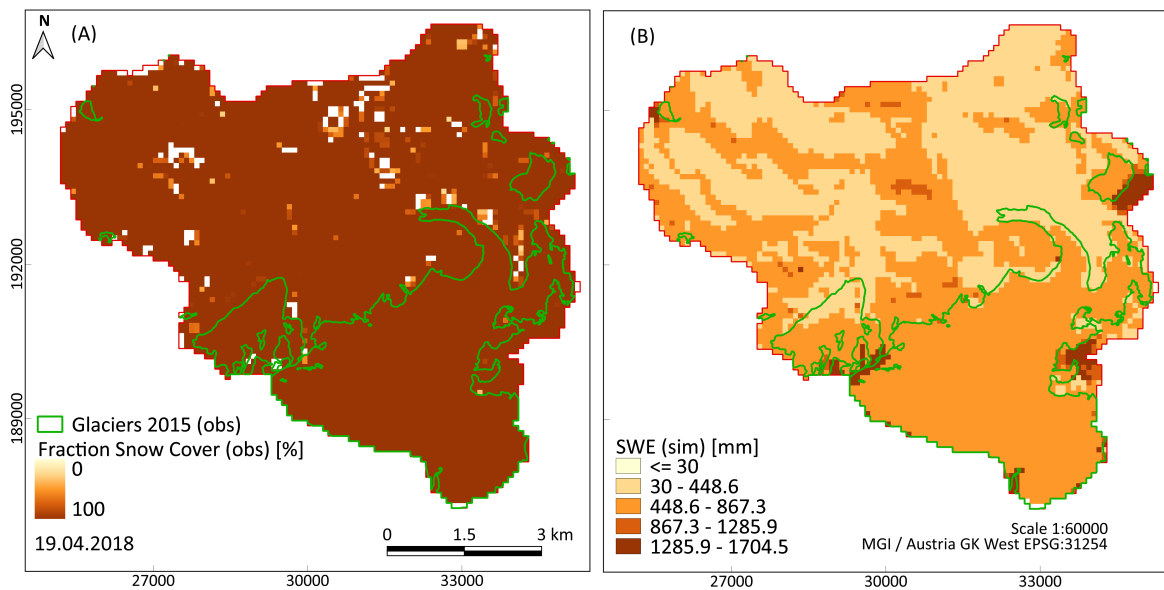


Figure C.4: Observed FSC (fraction of snow coverage) and simulated snow storage, given in SWE, for the day 19.04.2018.

## C.2 Additional results: OGGM run and processing of glacier outputs

These results complement Section 7.2. First, results from the sensitivity analysis of the mass balance model parameters for the glaciers *Weißseeferner* and *Östlicher Wannetferner* (Figure C.5). Second, the calibrated *prcp\_fac* for all the glaciers is shown (Figure C.6). Third, additional results on ice thickness are presented (Table C.3).



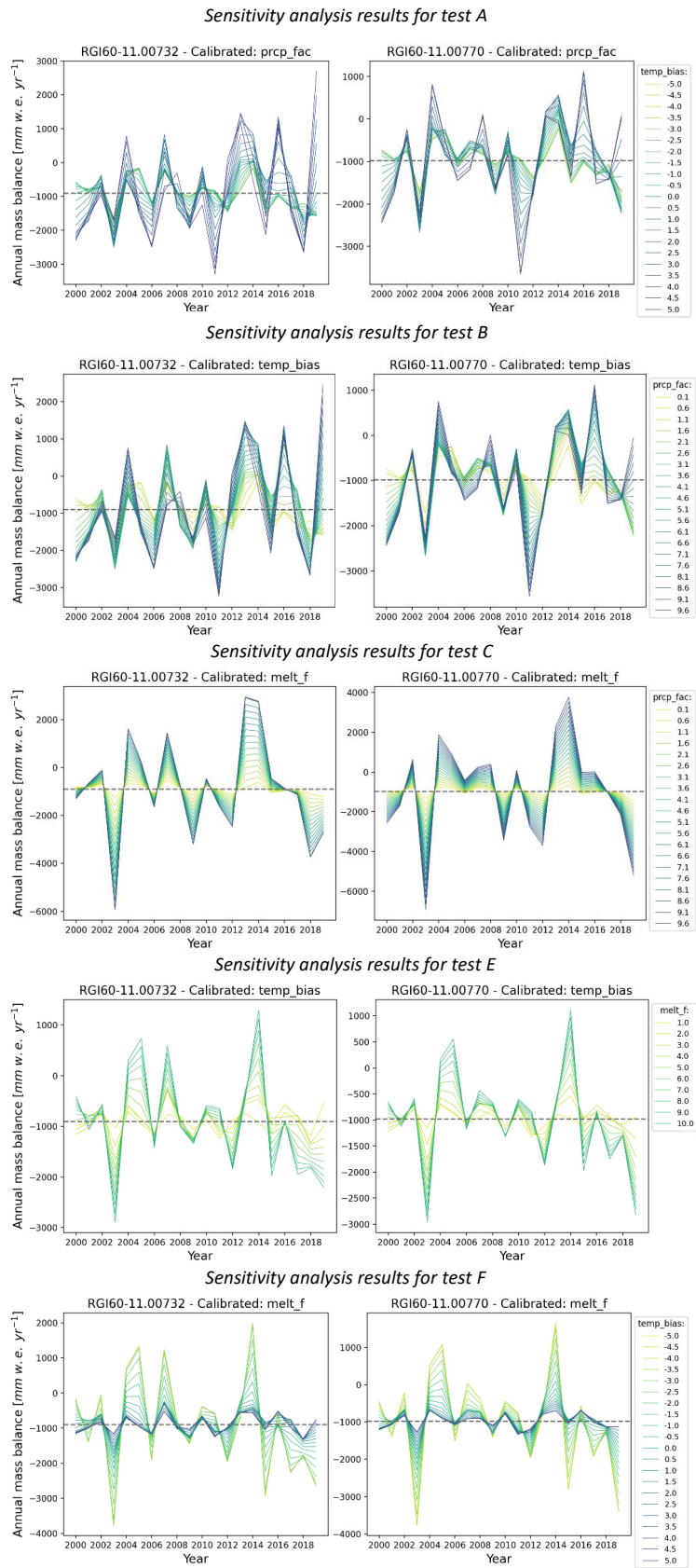


Figure C.5: Additional results from the sensitivity analysis of the mass balance model parameters in OGGM, for the glaciers Östlicher Wannetferner (RGI60-11.00732) and Weißseeferner (RGI60-11.00770).

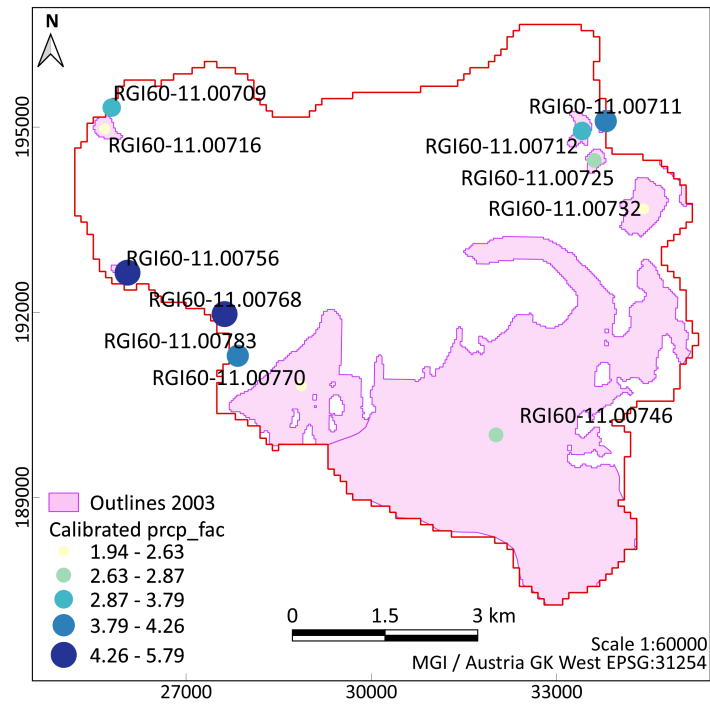


Figure C.6: Precipitation factors (*prcp\_fac*) values obtained after calibration of the mass balance model in OGGM for every glacier within the study area. The glacier outlines and IDs refer to the RGI.

Table C.3: Simulated mean and maximum thickness values for the glaciers Gepatschferner, Östlicher Wannetferner and Weißseeferner and for the years 1969, 1996, 2001, 2010 and 2019. For each glacier, mean observed values (*obs*) are also indicated in the corresponding year, when available. Values are given in m.

Year	Value	Gepatschferner	Östlicher Wannetferner	Weißseeferner
1969	mean	151	38	68
	max	493	102	174
	<i>obs</i>			
1996	mean	121	30	51
	max	407	87	144
	<i>obs</i>			31
2001	mean	115	29	50
	max	387	84	137
	<i>obs</i>	94		
2010	mean	106	28	49
	max	356	81	126
	<i>obs</i>		28	
2019	mean	102	27	47
	max	338	81	119
	<i>obs</i>			

### C.3 Additional results: coupling scheme

These results complement Section 7.3. First, complementary results related to the optimization of the coupling scheme are provided (Figure C.7). These include also the optimization of the two further set ups, in which the simulations begin in the year 1984 (and optimized during the period 1985-1998) and in the year 2003 (and optimized during the period 2005-2015) (Figures C.8, C.9 and C.10).

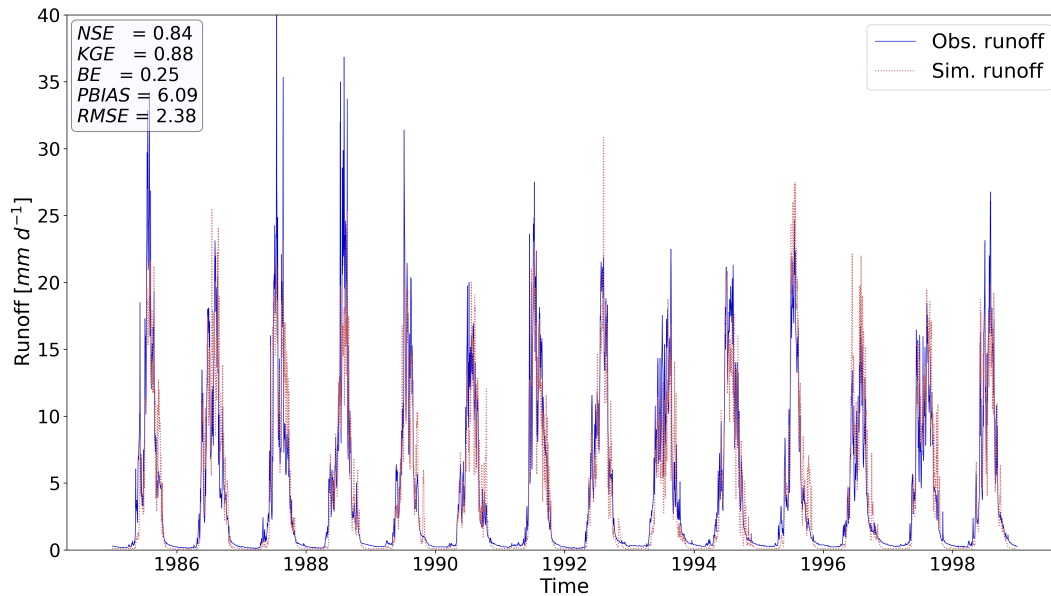


Figure C.7: Observed and simulated runoff at the outlet of Gepatschalm during the optimization period (01/1985 - 12/1998) obtained from the coupling scheme and with the model initialized in 1969. Blue solid line: observed runoff, red dashed line: simulated runoff.

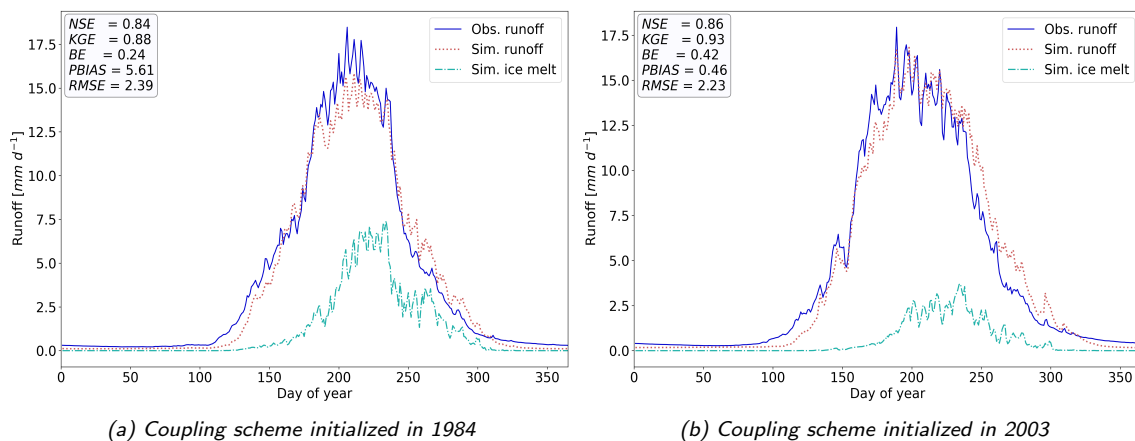


Figure C.8: Mean daily observed and simulated runoff at the outlet of Gepatschalm, including the mean daily simulated ice melt component, obtained from the optimized coupling scheme for the two other model configurations: (a) coupling scheme starting in 1984 and optimized for the period 1985-1998; (b) coupling scheme starting in 2003 and optimized for the period 2006-2015. Blue solid line: observed runoff, red dashed line: simulated runoff, light blue line: simulated melt from ice.

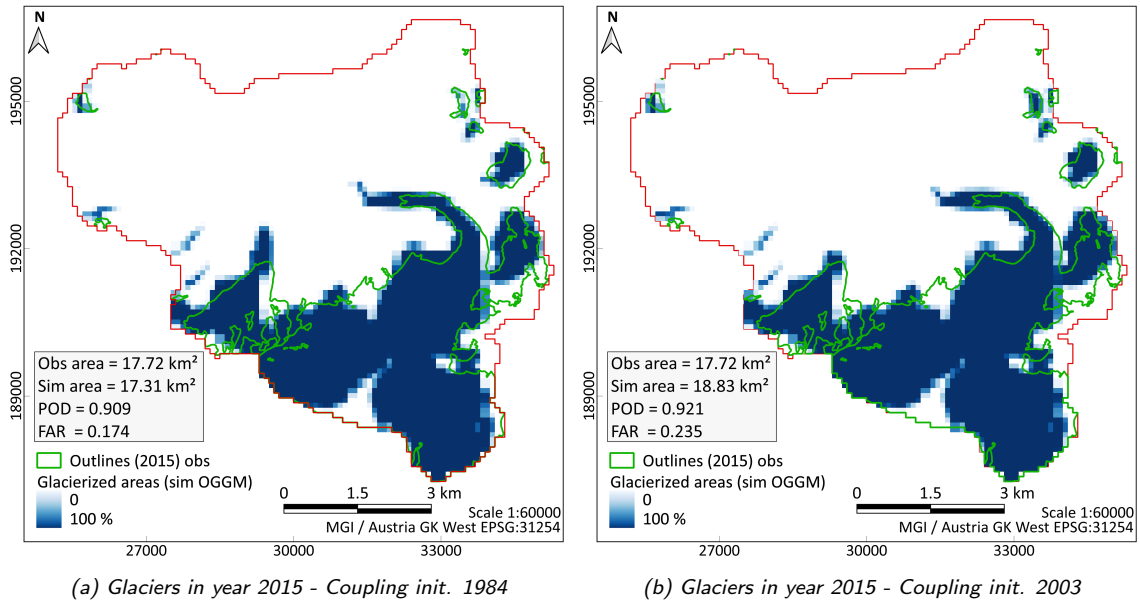


Figure C.9: Observed and simulated glacier areas for the year 2015 for the two other model set ups: (a) coupling scheme starting in 1984 and optimized for the period 1985-1998; (b) coupling scheme starting in 2003 and optimized for the period 2006-2015. The observed outlines belong to the AGI.

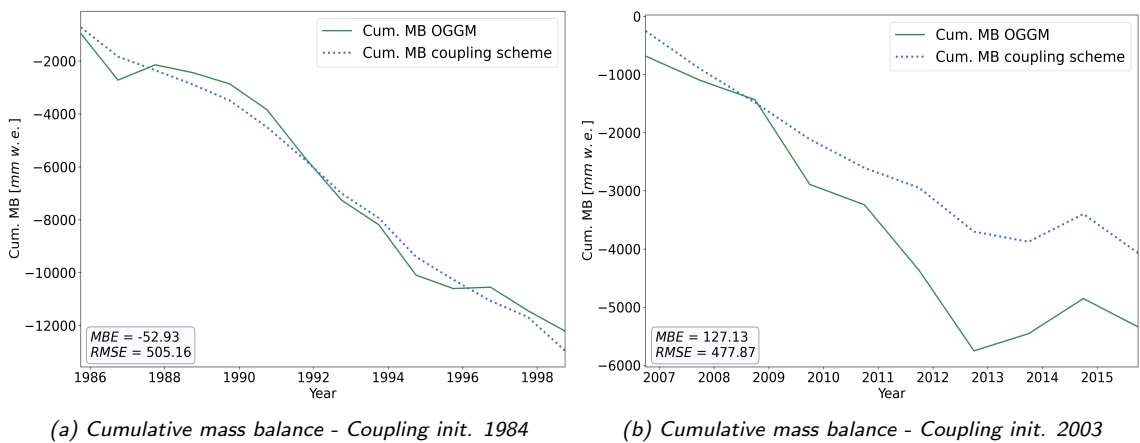


Figure C.10: Cumulative mass balances for Gepatschferner simulated with OGGM and with the optimized coupling scheme for the two other model set ups: (a) coupling scheme starting in 1984 and optimized for the period 1985-1998; (b) coupling scheme starting in 2003 and optimized for the period 2006-2015.

## C.4 Additional results: comparison WaSiM VA scaling vs. WaSiM-OGGM coupling scheme

These results complement Section 7.4. First, mass balance observations at the tongue of Gepatschferner are compared to the simulation results from WaSiM with VA scaling and the coupling scheme (Figure C.12 and Figure C.12, following the procedure described in Section 7.2.2). Second, a comparison between projected glacier coverage simulated by the different models (WaSiM with VA scaling and WaSiM-OGGM coupling scheme) is shown, for the ICHEC-EC-EARTH climate model and under different RCPs (Figure C.13). Finally, the evolution of annual runoff at Gepatschalm (only due to *Gepatschferner's* contribution)

determined by OGGM is presented. On the one hand, simulation results by using the future projections based on the INCA-kNN climate dataset and, on the other hand, using the OGGM's default climate dataset (CMIP 6, based on the W5E5 climate dataset).

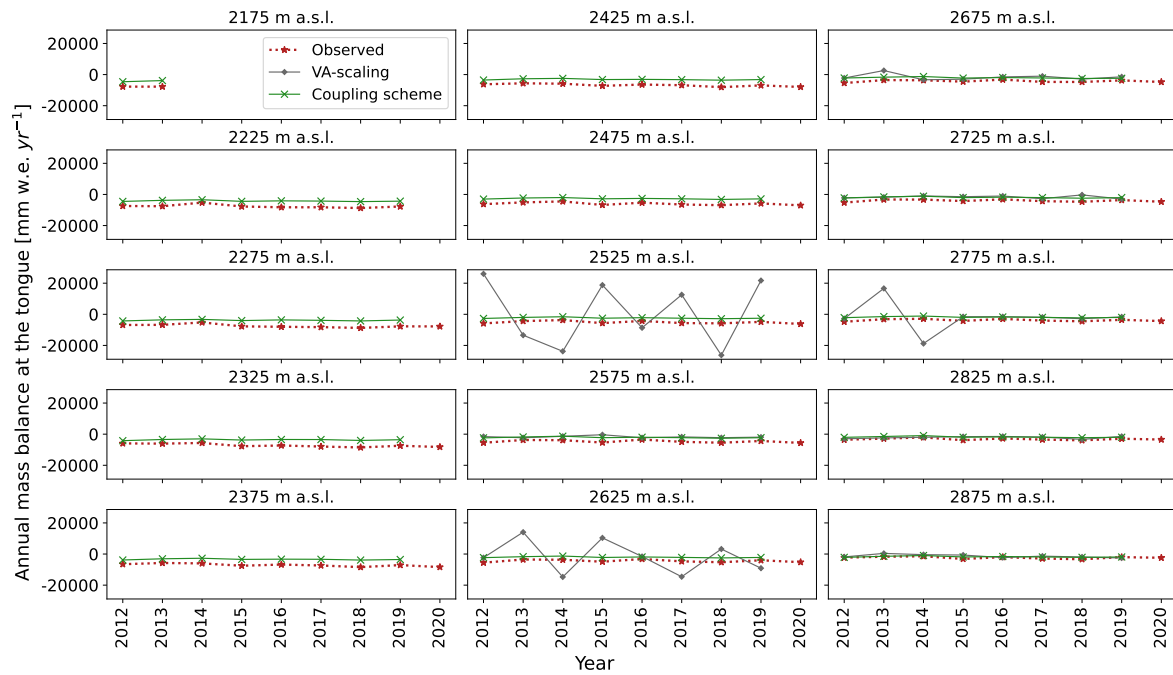


Figure C.11: Observed and simulated mass balance values at the tongue of Gepatschferner for different elevations. Observations: red dashed line with \*, simulation with WaSiM with VA Scaling: gray solid line with  $\diamond$ , simulation with coupling scheme: green solid line with  $\times$ .

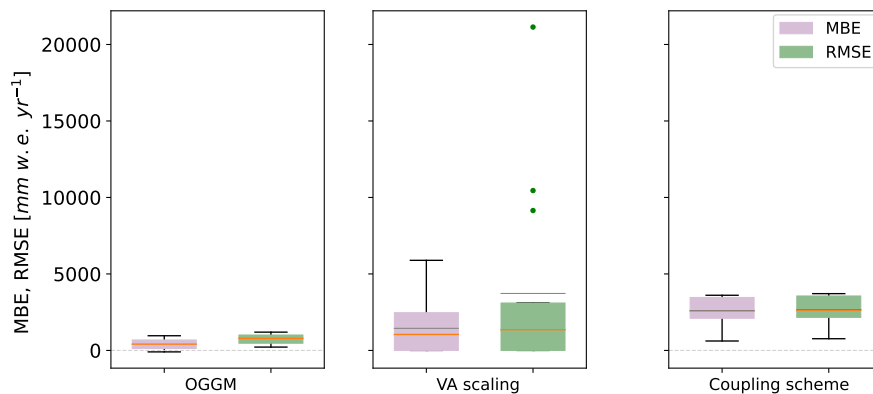


Figure C.12: MBE and RMSE [ $\text{mm w.e. yr}^{-1}$ ] between observations and simulations at the tongue of Gepatschferner and as an average of all elevations. The first case OGGM refers to the calibrated mass balance model from OGGM (Section 7.2.2), VA scaling refers to the first WaSiM run with integrated VA scaling (Section 7.1.2) and Coupling scheme refers to the third step of the coupling scheme, WaSiM with explicit ice-flow dynamics (Section 7.3).

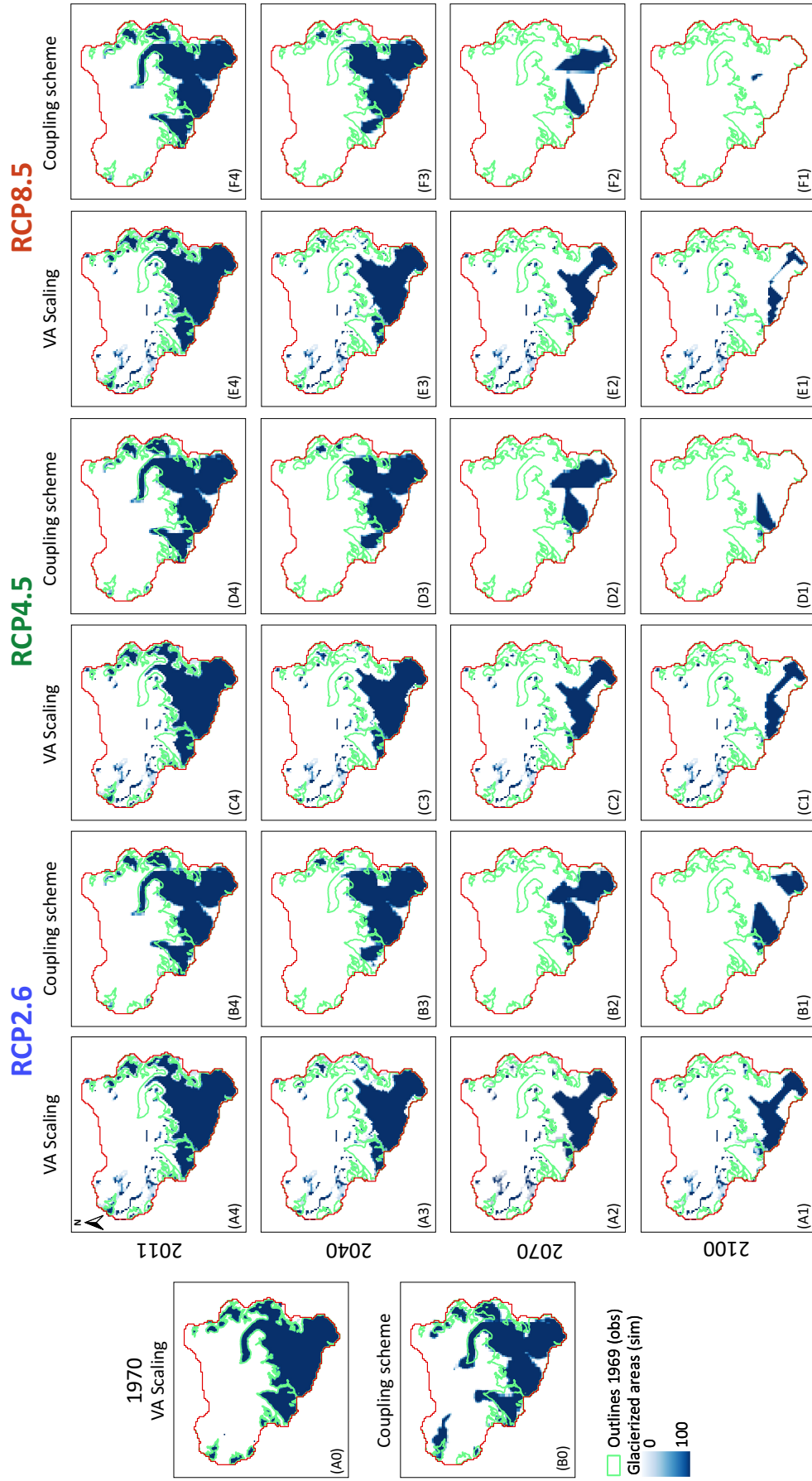


Figure C.13: Projected glacier coverage for the years 2011, 2040, 2070 and 2100, under the three different RCPs for the ICHEC-EC-EARTH GCM/RCM climate model combination. The columns indicate the RCP and model (VA scaling or coupling scheme results) and the rows, the different years. If a model cell is completely glaciated, it is represented by the dark blue color. The observed glacier outline of 1969 is also included in the figures. Moreover, the comparison for the year 1970 is also shown at the left of the figure.

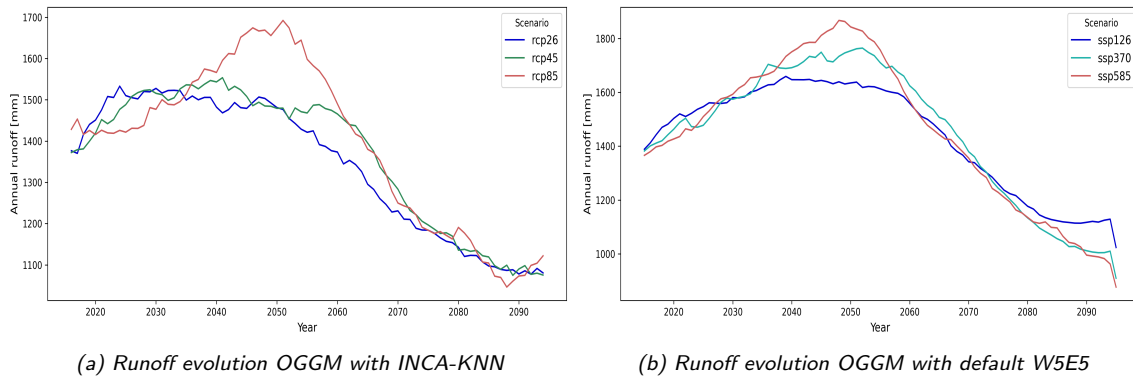


Figure C.14: Future evolution of annual runoff, computed considering only Gepatschferner, obtained from OGGM. (a) normal set up used in this thesis, the lines represent the ensemble mean of the three GCM/RCMs combinations and for RCP2.6 (blue), RCP4.5 (green) and RCP8.5 (red). (b) OGGM's default run with W5E5 (Section 6.4.3.1) as driven climate dataset in the past, the lines represent the ensemble mean of five GCM from the ISIMIP3b (Inter-Sectoral Impact Model Intercomparison Project, third simulation round, Lange et al., 2023; Maussion et al., 2023, bias adjusted and statistically downscaled from the more recent CMIP6 climate data (Coupled Model Intercomparison Project, Phase 6 (Eyring et al., 2016)). The colors represent the three different Shared Socioeconomic Pathways (SSPs): blue for SSP126, turquoise for SSP370 and red for SSP585. In both figures, the lines represent the 10-year moving average.

## C.5 Additional results: application of the coupling scheme in another catchment

These results complement Section 7.5. First, intermediate results from the dynamic run performed by OGGM in terms of volumes and areas are shown, where two initialization years are considered (1969 and 1998, Figure C.15). Second, a summary of calibrated parameters from OGGM (Figure C.16) and the optimized parameters from the coupling scheme are included (Table C.4). Finally, the comparison between (mean) observed and simulated ice thickness for the three reference glaciers and for the available years is depicted in Figure C.17.

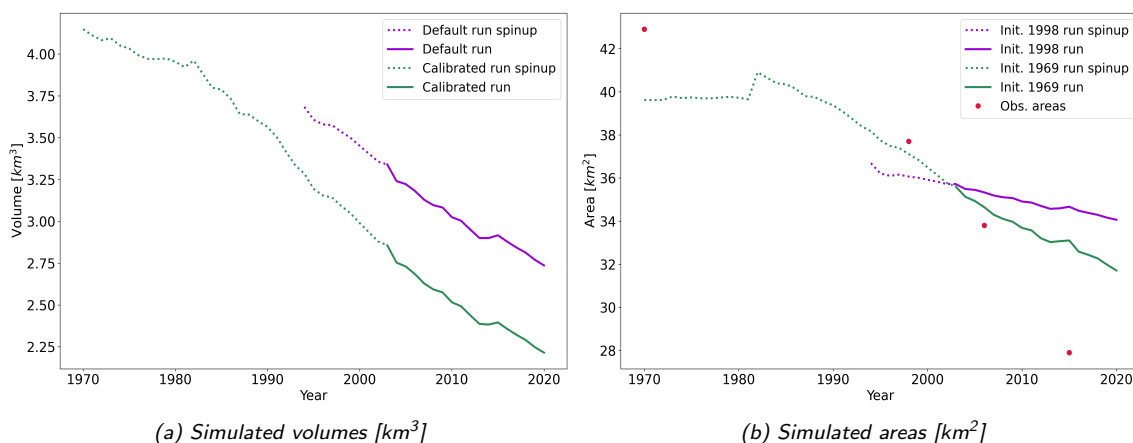


Figure C.15: Simulation results of the OGGM's dynamic runs in Rofenache: in green, calibrated run initialized in 1969 (34 years spinup) and in purple, calibrated run initialized in 1998 (5 years spinup). The dashed lines indicate the spinup period, whereas the solid lines indicate the dynamic run from 2003 onward. The red points indicate the observed areas for the selected years.



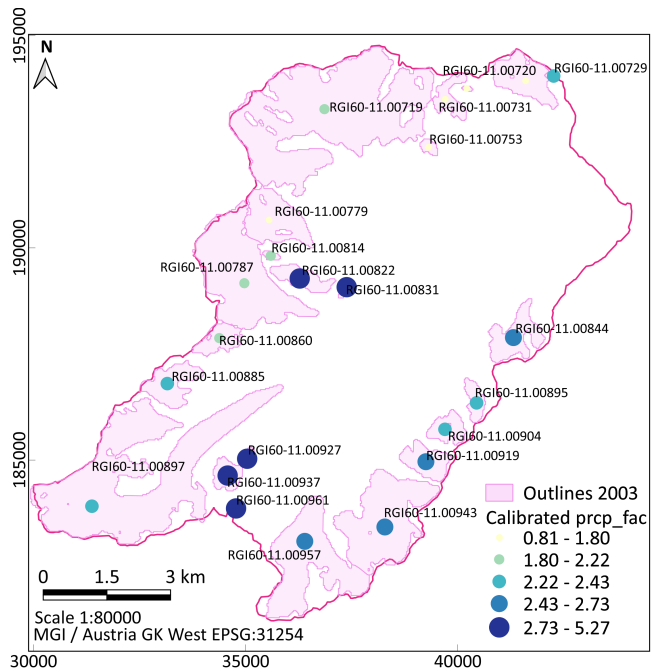


Figure C.16: Precipitation factors (*prcp\_fac*) values obtained after calibration of the mass balance model in OGGM (for the Rofenache catchment).

Table C.4: Parameters adjusted during optimization of the coupling scheme for Rofenache, including their values and units.

Parameter	Unit	Calibrated value
$k_d$	h	212.7
$k_i$	h	53.5
$q_0$	mm h <sup>-1</sup>	0.43
$t_0$	°C	0.40
$min_{slope}$	-	71.6
$lw_{out}$	-	1.07
$mf$	mm °C <sup>-1</sup> d <sup>-1</sup>	3.71
$k_{ice}$	h	18.5
$k_{firn}$	h	446.8
$k_{snow}$	h	82.3

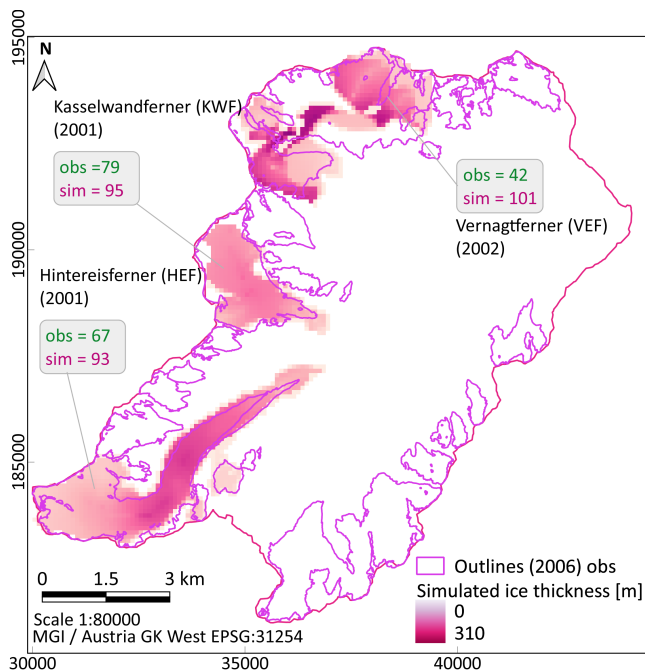


Figure C.17: Simulated ice thickness for three glaciers in the Rofenache catchment: Hintereisferner, Kasselwandferner and Vernagtferner at years in which point observations are available (years are indicated in brackets). The observed and simulated values given for each glacier refer to the mean value at the corresponding year.



# Appendix D

## GitHub repository

This Appendix includes the workflow followed in the [mariapesci/WaSiM-OGGM](#) repository and an example of the required input and output files created by the models or required from the user, as well as the corresponding scripts to run the coupling.

# Coupling scheme workflow

This text summarizes the main steps needed to follow for running WaSiM-OGGM

---

## 1. Run WaSiM

Daily (or sub-daily) simulations. Monthly mean and sum grids for temperature and precipitation have to be created, respectively. This is done in the interpolation section of the control file.

Variable	Write code	Output
temperature	73	mean monthly values
precipitation	33	total monthly values

Since we are going to update the glacier model with OGGM's output afterwards, the glacier model in WaSiM can be deactivated.

---

## 2. Convert grids to nc files

Use the file: [Convert WaSiM grids to netCDF files](#)

Results: one netCDF file (i.e.: 'monthly\_meteo.nc') containing monthly values of temperature and precipitation.

---

## 3. Run OGGM

OGGM calculates the monthly mass balance based on the Temperature index model ([Marzeion et al., 2012](#)) calibrated on geodetic mass balance observations ([Hugonet et al., 2021](#)). The description of the T-index model can be found here: [T-index model calibrated on geodetic MB data](#).

- Define the initialization method:
  - No initialization: if OGGM starts its simulation from the RGI inventory's date (e.g. 2003)
  - Dynamic spinup: if OGGM starts its simulation no more than 40 years before the RGI inventory's date (e.g. in 1970). Either no initialization or with a dynamic spinup, the script [coupling\\_oggm\\_user.py](#).
  - Initialization\_Eis: if OGGM starts its simulations far away in time, the method developed by Eis et al. (2021) will be applied. In this case, the script [coupling\\_initialization.py](#) needs to be run beforehand

Based on the [ice dynamics flowline model](#), an outline is created for each of the glaciers and each year within the simulation period. The outlines are converted into polygons and saved as shapefiles for posterior use.

Similarly, the glacier's thickness distribution within the previously defined outline, is obtained for each of the glaciers and years, adapted from the function [distribute\\_thickness\\_per\\_altitude](#).

Two new files are created for WaSiM:

- glaciercells\_year: an ASCII format file (raster) containing the volume of ice for each grid cell and for each of the years

- glaciercodes\_year: an ASCII format file (raster) containing the glacier codes needed to run the glacier module in WaSiM (which corresponds each year with the glaciercells file).

---

#### 4. Re-run WaSiM with initial states from OGGM outputs and optimize results

In WaSiM, the dynamic glacier model is selected. This model is based on the volume-area scaling approach ( $V = b \cdot A^f$ ) and depends on two empiric factors ( $b$  = mean glacier thickness of a 1 km<sup>2</sup> glacier and  $f$  = scaling factor).

Now, a new simulation with WaSiM can be performed. Each year, the integrated VA-scaling model in WaSiM is then "replaced" by OGGM's outputs (area x ice thickness = volume).

WaSiM is run annually: at the beginning of each year, the glaciers' volume is known (OGGM outputs). At the end of each year, the outputs from WaSiM serve as initial states for the following year, thus ensuring a continuous simulation through the entire simulation period.

WaSiM determines the mass balance of the glaciers on a daily basis and based on their own parameter set. The results differ from OGGM mass balances, since other parameters set is used (inherent to OGGM). Thus, a calibration based on the annual (or monthly) mass balances must be performed, in order to integrate OGGM's results.

An automatic calibration is performed in which selected parameters (affecting the MB in WaSiM) are adjusted, while running the coupling scheme in a yearly basis. The [Statistical Parameter Optimization Tool for Python, SPOTPY \(Houska et al., 2015\)](#) is linked to the coupling scheme. Since the parameters affecting the mass balance also influences the ice melt contribution to the total runoff, a multi-objective calibration approach based on a multi-objective function is applied. In this way, the model is calibrated against observed runoff and OGGM-mass balance data.

Post-processing of OGGM output data:

- Determine volume from thickness and outlines: with the script [init\\_vol\\_from\\_thickness.py](#), the grids containing the distributed thickness for each glacier are read and merged all together for each individual year. The volume is then corrected with the calculated values from the dynamic run performed by OGGM. A new ASCII file is saved as "glaciercells", containing the initial volume of the glacierized cells, similar to the grid containing the fraction of glacierization per cell.
- Convert ASCII grids to binary files: this step is required before running WaSiM and can be done with [ascii\\_to\\_grid.py](#).
- A small trick has to be performed before running the coupling: an initial grid file containing the mass balance values for the glaciers has to be created at the beginning of the simulations, then, while running the coupling with annual updates of the glaciers, the mass balance grid will be created automatically. This initial mass balance grid (glmb and glmb\_old) only needs to contain 0 values in all active model cells, and -9999 in the inactive cells (a simple approach is to copy one of the 'glaccells.grd' and replace non -9999 values with 0).
- Set up the multi-objective optimization of the coupling scheme: within this script [spotpy\\_coupling\\_settings.py](#), where simulation period, input data, observed data, target variables and maximum number of iterations are defined.
- Finally, the actual coupling with optimization: [spotpy\\_calibration.py](#). Here, different weights are assigned to the multi-objective function, together with the algorithm used during the optimization.

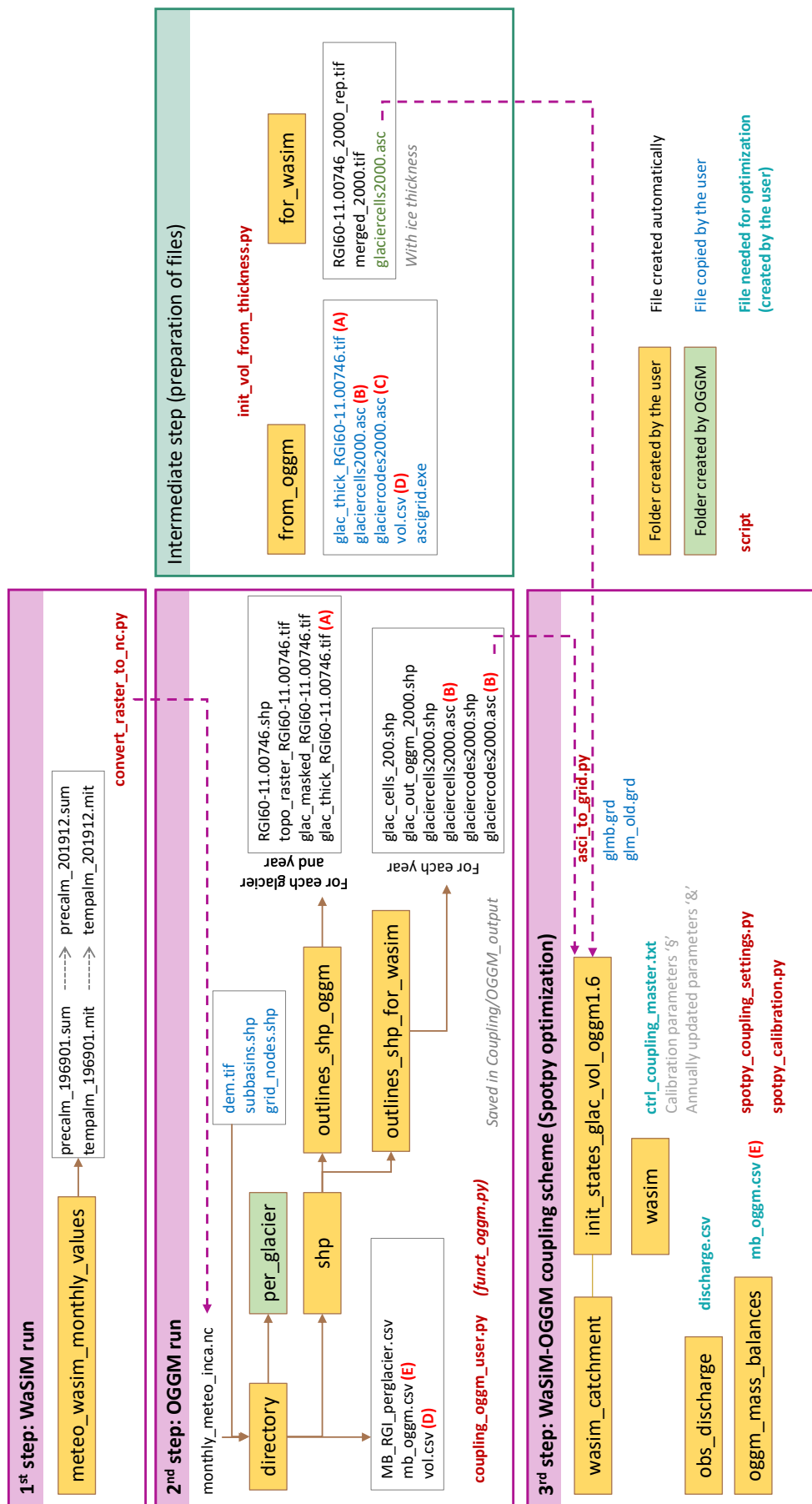


Figure D.1: Detailed flow of files and scripts needed to run the WaSiM-OGGM coupling scheme.



Herausgegeben im Selbstverlag  
des Institutes für Hydrologie und Wasserwirtschaft  
Gottfried Wilhelm Leibniz Universität Hannover  
Appelstraße 9a; D-30167 Hannover  
Tel.: 0511/762-2237  
Fax: 0511/762-3731  
E-Mail: [info@iww.uni-hannover.de](mailto:info@iww.uni-hannover.de)

2024

Alle Rechte beim Autor